DEPARTMENT OF TRANSPORTATION

An Innovative Practical Approach to Assessing Bitumen Compatibility as A Means of Material Specification

Eshan V. Dave, Principal Investigator
Department of Civil and Environmental Engineering
University of New Hampshire

January 2025

Final Report NRRA202501

NRRA National Road Research Alliance

To get this document in an alternative format or language, please call 651-366-4720 (711 or 1-800-627-3529 for MN Relay). You can also email your request to ADArequest.dot@state.mn.us. Please make your request at least two weeks before you need the document.

Technical Report Documentation Page

1. Report No.	2.	3. Recipients Accession No.	
MN NRRA202501			
4. Title and Subtitle An Innovative Practical Approach to Assessing Bitumen Compatibility as A Means of Material Specification		5. Report Date January 2025 6.	
7. Author(s) Eshan V. Dave, Jo E. Sias, Shubham H. Modi, Zheng Wang		8. Performing Organization Report No.	
9. Performing Organization Name and Address Department of Civil and Environmental Engineering University of New Hampshire 33 Academic Way, Durham, NH, 03824		10. Project/Task/Work Unit No. 11. Contract (C) or Grant (G) No. (c) 1003326 (wo) 2	
12. Sponsoring Organization Name and Address Minnesota Department of Transportation Office of Research & Innovation 395 John Ireland Boulevard, MS 330 St. Paul, Minnesota 55155-1899		13. Type of Report and Period Covered Final Report 14. Sponsoring Agency Code	
15. Supplementary Notes http://mdl.mndot.gov/			

16. Abstract (Limit: 250 words)

Modern asphalt mixtures are usually a combination of various materials from different sources, including reclaimed asphalt pavement (RAP) and recycling agents (RAs), and are used to attain sustainable growth. However, the lack of a well-established method for determining compatibility between various sources and types of virgin binder, aged binder within RAP, and RAs has been a major impediment in current asphalt material selection and specification. Therefore, the objective of this study was to evaluate various binder and mixture testing methods to characterize the compatibility between complex components of asphalt mixtures, specifically from the perspective of assessing their cracking performance. The primary evaluation consisted of laboratory-prepared materials that used three RAP sources, three asphalt binders (one PG 58–28, two PG 64–22), and two RAs (petroleum-based and bio-oil-based) for both binder and mixture characterization. The binder tests consisted of rheological characterization using the dynamic shear rheometer (DSR) and thermal analysis using the differential scanning calorimeter (DSC), whereas the mixture tests included complex modulus (E*), semi-circular bend (SCB), and disk-shaped compact tension (DCT) tests. The results indicated that the rheological characterization of asphalt binder and mixture may not adequately capture the incompatibility between virgin binder, RAP, and Ras. However, binder DSC analysis and mixture fracture tests have shown promising results for evaluating the compatibility of various mixture components. Therefore, the findings of this study provide agencies with a framework to select the most compatible component materials from various sources for their projects.

17. Document Analysis/Descriptors	18. Availability Statement		
Recycled materials, Fracture tests, Shear modulus, Rheometers, Calorimeters, Asphalt tests	No restrictions. Document available from: National Technical Information Services, Alexandria, Virginia 22312		
19. Security Class (this report)	20. Security Class (this page)	21. No. of Pages	22. Price
Unclassified	Unclassified	202	

AN INNOVATIVE PRACTICAL APPROACH TO ASSESSING BITUMEN COMPATIBILITY AS A MEANS OF MATERIAL SPECIFICATION

FINAL REPORT

Prepared by:

Eshan V. Dave, Jo E. Sias, Shubham H. Modi, and Zheng Wang
Department of Civil and Environmental Engineering
University of New Hampshire

Hassan Tabatabaee and Tony Sylvester
Cargill Bioindustrial

January 2025

Published by:

Minnesota Department of Transportation
Office of Research & Innovation
395 John Ireland Boulevard, MS 330
St. Paul, Minnesota 55155-1899

ACKNOWLEDGMENTS

The authors would like to begin by acknowledging the Technical Advisory Panel (TAP) members on this project: Andrew Cascione, Mohamed Elkashef, Brian Hill, Brett Lambden, Erik Lyngdal, Tirupan Mandal, Kiran Mohanraj, Dan Oesch, Michael Vrtis, Richard Willis, and Ben Worel. The TAP members provided guidance and improvements throughout the entirety of the project.

In addition, the authors would like to thank the National Road Research Alliance (a USDOT Pooled Fund led by the Minnesota Department of Transportation) for their support of this project. In particular, we thank MnROAD, NCAT, and the Department of Transportations of Alabama, Missouri, Texas, Illinois, Virginia, Wisconsin, and their staff members for their substantial help in material sampling during the COVID pandemic.

TABLE OF CONTENTS

LIST OF FIGURES

LIST OF TABLES

LIST OF ABBREVIATIONS

|E*|	Dynamic Modulus
AFM	Atomic Force Microscopy
AFT	Asphalt Binder Film Thickness
APC	Advanced Polymer Chromatography
ASTM	American Society for Testing and Materials
BBR	Bending Beam Rheometer
CII	Colloidal Instability Index
CMRI	Complex Modulus Based Rutting Index
CTOD	Crack Tip Opening Displacement
DCT	Disk-Shaped Compact Tension
D-EMT	Differential Effective-Medium Theory
DENT	Double-Edge-Notched Tension
D^R	Average Reduction in Integrity Up to Failure for Mixture
DSC	Differential Scanning Calorimetry
DSR	Dynamic Shear Rheometer
DTCF	Direct Tension Cyclic Fatigue
EBBR	Extended Bending Beam Rheometer
E_f	Strain Energy Tolerance
EMHP	Elastin-Mimetic Hybrid Polymers
EPDM	Ethylene-Propylene-Diene Rubber
EWF	Essential Work of Ductile Failure
FHWA	Federal Highway Administration
FI	Flexibility Index

FID	Flame Ionization Detector
FKM	Fluororubber
FST	Fracture Strain Tolerence
FTIR	Fourier-Transform Infrared
G_f	Fracture Energy
G-R	Glover-Rowe
G-R_m	Mixture Glover-Rowe
GTR	Ground Tire Rubber
HBRR	High Binder Replacement Ratio
HMW	High Molecular Weight
HPLC	High-Performance Liquid Chromatography
HTPG	High Temperature Performance Test
HWTT	Hamburg Wheel Tracking Test
I_A	Asphaltene Index
I_C	Gaestel Index
ICP-AES	Inductively Coupled Plasma Atomic Emission Spectroscopy
IR	Infrared
I^R	Average Reduction in Integrity up to Failure for Binder
J_{nr}	Non-Recoverable Creep Compliance
LAS	Linear Amplitude Sweep
LBRR	Low Binder Replacement Ratio
LMW	Low Molecular Weight
LTPG	Low Temperature Performance Grade
LTPP	Long-Term Pavement Performance
LVE	Linear Viscoelastic

MESAL	Million Equivalent Standard Axle Load
MMW	Medium Molecular Weight
MSCR	Multiple Stress Creep Recovery
m-value	Relaxation Rate
Mw	Molecular Weight
n	Ozawa Exponent
NMR	Nuclear Magnetic Resonance
NRRA	National Road Research Alliance
PEG	Polyethylene Glycol
PG	Performance Grade
PIB	Polyisobutylene
PMB	Polymer Modified Binder
ppm	Parts Per Million
RA	Recycling Agent
RAF	Roofing Asphalt Flux
RAP	Reclaimed Asphalt Pavement
RB	Rejuvenated Binder
RBR	Recycled Binder Ratio
RDCI	Rate-Dependent Cracking Index
REOB	Recycled Engine Oil Bottoms
RPE	Recycled Polyethylene
S	Creep Stiffness
S_{app}	Accumulated Damage
SARA	Saturates, Aromatics, Resins, and Asphaltenes
SB	Softer Binder

SBS	Styrene-Butadiene-Styrene
SCB	Semi-Circular Bend
SEC	Size Exclusion Chromatography
SEM	Scanning Electron Microscopy
STM	Scanning Tunneling Microscopy
S-VECD	Simplified Viscoelastic Continuum Damage
Tg	Glass Transition Temperature
TGA	Thermo-Gravimetric Analysis
THF	Tetrahydrofuran
T_t	Viscoelastic (Crossover) Transition Temperature
UV	Ultraviolet
VB	Virgin Binder
VECD	Viscoelastic Continuum Damage
VFA	Voids Filled with Asphalt
VMA	Voids in the Mineral Aggregate
WEO	Waste Engine Oil
WMA	Warm Mix Asphalt
XRF	X-Ray Fluorescence
δ	Phase Angle
ΔT_{IR}	Intermediate Region Temperature Range
ε_T	Stain Tolerance up to Failure

EXECUTIVE SUMMARY

Modern asphalt mixtures are usually a combination of various materials from different sources, including reclaimed asphalt pavement (RAP) and recycling agents (RAs), and are used to attain sustainable growth. However, the lack of a well-established method for determining compatibility between various sources and types of virgin binder, aged binder within RAP, and RAs is a major impediment to current asphalt material selection and specification. This knowledge gap leads to inferior pavement performance and longevity, hinders the adoption of higher recycled materials than that in typical asphalt mixtures, and complicates the selection of appropriate binders and rejuvenators by agencies. Furthermore, one of the main issues that limits the use of RAP is related to the cracking performance of recycled mixtures at both intermediate and low temperatures, as RAP increases its stiffness. Therefore, this study evaluates various binder and mixture testing methods to characterize the compatibility between complex components of asphalt mixtures and attempts to develop a robust method to characterize the compatibility. The main objectives of this research study are as follows:

- Explore a practical and implementable compatibility characterization system
- Build a methodology for adopting the compatibility characterization system
- Provide guidance to agencies on the implementation of the compatibility-based material selection methodology

The primary evaluation consisted of laboratory-prepared materials that used three RAP sources, three asphalt binders (one PG 58–28, two PG 64–22), and two RAs (petroleum-based and bio-oil-based) for both binder and mixture characterization. These materials are referred to as “core materials” in this report. In addition, eight plant-produced validation mixtures and their limited field performance were also assessed to verify the findings from laboratory-prepared materials. These materials are referred to as “validation materials” in this report.

This project included seven research tasks. Task-1 consisted of performing a thorough state-of-the-art review regarding the available tools and techniques to assess the compatibility of asphalt binders with respect to virgin and recycled asphalt sources as well as rejuvenators and polymers. The review conducted focuses on literature both in the asphalt materials domain as well as those available in the fields of organic chemistry and polymer science. Task-2 focused on carefully selecting and collecting the core material to cover the possible geographical variation and different varieties of the materials for the study. It also included screening and prioritizing the core materials evaluated in this study. The efforts undertaken in Task-2 have allowed the research team to select the control materials from core materials and thus accommodate various test methods without increasing the test burden. Task-3 focused on the characterization of control materials and allowed the screening of promising methods for compatibility characterization. Preliminary statistical analysis was conducted as part of Task-3 and revised with the results of remaining core materials over the course of the project in subsequent task reports. Next, Task-4 was dedicated to the evaluation of all core materials using screened test methods of Task-3. The preliminary compatibility characterization system was proposed based on the findings of Task-4 results. Task-5 focused on validating the recommendations of Task-4 by evaluating eight validation materials

collected across the United States. The laboratory performance of validation mixtures was also compared with the available field performance data within this task.

The innovations from this project are expected to result in novel applications of material characterization methods and provide recommendations for material selection and specification processes. The expected outcomes will allow National Road Research Alliance (NRRA) agencies and producers to improve their understanding of RAP materials, thereby enabling the selection of appropriate additives for enhanced performance and sustainability of pavement materials. There were several significant findings and recommendations made based on the research conducted in this study. Based on the test efforts, rheological and thermal parameters for binder and cracking parameters of mixtures were proposed for compatibility characterization of asphalt mixture components. Finally, the methodology to develop the thresholds for the proposed binder parameters was presented.

Chapter 1: INTRODUCTION

A major challenge in current asphalt pavement material selection, specification, and mix design processes, is the lack of knowledge in determining compatibility between virgin binders and binders in recycled materials as well as those between binders (new and recycled) and rejuvenators. This lack of a characterization process to evaluate compatibility is a significant issue in the currently adopted U.S. practice for asphalt specification and purchase, whereby multiple sources of binders are often blended, and most agencies allow for the use of recycled asphalt pavements (RAP) in the mixtures. The consequence of this is manifested in the form of inferior pavement performance and longevity and lack of guidance to agencies in adopting higher amounts of asphalt recycling, as well as selection of appropriate binders and rejuvenators.

The primary objective of this project is to develop a practical and implementable characterization system to determine the compatibility between virgin asphalt binder and RAP as well as that between virgin asphalt binder, RAP, and rejuvenating agents. The innovations from this project will be realized in terms of novel applications of material characterization methods as well as recommendations for material selection and specification processes. Furthermore, the outcomes of the proposed study will allow National Road Research Alliance (NRRA) agencies and producers to improve their understanding of the RAP materials by correctly being able to identify their compatibility and therefore select the right additives to use. This would then lead to higher performance and overall greater sustainability for pavement materials. Both analytical and mechanical testing methods as well as advanced analyses are evaluated in the study to develop a practical and readily implementable protocol for binder compatibility evaluation.

Chapter 2: STATE-OF-THE-ART REVIEW, SAMPLING, AND TEST PLAN

2.1 CHAPTER INTRODUCTION

This chapter summarizes a thorough state of the art review regarding the available tools and techniques to assess the compatibility of asphalt binders with respect to virgin and recycled asphalt sources as well as rejuvenators and polymers. The review focuses on literature in the domain of asphalt materials and those available in organic chemistry and polymer science. This report incorporates research that has been conducted worldwide on these topics in recent years. The existing body of knowledge and current methods are used as important references to adjust and finalize the proposed testing plan and as the starting point to develop an innovative, practical, and implementable characterization system to determine the compatibility of complex binders.

2.2 DEFINITIONS OF BINDER COMPATIBILITY

There has been a lack of consensus about the standardized definition of binder compatibility in the asphalt materials field. However, binder compatibility can be typically described from two different perspectives: (1) compatibility in terms of the asphalt component; and (2) compatibility between asphalt and additives.

2.2.1 Asphalt Component Compatibility

Historically, asphalt component compatibility has been described in terms of a colloidal model, which depicts asphalts as dispersions of asphaltenes in petrolenes (maltenes). Asphalt component compatibility is believed to be directly tied to colloidal composition, where asphalts with low asphaltene content are designated as more compatible. Asphalt component compatibility can also be explained by the sol-gel structure of asphalt binders. Typical asphalts can be classified into sol, gel, or intermediate categories. Sol and gel type asphalts exhibit differences in physical and chemical behavior. Sol asphalts can be described as compatible, while gel asphalts are generally described as non-compatible.

2.2.1.1 Based on Colloidal Model

Based on Corbett's method (Corbett, 1969), asphalt binders can be represented by a colloidal model consisting of a highly polar asphaltene phase dispersed in a maltene phase. The concept of binder compatibility or stability refers to the balance between soluble and insoluble fractions in the colloid, which controls the flow properties of the colloid. Based on this model, asphalt binders can be separated into four different fractions based on increasing polarity: saturates, aromatics, resins, and asphaltenes (SARA), as shown in **Figure 2-1**. The balance between SARA fractions has been related to physical properties, and this balance is a common compatibility indicator (Corbett, 1970; Petersen, 2009). A more compatible asphalt binder has a larger proportion of soluble fractions, resulting in a softer binder with increased ductility. Loss of binder compatibility with short- and long-term aging (stiffening and

embrittlement) is attributed to volatilization of lighter oils in the asphalt binder and the increased asphaltene content formed upon binder oxidation (Petersen, 2009).

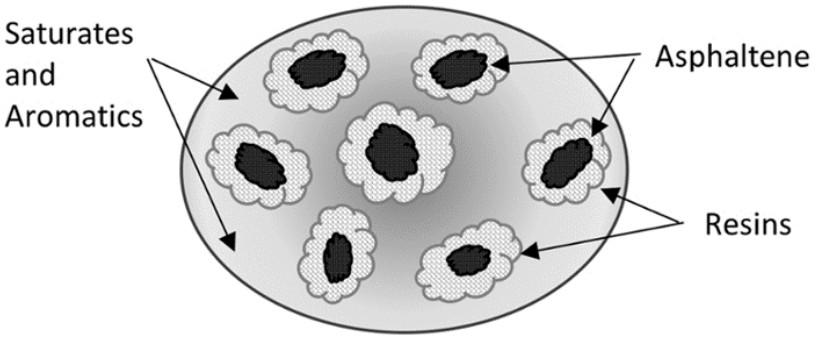

Figure 2-1 Typical asphalt components

2.2.1.2 Based on Binder Sol-gel Structure

The compatibility of asphalt component can also be described by looking at its sol-gel structure (related to the colloidal composition of binders). Generally, asphalts can be classified as either exhibiting gel-type (less compatible) or sol-type (more compatible) (Barth, 1962) characteristics in terms of their flow properties. With "more" compatible asphalts, the material structure referred to as "dispersed-phase" asphaltenes is generally lower in natural abundance and well dispersed or peptized by the maltene solvent "continuous" phase. Compatible asphalts also exhibit more Newtonian-like flow properties and are generally more ductile than less compatible asphalts. Conversely, "less" compatible asphalts exhibit more elastic behavior, have a higher natural abundance of asphaltenes, and are less ductile (or more brittle) than more compatible asphalts. Several researchers (Sheu et al., 1991&2002; Pauli et al., 1998&1999) have considered the Pal-Rhodes model (Sheu et al., 1991), which builds upon Einstein's colloid theory of dilute suspensions (Einstein, 1996), to construct the relationship between asphalt compatibility and its physical properties. Bullard et al. (Bullard et al., 2009) have recently applied differential effective-medium theory (D-EMT) to derive solutions to the Pal-Rhodes model. In D-EMT, the properties of a composite material (the effective medium) are shown to be directly related to the relative amounts of the starting fractions (indicating the compatibility) of a given binder sample. For instance, the effective viscosity η of an asphalt is modeled in terms of the viscosity of the solvent phase maltenes, η_0, and the mass fraction of suspended phase asphaltenes, *x*. The final conserved solution to the Pal-Rhodes model is generally expressed by,

$$\eta = \eta_0(1 - Kx)^{-2.5} \tag{2.1}$$

where *K* is a solvation factor and is assumed to be shear rate and temperature dependent.

In addition, there are also studies that discuss the asphalt component compatibility in ways outside these two traditional definitions, such as explaining the compatibility in terms of the crystallized fraction, glass transition, Heithaus theory. Compatibility in terms of binder performance criteria will be discussed in section 2.3.

2.2.2 Compatibility between Asphalt and Additives

As refinery efficiency allows extraction of more gasoline and other petroleum products from crude oil and as the source of crudes that yield quality asphalt residua decreases, the need for additives to upgrade straight-run asphalts increases. Further, the physical specifications for asphalt defined by the PG system have prompted the use of more additives to meet state DOT requirements. Highway agencies have also recognized the benefits of using modified asphalt to reduce the amount and severity of pavement distresses and to increase service life. Therefore, the use of additives in the asphalt materials field has become increasingly popular.

There are generally three typical types of asphalt additives: recycled materials (e.g., RAP and reclaimed asphalt shingles (RAS)), rejuvenators (e.g., aromatic extracts, paraffinic oils, tall oils, organic/vegetable oils), and modifiers (e.g., elastomers, plastomers, and rubbers). The compatibility between the virgin binder and these different additives is usually described as blend effectiveness, as well as the performance difference between the blends and the virgin binders (Spadafora et al., 1985; Turner et. al., 1997; Qin et. al., 2014; Wang et al., 2014&2015; Liang et al., 2018; Adams et. al., 2019; Apostolidis et. al., 2019). A well-blended binder with improved performance is generally considered as the compatible binder sample, e.g., a polymer modified binder with the cross-linking structure and a rejuvenated binder with the well-diffused rejuvenator in the RAP. The blend effectiveness of these complex binder blends can be characterized by morphology analysis methods, as well as thermal analysis instruments, while their performance can be directly measured and compared by the different binder performance tests. These different measurements, as well as their typical outputs that can be used to characterize the compatibility of the complex binder blends will be discussed in detail in section 2.3.

There are also some overlapping areas between the asphalt component compatibility and the compatibility between the asphalt and additives. For example, RAP binder is aged asphalt; when it is blended with virgin binder, the compatibility of the blend can also be discussed in terms of the blend's colloidal model and sol-gel structure. For certain types of rejuvenators (e.g., aromatic extracts), methods for characterization of the compatibility of asphalt components can also be potentially used to describe the compatibility of the final blends.

2.3 CURRENT METHODS AND PRACTICES FOR EVALUATION OF COMPATIBILITY (IN ASPHALT DOMAIN)

Currently, there are no standardized methods to identify compatible or incompatible binder and binder blends. This section summarizes the review of literature on various methods and practices that have been used to evaluate the compatibility of binder samples, as well as characterize the properties of complex binder blends (e.g., a mixture of binders from different sources, RAP, rejuvenator, and modifier) within the asphalt materials domain.

2.3.1 Analytical Method

2.3.1.1 Measurement of the Colloidal Indices

In order to determine chemical/colloidal compositions, column chromatography or the SARA separation method can be performed on the binder samples. In this method, asphaltenes are precipitated in n-heptane and separated from n-heptane soluble Petrolenes. Afterward, Petrolenes are fractionated into saturates, aromatics and resins by descending in a glass chromatographic column. Finally, eluted fractions are recovered by removing the solvent before weighing (Mansourkhaki et al., 2020). **Figure 2-2** shows the typical process for the SARA fractionation test.

Figure 2-2 SARA fractionation test (column chromatography) (Mansourkhaki et al., 2020)

To characterize the binder colloidal system, several indices, such as the Asphaltene Index (I_A) and Gaestel Index (I_C), have been proposed. These two indices are calculated by Eqs. (2.2), (2.3) (Oyekunle et al., 2006; Paliukaite et al., 2014).

$$I_A = (A_S + R)/(A_R + S) \tag{2.2}$$

$$I_C = (A_S + S)/(A_R + R) \tag{2.3}$$

where,
A_S = denotes the asphaltene content;
S = saturate content;
R = resin content; and
A_R = Aromatic content.

The I_C, also known as the colloidal instability index (CII), is one of the most common indices demonstrating binder colloidal compatibility and stability. If the I_C increases, the colloidal compatibility of the system decreases (Kim et al., 2018). A colloidal stable binder has an I_C value between 0.22 and 0.5, and for I_C between 0.5 and 2. 7, the binder is considered unstable (Paliukaite et al., 2014; Oliver, 2009). Gaestel Index itself can be used to evaluate and compare the compatibility of different binders and blends, the trend of changing the I_c with change of additives can be also used to evaluate the compatibility of the binder blends (Mansourkhaki et al., 2020).

Figure 2-3 shows an example of using the Gaestel Index to evaluate the compatibility or stability of binder blends. As shown in the figure, blends modified with softer binder (SB) and polymer modified binder (PMB) tend to move toward upper boundary area (unstable zone) with the increase in RAP content. By adding RAP up to 50%, the colloidal system of the binder modified with SB is still in the stable area. However, for the rejuvenated binder the trend is not the same. As can be seen in **Figure 2-3**, I_C increases with an increase in RAP content from 25 to 50%. Further increase in RAP content causes a decrease in I_C, resulting in the incompatible blended binders.

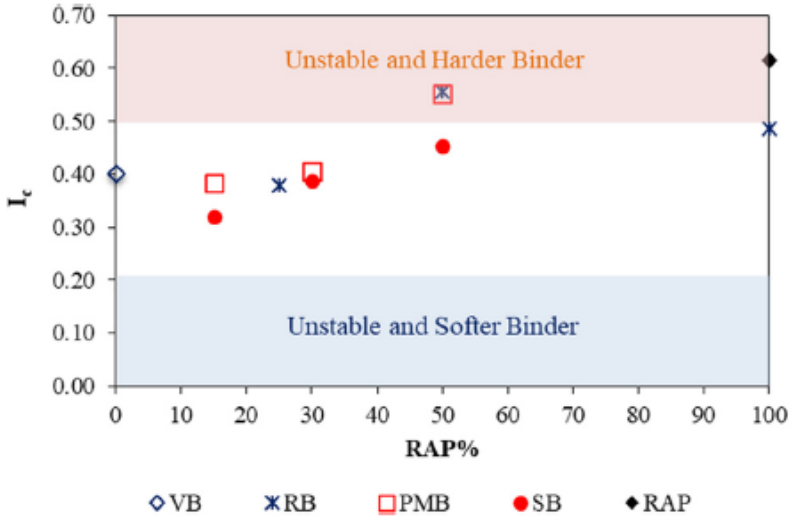

Figure 2-3 I_C versus RAP content for RAP binder, virgin binder (VB) and blends modified with soft binder (SB), rejuvenated binder (RB), polymer modified binder (PMB) (Mansourkhaki et al., 2020)

2.3.1.2 Heithaus Method

Based on Heithaus' theory (Heithaus, 1960), the binder compatibility is a function of the maltene solvent power and the asphaltene dispersion, which is generally measured by the Heithaus titration test or variations of the test (e.g., Asphaltene Flocculation Titration test). Asphalt compatibility is determined and evaluated from three calculated parameters that measure the state of peptization of an asphalt or asphalt blend.

Generally, asphaltenes are solid materials that precipitate when asphalt is treated with solvents such as n-pentane, n-hexane, n-heptane, etc. Maltenes are the components of asphalt not precipitated by n-alkane solvents. Asphaltenes are more aromatic than maltenes and contain more heteroatoms. Thus, intermolecular interactions are more extensive in asphaltenes than in maltenes. This is reflected in the greater molecular weights of asphaltenes than maltenes (Koots et al., 1975). In the colloidal model of asphalt structure, asphaltenes are believed to correspond to the dispersed materials and maltenes to the solvent. Therefore, asphaltenes will be mainly responsible for the internal structure of asphalt and will dominate many physical properties (Boduszynski et al., 1981). Thus, the amount of asphaltenes in asphalt is a rough measure of compatibility. Compatible asphalts generally have smaller amounts of asphaltenes than incompatible asphalts. Oxidative aging of asphalt will decrease compatibility by the

formation of polar molecules, which cause increasing associations and result in more asphaltenes. The ease with which asphaltenes are dispersed is highly dependent on the dispersing power of maltenes, which is also a very important contributing factor to asphalt compatibility. The best-known measurement of the compatibility of asphalt that considers all the above factors is the Heithaus method.

Three important parameters can be calculated and directly used from the Heithaus tests to evaluate the compatibility of asphalt binders, as shown in Equations 2.4-2.6. The parameter P_a is a measure of the peptizability of asphaltenes. The parameter P_0, is a measure of the peptizing power of the maltenes, and the parameter P, derived from P_a and P_0. values, is a measure of the overall state of peptization of the asphalt or asphalt blend.

$$P_a = 1 - FR_{max} \tag{2.4}$$

$$P_0 = FR_{max}(C_{min}^{-1} - 1) \tag{2.5}$$

$$P = \frac{P_0}{1-P_a} \tag{2.6}$$

where *FR* is the flocculation ratio and *C* is the concentration; both can be directly measured from the Heithaus tests (Heithaus, 1960; Boduszynski et al., 1981).

2.3.1.3 Fourier-Transform Infrared (FTIR) Spectrometer

A Fourier-transform infrared spectrometer emits infrared photons at the sample. These photons can be absorbed by the sample, exciting parts of the molecule to vibrate or rotate. Different molecules absorb different wavelengths of photons depending on their structure and the types of bonds and functional groups in the molecule. Thus, the infrared peak intensities measured from FTIR analysis have been widely used for identifying and characterizing important elements and functional groups in asphalt, as well as for studying the structure of binder samples (Pieri et al., 1996; Kudva et al., 1998; Bahia et al., 2001; Lima et al., 2004; Pasandín et al., 2015).

FTIR is an effective tool for evaluating the compatibility of complex binder blends, such as modified asphalt binder, virgin binder mixed with RAP, as well as rejuvenated asphalt binders (Lamontagne et al., 2001; Gulmine et al., 2002; Polacco et al., 2004; Canto et al., 2006; Pasandín et al., 2015). For example, in the study conducted by Lamontagne et al. (2001), through testing every point of the sample and considering the specific absorption peaks (965 cm^{-1}) of the Styrene-Butadiene-Styrene (SBS) polymer, the modified asphalt can be mapped as shown in **Figure 2-4**. This kind of microscopic map (will be discussed in section 2.3.2) can be used to evaluate the blending sufficiency and study the compatibility of complex binder blends. A similar method was used by Bowers (2014) to characterize the combability between the virgin binder and the RAP material.

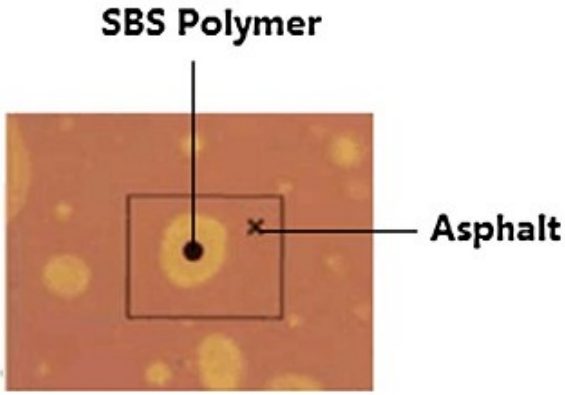

Figure 2-4 Mapping of SBS modified asphalt (Lamontagne et al., 2001)

The efficiency of diffusion between rejuvenator and binder including the new binder and aged/recycled binder is a key factor to produce high quality recycled asphalt materials, and the diffusion mechanism is complex and related to multiple factors (e.g., moisture content, mixing and compaction temperature). Oliver et al. (1974) and Karlsson et al. (2003&2007) have conducted laboratory experiments using FTIR to study the asphalt rejuvenator diffusion in the RAP binder. The results showed that FTIR was suitable for analyzing the diffusion process (Karlsson et al., 2003). In addition, the methyl-methylene stretch absorption bands as well as the carbonyl stretch bands were found as potential indices to characterize the rejuvenator's diffusion degree in asphalt (Karlsson et al., 2003).

Finally, FTIR has also been extensively used to evaluate the aging effect on virgin binders (Lu et al., 2002; Liu et al., 2014; Qin et al., 2014; Yang et al., 2015; Soenen et al., 2016) and complex binder blends, including SBS modified binders (Lu et al., 1998; Cortizo et al., 2004; Ma et al., 2012), crumb rubber modified asphalt (Huang et al., 2008; Yani et al., 2013; Ning-Li et al., 2015; Yu et al., 2015), asphalt modified by warm mix asphalt (WMA) additives (Trujillo et al., 2011; Xiao et al., 2013), anti-ultraviolet modified asphalt (Kuang et al., 2014; Liu et al., 2015; Zhang et al., 2015), etc. Among these studies, in terms of the change of binder compatibility with aging, Mouillet et al. (2008) found that that the aging process accelerated the degradation of SBS polymer and resulted in a better compatibility between these two phases (binder and modifier) by evaluating the FTIR mapping results of the SBS modified asphalt.

2.3.1.4 X-Ray Fluorescence (XRF)

X-Ray Fluorescence is a simple and widely accepted technique for the quantitative analysis of elements, typically from Sodium to Uranium in the Periodic Table. An energy-dispersive X-ray fluorescence analyzer emits high energy (40 keV) X-ray photons at a sample and measures the energy of the fluorescent photons emitted by the sample (Hesp and Shurvell, 2010). Because samples contain different elements in different proportions, their spectra are different. The XRF technique has been used by many studies in the asphalt field to identify and detect the composition of binders (Shastry et al., 2015; Barborak et al., 2016; Arnold, 2017). **Figure 2-5** below shows an example of using XRF to detect the amount of recycled engine oil bottoms (REOB) (estimated from the zinc and molybdenum peak heights in the XRF spectrum) within different binder samples.

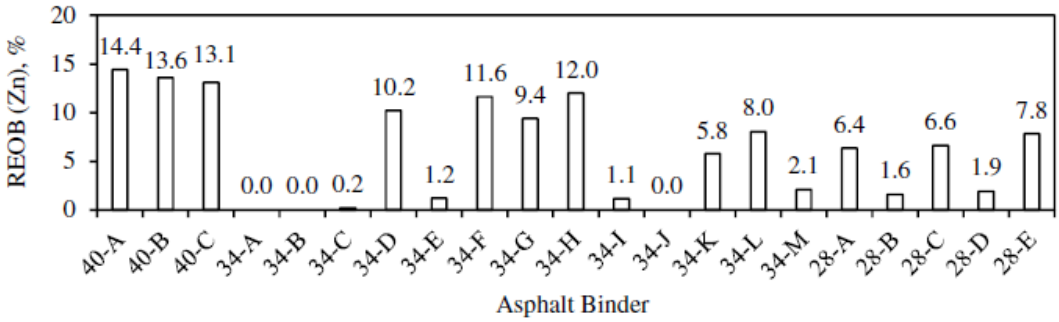

Figure 2-5 REOB contents in samples using X-ray fluorescence spectra (Hesp and Shurvell, 2010)

The XRF is useful to determine the presence of certain elements to help fingerprint the sources of various binders/RAP/rejuvenators that are sampled from different locations/projects in this proposed study, especially when the binders from different resources are blended for the purpose of evaluating the compatibility of the complex blends.

2.3.1.5 Nuclear Magnetic Resonance (NMR)

Nuclear magnetic resonance involves emitting radio waves at a sample to cause a change in the alignment of nuclei with respect to an applied magnetic field. The signal varies slightly depending on the other atoms and bonds surrounding the NMR active nucleus, which affect the local magnetic field. Results are measured relative to a standard in parts per million (ppm); this measurement is called chemical shift (Paliukaitė et al. 2017). For a binder sample that contains specific elements or organic molecules, the protons in these molecules have different bonds and nuclei surrounding them, and thus will have different chemical shifts as measured by NMR. An example result from NMR analysis within the asphalt materials field is shown in **Figure 2-6**; the difference in the spectra is believed to come from polyisobutylene (PIB), a common additive in engine oil.

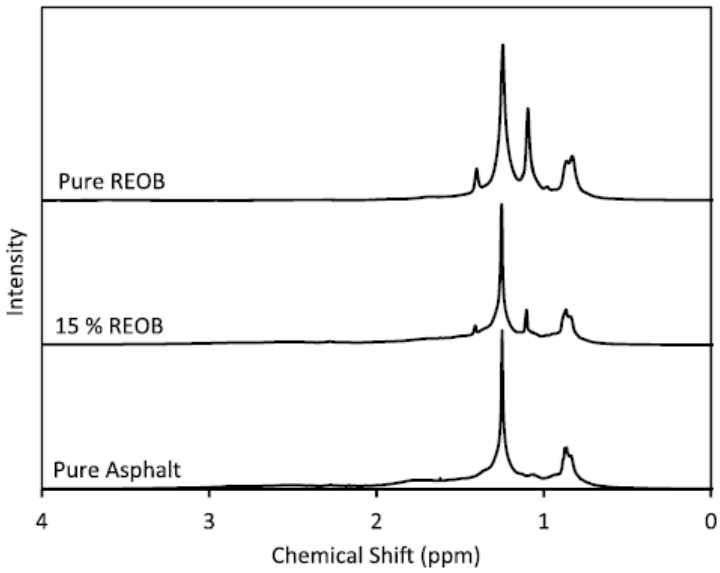

Figure 2-6 NMR spectra of REOB, virgin asphalt, and a mixture of REOB and virgin asphalt (Paliukaitė et al. 2017)

The NMR technique has been widely employed for analyzing asphalt binders, such as evaluation of the aging effect (Menapace et al., 2015), impact of modifiers (Miknis et al., 1998) and rejuvenators (Menapace et al., 2018) on virgin binder properties. For assessing binder compatibility, the NMR analysis could be of help since it may determine the presence of certain elements to help fingerprint various binder sources, evaluate the blended binders containing polymers and rejuvenators, and study the property changes with aging.

2.3.1.6 Inductively Coupled Plasma Atomic Emission Spectroscopy (ICP-AES)

Inductively coupled plasma atomic emission spectroscopy involves using a nebulizer to spray the sample into an argon plasma as a mist, where the atoms in the sample are excited. When the atoms return to a ground state, they emit photons. Each element has its own characteristic radiation signature, and thus it emits photons at unique wavelengths. This radiation is measured by a detector and can be used to determine the concentrations of each element in the sample. ICP-AES analysis has been used in asphalt materials field to primarily identify and track the sources of various binder, RAP and rejuvenators for evaluation of the binder blends (Zhou et al., 2013; Kaskow et al., 2018).

2.3.2 Morphology Analysis (Microscopy Technique)

With the progress of research and development of microscopy technology, many techniques have been applied to the microscopic study of asphalt binders, including ultraviolet, infrared and fluorescence microscopy, scanning electron microscopy (SEM), atomic force microscopy (AFM) and so on. In contrast to other technologies, the microscopic technique is instrumental in the observation and quantitative analysis of the asphalt microscale morphology which plays a significant role in properties of binder blends, including compatibility, because of its high resolution and ability to obtain nanomechanical properties (Spadafora et al., 1985; Wang et al., 2014&2015; Liang et al., 2018).

Ultraviolet (UV) microscopy is a type of light microscopy that utilizes UV light to generate a magnified image of the sample being analyzed. While Infrared (IR) microscopy, also known as infrared microspectroscopy, is a type of light microscopy that uses a source that transmits infrared wavelengths of light to view an image of the sample. Fluorescence microscopy is an optical microscopy that uses the emission of fluorescence to study properties of organic or inorganic substances. AFM is an advanced surface structure technology developed based on scanning tunneling microscopy (STM). AFM can obtain surface topography by the interaction between probes and samples of the tested material. AFM can measure both topography and nanomechanical properties of the given binder samples.

Fig. 2-7 presents an example of using fluorescence micrographs to evaluate the compatibility of complex binder blends – asphalt with different percentages of ground tire rubber (GTR) and recycled polyethylene (RPE), and SBS modified asphalt. It can be clearly seen that the ratio of GTR to RPE has an influence on the dispersion state of modifier in asphalt. Three phases are shown in the micrographs. The light area is the RPE phase and black stains represent rubber domains. In the case of low ratio of GTR to RPE, large and irregular shaped RPE phase enveloping GTR particle disperses in the continuous asphalt phase (yellow background). The coarse RPE phase works like aggregate particle and the interface

boundary is clear, which means that the compatibility among RPE, GTR and asphalt are not good. As the ratio of GTR/RPE increases, a more homogeneous dispersion of modifier is presented in micrographs. The size of RPE phases decreases significantly and the rubber phase is not obvious. Also, the interface boundary between modifier and asphalt becomes less remarkable. The degree of dispersion for modifier is enhanced with increase of ratio of GTR/RPE, which indicates the improvement in compatibility (Wang et al., 2014&2015; Ge et al., 2016). In addition, SBS in this study has a fine dispersion in modified asphalt (**Fig. 2-7e**), which indicates good compatibility. Overall, in terms of morphology, high ratio of GTR/RPE seems to be more ideal, which morphology more similar to SBS indicating the compatibility of different phases.

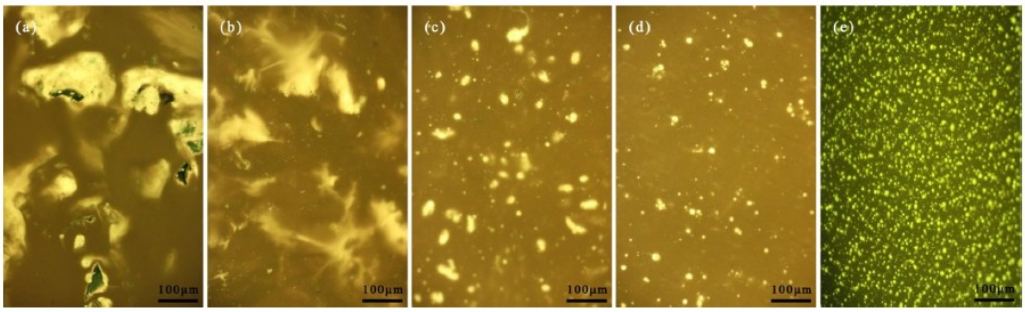

Figure 2-7 Morphological properties of asphalt with the ratio of GTR to RPE equaling (a) 5:5, (b) 6:4, (c) 7:3, (d) 8:2, and (e) SBS modified asphalt (Liang et al., 2020)

2.3.3 Thermal Analysis

As the causal mechanisms of compatibility are postulated to be related to the intermolecular interactions and associations, it becomes critical to be able to evaluate such behavior in the natural state of asphalt. Use of solvents can affect and modify the molecular association, therefore confounding results of compatibility analysis carried out using analytical methods (discussed in section 2.3.1) that study asphalt in solution. Therefore, thermal analysis methods overcoming the problem listed above have shown promise as a means of investigating binder properties, including compatibility (Kriz, et. al., 2008).

2.3.3.1 Differential Scanning Calorimetry (DSC)

Differential scanning calorimetry (DSC) is the most widely used approach to determine the enthalpy related transitions of asphalt binders (Harrison et. al., 1992; Planche et. al., 1998) and of polymeric materials (Yousefi et. al., 1997). DSC monitors the endothermic or exothermic heat flow of a sample under a controlled temperature program, considering that the heat generation and its rate is proportional to the reaction rate when crosslinking polymers are studied (DiBenedetto et al., 1987) and to thermal events, such as glass transition (Kamal et al., 1973).

DSC analyses have been used successfully to evaluate the glass transition temperature (Tg) of asphalt binders and of different origins as well as the effect of various asphaltic fractions (Claudy et. al., 1991&1992; Jimenez-Mateos et. al., 1996), modifiers (Turner et. al., 1997; Qin et. al., 2014; Adams et.

al., 2019; Apostolidis, et. al., 2019) and rejuvenators (Lei et. al., 2015; Elkashef et. al., 2019) on their glass temperature region. The Tg can be used to interpret thermal-related defects in asphalt pavements, such as thermal cracking. For instance, binders with high Tg accumulate less thermal stress build-up under a given thermal history and thus are more resistant to low temperature cracking. In addition, the glass transition region as well as Tg has shown potential to be used to evaluate the binder compatibility.

Figure 2-8 shows the glass temperature regions for three binder samples (a, b, and c) (Kriz et al., 2008). Clearly, as compared to the two incompatible binders a and b, compatible binder c shows no separate glass transition outside the main glass transition. **Figure 2-9** shows the clear difference in transition behavior for an incompatible (AC #2 with multiple transitions) and a compatible bitumen (AC #1 with a single transition), as well as the impact of subsequent aging. A study conducted by Apostolidis et. al. (2019) also showed that incompatible binders typically result in high Tg temperatures. In polymer modified binders, the compatibility of a certain polymeric formulation to asphalt binder is affected negatively when a binder has high asphaltene content. Improvement of polymer-asphalt binder miscibility (compatibility) is reached when the aromaticity of maltenes decreased to certain values (Laval et al., 2017).

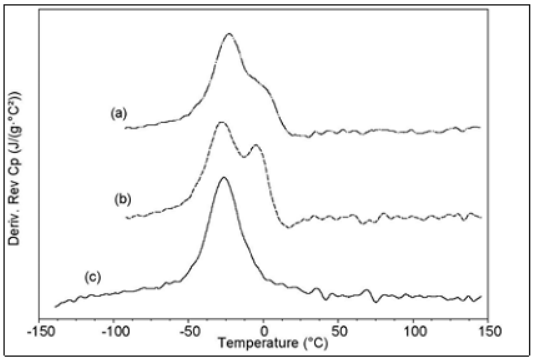

Figure 2-8 Glass transition regions of different binder samples (Kriz et al., 2008)

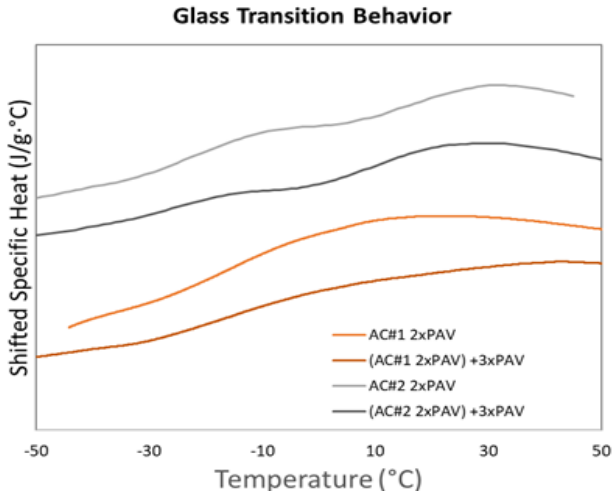

Figure 2-9 Impact of aging on compatible (AC#1) and incompatible (AC#2) bitumen, measured by the proposers (Cargill).

In addition to the glass transition region/temperature, the crystalized fraction (wax crystallization/ precipitation) C(T) can be calculated from the DSC measurement and has been used to evaluate the compatibility of asphalt binders. Waxy constituents of binders are significant contributors to their temperature sensitivity. At only a few percent by weight, waxes significantly lower viscosity when molten but solidify (gel) the binder when crystalline at cold temperatures (Thomas et al., 1933; Le Guern et al., 2010; Polacco et al., 2012; Rebelo et al., 2014). Higher contents of solid wax in asphalt binder usually contribute to poor performance of the asphalt pavement. Crystallized wax in the asphalt binder generally promotes phase separation (incompatibility) (Traxler et al., 1952; Romberg et al., 1959; Hesp et al., 2007; Schmets et al., 2010), which can directly lead to lower cracking resistance (Redelius et al., 2015; Nahar et al., 2016). Further, wax acts as a flocculant for the asphaltenes that are dispersed in the maltenes, so the colloidal system is easily destabilized at cold temperatures, and/or in old age when asphaltene contents increase (Thomas et al., 1933; Rebelo et al., 2014; Le Guern et al., 2010).

Several researchers have used the Ozawa exponent (n) calculated from the Ozawa function (theory) (by fitting the heat flow curves measured from DSC) that is typically used to analyze the non-isothermal kinetics for crystallizing systems, to evaluate the compatibility of asphalt binders. Generally, smaller values of n indicated slower rates of hardening through crystallization, and the binder sample is believed to have good compatibility and is expected to show better thermal cracking performance, and vice versa. **Figure 2-10** below shows a consistent trend between the Ozawa exponent n and the measured thermal cracking on the top of asphalt pavement in different sections.

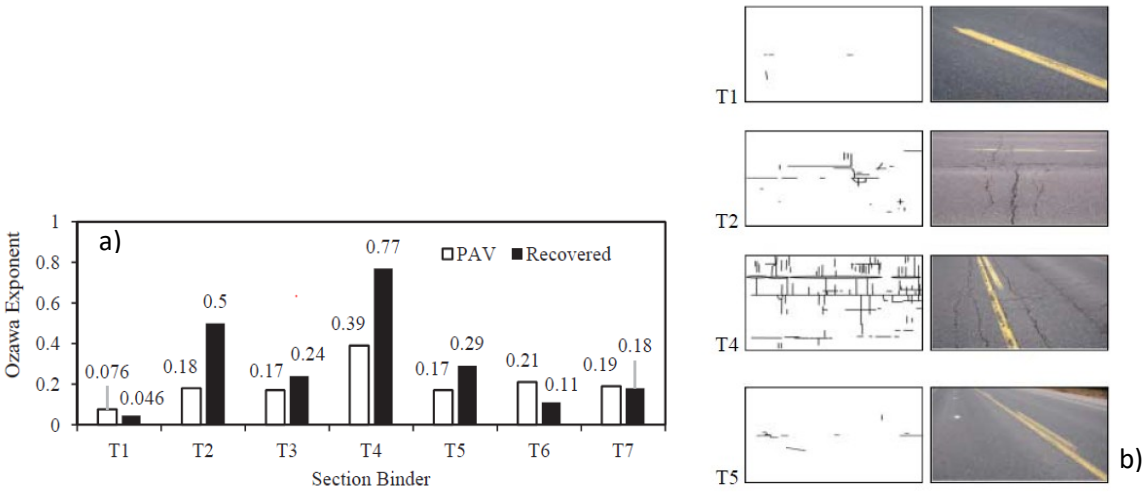

Figure 2-10 (a) Ozawa DSC exponents determined on PAV residues and recovered asphalt samples; (b) crack maps and photographs for corresponding sections (Rigg et al., 2017)

In summary, DSC measurement together with the corresponding output parameters have been shown to be a powerful tool to evaluate binder compatibility.

2.3.3.2 Frequency and Temperature Sweep Test by Dynamic Shear Rheometer (DSR) with a 4mm plate

The thermal properties of asphalt binders can also be measured using a Dynamic Shear Rheometer (DSR) with a 4-mm plate (Glaser et al., 2015). This test covers a wide range of temperatures (-36 °C to 36 °C, usually in 3-degree increments), and frequencies (15 frequencies from 100 rad/sec to 0.2 rad/sec), by using the appropriate strain level at each combination of test temperature and frequency. The isotherm tests are conducted from the coldest to the warmest temperature and from the highest to the lowest frequencies.

The transition temperatures (Tg, viscoelastic (crossover) transition temperature (T_t), and the intermediate region temperature range (ΔT_{IR})) can be measured from the 4mm DSR test and have correlated well with the measurements from DSC method (Elwardany at el., 2019). These three temperatures are typically calculated from the storage and loss modulus master curves in the temperature domain with a frequency of 10 rad/s or 1.59 Hz (as shown in **Figure 2-11**). The T_t is the temperature where loss modulus is equal to storage modulus in between the intermediate and terminal region (this temperature is close to the point of gelation, thus can be potentially used to evaluate the compatibility of different binders). The ΔT_{IR} is the difference between the viscoelastic temperature and the glassy transition temperature, indicating the "length" of the intermediate "transition" region.

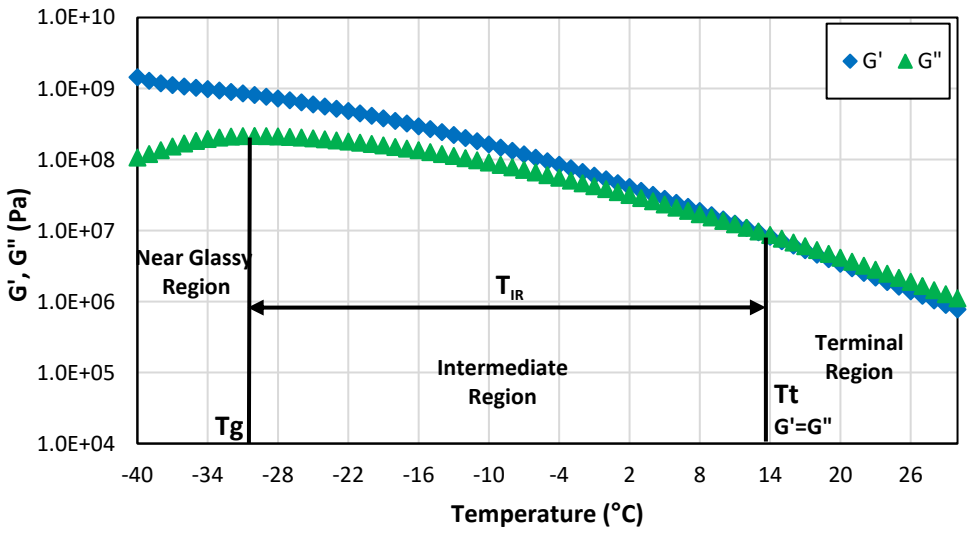

Figure 2-11 Tg, T_t, and T_{IR} in G' and G" master curve (temperature domain)

2.3.4 Binder Performance Tests

In addition to the analytical methods, morphology techniques and thermal analysis methods, there are also many binder performance tests that can be employed to evaluate the compatibility of different binder samples.

2.3.4.1 Traditional Tests in Superpave Specification

Common parameters and criteria that are directly measured from the traditional binder tests in the Superpave specification have often been employed for assessing binder compatibilities. These include the ΔT_c parameter (defined as the difference in critical temperature for the creep stiffness (S) and relaxation rate (m-value) passing values from bending beam rheometer (BBR) test), indices from Black space diagrams which are two dimensional representations of dynamic modulus and phase angle of viscoelastic materials measured from temperatures and frequencies sweep tests performed on the DSR (e.g., the binder Glover-Rowe (G-R) parameter), and mastercurve shape parameters (such as R-value, the difference between the glassy modulus and equilibrium modulus in logarithmic scale). The advantages of employing these parameters are: (1) They have been extensively used in recent decades and are valuable tools for characterizing binder properties; (2) Studies have established threshold values for these parameters through field validations (e.g., ΔT_c = -2.5 °C is typically used as a crack warning limit and ΔT_c = -5.0 °C as the cracking limit; G-R = 180 kPa is proposed as a crack warning limit, G-R = 600 kPa for the development of significant cracking), thus, it is simpler and more convenient for researchers and agencies to evaluate the different asphalt materials in a "pass" or "fail" manner.

Black space diagrams can be used to characterize asphalt binders as either rheologically simple or complex. Rheologically simple binders (with the more sol-type or compatible structure) exhibit a single-phase system over the temperature and time domains studied whereas rheologically complex binders (with the more gel-type or incompatible structure) typically exhibit two or more phase systems. This implies that at varying temperatures, a rheologically simple binder would show continuity in the progression of curves of logG* versus phase angle. On the other hand, a complex binder would show significant discontinuity due to phase separation. **Figure 2-12** below shows an example comparing a compatible binder with an incompatible binder by using the Black space diagram (logG* versus phase angle plot). The rheologically complex behavior as shown in **Figure 2-12(b)** could be explained by the occurrence of phase separation (incompatibility) at high temperatures where the RAF with 20% RAP and 2% oxidized polyethylene wax changes from a sol-type material to a predominant gel-type material. A sol is defined as a largely Newtonian liquid with little or no elasticity, delayed elasticity, or non-linearity whereas a gel is defined as a material with significant non-linear behavior. Gels are less able to flow at ambient and warmer temperatures compared to sols and therefore produce asphalt binders that are more prone to thermal and fatigue cracking distress.

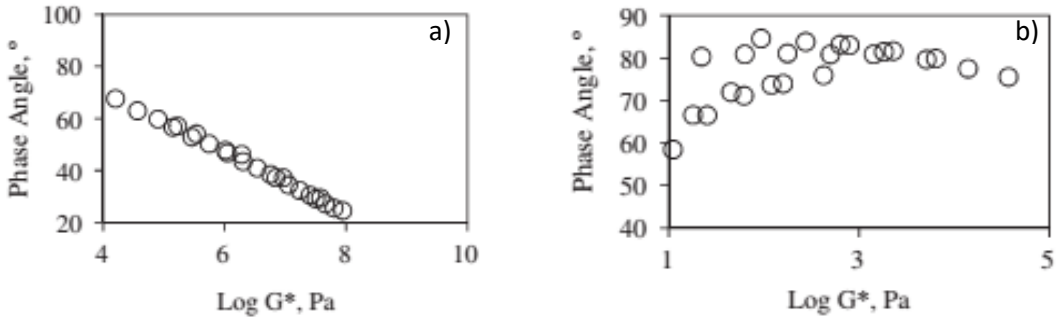

Figure 2-12 Black space diagram for (a) base binder with RAF + 20%, RAP + 1%, and siloxane; (b) base binder with RAF + 20%, RAP + 2%, and oxidized polyethylene wax (RAF is the roofing asphalt flux) (Omari et al., 2016)

Even though these parameters described above have been used for characterization of binder properties including the compatibility, there are also many existing concerns for using these traditional methods in the Superpave system for characterizing the compatibility or incompatibility for today's complex binder blends: (1) these parameters and criteria have been demonstrated only as empirical circumstantial evidence of compatibilities, not direct measurements of asphaltene association, compatibilization, and sol/gel morphology; (2) current accepted limits for existing indirect compatibility tests are based on limited historical datasets, yet are being considered for many different regions and diverse binder sources today (Roberts et al., 1977; Anderson, et. al., 2011); (3) the Superpave system was developed based on a number of assumptions and simplifications that have since proven to be serious limitations (Hesp et al., 2014) and the asphalt supply chain has continued to evolve with increasing amounts of recycled materials and use of various innovative materials; (4) the traditional tests in the Superpave specification are mainly designed to measure the materials' behavior within relatively low strain levels, therefore, they do not capture the whole picture of how the materials behave under the complicated traffic and climatic loading conditions today. Because of the limitations listed above, many other more fundamental and advanced binder tests (discussed in the sections below) have been developed in recent years for characterizing today's complex binder blends.

2.3.4.2 Extended Bending Beam Rheometer (EBBR)

Over the past 10 years, significant research has shown that physical hardening is able to explain vast performance differences considering the material design, climate, and aging conditions (Hesp et al., 2007&2009; Erskine, et. al., 2012). The EBBR protocol is thus specifically designed to assess a binder's tendency to physically harden during conditioning. The test procedure conditions samples for one, 24 and 72 h at T_d + 10 and T_d + 20, where T_d is the temperature of the pavement design before pass/fail testing. The continuous grade is obtained as the warmest of all temperatures measured for the two conditioning temperatures and three conditioning times. The grade loss from the one-hour result at T_d + 10 (roughly equal to the AASHTO M320 grade) is calculated and serves as a measure of durability. A 6 °C loss in low temperature grade reduces the chance that no damage occurs in any given winter from the intended 98% to around 50% reliability. A 12 °C loss reduces this to less than 10%. The low temperature grade and the grade loss after 72 hours of conditioning measured from EBBR test have been shown to

correlate well with the long−term pavement performance (Hesp et al., 2007&2009; Erskine et. al., 2012; Johnson et al., 2014).

Figure 2-13 shows an example of using the EBBR test to evaluate the compatibility of binder samples. As shown in figure below, the grade losses in AAK, ABG, and CL (high asphaltene binders as compared with other) are significantly higher when waste engine oil (WEO) is added, compared with straight material, indicating the incompatibility of these three modified binder samples, which can be attributed to the fact that these modified binders are more gelled than unmodified ones.

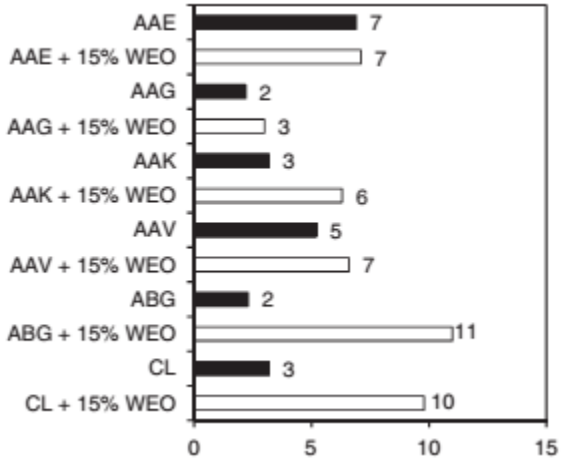

Figure 2-13 Three-day grade loss (degree) (Johnson et al., 2014)

In addition, recent research has shown that the limiting phase angle temperature T (30) (when measured phase angle is equal to 30), as measured with a regular DSR temperature sweep protocol with 15 min conditioning steps, provides a very high degree of correlation with the limiting extended BBR temperature after three days of cold conditioning (R^2 = 0.90–0.96) (Angius et al., 2018; Ding et al., 2017&2018). This suggests that the measurement of phase angle, at temperatures around the freeze–thaw transition (around 10 °C) and after much shorter conditioning, can provide an equally accurate limiting low temperature grade to the extended BBR protocol (Rigg et al., 2017), thus, can be used as a parameter for evaluation of binder while considering the physical hardening process.

2.3.4.3 Double-edge-notched Tension (DENT) Test

DENT test is designed to model ductility of asphalt material in a more fundamental and refined framework. The DENT test is created to control fatigue-type cracking distress (Andriescu et al., 2004&2009). It is based on a fundamental essential work of ductile failure (EWF) analysis by Cotterell and Reddel (1977). The DENT test is conducted at a relatively fast rate of 50 mm/min and moderate temperature of 15 °C to speed up the analysis. These conditions were chosen to mimic significantly slower speeds at lower temperatures around the freeze–thaw regime, where significant cracking is believed to occur. The test is typically conducted on three DENT specimens with varying notch depths, providing ligaments of 5, 10 and 15 mm. The most important output parameter from the DENT test is the crack tip opening displacement (CTOD). The CTOD is the amount by which a tiny fibre (fibril) of

asphalt cement can be stretched under severe constraint in the ductile state until it fails. A higher CTOD allows the pavement to flex more under traffic and therefore provide better resistance to fatigue cracking.

Figure 2-14 shows an example of using CTOD measured from the DENT test to evaluate the potential incompatibility of binder samples. As shown in the figure, binders 5% SBS D1192 and 3% SBS D1192+8% REOB initially have high CTOD values, however, after adding 20% RAP, the CTOD value significantly decreases. One of the potential reasons provided by the researchers is that this significant deterioration of failure properties can be attributed to the incompatibility between the SBS, and the RAP used in this study.

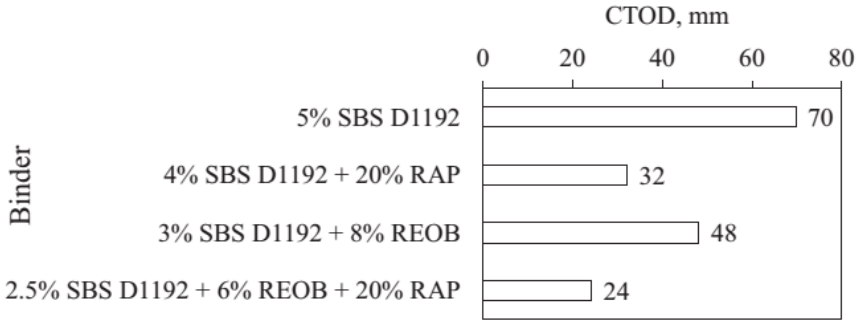

Figure 2-14 Measured CTOD (Paliukaite et al., 2016)

2.3.4.4 Linear Amplitude Sweep (LAS) Test

The LAS test evaluates the ability of asphalt binder to resist fatigue damage. Studies (Zhou et al., 2012; Clopotel et al., 2012) have shown that the LAS test is an effective test method to evaluate binder fatigue properties and has been shown to correlate fairly well with the Long-Term Pavement Performance (LTPP) field fatigue cracking data (Hintz et al., 2011). Zhang et al. (2020) recently developed new parameters from the LAS test to better evaluate the fatigue properties of asphalt binders by incorporating the effect of aging and polymer modifiers on binder properties. These parameters include the Average Reduction in Integrity up to Failure (I^R), Stain Tolerance up to Failure (ε_T) and Strain Energy Tolerance (E_f). The I^R parameter was developed based on the Viscoelastic Continuum Damage (VECD) principle for characterizing materials' behavior under the repeated loading condition, while the ε_T and E_f parameters were developed from the stress versus strain curve during the test for more appropriately evaluation of the effect of additives on binder behavior under the loading conditions. Thus, the LAS test and the corresponding parameters would be applicable for this project to evaluate the complex binder blends.

2.3.4.5 Multiple Stress Creep Recovery (MSCR) Test

The Multiple Stress Creep Recovery (MSCR) test is the latest improvement to the Superpave Performance Grade (PG) Asphalt Binder specification - providing a new high temperature binder specification that more accurately indicates the rutting performance of the asphalt binder and is blind to

modification. A major benefit of the new MSCR test is that it eliminates the need to run tests such as elastic recovery, toughness and tenacity, and force ductility, procedures designed specifically to indicate polymer modification of asphalt binders. A single MSCR test can provide information on both performance and formulation of the asphalt binder. Thus, this method could be included in this project for evaluation of the various binder blends.

There are two important parameters that are generally measured from the MSCR test: the non-recoverable creep compliance (J_{nr}) and MSCR %recovery. The J_{nr} is a measure of the amount of residual strain left in the specimen after repeated creep and recovery, relative to the amount of stress applied. The MSCR %recovery is a measure of how much the sample returns to its previous shape after being repeatedly stretched and relaxed. In recent years, this test has been shown to be an effective tool to capture the field rutting performance of the materials (Anderson et al., 2010; Horan et al., 2011; Zelelew et al., 2011; Morea et al., 2012).

2.4 CURRENT METHODS AND PRACTICES FOR EVALUATION OF COMPATIBILITY (IN FIELDS OF ORGANIC CHEMISTRY AND POLYMER SCIENCE)

This chapter summarizes the common tools and methods for characterization of the compatibility between the different components/phases for a given sample in the fields of organic chemistry and polymer science.

2.4.1 Chromatography Analysis

Chromatography is a laboratory technique for the separation of a mixture. There are two popular methods including the Size Exclusion Chromatography (SEC) and High-Performance Liquid Chromatography (HPLC) (polymer) in the field of chemistry. SEC is also called gel-filtration or gel-permeation chromatography. This method uses porous particles to separate molecules of different sizes. It is generally used to separate biological molecules and to determine molecular weights and molecular weight distributions of polymers, and the separation of molecules which is also called fractionation. It is usually applied to large molecules or macromolecular complexes such as proteins and industrial polymers.
HPLC is a technique in analytical chemistry used to separate, identify, and quantify each component in a mixture. It relies on pumps to pass a pressurized liquid solvent containing the sample mixture through a column filled with a solid adsorbent material. HPLC has also been used for separating the components of a complex biological sample or of similar synthetic chemicals from each other.

Figure 2-15 shows an example archetypal elution curve measured by the SEC technique to evaluate the sample compatibility from the study conducted by Grieshaber et al. (2009). Grieshaber et al. (2009) used the SEC as one characterization technique to confirm the formation of the multiblock product. They synthesized elastin-mimetic hybrid polymers (EMHPs) containing flexible synthetic segments based on polyethylene glycol (PEG) alternating with alanine-rich, lysine-containing peptides and monitored the

change in molecular weight from the starting materials to the hybrid product by SEC technique. According to the SEC analysis data, the resulting hybrid polymers contain PEG and peptide alternating along the polymer backbone, with an estimated molecular weight (Mw) of 34 kg/mol and a polydispersity index of 4.3. It needs to be mentioned that the polydispersity index is an important parameter to explain the size distribution in a sample or agglomeration or aggregation of the sample during analysis (Gilar et. al., 2005; Buszewski et. al., 2012; Kartsova et. al., 2019) which can be used to indicate the sample compatibility.

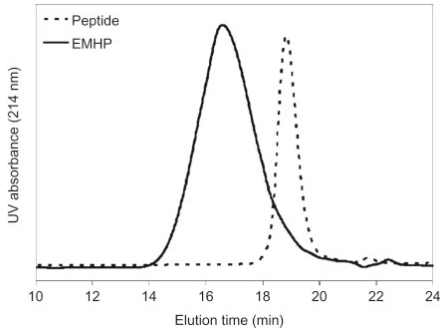

Figure 2-15 SEC analyses of the peptide and elastin-mimetic hybrid polymers (EMHP) (Grieshaber et al., 2009)

Chromatography is one of the most commonly used methods in the analysis of size distribution and structure of polymers and biomass, therefore, its applicability for analyzing the molecular sizes and their distribution in binder blends is promising, especially those with RAP, rejuvenators, as well as polymer modifiers.

2.4.2 Thermal Analysis

The DSC discussed in section 2.3 is also the most widely used instrument to determine the enthalpy related transitions of polymeric materials. The heat flow curve, glassy transition temperature and the degree of crystallization are critical for evaluation of the compatibility of synthesized polymers as well. In addition to the DSC technique, thermogravimetric analysis is another popular method for characterizing the thermal behavior of polymeric materials. Thermogravimetry is a process of determining material weight with respect to a combination of temperature and time. Thermo-gravimetric Analysis (TGA) is a commonly used instrument based on this process to investigate thermal characteristics of a substance under heating environments (Das et al., 2019). Generally, two types of plots are available as a result. A plot of specimen weight against temperature (TGA curve) provides thermal decomposition temperatures with residue amount as a function of temperature. The second plot, a derivative of the TGA curve, indicates mass loss rate depending on an increase in temperature. These curves can also be used to derive other parameters, such as the kinetics of the reaction. Since the thermogravimetric analysis is a powerful technique for the measurement of the thermal stability and weight reduction of polymer composites and biomass, it is also expected to be able to assess the stability of binders under temperature changes, as well as various fractions within the bitumen in terms of volatility (volatilization spectra) which is an important factor that impacts the compatibility of the binders (Pauli et al., 1998&1999; Petersen, 2009). **Figure 2-16** shows an example of thermal-

decomposition curves measured using the TGA method. The two ethylene-propylene-diene rubber (EPDM) samples generally show a relatively flat curve as compared to the two fluororubber (FKM) ones, indicating higher thermal stability and less temperature susceptibility.

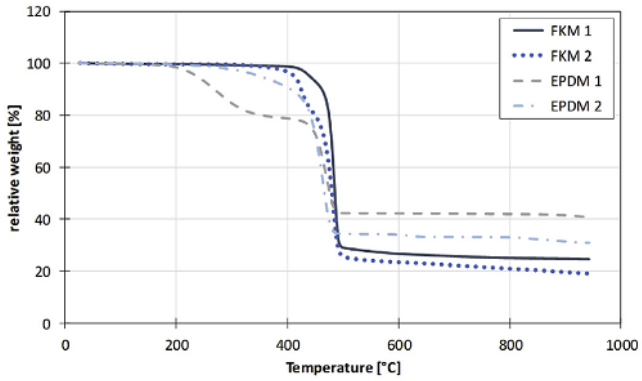

Figure 2-16 TGA-decomposition curves of ethylene-propylene-diene rubber (EPDM) and fluororubber (FKM) compositions (Eyerer et al., 2018)

2.4.3 Morphology Analysis (Microscopic Technique)

The microscopic techniques discussed in section 2.3 have also been widely used to determine microscale morphology of polymeric materials (Desbief et. al, 2012; Gutierrez et. al., 2014; Jafarzadeh et. al., 2014). **Figure 2-17** below shows an example of using the SEM to evaluate the compatibility of the study blends. Morphologies of the cryogenically fractured surfaces of the as-extruded and nanofibrillated poly (ε-caprolactone) (PCL) and poly (lactic acid) (PLA) blends with different PLA concentrations, 5–15% by weight (wt%), are shown**.** In the case of the as-extruded blends, as shown in **Figure 2-17**(a), (c), and (e), typical sea-island phase morphologies (phase separation) are observed with PLA spheres dispersed in the PCL matrix, indicating the low level of compatibility between the PCL and PLA phases in the as-extruded samples. This behavior is evidenced by the existence of gaps between the phases as well as the presence of many holes on the fractured surfaces of the blends which were caused by facile debonding between the PCL and the PLA during the fracture. Remarkably, for the nanofibrillation of the PCL/PLA blends (shown in **Figure 2-17**(b), (d), and (f)), the surfaces of the cryo-fractured NFCs, with PLA nanofibril contents of up to 15 wt%, show no signs of the dispersed PLA phase (smooth fracture surfaces). Such a dramatic change in the compounds' morphologies is ascribed to the achievement of an extraordinary level of compatibility between the PCL and PLA phases after nanofibrillation.

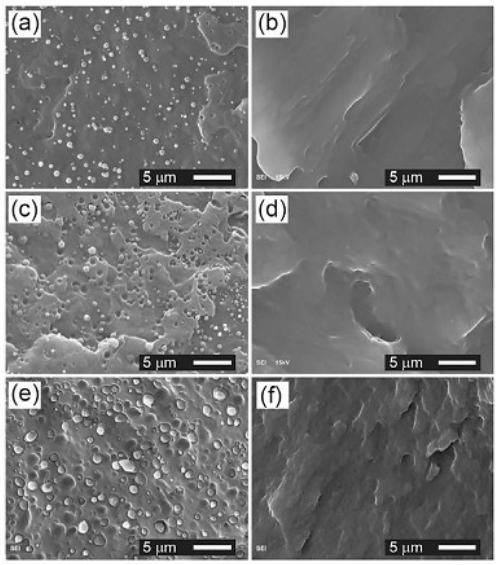

Figure 2-17 SEM micrographs of the cryo-fractured surfaces of PCL/PLA blends with 5 wt% (a and b), 10 wt% (c and d), and 15 wt% (e and f) of spherical (a, c, and e) and nanofibrillar (b, d, and f) PLA domains (Kakroodi et. al., 2018)

2.5 SUMMARY OF FINDINGS FROM LITERATURE

The summary of findings from literature review of available methods and tools for characterization of the binder blends and the compatibility between the different composition of the binder samples is presented in this chapter, in tabular form (**Table 2-1**) shown below. These methods are organized into four categories and their corresponding key outputs that can be used to evaluate the compatibility of binder samples are discussed in the table.

It needs to be noted that for study of the complex binder blends, coupling methods will become more affordable and usable, thus can be used to evaluate the compatibility of the blends appropriately and comprehensively from various perspectives. For example, analytical methods can provide researchers the fundamental information of the chemical composition of the binder blends, but requires the use of solvent, while the thermal analysis tools can provide transition behaviors and the change of sample structure with varying the temperatures, in the natural state of asphalt without use of solvent. This is important and has been considered by the research team when finalizing the testing plan (presented in section 2.6).

Table 2-1 Summary of different methods for evaluation of binder compatibility

Methods and tests		Corresponding key outputs from the testing
Analytical methods	SARA separation	Colloidal Indices (Asphaltene Index I_A; Gaestel Index I_C)
	Heithaus method	Measure of the peptizability: peptizability of the asphaltenes (Pa); peptizing power of the maltenes (P_0): overall state of peptization of the asphalt blend (P)
	Fourier-transform infrared (FTIR) spectrometer	Infrared peak intensities for identifying and characterizing the important elements and functional groups; FTIR map for evaluation of the microscale structure
	X-ray fluorescence (XRF)	Detect the specific elements or organic molecules in binder blends to help identify and track the binder source/RAP/Rejuvenator/Modifier
	Nuclear magnetic resonance (NMR)	
	Inductively coupled plasma atomic emission spectroscopy (ICP-AES)	
	Chromatography analysis (size exclusion chromatography (SEC) and high-performance liquid chromatography (HPLC)	Determine molecular weights and size distribution (agglomeration or aggregation of the sample)
Morphology analysis (microscopy technique)	Ultraviolet, infrared microscopy	Mapping the micro-structure; evaluate the blend effectiveness
	Fluorescence microscopy	
	Scanning electron microscopy (SEM)	
	Atomic force microscopy (AFM)	

Table continues the next page.

Table continued from previous page.

Methods and Tests		Corresponding Key Outputs from the Testing
Thermal analysis methods	Differential scanning calorimetry (DSC)	Measure of the glassy transition temperature (Tg); wax crystallization/ precipitation (C(t)); Ozawa exponent (n)
	Thermo-gravimetric analysis (TGA)	Thermal decomposition curves
	Frequency and temperature sweep test by dynamic shear rheometer (DSR) with a 4-mm plate	Transition Regions and Temperatures (glassy transition temperature (Tg); viscoelastic (crossover) transition temperature (T_t,); and the intermediate region temperature range (ΔT_{IR}))
Binder performance tests	Traditional tests in Superpave specification	ΔT_c parameter; Glover-Rowe parameter; R-value; Black space diagram etc.
	Extended bending beam rheometer (EBBR)	Low temperature grade and the grade loss after 72 hours of conditioning
	Double-edge-notched Tension (DENT) Test	Crack tip opening displacement (CTOD)
	Linear amplitude sweep (LAS) test	Average reduction in integrity up to failure (I^R), stain tolerance up to failure (ε_t) and strain energy tolerance (E_f)
	Multiple stress creep recovery (MSCR) test	Non-recoverable creep compliance (J_{nr}) and MSCR %recovery

2.6 MATERIAL SAMPLING AND TESTING PLAN

This section briefly presents and discusses the proposed sampling and testing plans as well as the overall structure for this project.

2.6.1 Material Selection Overview

Tables 2-2 and 2-3 below show the overall material matrix considered in the study. **Table 2-2** covers three core materials, and **Table 2-3** covers the eight validation materials.

Table 2-2 Information for core materials

Material Type	Material ID	Binder Grade	Source	Binder Content	Corresponding Field Section
Binder	A	PG 58-28	Minnesota	--	MnROAD/NRRA
	B	PG 64-22	Alabama	--	NCAT
	C	PG 64-22	Wisconsin	--	Wisconsin
RAP	1	PG 103-5	Minnesota	3.9%	MnROAD/NRRA
	2	PG 104-6	Alabama	4.5%	NCAT
	3	PG 87-26	Texas	3.8%	Field Section for RAP in Texas

Table 2-3 Information for validation materials

Material Group	Mixture ID	Base Binders	Binder Sources	RAP Source	Corresponding Field Section/Pavement Built
Validation	MO-VL	PG 46-34	Missouri	Missouri	Route T, St. Charles County
	IL-VL	PG 58-28	Illinois	Illinois	Field Section Location is not disclosed by IDOT District-1 (Chicago)
	VA-VL	PG 58-28	Virginia	Virginia	Rt. 903, Richmond District
	MN-VL	PG 58-28	Minnesota	Minnesota	MnROAD Test Cell
	NCAT30-VL	PG 64-22	Alabama	Alabama	NCAT Test Section
	NCAT45-VL	PG 64-22	Alabama	Alabama	NCAT Test Section
	TX10-VL	PG 70-22	Texas	Texas	State Highway 71, Yoakum District
	TX30-VL	PG 64-22	Texas	Texas	State Highway 71, Yoakum District

For core materials, asphalt binder performance modifiers (such as polymer modification) are not included. Instead, modifiers are considered to increase the material base evaluated in this project via the validation materials. The core materials are primarily used to evaluate the compatibility and incompatibility between the binders (different sources), RAP (sources and dosages), and the rejuvenator additives (sources).

Since the focus of this research is on compatibility between various asphalts, the core experiment mixture testing is focused on the use of a single aggregate skeleton, the one used in core mix A. The lab-produced asphalt mixtures for all three core group materials are manufactured using a fractional

factorial design to generate additional mixtures (in addition to proportions similar to their actual plant-produced counterparts) and binder blends for evaluation purposes. The binder sources and RAP content are also varied when designing the mixtures, while keeping the aggregate source (from A) and gradation (the gradation of the plant-produced A mixture) the same for all the mixtures that are generated. This resulted in a wider core material base and proved to be critical to evaluate how the compatibility would change with the change of component sources and dosages. For the eight validation materials, the plant-produced mixtures are directly sampled.

2.6.2 Test Method Selection

Based on the discussions between the research team and the TAP, as well as the important findings from the literature review, selection of test methods for evaluation of compatibility of the binder blends has been finalized and presented in **Table 2-4** below. The various tests suggested and included have provided a comprehensive way to evaluate the compatibility of different blends from disparate perspectives. As the project evolved, these testing methods were narrowed down depending on the preliminary results.

Table 2-4 Binder testing plan

	Test Method	Expected Results
Analytical methods	Iatroscan	SARA fractionation
Thermal analysis	Modulated differential scanning calorimeter (DSC)	Tg, phase miscibility
Binder performance tests	Dynamic shear rheometer testing (4-mm, 8-mm and 25-mm)	Superpave PG parameters, linear viscoelastic characterization, thermal-rheological indices and aging index parameters
	Linear amplitude sweep (LAS) testing	Binder damage characteristic curve, fatigue performance indices
	Multiple stress creep recovery (MSCR) testing	Recoverable and non-recoverable portion of binder creep compliance as a rutting performance parameter

In addition to the binder tests, mixture performance assessment is also critical in this study due to the presence of RAP in the mixtures, which makes it challenging to conduct only binder performance assessment where new and recycled binder as well as rejuvenators fully blend during the recovery process. Due to this challenge, it is essential that mixture performance evaluations are also conducted to support the expansion of the dataset generated from the binder tests. A list of mixture performance tests that are employed in the study is shown in **Table 2-5**. In some instances, instead of specific test method a test category has been identified (such as, fracture test for asphalt mixtures). These mixture tests have been widely accepted in the asphalt materials field and have been shown as effective and efficient tools for characterization of asphalt mixtures (Glover et al., 2005; Rowe et al., 2011; Martin et al., 2015&2018; Ozer et al., 2016; Al-Qadi et al., 2017; Mensching et al., 2017; Nemati et al., 2017; Wang et al., 2017; Zhu et al., 2017; Sias et al., 2019).

Table 2-5 Mixture testing plan

Test Method	Expected Results	Significance
Complex (dynamic) modulus	Linear viscoelastic (LVE) characterization, mix rheological indices (such as, mix Glover-Rowe parameter and mastercurve shape factors), and aging index parameters	Similar to binder testing, full LVE characterization allows to look at rheological cracking and rutting performance indices for mixtures to expand the field performance datasets.
Direct tension cyclic fatigue (DTCF)	Mixture damage characteristic curve, fatigue performance indices	On the baseline samples at various lab aging levels, this test determines fatigue cracking performance. The outcomes of this test are also input to Federal Highway Administration's (FHWA) FlexPAVE performance prediction system.
Fracture and cracking tests (such as disk-shaped compact tension (DCT) and semi-circular bend (SCB) tests)	Cracking performance parameters	In addition to full LVE and fatigue cracking performance testing, various cracking lab performance tests, that are currently being adopted by several NRRA partners, are also included. Often times these have simpler testing procedures, and these can serve as quicker proofing tests for validating the findings from binder analytical and performance assessment tasks.

Note that the suggested binder and mixture tests are conducted on the core materials first. The tests/methods which showed the most promise in identifying the compatibility/incompatibility of the core materials are applied on the validation materials to further evaluate their effectiveness. The section below discusses the detailed material base that is generated and the corresponding tests that are performed on the materials within this project.

2.6.3 Overall Sampling and Test Plan

Overall, the project is divided into three phases based on the proposed sampling and testing plans, the project proposal, and the work plan. This helps to make it easier to understand and explain the research process of the study. **Figure 2-18** depicts a schematic of the project structure in terms of material sampling and laboratory testing.

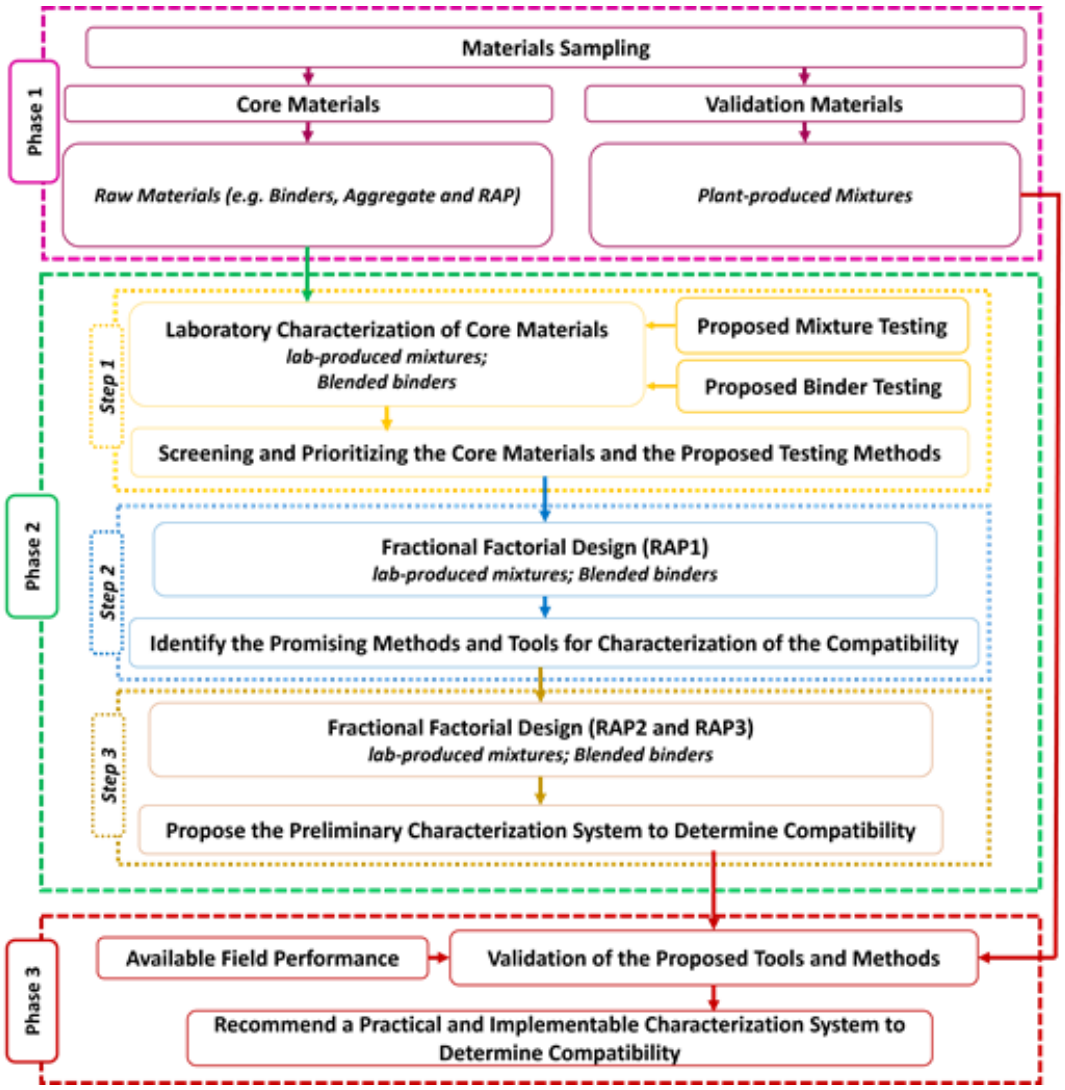

Figure 2-18 Overall structure of the research study

Phase 1: Materials Sampling

Significant quantities of component materials such as binder (3), aggregates, and RAP (3) were sampled for core materials. For validation materials, eight plant-produced mixtures were sampled in a limited amount.

Phase 2: Propose the Preliminary Characterization System to Determine Compatibility

This phase focused on identifying and proposing the preliminary system for characterization of binder compatibility based on the three sets of core materials. It has been further divided into three steps:

Step 1: Screening and Prioritizing the Core Materials and the Proposed Testing Methods

First, all three core RAP materials were characterized using the proposed binder tests (including the analytical and performance tests), which allowed research team to identify a control RAP in the study. The control RAP was chosen such that yields most inferior properties (specifically in terms of

performance properties obtained from binder tests), based on testing results available to researchers, core RAP1 has shown most inferior performance properties. This RAP material was referred to as “RAP1 (control)” and it was used for extensive evaluations of binder blends in this project. Three virgin binders were also characterized and the dosages of two rejuvenators were also determined in this step blending with RAP1. Finally, the RAP1 is blended with all three virgin binders (with high binder replacement ratio (HBRR)), generating three blends.

For the mixture evaluation in this step, all three virgin binders were first blended and mixed with the aggregate sampled in order to design and fabricate the virgin mixtures (with the gradation of plant-produced mixture) as the control/base mix within this project. Then, three mixtures with high RAP content were fabricated.

With the material base generated in this step, all the proposed binder and mixture tests were performed on these blends and mixtures to determine the priority of the tests and screen out the methods and tools that were sensitive and able to differentiate the compatibility of these materials caused by change of blend/mix components. These methods and tools were further evaluated in the next step.

Step 2: Identify the Promising Methods and Tools for Characterization of the Compatibility

In this step, the RAP1 (control) was mixed with all three virgin binders with HBRR (same content as the blends created in step 1). Then, these blends were mixed with the two rejuvenators that were part of this project. This generated a total of six blended binder samples that were evaluated using the methods identified in step 1.

Second, the RAP-1 (control) was blended with virgin binders but with low binder replacement ratio (LBRR) to generate 3 binder blends which were also used to produce three corresponding mixtures. The proposed binder evaluation methods from step 1 were performed on these materials to further investigate whether these tools can effectively capture the change of material compatibility with change of RAP dosage and evaluate the trend in change of compatibility with change of binder.

From each of the above-described binder blends, approximately one-third was used to make lab produced asphalt mixtures for conducting mixture evaluations using the methods identified in step 1. The selection of binder blends for mixture evaluation was based on binder blend results and was an attempt to encompass the most varied binder blend properties.

At the end of this step, the most promising and effective methods, and tools for characterization of the compatibility were identified and reported after evaluation of the material base generated.

Step 3: Propose the Preliminary Characterization System to Determine Compatibility

In addition to the control RAP, other two RAP materials (RAP2 and RAP3) were also evaluated in this step. They were blended with the virgin binders (A and C with PG 64-22; with HBBR) respectively for the binder evaluations. The two rejuvenators were also added into the blends to specifically investigate the compatibility between the rejuvenators, RAP and virgin binders.

The identified and selected binder and mixture testing methods from step 2 was further validated in this step. Binder from A and C with same PG 64-22 are blended and then mixed with aggregate for evaluation purposes. The material base created from this step was mainly used to validate the selected testing approaches from step 1 and 2 with respect to their effectiveness to capture the different compatibility of these designed materials.

As the end result of phase 2, a preliminary characterization system to determine compatibility after investigation and validation based on the wide material base created and evaluated from these three steps was finally proposed.

Phase 3: Recommend a Practical and Implementable Characterization System to Determine Compatibility.

In phase 3, the eight validation materials were used to further validate the effectiveness of the proposed preliminary characterization system inducing the potential binder and mixture tests from phase 2. In addition, the field performance that was measured from the test sections was also employed in this step to compare with the laboratory measurements on the study materials. Finally, the research team provided and recommended a practical and implementable evaluation system that can be used as a screening tool for identifying the compatible and incompatible materials during material selection.

2.7 CHAPTER SUMMARY

This chapter presented a detailed literature review regarding the available tools and techniques to assess the compatibility of asphalt materials. It has covered the asphalt materials domain as well as organic chemistry and polymer science domains. Material sampling plan (core materials and validation materials) along with characteristics was also presented in the chapter. Three RAP sources and three virgin binders across the country were selected as core materials, whereas eight plant-produced mixtures were selected as validation materials. The testing methods for binders and mixtures were selected based on the findings of the literature review for characterization of the sampled materials. Finally, the research plan of the study was presented and explained. It has been divided into three phases each focusing on material sampling, laboratory characterization (to develop a preliminary system to evaluate the compatibility) and validation of the proposed system and findings.

Chapter 3: SCREENING AND PRIORITIZING THE CORE MATERIALS AND THE PROPOSED TESTING METHODS

3.1 CHAPTER INTRODUCTION

A state-of-the-art review regarding the available tools and techniques to assess the compatibility of asphalt binders with respect to virgin and recycled asphalt sources as well as rejuvenators and polymers was summarized by the research team in the previous chapter. This chapter discusses the core materials evaluated in this study and the testing methods used to characterize these materials.

3.2 MATERIAL AND TESTING METHODS

This section discusses the various testing methods included in this chapter as well as the core materials and blends evaluated. The core materials include three virgin binders, three RAP sources and two recycling agents.

3.2.1 Testing Methods

As identified from the literature review (described in previous chapter), binder analytical analysis methods are the fundamental methods to evaluate the colloidal structure or sol-gel structure of the binder sample to directly determine compatibility, while the thermal analysis approach is a valid method that has been shown by many studies to indicate and differentiate compatible and incompatible asphalt materials. The rheological characterization and other binder performance tests provide an indirect measure of compatibility but have been used by many studies to evaluate compatibility. In this chapter, these binder testing methods are evaluated using the core materials sampled in this project. In addition to binder evaluations, mixture performance assessment is also critical in this study due to the presence of RAP in the mixtures, which makes it challenging to conduct performance assessment on just binders because new and recycled binder as well as rejuvenators fully blend during the recovery process.

The binder and mixture testing methods in this study are presented in **Table 3-1** and **Table 3-2,** respectively. The various tests included in this chapter provide a comprehensive set of tools to evaluate the compatibility of different binder blends and mixtures from various perspectives.

Table 3-1 Binder testing methods

Test Method		Test Results
Analytical methods	Iatroscan	SARA fractionation
	Advanced permeation chromatography (APC) (Size exclusion chromatography (SEC))	Molecular size distribution
Thermal analysis	Modulated differential scanning calorimeter (DSC)	Tg, Phase Miscibility
Binder performance tests	Dynamic shear rheometer testing (DSR; with 4-mm, 8-mm and 25-mm plates)	Superpave PG parameters, linear viscoelastic characterization, thermal-rheological indices and aging index parameters

Table 3-2 Mixture testing methods

Test Method	Test Results
Complex (dynamic) modulus	Linear viscoelastic (LVE) characterization, mix rheological indices (such as, mix Glover-Rowe parameter and mastercurve shape factors), and aging index parameters
Direct tension cyclic fatigue	Mixture damage characteristic curve, fatigue performance indices
Fracture and cracking tests (DCT and I-FIT)	Cracking performance parameters

3.2.2 Materials

Table 3-3 below shows the overall information for the core materials sampled and received in this study, including three virgin binders and three individual sources for RAP stockpiles (Gradation of the RAP can be found in Section 3.3).

Table 3-3 Information for core materials

Material Type	Material ID	Binder Grade	Source	Binder Content	Corresponding Field Section
Binder	A	PG 58-28	Minnesota	--	MnROAD/NRRA
	B	PG 64-22	Alabama	--	NCAT
	C	PG 64-22	Wisconsin	--	Wisconsin
RAP	1	PG 103-5	Minnesota	3.9%	MnROAD/NRRA
	2	PG 104-6	Alabama	4.5%	NCAT
	3	PG 87-26	Texas	3.8%	Field Section for RAP in Texas

The overall material base that was generated based on the sampled core materials and evaluated in this chapter is summarized and presented in **Table 3-4** below. First, the core binders and RAP from different sources were evaluated. Then the RAP with the most inferior properties was identified as the control RAP (RAP1; discussed in detail in this chapter) for extensive evaluation in the binder blends and mixtures. In total, six mixtures were designed and evaluated within this chapter, the detailed design information for the remaining mixtures will be discussed in chapter 4.

The binder from RAP and loose mix samples was extracted by two step centrifuging using a standard explosion-proof centrifuge in accordance with ASTM D2172, followed by a high-speed centrifuge to remove the fines. Toluene was selected as the solvent of choice based on extensive prior experience of use for such applications. The asphalt was recovered from the solution using the Abson recovery method following ASTM D1856, modified for ideal toluene removal conditioning using the methodology described by ASTM D7906 for asphalt recovery from toluene solutions.

Table 3-4 Material base generated from step 1

	Material Base		Testing Methods
Binder Evaluation	Virgin Binder	A	Binder Tests
		B	
		C	
	RAP	1	
		2	
		3	
	Blends	RAP1 (control) + Rejuvenator A	
		RAP2 + Rejuvenator A	
		RAP3 + Rejuvenator A	
		RAP1 (control) + Rejuvenator B	
		RAP2+ Rejuvenator B	
		RAP3 + Rejuvenator B	
		RAP1 (control) + Binder A (HBRR)	
		RAP1 (control) + Binder B (HBRR)	
		RAP1 (control) + Binder C (HBRR)	
Mixture Evaluation	Virgin Mixtures	Binder A + Aggregate A	Mixture Tests
		Binder B + Aggregate A	
		Binder C + Aggregate A	
	Mixtures with RAP	RAP1 (control) + Binder A + Aggregate A (HBRR)	
		RAP1 (control) + Binder B + Aggregate A (HBRR)	
		RAP1 (control) + Binder C + Aggregate A (HBRR)	

HBRR: High Binder Replacement Ratio (34%)

3.3 CORE RAP MATERIALS CHARACTERIZATION

This section presents the results of the tests conducted on the core materials. **Table 3-5** summarizes the testing and aging conditions that were performed on the core RAP materials. The testing results are discussed in the corresponding subsections. Based on the rheological, thermal, and SARA analysis (discussed in the following sections), RAP1 was selected as the control RAP for this project due to its overall inferior properties as compared to RAP2 and RAP3. The gradation curve of RAP1 is shown in **Figure 3-1** below.

Table 3-5 Testing types and aging levels for evaluation of core RAP

Material ID / Testing Type	RAP1			RAP2			RAP3		
	As-extracted	1xPAV	2xPAV	As-extracted	1xPAV	2xPAV	As-extracted	1xPAV	2xPAV
DSR	√	√	√	√	√	--	√	√	√
DSC	√	√	√	√	√	√	√	√	√
APC	√	--	--	--	--	--	--	--	--
Iatroscan (SARA)	√	--	--	√	--	--	√	--	--

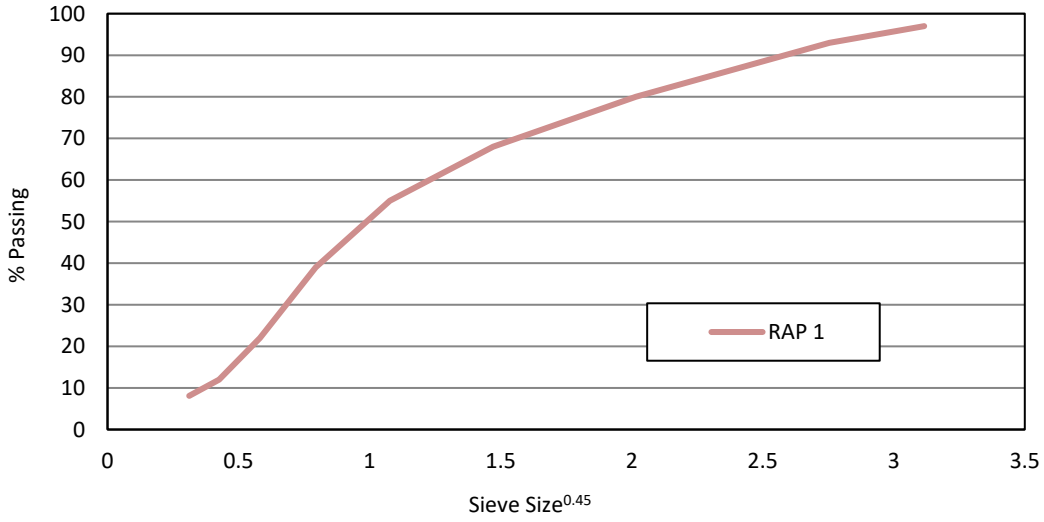

Figure 3-1 Gradation curve for control RAP

3.3.1 Rheological Measurements (DSR Testing)

The temperature and frequency sweep test using a DSR with 4- and 25-mm plates was conducted to measure the PG and the rheological parameters of the core RAP materials. The Christensen-Anderson model was used to fit the isotherms measured from the test to construct a mastercurve using a minimization technique to determine the shift factors and derive the mastercurve shape parameters, as shown below in equation 3.1.

$$G^* = G_g^* \left(1 + \left(\frac{\omega}{\omega_c}\right)^{log2/R}\right)^{R/log2} \quad (3.1)$$

Where,

G* is the complex modulus in Pa at frequency ω in Hz,

G_g^* is the glassy modulus asymptote variable (assumed 1 GPa),

ω_c is the cross-over frequency,

R is the Rheological Index or “R-Value”.

The rheological indices include the ΔT_c parameter, defined as the difference in critical temperature for the S and m-value passing values from BBR (Anderson et al., 2011), and the G-R parameter (Rowe et al., 2011) can be also calculated from the DSR measurements (Zhang, 2020).

Table 3-6 and **Figure 3-2** below summarize the measured continuous PG and rheological parameters for the study core RAP materials with different aging conditions. RAP1 and RAP2 have comparable PG with RAP1 having slightly higher value of low temperature PG (LTPG), while RAP3 has the lowest high temperature PG (HTPG) and LTPG. There is not a clear trend in ΔT_c parameter for three study RAP with different aging conditions, the ΔT_c values for RAP1 with as-extracted and 2xPAV aging levels and RAP2 with 1xPAV aging are lower the cracking limit threshold of -5 °C. In terms of G-R parameter, RAP1 and RAP2 have higher values than RAP3 after each aging condition and all exceed the cracking limit threshold value of 600 kPa, indicating inferior cracking properties.

Table 3-6 Rheological characterization of the core RAP materials

Material ID / Parameters	RAP1			RAP2			RAP3		
	As-extracted	1xPAV	2xPAV	As-extracted	1xPAV	2xPAV	As-extracted	1xPAV	2xPAV
Continuous PG	103-5	103+1	N/A+4	104-6	104-0	N/A	87-26	87-20	N/A-16

N/A: Resulting binder was too brittle for proper grade testing.

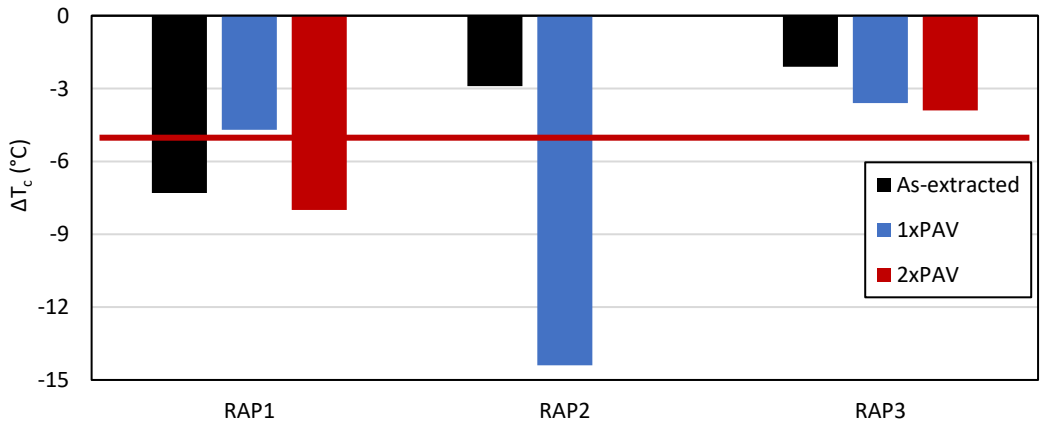

(a)

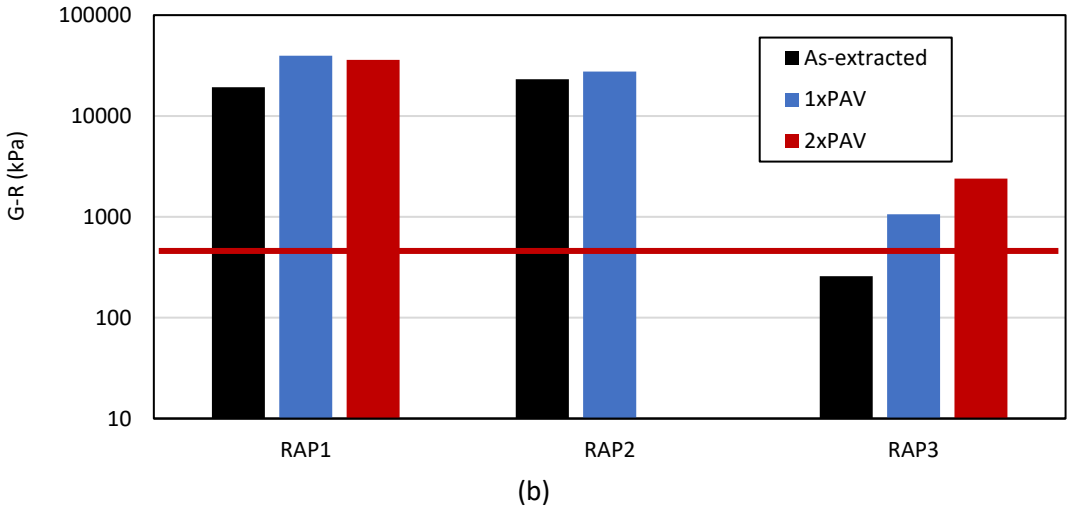

Figure 3-2 (a) ΔT_c and (b) G-R parameter for study core RAP

3.3.2 Thermal Analysis (DSC Testing)

DSC is the most widely used approach to determine the enthalpy related transitions of asphalt binders (Planche et al., 1998) and of polymeric materials (Yousefi et al., 1997). The Tg of asphalt binders measured from DSC analysis can be used to interpret thermal-related defects in asphalt pavements, such as thermal cracking. For instance, binders with low Tg accumulate less thermal stress under a given thermal history and thus are more resistant to low temperature cracking. In addition, studies (Jimenez-Mateos et al., 1996; Apostolidis et al., 2019) have shown that incompatible binders typically have high Tg temperatures.

In this study, a TA DSC250 DSC was used to measure the glass transition range of binders using a modulation method. The heating rates, rest rates, and increment periods selected were:

- Hold for 1 minute at 150 °C to erase thermal history
- Cool from 150 °C to -100 °C at a rate of 20 °C/min
- Hold for 5 minutes at -100 °C to achieve equilibration
- Modulate from -100 °C to 100 °C in 2 °C modulation periods at an average heating rate of 5 °C/min.

The modulation analysis can be used to separate the thermally reversible and irreversible response from the spectra. Analysis of the DSC data required the development of a protocol for reduction and smoothing of the initial dataset. Data below -88 °C was discarded to remove the impact of test artifacts occurring at the start of the modulation step in this study. The modulated step collected approximately 55,000 datapoints over the 200 °C span. The data was first uniformly reduced to 1000 data points (~1 point per every 0.2 °C). Smoothing was performed using the TA TRIOS software's "Least Square Moving Window" smoothing technique, for a 40 data point window. The transition temperatures were then determined as the local maxima on the derivative of the heat capacity spectra. As shown in **Figure 3-3**, The "transition region" was defined by the temperatures at which reversible heat flow curve

approximately achieves its linearity at either tangent (between $Tg_{,onset}$ and $Tg_{,endpoint}$). The central temperature of the glass transition can be defined at the mid-height of the tangents ($Tg_{(H)}$) or by the inflection point $Tg_{(I)}$. The glass transition temperature (Tg) used in this study for evaluation of the binders and mixtures is the $Tg_{(I)}$ which corresponds to the inflection point as shown in **Figure 3-3**.

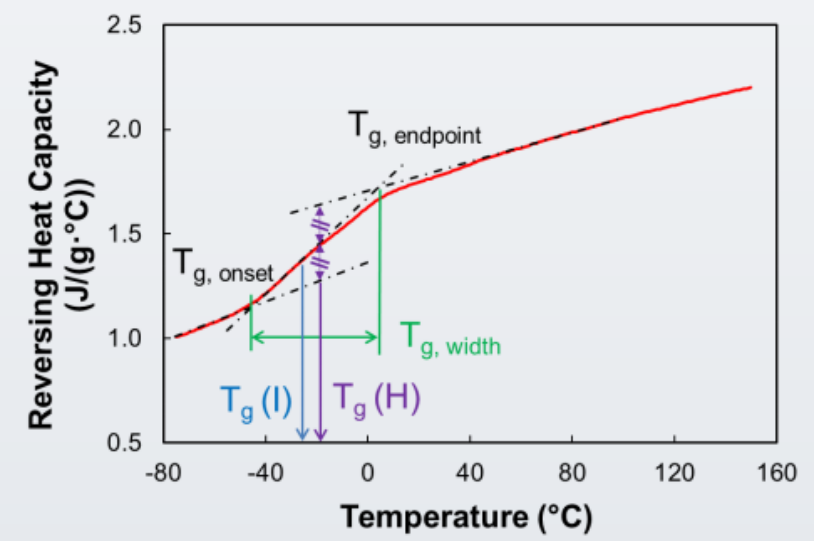

Figure 3-3 Glassy transition region and temperatures (Elwardany et al., 2019)

The Tg values measured from the DSC analysis for the study RAP material with different PAV aging cycles are shown in **Figure 3-4** below. RAP1 and RAP2 have significantly higher Tg values than RAP3 after each aging condition. RAP1 shows the warmest Tg value indicating inferior thermal properties and potential incompatibility.

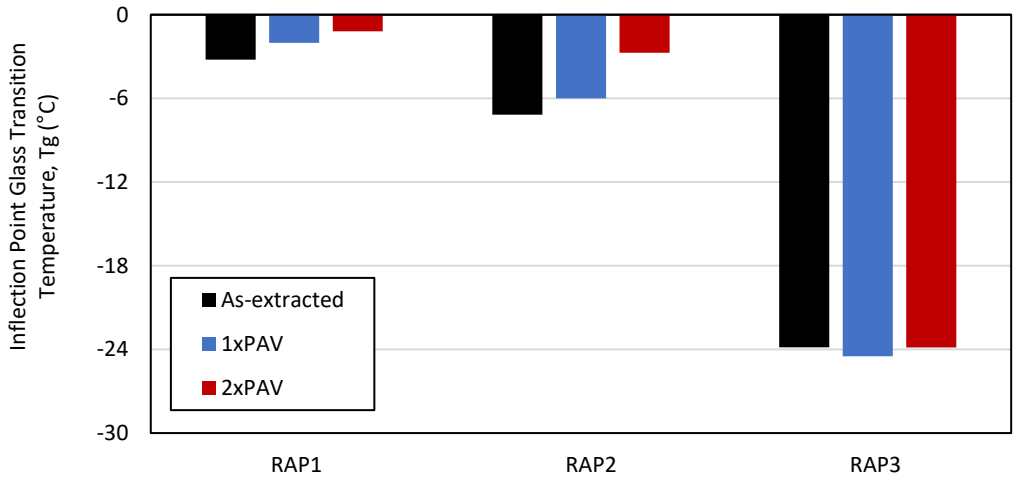

Figure 3-4 Tg values for study rap material

Some studies have proposed deconvoluting the heat flow derivative curve into the underlying Tg events in order to quantify indices based on the relative intensity of the corresponding peaks in different

binders, with different aging conditions, and with or without rejuvenators (Tabatabaee et al., 2021; Tabatabaee and Sylvester, 2021).

Figure 3-5 shows an example of the deconvolution of the heat flow derivative peak to two glass transition distributions. The main peak, typically occurring at the lower temperature is hereby referred to as Tg_{α} (shown in **Figure 3-5a**). It can be seen that the sum of the peak heights at each given temperature (shown in **Figure 3-5c**) corresponds closely to the experimentally derived |dH/dT| (shown in **Figure 3-5b**). The area under each of these curves after deconvolution was calculated and defined as ΔH. The following parameters are hereby defined:

$$\phi_{\alpha,\beta} = \frac{\Delta H_{\alpha,\beta}}{\sum \Delta H} \tag{2}$$

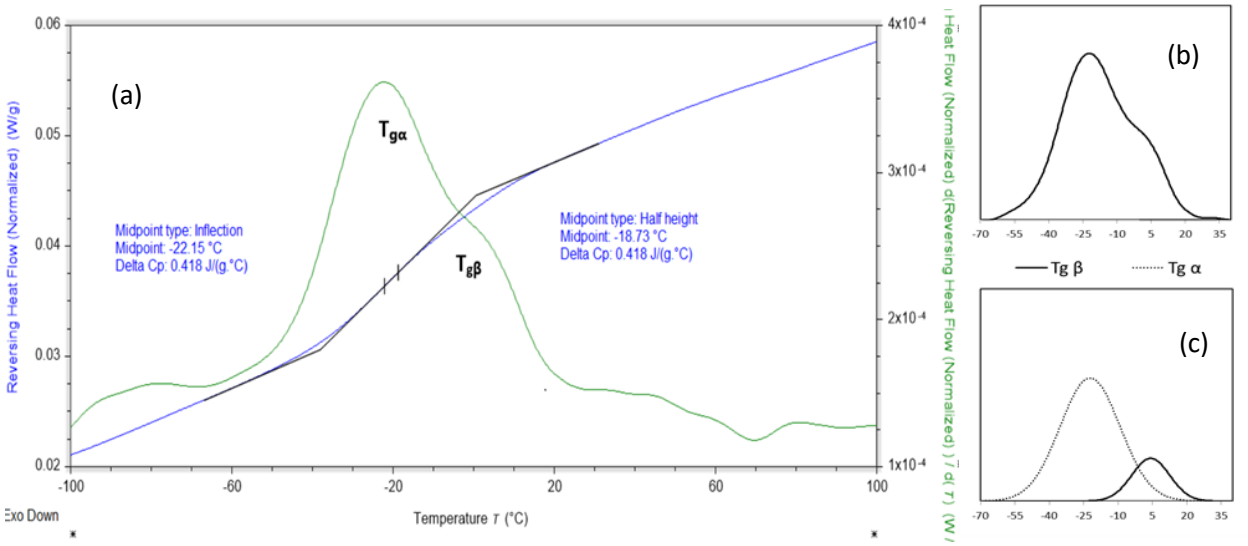

Figure 3-5 Definition of the deconvolution and analysis of DSC curves for an RTFO aged PG 64-22 binder

Based on Tabatabaee & Sylvester (2021), more compatible binders are expected to have a higher ϕ_{α} index. Furthermore, aging would be expected to reduce the ϕ_{α} index as the binder becomes less compatible with the evolution of its composition. Another parameter calculated based on the deconvoluted peaks is the Tg_{Aave} parameter. This parameter is essentially a "recombination" of the peaks, in which each peak contributes to the average weighted by its corresponding ϕ (area ration from total of all peak areas). The Tg_{Aave} can be thought of as an idealized version of the total glass transition, and for a glass transition well described by the applied deconvolution the numeric value will be well correlated to the inflection point glass transition temperature defined on the entire thermal response spectra (Tg).

Figure 3-6 shows the values of the ϕ_{α} parameter for RAP1, RAP2, and RAP3 with three aging levels. The ϕ_{α} parameter decreases with increase of aging condition as expected. RAP1 clearly shows the lowest ϕ_{α} value as compared to the other two RAP materials after each aging condition, indicating that RAP1 has an inferior thermal property and potential incompatibility.

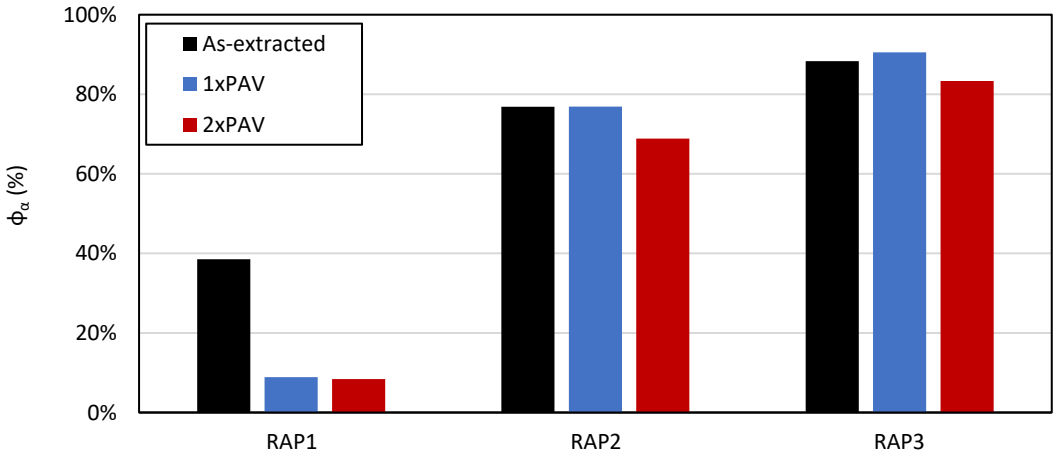

Figure 3-6 ϕ_α index for RAP1, RAP2, and RAP3 samples

3.3.3 SARA Separation (Iatroscan)

Classifying and understanding the chemical composition of asphalt binders has been of significant focus in asphalt research for many decades. Various methods have been proposed and used for separating asphalt into its chemical building blocks, or "fractionation". Such methods often rely on one or a combination of methods such as solvent solubility, separation by molecular size or polarity through various size exclusion or column separation methods, and thin layer chromatography such as with an Iatroscan. Most commonly, asphalt is split into four fractions in terms of solvent affinity (polarity and molecular weight): Saturate, Aromatic, Resin and Asphaltene, also known as SARA fractionation. In this study, the SARA factions are characterized using an Iatroscan Thin Layer Chromatography methodology. Using this method, the saturate fraction is separated through an N-Pentane elution, followed by the elution with a Chloroform-Toluene blend (90:10 by volume) to separate the aromatic phase from the polar aromatic (resin) fraction. The Iatroscan employs a Flame Ionization Detector (FID) to quantify the fractions separated by each elution.

Based on the measured fractions of the binder, the CII can be calculated as shown in **Equation 3** below. A higher CII value generally indicates a binder that may have compatibility issues.

$$CII = \frac{A_S+S}{A_R+R} \quad (3)$$

where,

AS = denotes the asphaltene content,
S = saturate content,
R = resin content, and
AR = Aromatic content.

The CII values measured from the SARA analysis for the study RAP materials are shown in **Figure 3-7** below. The CII values for RAP1 and RAP2 are comparable, while RAP3 shows the highest value due to a higher asphaltene content.

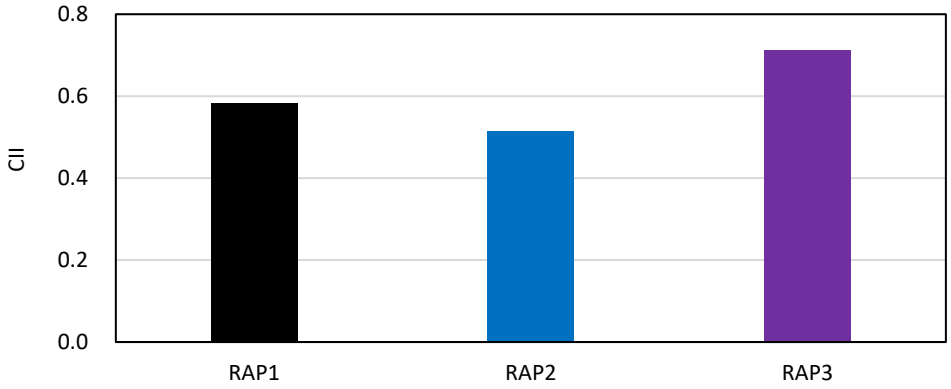

Figure 3-7 SARA analysis of RAP1, RAP2, and RAP3 samples

3.3.4 Chromatography Analysis (APC Testing)

The molecular size distribution of the asphalt binders was determined through the SEC method using the ACQUITY Advanced Polymer Chromatography (APC) system manufactured by Waters. This test was only conducted on the selected control RAP (RAP1). Liquid chromatography methods generally work using the principles of size exclusion. The sample is solubilized in an appropriate solvent and injected into packed columns. The columns have specific distributions of molecular scale pore sizing that will retain like-sized molecules, thus delaying their elution through the columns. As a result, larger molecules are less frequently retained and elute earlier, while the smaller particles are retained by a higher proportion of pores and therefore elute later, thus effectively separating into a molecular size-distribution on an elution time scale.

The system configuration for the tests performed in this study was as follows:

- Three columns in the following order: Two Acquity APC XT 125 2.5 micrometers 4.6x150mm columns, one Acquity APC XT 125 2.5 micrometers 4.6x150mm column, and one Acquity APC XT 45 1.7 micrometers 4.6x150mm column.
- Columns Temperature: 35 °C.
- Solvent type: Tetrahydrofuran (THF) non-UV, HPLC grade. Flow Rate: 0.6 mL/min
- Detector type: RI Detector at 35 °C.

The APC data was analyzed through the creation of a response histogram. Many petrochemical hydrocarbon products such as asphalt yield broad and continuous molecular size distribution histograms, without distinct peaks. Therefore, analysis of such curves was performed using two methods:

A. Slicing: The continuous curve is split into multiple areas at certain elution times (corresponding to specific molecular sizes). The area under the curve for these areas can be calculated as a percentage of the area under the total histogram. In this study the histogram was split into three areas: HMW (High Molecular Weight), MMW (Medium Molecular Weight), and LMW (Low Molecular Weight). A RAP binder typically has higher proportion of HMW fraction while the virgin binder and the RA treated binder generally show higher LMS fraction (Daly et al., 2013; Dong et al., 2013). This is shown in **Figure 3-8(a).**

B. Deconvolution: The deconvolution method employed was similar to that used for the DSC analysis described in section 3.3.2. The analysis assumed a normal gaussian distribution for each sub-species. For the current analysis, three underlying curves (Peak α, β and γ) were assumed, and the width, intensity, and the area under each peak were determined through a Sum of Squared Errors minimization. This is shown in **Figure 3-8(b).** The area under each peak is directly related to the molecular weight parameters; higher area of peak γ, β and α correspond to higher HMW, MMW and LMW respectively.

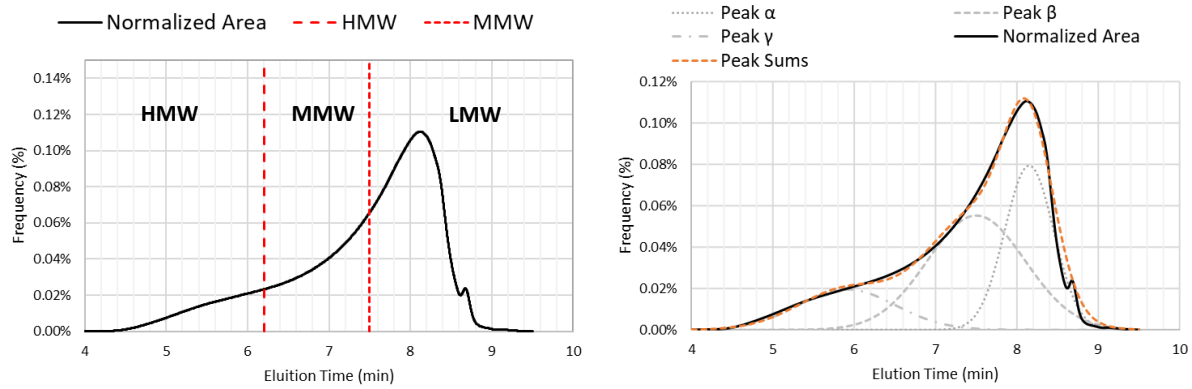

(a) (b)

Figure 3-8 APC molecular size distribution analysis through (a) slicing method and (b) deconvolution analysis

The results from the APC analysis for the selected control RAP (RAP1) are shown in **Table 3-7** below.

Table 3-7 APC parameters for the control RAP (RAP1)

HMW	MMW	LMW	Peak γ	Peak β	Peak α
11.60%	30.1%	58.3%	17.1%	48.3%	34.7%

3.4 MIXTURE EVALUATION

As per the testing plan, in this stage only one RAP was to be selected for mixture evaluation. RAP1, with inferior binder properties and therefore a higher potential for incompatibility as compared to the other two RAP materials, was designated as the control RAP and further evaluated through mixture testing. This section summarizes the results from different mixture performance testing, including the Complex Modulus (E*), DTCF, I-FIT and DCT tests. The focus was to compare the binder-based compatibility evaluation tests with mixture performance indices obtained from different tests.

3.4.1 Mixture Design

Using the reference mix design (45% RAP mix) provided by MnDOT, the control RAP (RAP1) was blended with three virgin binders to design (following AASHTO M 323) and generated three RAP mixtures with high (45% RAP) content as indicated in **Table 3-8**. In addition, a virgin mixture was designed to match the gradation of the 45% RAP mix (gradation curve shown in **Figure 3-9**). Three virgin mixtures with three binder sources were then produced as the control mix to compare the properties with 45% RAP mixtures. All mixtures used the same virgin aggregates.

Table 3-8 Mix information and volumetric parameters

Mix ID	Binder ID	RAP Content	Optimum Asphalt Binder Content (AC; %)	Voids in the Mineral Aggregate (VMA; %)	Voids Filled with Asphalt (VFA; %)	Asphalt Binder Film Thickness (AFT; µm)
V-A	A	0%	5.8	18.2	78	13.3
V-B	B					
V-C	C					
HRAP-A	A	45% by wt of mixture (34% RBR)	5.3	15.3	75.2	9.6
HRAP-B	B					
HRAP-C	C					

RBR: recycled binder ratio

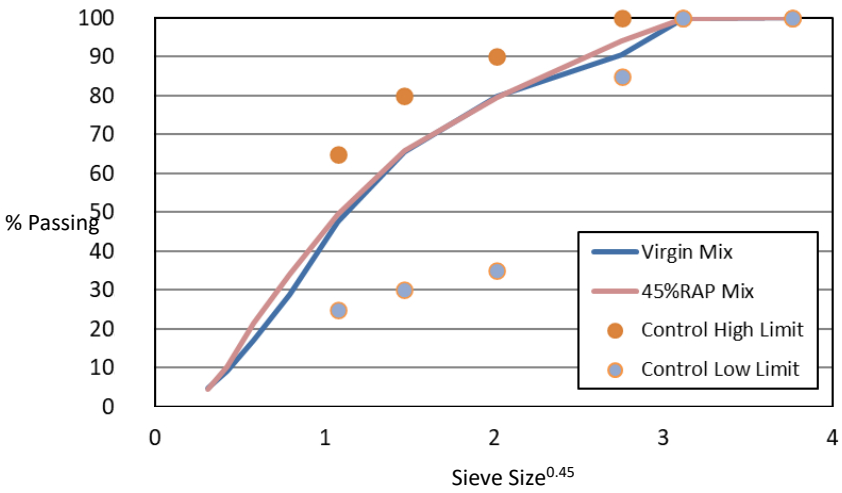

Figure 3-9 Gradation information for the two mixture designs

3.4.2 Complex Modulus Testing

The Complex Modulus (E*) tests were conducted following the AASHTO T 342 procedure to evaluate the fundamental viscoelastic properties of asphalt mixtures. Dynamic modulus (|E*|) and phase angle (δ) master curves measured from the E* test are presented in **Figure 3-10;** each series represents the average of three replicates. The mixtures with the control RAP typically show significantly higher stiffness (|E*|) and lower phase angle (δ) than the corresponding virgin mixtures, as expected. Comparing the virgin and RAP mixtures, mixtures HRAP-A and V-A show the lowest |E*| and highest δ

value as compared to others due to the softer, more compatible base PG 58-28 binder. The mixture with the potentially incompatible binder (binder B) and control RAP shows the highest stiffness and lowest relaxation capability. While this observation is for a single mixture and additional confirmation is necessary, this result indicates that mixture rheological characterization should be further explored to identify incompatible binders. Mixtures with binder C typically show comparable |E*| and δ values as compared to mixtures containing binder B due to the similar grade binders used in the two mixtures.

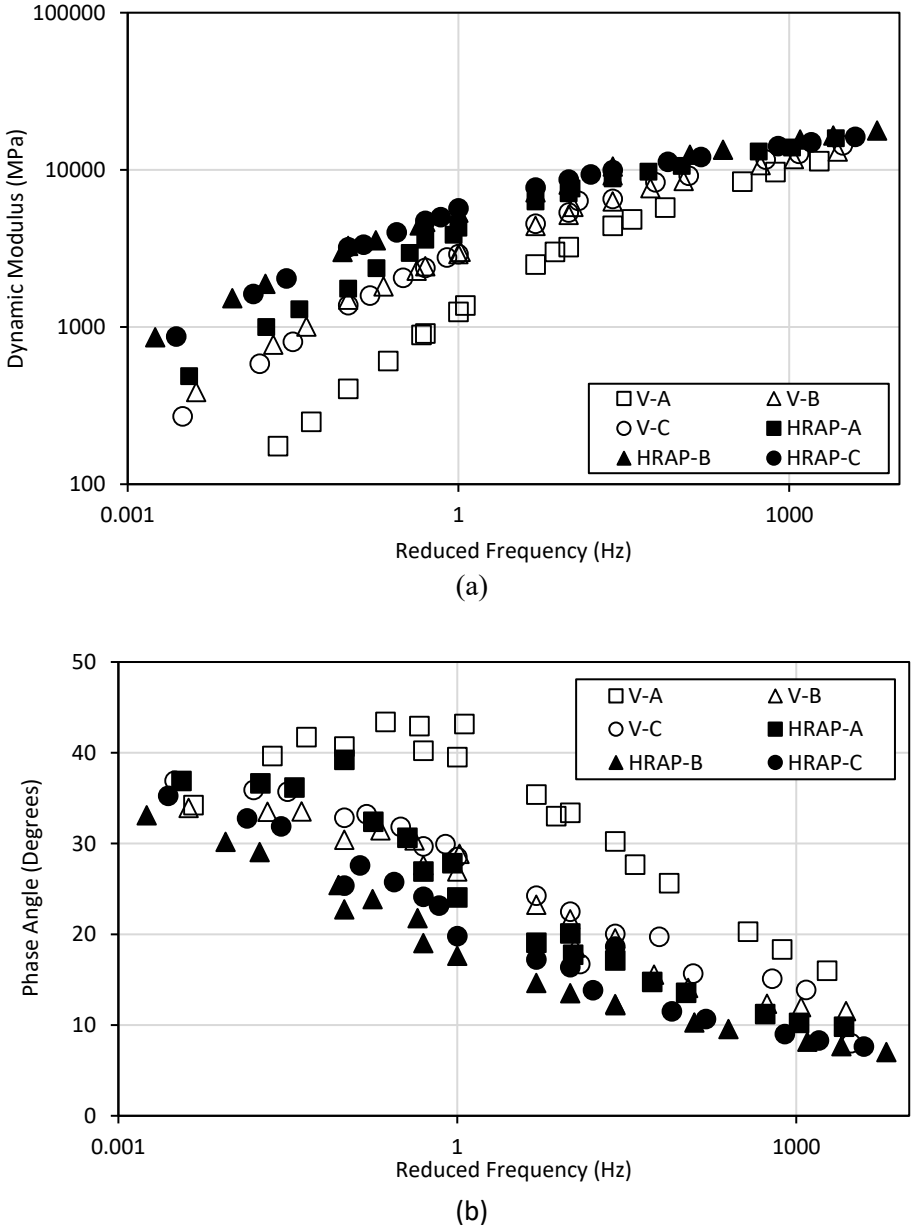

Figure 3-10 E* testing results: (a) dynamic modulus (|E*|) mastercurves and (b) phase angle (δ) mastercurves

From the constructed mastercurves, several rheological based performance parameters can be calculated, including the mixture Glover-Rowe (G-R_m) parameter and complex modulus based rutting index (CMRI). The G-R_m parameter was initially proposed to assess the cracking resistance of asphalt binders. The basis of this approach was originally proposed by Glover et al (2005). Later, Mensching et

al. (2017) developed a parameter to evaluate the cracking performance of asphalt mixture in the format of the binder Glover-Rowe parameter, but employing stiffness and phase angle measured on the mixture (|E*| and δ), as shown in **Eq. 4**.

$$G - R_m = \frac{|E^*|(cos\delta)^2}{sin\delta} \quad (4)$$

In this study, the parameter is calculated at the temperature-frequency combination of 20 °C and 5Hz, following additional development of the G-R_m parameter to use a typically measured point to evaluate the cracking performance of asphalt mixtures in the NCHRP 09-58 project (Epp Martin et al., 2018).

A CMRI was developed by Nemati et al. (2020), which has been shown to correlate well with the Hamburg Wheel Tracking Test (HWTT) results, as well as the actual field rutting performance of asphalt pavement. The calculation of the CMRI parameter is shown below:

$$CMRI = \frac{|E^*_A| - |E^*_B|}{(f_A - f_B)^2} \quad (5)$$

$|E^*_A|$: dynamic modulus corresponding to peak phase angle;
$|E^*_B|$: dynamic modulus corresponding to the HWTT testing condition (45 °C at 0.866Hz);
f_A: logarithm of frequency corresponding to peak phase angle;
f_B: logarithm of frequency corresponding to HWTT testing condition (45 °C at 0.866Hz).

Figures 3-11 and 3-12 below show the calculated G-R_m and CMRI for the study mixtures, respectively. The mixture G-R_m parameter indicates the general cracking properties and lower G-R_m value indicates better cracking resistance. The CMRI indicates the rutting properties of asphalt mixture and a higher CMRI value indicates better rutting resistance. The three mixtures with 45% RAP generally show higher G-R_m and CMRI values than the three virgin mixtures, as expected. Comparing the virgin and RAP mixtures, mixtures HRAP-A and V-A typically have lower G-R_m indicating better cracking properties but lower CMRI value indicating higher susceptibility to rutting as compared to the mixtures with the PG 64-22 binders. Mixtures with binder B have the highest G-R_m values, while mixture HRAP-C with binder C has the highest CMRI value.

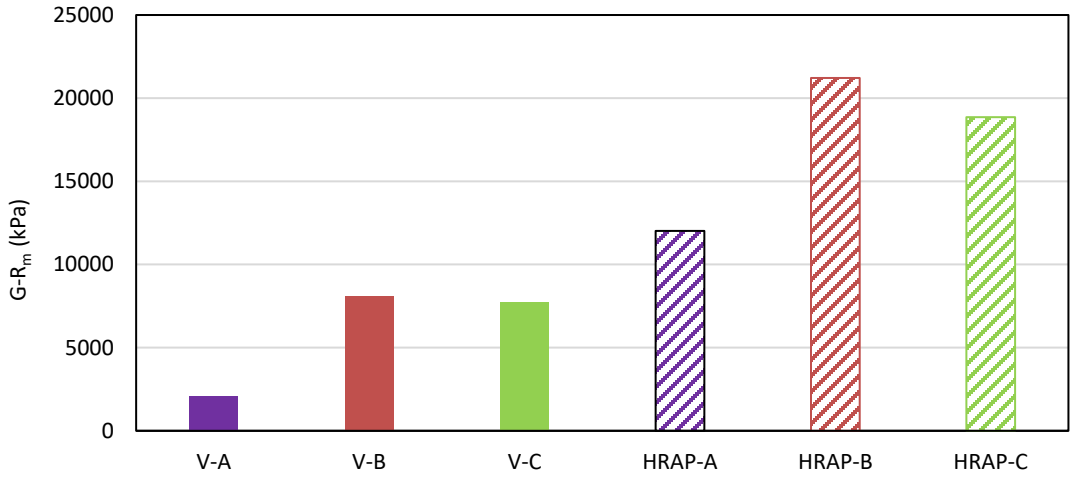

Figure 3-11 G-R_m parameter for the study mixtures

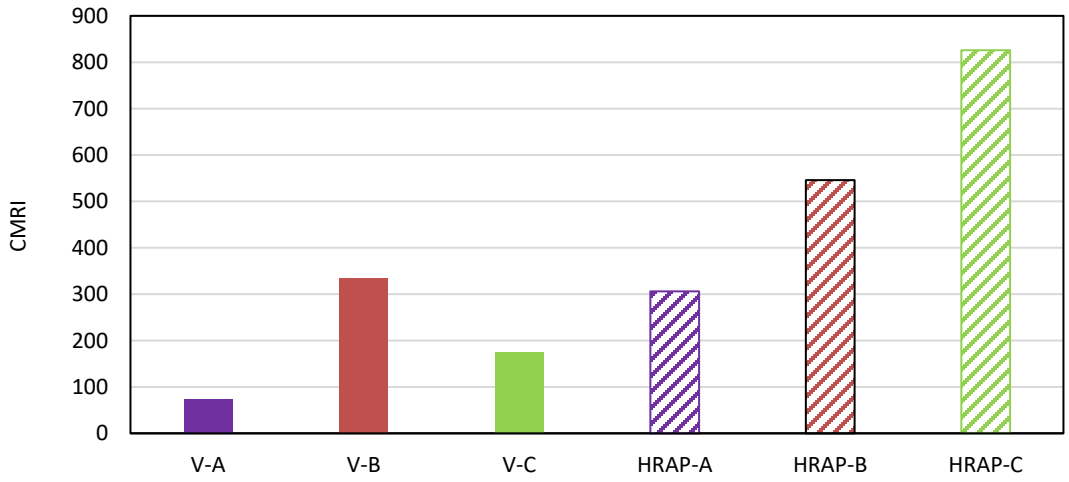

Figure 3-12 CMRI parameter for the study mixtures

3.4.3 Direct Tension Cyclic Fatigue (DTCF) Test

DTCF test was conducted in accordance with AASHTO TP 107 to evaluate the fatigue properties of asphalt mixtures. The performance parameter D^R (average reduction in integrity up to failure) and S_{app} (the accumulated damage when C (pseudo stiffness) is equal to 1-D^R) calculated from the simplified viscoelastic continuum damage (S-VECD) approach are used to evaluate the ability of the mixtures to resist fatigue cracking (Wang et al., 2017). The D^R parameter is calculated primarily based on the reduction of the stiffness of sample during the test, thus, is more related to the damage tolerance of the asphalt mixture; the S_{app} parameter is calculated based on the dissipated energy of the sample with increase of cycles, therefore, is more representative of the trade-off between the applied stress and strain, material stiffness and relaxation capability. Typically, a higher value is preferred for both parameters.

Figures 3-13 and 3-14 below show the D^R and S_{app} values measured from the DTCF test for the study mixtures. The virgin mixtures have higher D^R and S_{app} values than the 45% RAP mixtures, indicating better fatigue properties as expected. Comparing the three RAP mixtures, mixture HRAP-A with the softer and compatible PG 58-28 binder has the highest D^R and S_{app} values, and HRAP-B shows higher values than HRAP-C. The virgin mixtures have a similar trend for the D^R values but the opposite trend for the S_{app} values. The different trend observed for the D^R and S_{app} parameters here can be attributed to the different background/theory for development of these parameters as described above. The D^R parameter shows the consistent decreasing trend with increase of binder stiffness (grade) and RAP content, however, the S_{app} parameter does not. Using a stiffer base binder and addition of RAP may increase the brittleness of mixture, but it will generate lower strain and potentially less dissipated energy, resulting in a higher S_{app} parameter.

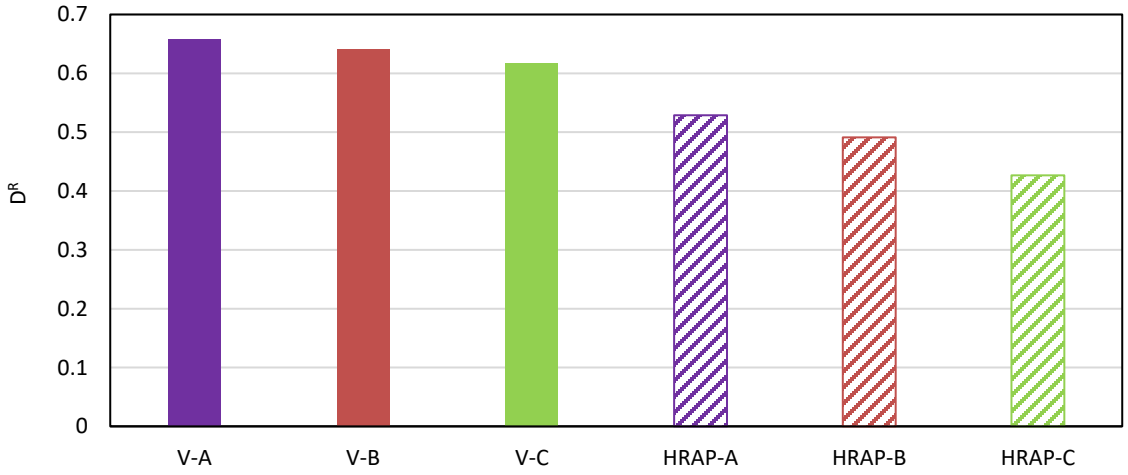

Figure 3-13 D^R parameter for study mixtures

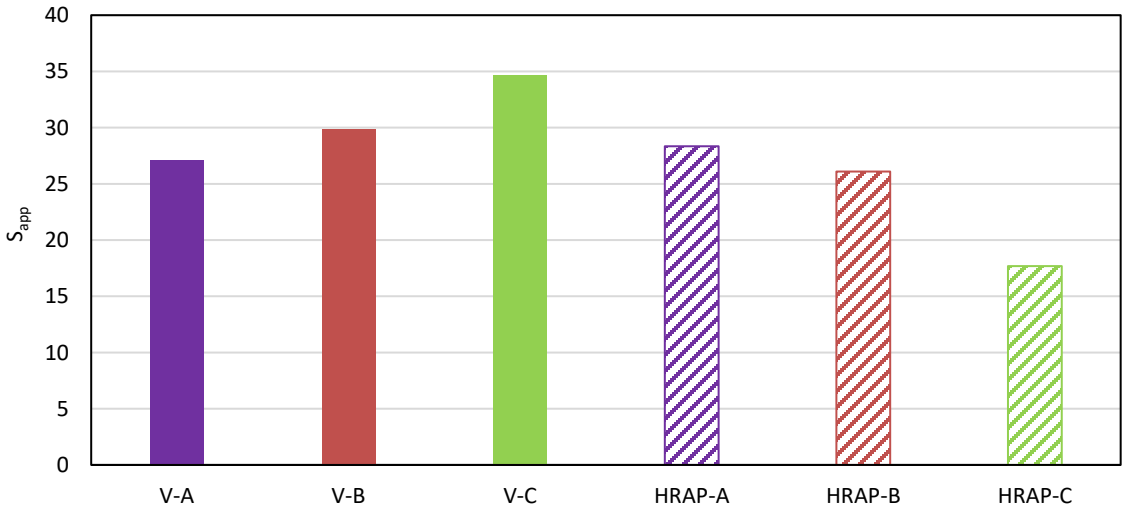

Figure 3-14 S_{app} parameter for study mixtures

3.4.4 Illinois Flexibility Index Semi-Circular Bend (SCB) Test (I-FIT)

The I-FIT was conducted following AASHTO T 393 procedure to evaluate the fracture characteristics of asphalt mixtures at an intermediate temperature. The measured data were analyzed to calculate the fracture energy (G_f) and flexibility index (FI) parameters (Ozer et al., 2016). A higher value for both parameters is generally preferred, indicating a better ability to resist cracking development. Nemati et al. (2020) developed the rate-dependent cracking index (RDCI) to better discriminate asphalt mixtures with various mix variables. The calculation of RDCI is shown below:

$$RDCI = \frac{\int_{t_{peak}}^{t_{0.1\,peak}} W_C\, dt}{P_{t_{peak}} \times ligament\ area} \times C \qquad (6)$$

where RDCI is the rate-dependent cracking index, $\int_{t_{peak}}^{t_{0.1\,peak}} W_C\ dt$ is the post-peak area under the cumulative work versus time curve, P_{tpeak} is the instantaneous power at peak force, C is the unit correction factor set to 0.01 and ligament area is the specimen thickness times the ligament length. Generally, a higher RDCI value is preferred.

Figures 3-15 and **3-16** below show the calculated G_f and FI parameters for the study mixtures, respectively. The three mixtures with 45% RAP have lower G_f and FI values than the three virgin mixtures, as expected. Mixture HRAP-A has the highest G_f parameter of the RAP mixtures, indicating the best cracking properties while the corresponding V-A mixture has the lowest G_f parameter of the three virgin mixtures. Adding RAP may decrease the damage tolerance and increase the brittleness of the mixture, but it can also increase the stiffness of the asphalt mixture; the G_f parameter is an energy-based parameter related to both damage tolerance and overall strength of the mixture. This explains the inconsistent trend observed between the virgin and RAP mixtures. Both the virgin and RAP mixture with binder A have the highest FI value, and mixtures with binder B have higher G_f and FI parameters than mixtures with binder C. Only the three virgin mixtures meet the current minimum threshold value of 8 for the FI parameter. The calculated RDCI values, shown in **Figure 3-17**, follow the same trends as the FI values.

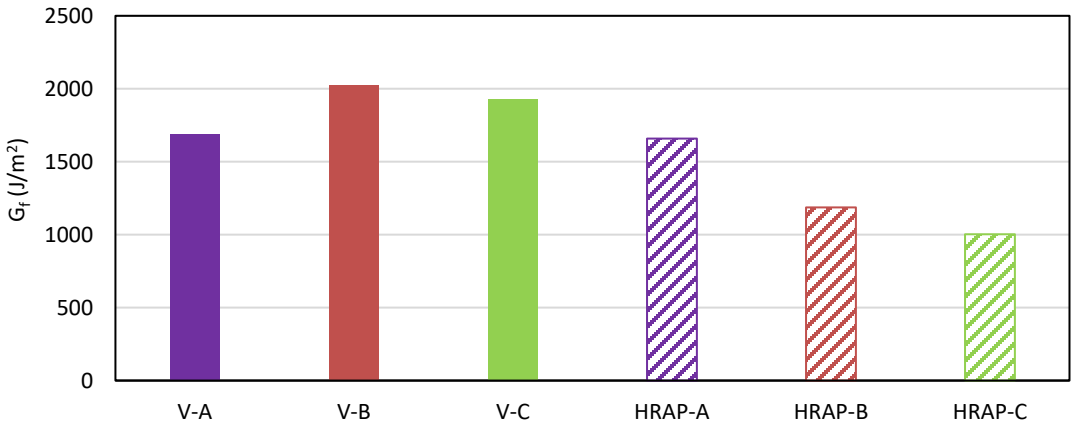

Figure 3-15 G_f parameter measured from I-FIT

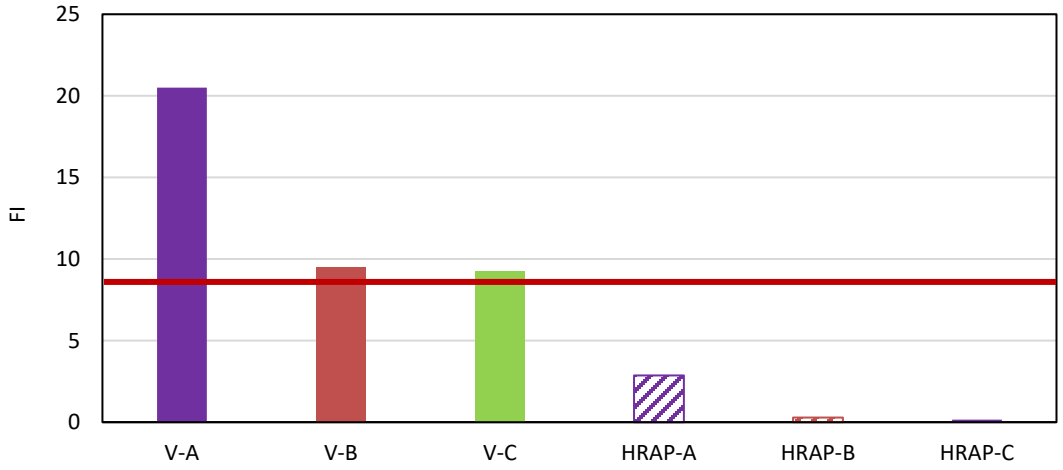

Figure 3-16 FI parameter measured from I-FIT

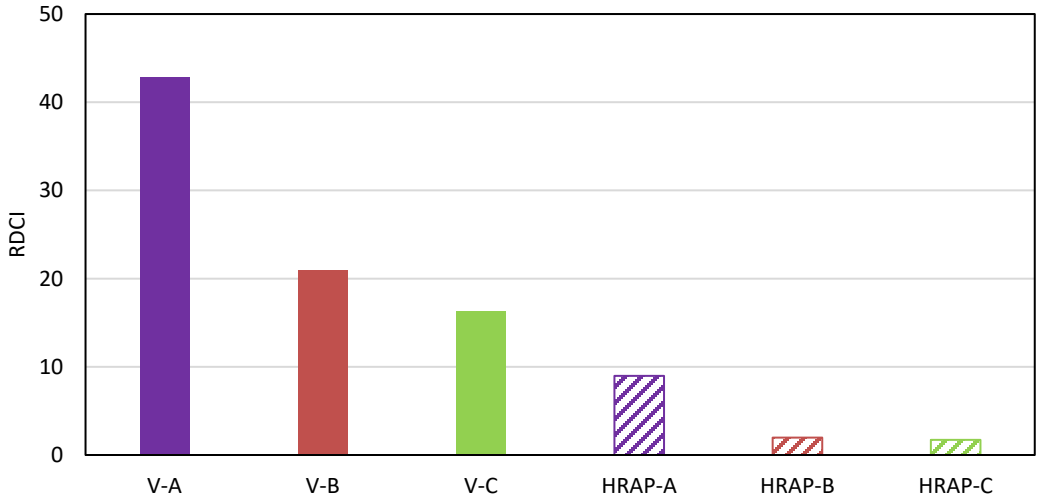

Figure 3-17 RDCI parameter measured from I-FIT

3.4.5 Disk-shaped Compact Tension (DCT) Test

The DCT testing (ASTM D7313) was conducted to compare the thermal cracking behavior as well as the fracture properties at low temperatures for the study mixtures. The test temperature is 10 °C warmer than the PG of the base binder. The measured data were analyzed to calculate the fracture energy (G_f) and fracture strain tolerance (FST) parameter (Zhu et al., 2017). Generally, a higher value is preferred for both parameters, indicating better ability to resist cracking.

Figures 3-18 and **3-19** below show the calculated G_f and FST parameter for the study mixtures. The RAP mixtures have lower G_f and FST values than the virgin mixtures, as expected. Both the virgin and RAP mixture with binder A have the highest G_f and FST values. Mixtures with binder B have higher G_f and FST values than the mixtures with binder C. All mixtures except HRAP-B and HRAP-C meet the current threshold value of 450 J/m^2 for the G_f parameter.

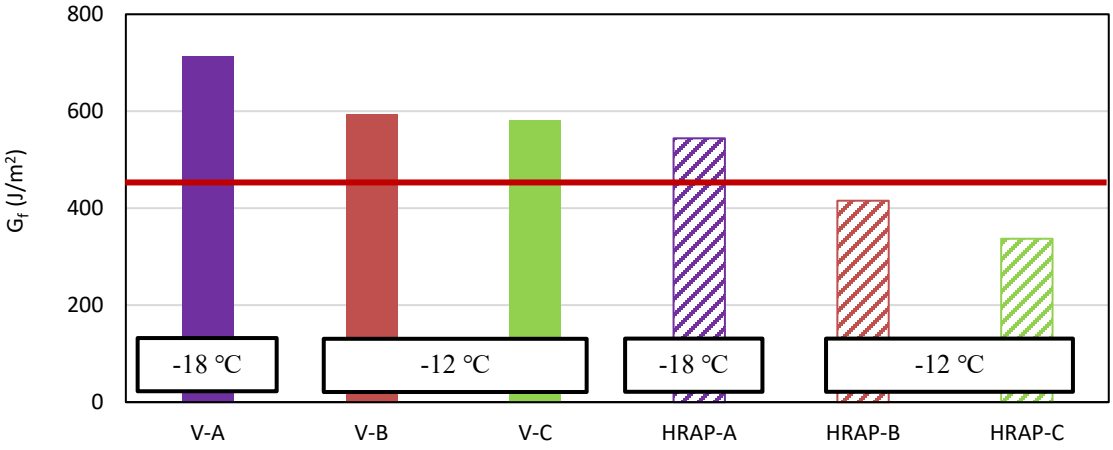

Figure 3-18 G_f parameter measured from DCT

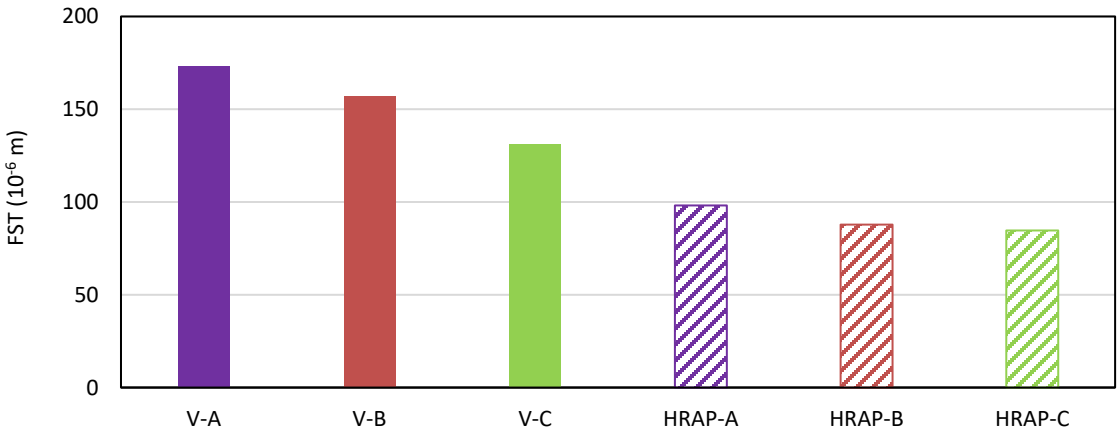

Figure 3-19 FST parameter measured from DCT

3.5 EVALUATION OF BINDER BLENDS

This section summarizes the results from the binder testing conducted on the RAP binder blended with two study recycling agents (5% RA1 and 8% RA2; percentage in terms of RAP binder weight) and the binders extracted and recovered from the three 45% RAP mixtures. The various binder tests were only conducted on the as-blended and as-extracted binders without further age conditioning. The results are discussed in the corresponding subsections.

3.5.1 Rheological Measurements

Table 3-9 below presents the measured continuous as extracted PG grade for the RAP and the RA treated RAP binders. The addition of RA1 can drop the LTPG of RAP1 and RAP2 by 10.5 and 8 °C respectively, while only decreases the LTPG of RAP3 by 2.8 °C. RA2 can drop the HTPG and LTPG of RAP1 and RAP2 by 6-9 °C, while only decreases of the LTPG of RAP3 by 0.6 °C.

Table 3-9 Continuous PG of RAP and RA treated RAP binders as extracted (no further aging)

Material ID	RAP1	RAP2	RAP3	RAP1 + 5% RA1	RAP2 + 5% RA1	RAP3 + 5% RA 1	RAP1 + 8% RA2	RAP2 + 8% RA2	RAP3 + 8% RA2
Continuous PG Grade	103-4.6	104-5.7	87-26	XX-15.0	XX-13.5	XX-28.8	97.5-8.3	97.1-15.1	79.8-26.6

XX-data not available

Figures 3-20 and **3-21** below summarize the measured ΔT_c and G-R parameter for the RAP and the RA treated RAP binders. Addition of RA1 decreased the ΔT_c value of RAP2 but increased it for RAP1 and RAP3. RA2 increased the ΔT_c value of RAP1, RAP2, and RAP3. RAP1 (untreated, and with both RA1 and RA2) have lowest ΔT_c values. For G-R parameter, both RA drop the G-R parameter of the RAP, indicating the improved properties. RA treated RAP3 (with both RA1 and RA2) have lowest G-R values.

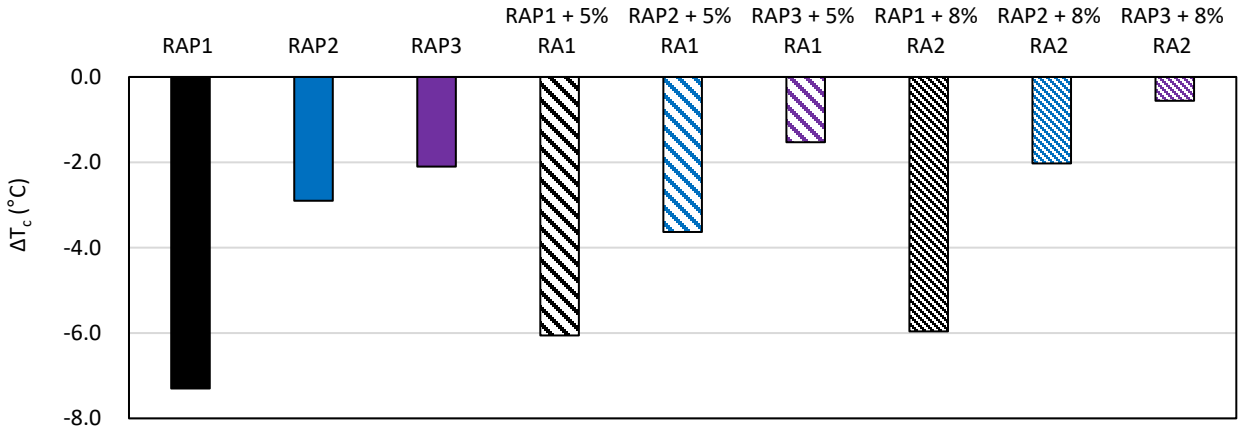

Figure 3-20 ΔT_c parameter of RAP and RA treated RAP samples

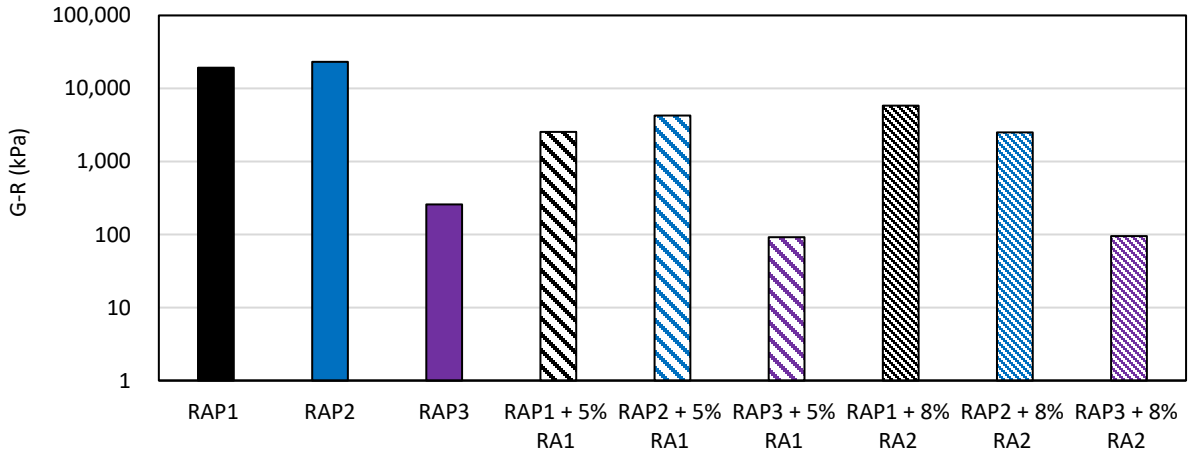

Figure 3-21 G-R parameter of RAP and RA treated RAP samples

Table 3-10 below summarizes the measured continuous PG and rheological parameters for the binders extracted and recovered from the three 45% RAP mixtures. HRAP-B has the worst values of all of the parameters and HRAP-A has the best values.

Table 3-10 Rheological characterization of the extracted and recovered binders

Material ID	HRAP-A	HRAP-B	HRAP-C
PG	75.9-26.9	82.7-22.3	79.2-25.2
ΔT_c Parameter	1.7	-3.2	-0.3
G-R Parameter	32	371.9	148.8

3.5.2 Thermal Analysis

The Tg values measured from the DSC analysis for the RAP and RA treated RAP binders are shown in **Figure 3-22** below. Both RAs can decrease the Tg value of the RAP material. RA2 appears to be more beneficial than RA1 due to the larger decrease in Tg for RAP1 and RAP2, however, RAP3 with RA2 shows a higher Tg value than with RA2. RAP3 with both RA1 and RA2 have the lowest Tg values, indicating potentially better thermal properties.

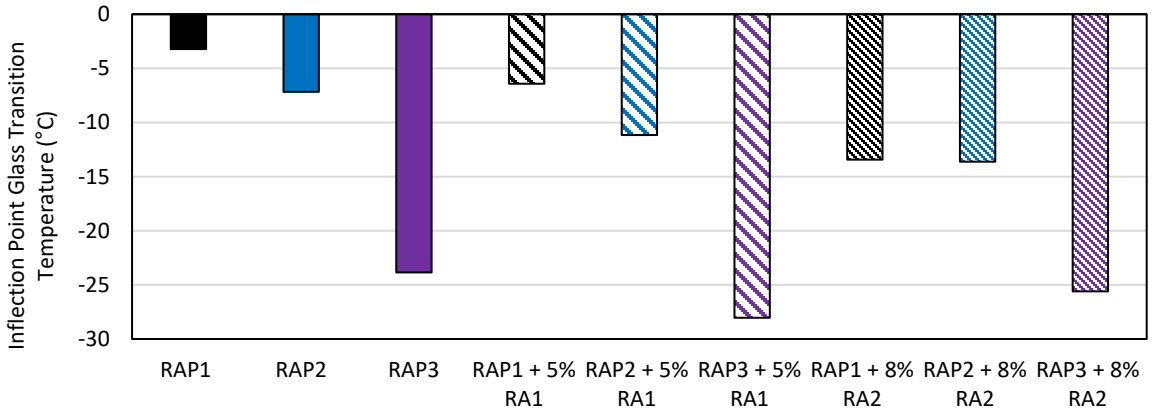

Figure 3-22 DSC analysis of RA treated RAP samples

The Tg values measured from the DSC analysis for the study RAP mixtures (RAP1 with virgin binders A, B, C) are shown in **Figure 3-23** below. Mixture HRAP-C shows the warmest Tg value, while mixture HRAP-B shows the lowest value.

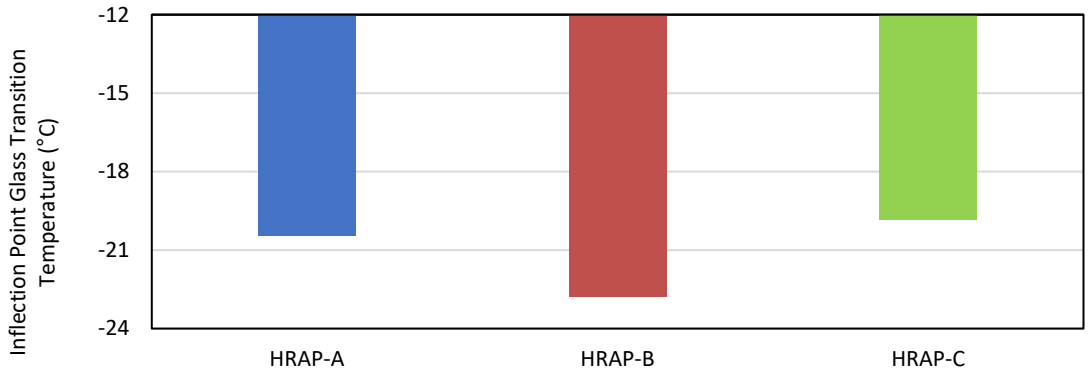

Figure 3-23 DSC analysis of three RAP mixtures

3.5.3 SARA Separation

The CII values measured from the SARA analysis for the RAP and RA treated RAP binders are shown in **Figure 3-24** below. Generally, addition of RA1 can increase the CII value of the three RAPs, while RA2 decreases the RAP CII value. When RA1 is used, RAP3 has a higher CII value while CII values for RAP1 and RAP2 are comparable. When RA2 is used, RAP3 has a lower CII value while CII values for RAP1 and RAP2 are comparable.

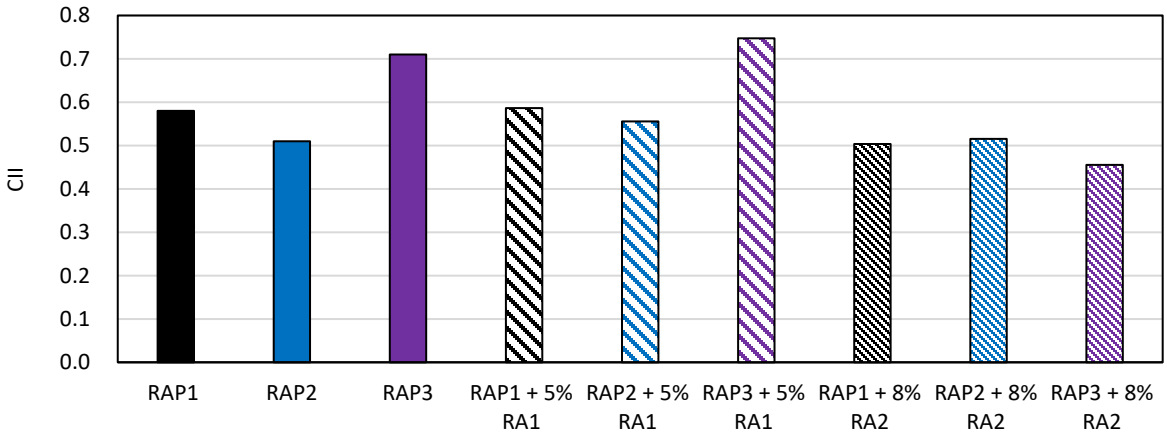

Figure 3-24 SARA analysis of RA treated RAP samples

The CII values measured from the SARA analysis for the study RAP mixtures are shown in **Figure 3-25** below. All mixtures show relatively similar CII values. Mixture HRAP-B and HRAP-C have slightly lower CII values.

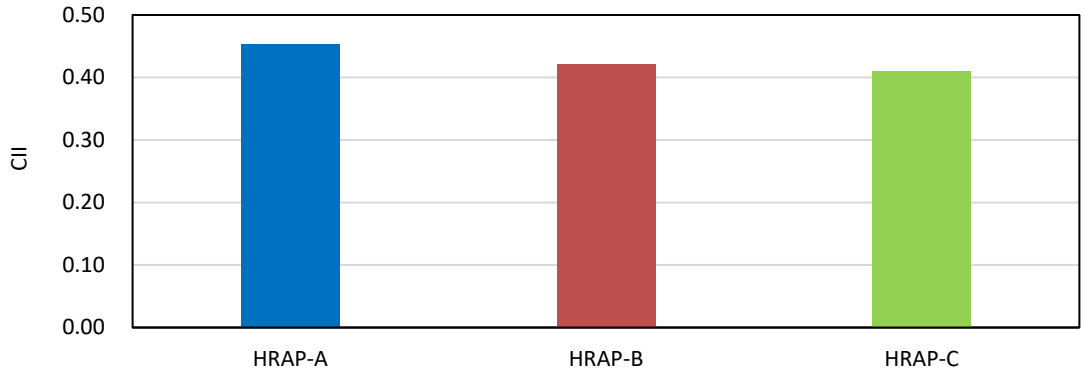

Figure 3-25 SARA analysis of three RAP mixtures

3.5.4 Chromatography Analysis

The HMW, MMW and LMW parameters, as well as the Peak α, β and γ parameters measured from the APC analysis for RAP1, and the RA treated RAP binders are shown in **Figure 3-26** below. Addition of RA1 slightly increases the HMW and MMW of RAP1, while decreasing the Peak β and γ. Comparing the RAP3 with RA1 and RA2, RAP3 with 5% RA1 generally shows higher HMW and Peak γ parameter, while RAP3 with 8% RA2 has the higher LMW and Peak α parameter. Comparing the three RAPs with RA1, RAP1 and RAP2 have comparable values, while RAP3 has lower HMW and MMW but higher LMW parameter, and higher Peak α but lower Peak β and γ parameters.

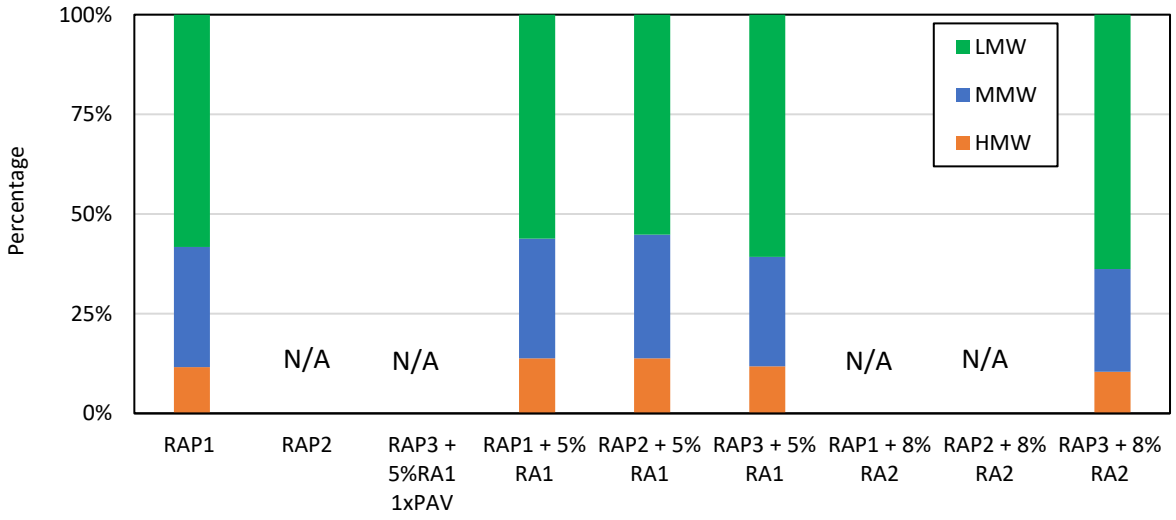

(a)

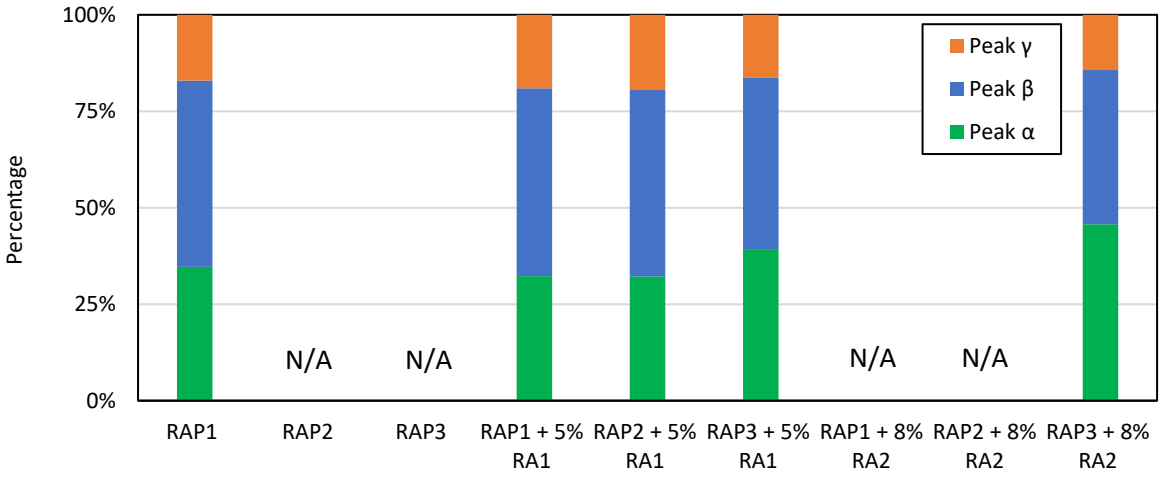

(b)

Figure 3-26 APC analysis of RA Treated RAP samples (a) parameters from slicing method and (b) parameters from deconvolution analysis

The HMW, MMW and LMW parameters, as well as the Peak α, β and γ parameters measured from the APC analysis for the study RAP mixtures are shown in **Figure 3-27** below. Mixture HRAP-C clearly shows the highest HMW indicating a potential compatibility issue, while HRAP-B has the highest LMW. Three mixtures have comparable Peak γ parameters, while mixture HRAP-A shows the highest Peak α value.

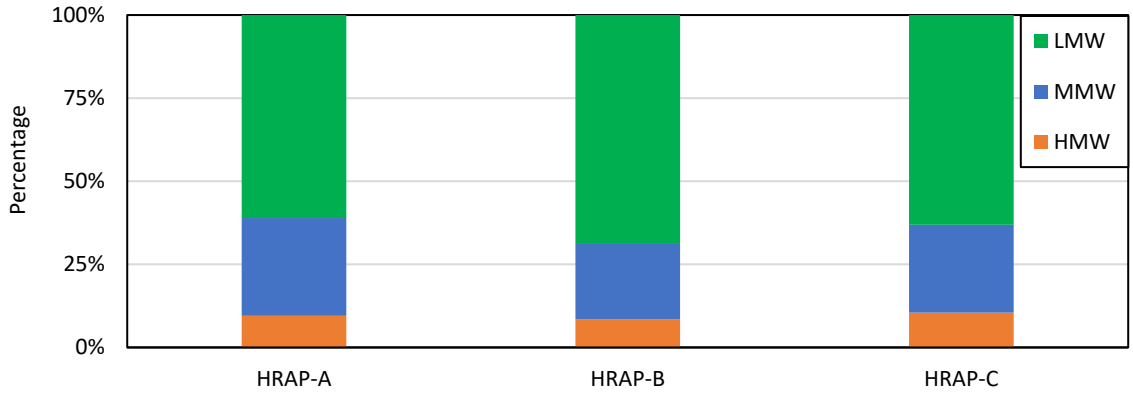

(a)

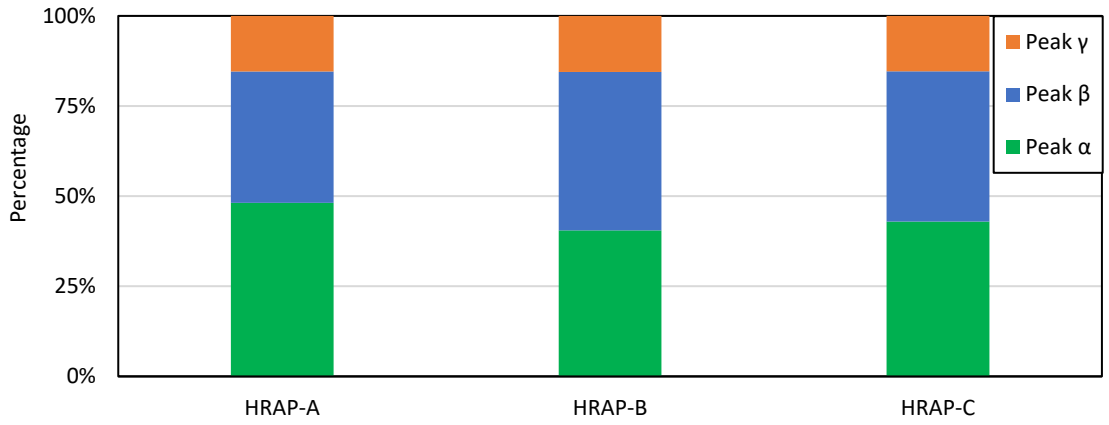

(b)

Figure 3-27 APC analysis of three RAP Mixtures (a) parameters from slicing method and (b) parameters from deconvolution analysis

3.6 CHAPTER SUMMARY

This chapter presented a summary of binder and mixture testing and analysis conducted in order to characterize the core materials. rom Rheological characterization it was observed that RAP1 and RAP2 have warmer PG (both high and low), lower ΔT_c parameter and higher G-R parameter than RAP3. DSC thermal analysis also showed that RAP1 has the warmest Tg after each aging condition indicating the inferior thermal property and potential compatibility issue. Hence, RAP1 was selected as the control RAP due to its inferior properties as compared to RAP2 and RAP3. Furthermore, the rheological, chemical and thermal analysis indicated that addition of RA1 and RA2 can improve the properties of the RAP material when evaluated with short term aging conditions.

The control RAP (RAP1) is blended with three virgin binders to design and generate three RAP mixtures with 45% RAP content (HRAP mixtures). Three corresponding virgin mixtures are also produced which were also designed with similar aggregate gradation to facilitate direct comparison. DTCF testing results indicate that the virgin mixtures show better fatigue properties than RAP mixtures. Mixtures with binder A generally have better fatigue resistance than mixtures with binders B and C. Similar observations were made from mixture fracture tests results (I-FIT and DCT).

Overall, based on the results from the binder and mixture evaluation within this chapter, the rheological characterization of binder and mixture, mixture fatigue and fracture tests, as well as the binder DSC analysis have shown promise to be able to capture the compatible and incompatible binders (virgin and RAP binders). Therefore, these tests are selected for further testing as they were most sensitive and able to differentiate the compatibility in both binder and mixture state.

Chapter 4: IDENTIFICATION OF PROMISING METHOD FOR CHARACTERIZATION OF COMPATIBILITY

4.1 CHAPTER INTRODUCTION

Previous chapter focused on the core material characterization and identified the promising test methods for compatibility evaluation. The main objective of the work conducted within this chapter is to evaluate these test methods and tools to determine those that are sensitive and able to differentiate the compatibility of the binders and mixtures based on the proposed testing plan. The promising methods and tools identified from this chapter are further validated in the next chapters.

4.2 MATERIAL BASE

The material base generated for this chapter is summarized and presented in **Table 4-1** below. Combined with the mixture results from chapter 3, a total of twelve mixtures (3 virgin mixtures, 3 HRAP mixtures, 6 RA treated mixtures) were designed and evaluated within this chapter. It should be noted that this chapter covers testing of control RAP (RAP1) only. Therefore, all the mixtures' and binder blends' ID include HRAP instead of HRAP1 for ease (for example HRAP-A-R1 for mixture having RAP1 (45%), binder A and RA1). This nomenclature is applicable for this chapter only. It should be noted that all LRAP materials have 25% RAP1 while all HRAP materials have 45% RAP1.

Table 4-1 Material base generated and used to identify promising methods for compatibility characterization

	Material Base		Binder/Mixture ID	Testing Methods	Chapter
Binder Evaluation	Virgin Binder	A	V-A	DSC, DSR, APC, SARA	Chapter 3
		B	V-B		
		C	V-C		
	Extracted Binder from HRAP mix	RAP1 + Binder A (HBRR)	HRAP-A		
		RAP1 + Binder B (HBRR)	HRAP-B		
		RAP1 + Binder C (HBRR)	HRAP-C		
	Extracted Binder from RA Treated mix	RAP1 + Binder A (HBRR) + RA1	HRAP-A-R1	DSC, DSR	Chapter 4
		RAP1 + Binder B (HBRR) + RA1	HRAP-B-R1		
		RAP1 + Binder C (HBRR) + RA1	HRAP-C-R1		
		RAP1 + Binder A (HBRR) + RA2	HRAP-A-R2		
		RAP1 + Binder B (HBRR) + RA2	HRAP-B-R2		
		RAP1 + Binder C (HBRR) + RA2	HRAP-C-R2		
Mixture Evaluation	Virgin Mixtures	Binder A + Aggregate A	V-A	E*, DTCF, I-FIT, DCT	Chapter 3
		Binder B + Aggregate A	V-B		
		Binder C + Aggregate A	V-C		
	Mixtures with RAP	RAP1 + Binder A + Aggregate A (HBRR)	HRAP-A		
		RAP1 + Binder B + Aggregate A (HBRR)	HRAP-B		
		RAP1 + Binder C + Aggregate A (HBRR)	HRAP-C		
	Mixtures with RAP and Bio-based RA	RAP1 + Binder A + RA1 + Aggregate A (HBRR)	HRAP-A-R1	E*, I-FIT, DCT	Chapter 4
		RAP1 + Binder B + RA1 + Aggregate A (HBRR)	HRAP-B-R1		
		RAP1 + Binder C + RA1 + Aggregate A (HBRR)	HRAP-C-R1		
	Mixtures with RAP and Petroleum-based RA	RAP1 + Binder A + RA2 + Aggregate A (HBRR)	HRAP-A-R2		
		RAP1 + Binder B + RA2 + Aggregate A (HBRR)	HRAP-B-R2		
		RAP1 + Binder C + RA2 + Aggregate A (HBRR)	HRAP-C-R2		

4.3 EXTRACTED BINDER PERFORMANCE TEST RESULTS

This section focuses on the testing results from the binders that are extracted and recovered from the RA treated RAP materials. The compatibility between two recycling agents (5% RA1 and 8% RA2; percentage in terms of RAP binder weight), three base binders (A, B, and C) together with control RAP material (RAP1) are evaluated in this section. **Table 4-2** summarizes the material combinations that were tested.

Table 4-2 Extracted and recovered blended binder information and aging level

Binder ID	Binder	RAP	RAP Content	Recycling Agent	Aging Level
HRAP-A	A	RAP1	45% by wt of mixture (34% RBR)	None	As-extracted
HRAP-B	B				
HRAP-C	C				
HRAP-A-RA1	A			RA1	As-extracted; 1xPAV; 2xPAV
HRAP-B-RA1	B				
HRAP-C-RA1	C				
HRAP-A-RA2	A			RA2	As-extracted; 1xPAV; 2xPAV
HRAP-B-RA2	B				
HRAP-C-RA2	C				

4.3.1 Rheological Analysis Results (DSR Testing)

Figure 4-1 and **Figure 4-2** summarizes the measured continuous PG for the extracted and recovered binders. The HTPG results for all binders with PAV aging are not presented because the aged binders were too brittle to conduct the grading. The HRAP mixtures with the three binders have different grades, with binder B having the warmest HTPG and LTPG values and Binder A the lowest values. The addition of RA1 increases the HTPG for all three binders in the as-extracted condition while RA2 decreases the HTPG for all three binders; the magnitude of the effect of the RAs is different with each binder.

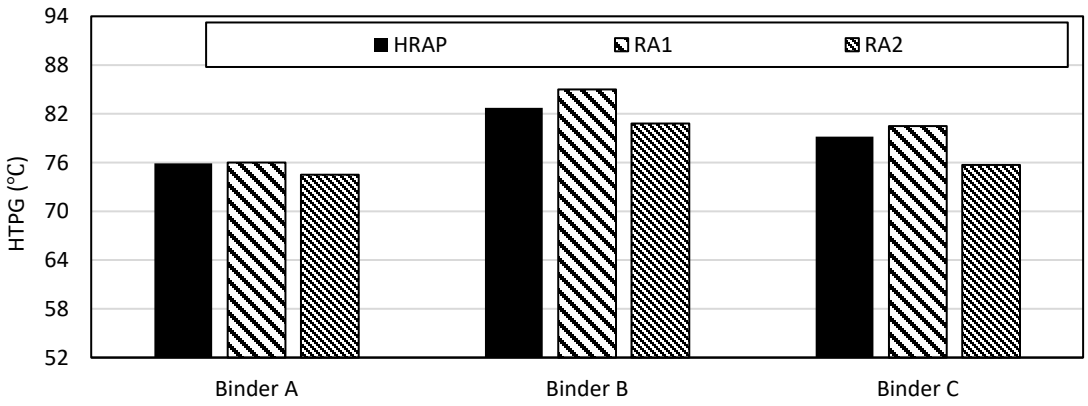

Figure 4-1 HTPG of the extracted and recovered binders

Figure 4-2 shows the LTPG and the percent change from the corresponding HRAP material in the as-extracted condition for the different aging levels. The addition of both RAs initially improves the LTPG, but the benefit is lost after PAV aging and continues to decrease at the higher aging level. The

magnitude of the change is different for the various binders, with binders B and C showing the largest changes (higher aging susceptibility) and warmest LTPG values. This indicates that both RA1 and RA2 may be incompatible with binders B and C together with the RAP1 material.

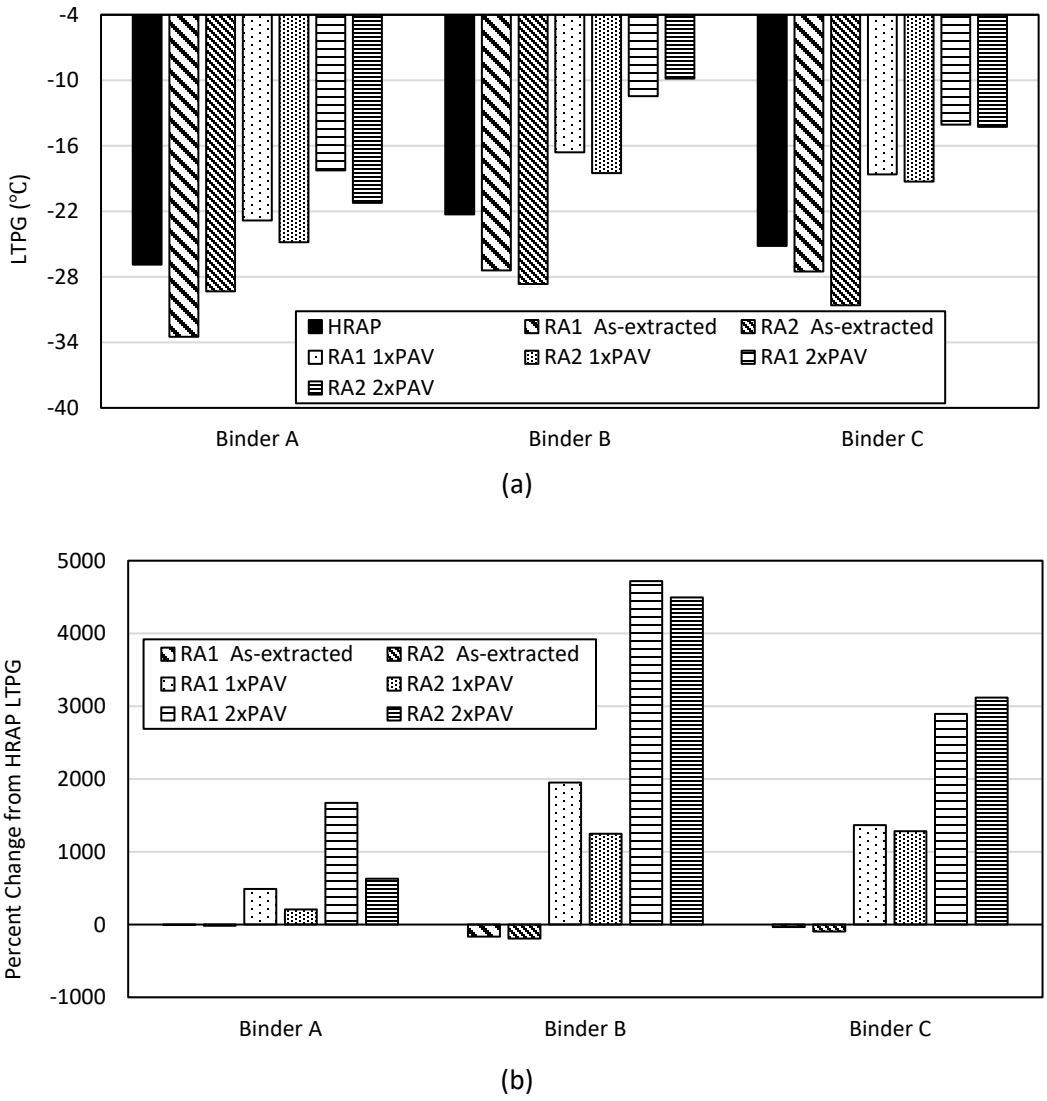

Figure 4-2 Comparison of (a) LTPG values and (b) percent change in LTPG as compared to HRAP materials

Figure 4-3 presents the ΔT_c values for all the binders. All as-extracted binders have ΔT_c values above the currently proposed cracking limit threshold of -5 °C and there is a consistent trend that binder B shows the lowest ΔT_c values, indicating inferior cracking resistance. The inclusion of the RA generally decreases the ΔT_c values for the blended binders, except for binder A where RA2 shows a higher ΔT_c value than the corresponding HRAP binder.

After both levels of PAV aging, all binders with RA1 are close to or exceed the cracking threshold, which indicates severe cracking potential. The ΔT_c values for binders with RA2 are generally better than those with RA1. Similar to the trend observed from the as-extracted materials, binder B has the worst ΔT_c

values at all long-term aging levels and therefore would be most susceptible to cracking. This is consistent with the assumption that binder B is more incompatible as compared to binders A and C.

The observations above indicate that binder B is more incompatible with the RAP1 material, and the RAs as compared to binders A and C. Also, both 1xPAV and 2xPAV can work with cracking limit of -5 °C to show the relative incompatibility of RA1 with all binders. RA2 shows higher compatibility with binder A and binder C together with RAP material.

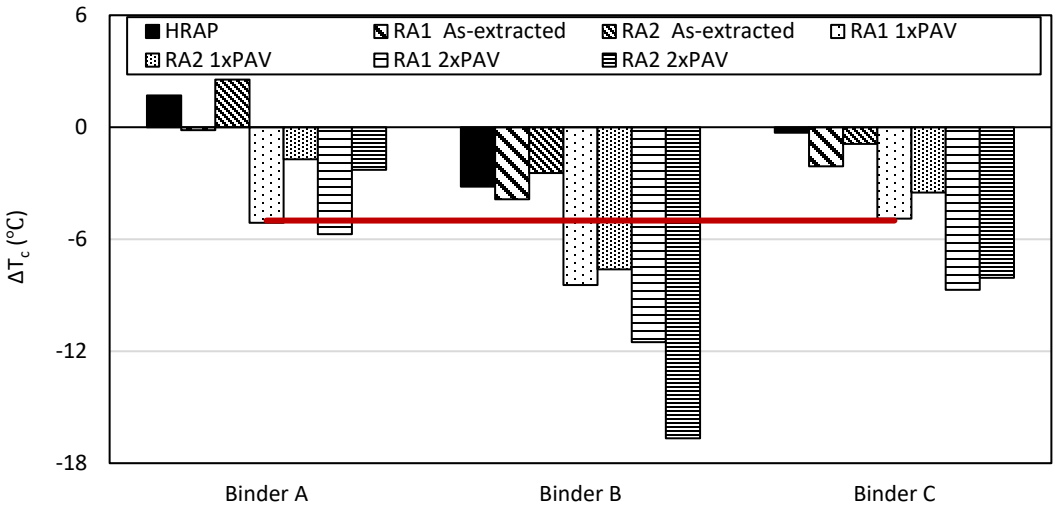

Figure 4-3 ΔT_c parameter of the extracted and recovered binders with aging

Figure 4-4 below shows the G* vs. phase angle of as-extracted binders in the Black space. For all three binders, both RA1 and RA2 show the softening effect and decreased stiffness on the HRAP mixtures. Also, the RA2 treated mixtures show lower G-R values than the RA1 treated mixtures for all three binder types. It indicates that RA2 might have a more significant softening effect on the mixture stiffness. **Figure 4-5** below shows the Black space diagram of the RA treated materials with at different aging levels.

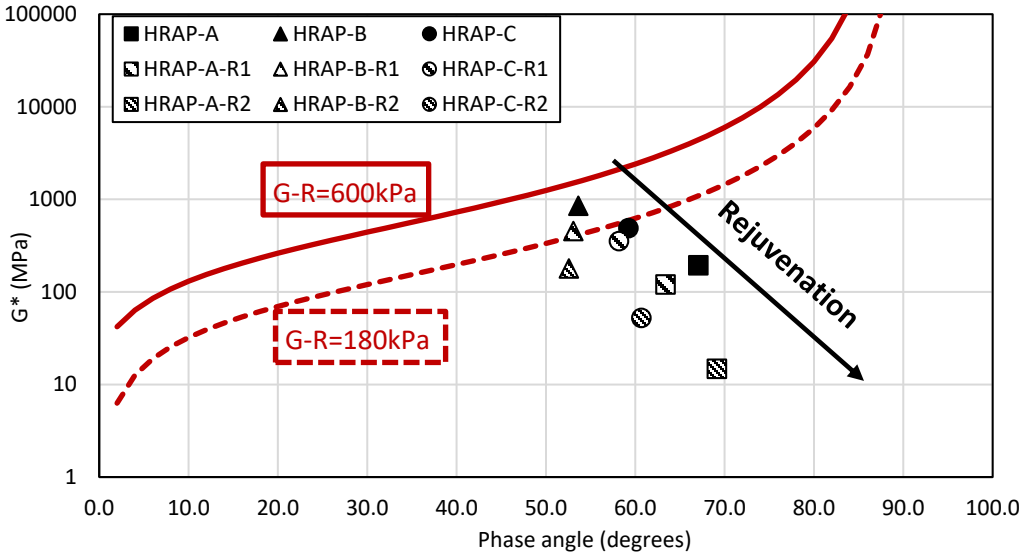

Figure 4-4 G-R Black space diagram for as-extracted binders

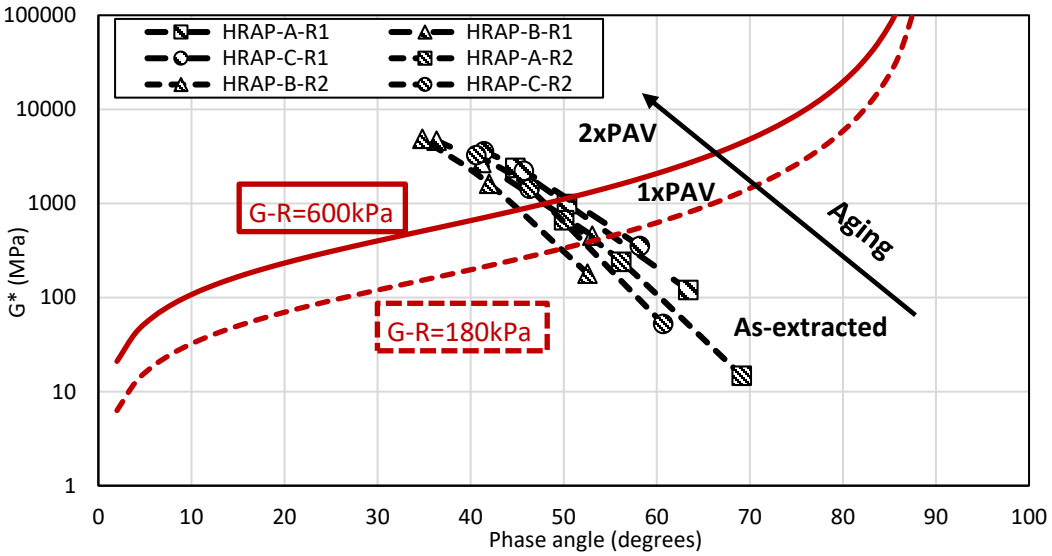

Figure 4-5 G-R Black space diagram for rejuvenated binders with aging

Figure 4-6 below presents the Glover-Rowe (G-R) parameters of extracted and recovered binders at different aging levels and the relative changes with respect to the control materials. All blended binders at the as-extracted level have G-R values that are lower than the cracking threshold of 600 kPa, with binder B having the highest G-R values and Binder A the lowest G-R values. The inclusion of RA improves (lowers) the G-R values for all three binders, with RA2 providing slightly more improvement than RA1. All G-R values increase with aging, with only Binder A material within the cracking threshold limit after 1xPAV. Both binder B and binder C have larger changes with aging, and the relative differences at the 2xPAV compared to the control materials indicate potential incompatibility of the RAP and both RAs. RA1 also shows the potential for incompatibility with binder A after the 2xPAV aging level.

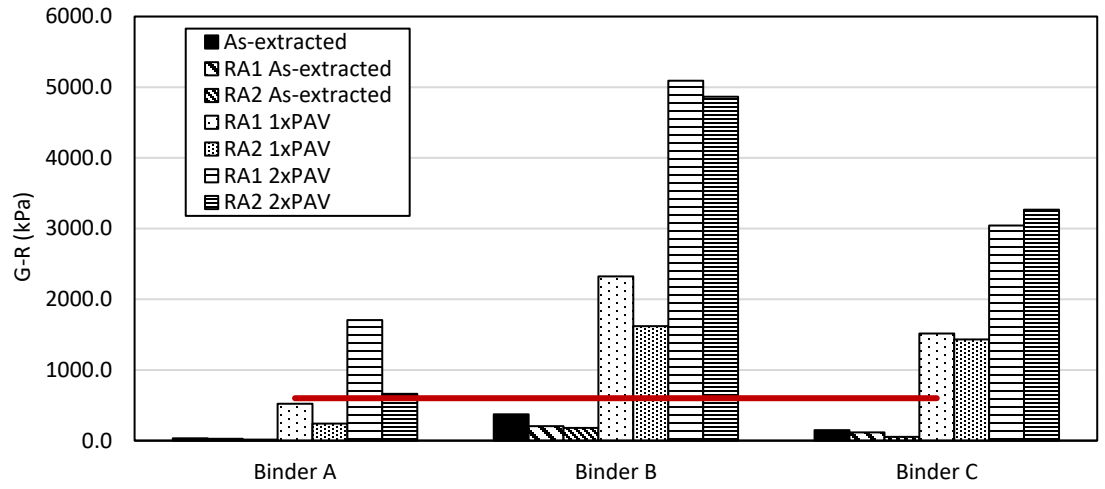

(a)

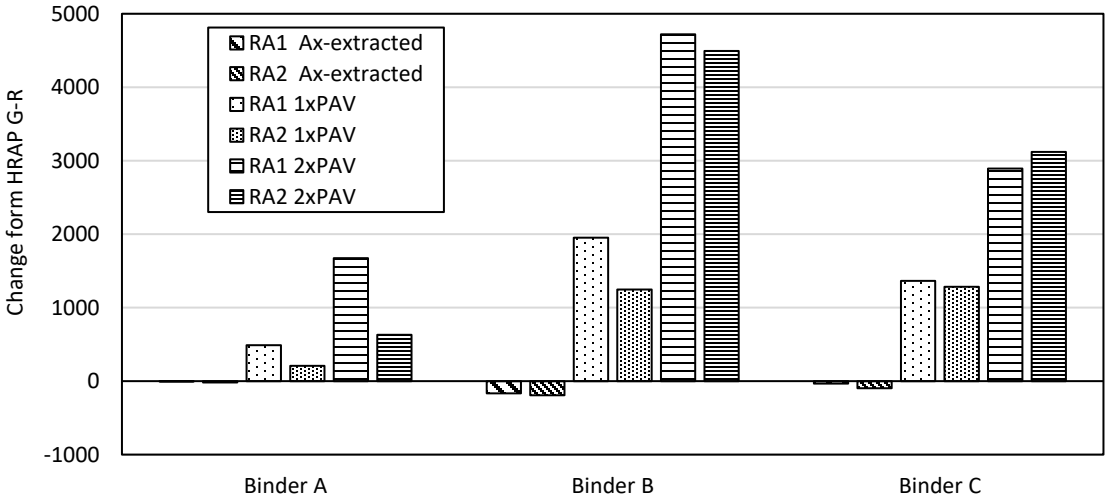

(b)

Figure 4-6 Comparison of (a) G-R parameter and (b) percent change in G-R compared to HRAP materials

Figure 4-7 below shows the R-values for all materials and aging conditions. Binder B consistently has the highest R-value for all conditions. The R-values of the as-extracted binder generally increase with the addition of both RAs and aging levels. There are differences in the R-values of the binder A materials, with the RA1 showing greater changes than RA2, which may indicate incompatibility with RA1 and the RAP1 material with Binder A. However, the R-value does not show differentiation for Binders B and C.

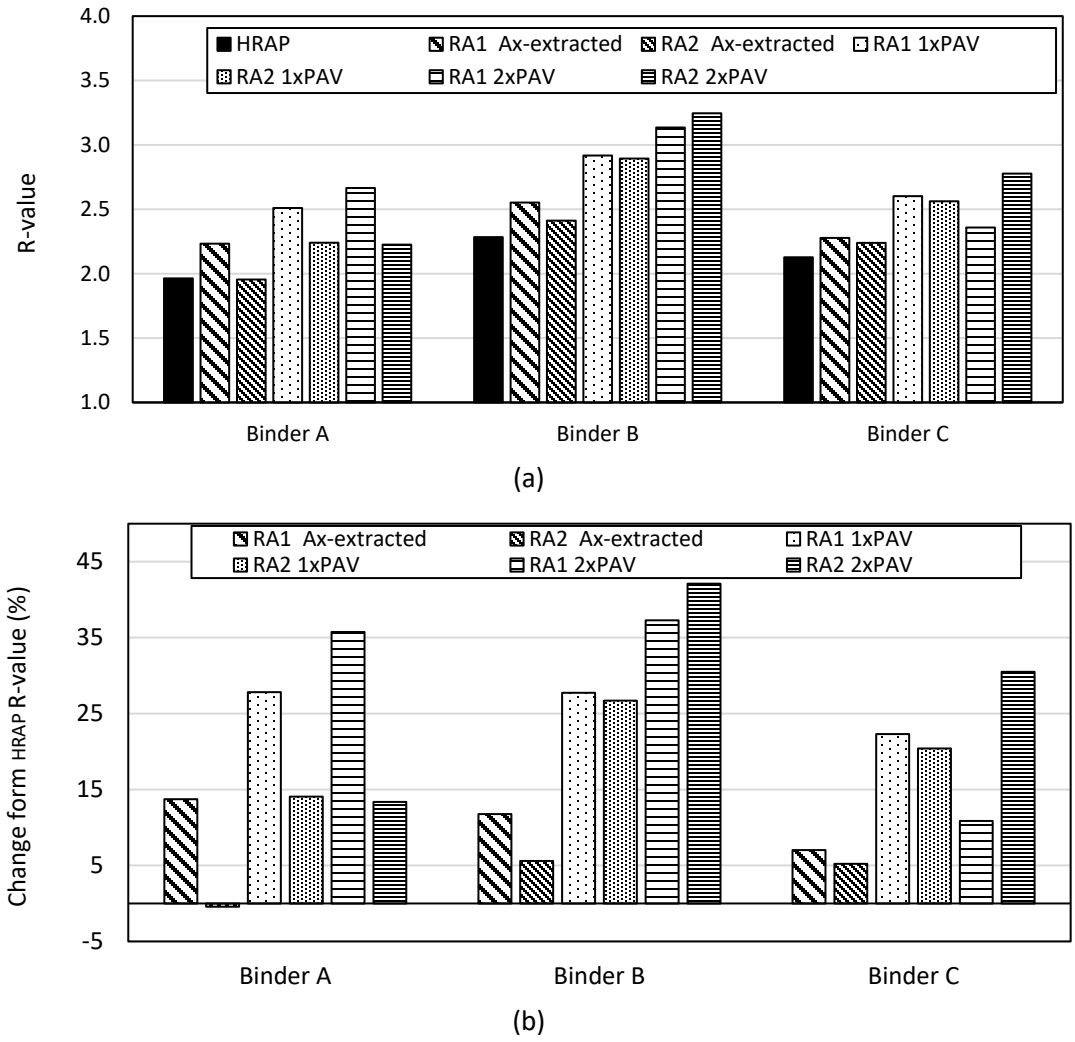

Figure 4-7 Comparison of (a) R-value parameter and (b) percent change in R-value compared to HRAP materials

4.3.2 Thermal Analysis Results (DSC Testing)

Figure 4-8 below shows the Tg_{α}, Tg_{β} and Tg values measured from the DSC test results for the extracted and recovered binders from the 6 RA treated mixtures and corresponding 3 control mixtures. With the inclusion of the RAs, both Tg_{α} and Tg_{β} show decreased values as compared to the corresponding untreated binder. Except binder B showing marginal lower value of Tg_{α} and Tg_{β}, there's no significant trend related to the compatibility from the results. Binder A and C have comparable Tg values which are slightly lower than the value for Binder B. The inclusion of RA results in slightly decreased Tg values, indicating inferior thermal properties. In general, there is no clear trend in the Tg parameter for comparing RA effect on these extracted binders.

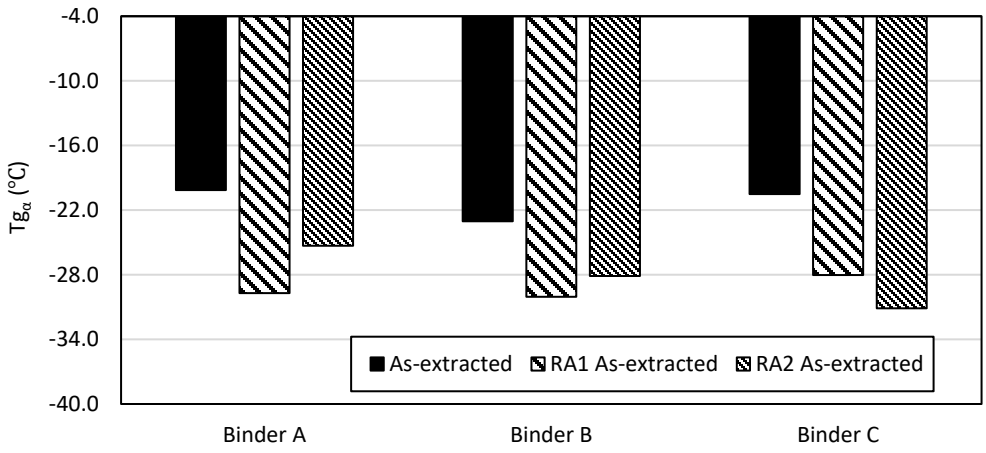

(a)

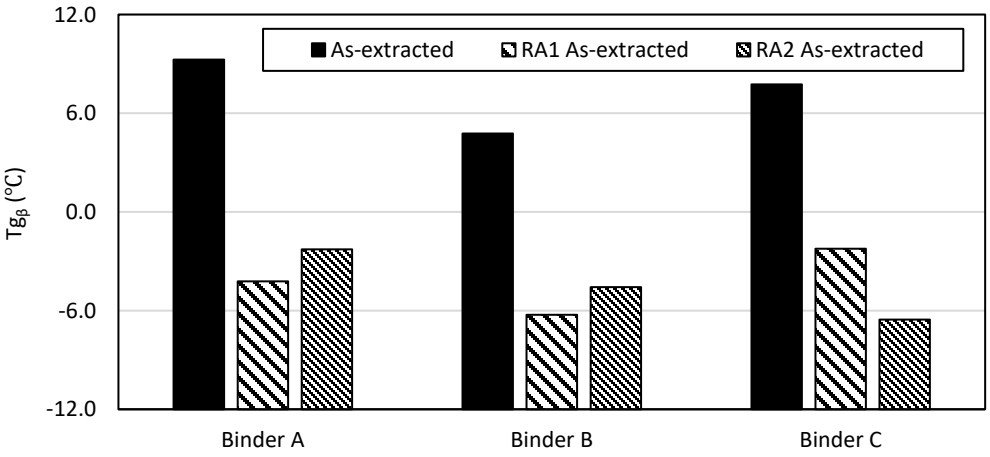

(b)

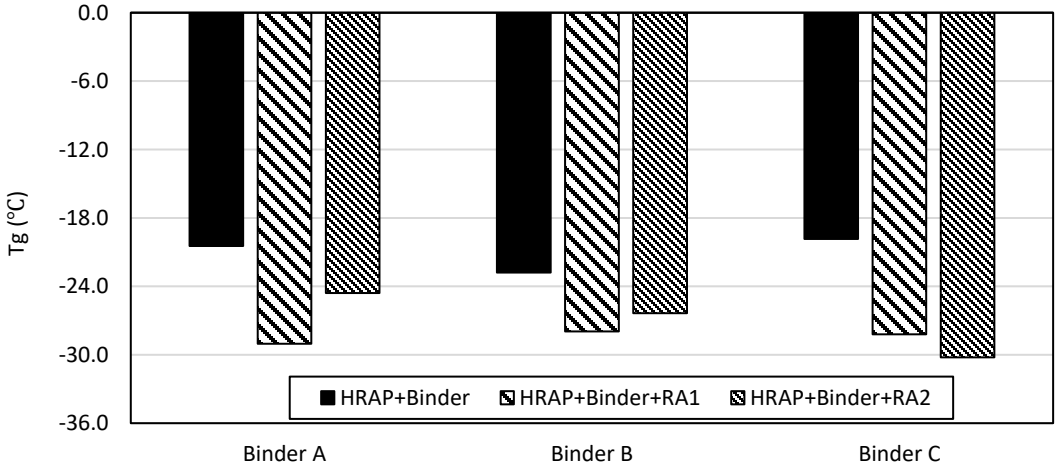

(c)

Figure 4-8 DSC analysis result of extracted and recovered binders: (a) Tg_{α}, (b) Tg_{β}, and (c) Tg

Figure 4-9 shows the ϕ_α parameter for the study binders. As expected, all RA treated binders have lower ϕ_α parameter than the corresponding extracted and recovered HRAP binders. The low ϕ_α parameter for binder B indicates that both RA1 and RA2 are potentially incompatible with Binder B and RAP1 material.

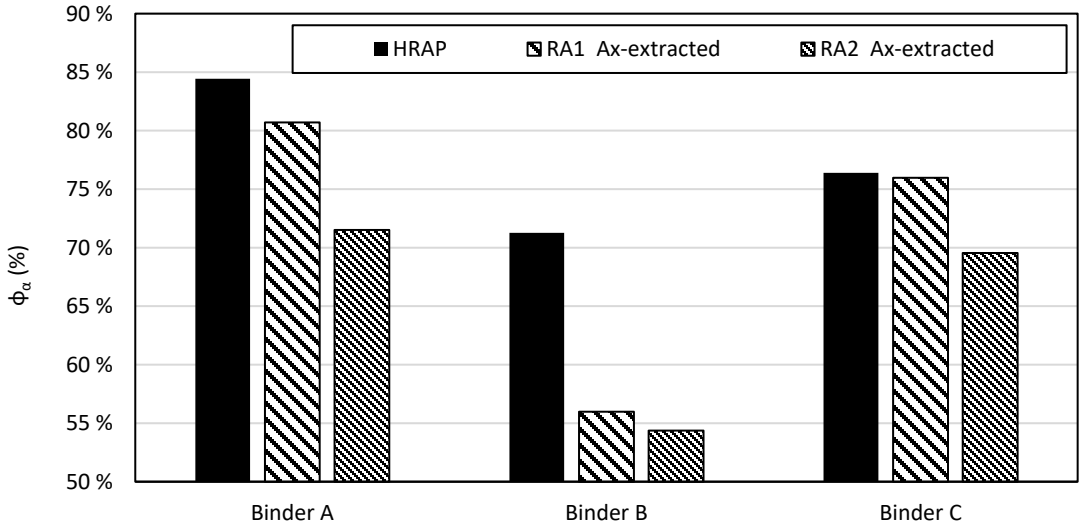

Figure 4-9 ϕ_α parameter for extracted and recovered binders

4.4 MIXTURE PERFORMANCE TEST RESULTS

In this section, results of various mixture tests on the lab-produced samples with 45% RAP and recycling agents are compared with their control groups (45% RAP without RA) and virgin mixtures (without RAP or RA).

4.4.1 Rheological Properties

Dynamic modulus and phase angle master curves constructed from the complex modulus testing are presented in **Figure 4-10**. Each series represents an average of three replicates. Compared to virgin mixtures, all HRAP mixtures show higher |E*| values and lower phase angle over all frequencies. The mixtures with binder A have significantly lower dynamic modulus and higher phase angles for both virgin mixtures and HRAP mixtures than those mixtures blended with binder B and binder C. The |E*| values for HRAP mixtures with binder B and binder C are statistically similar over all frequencies (based on t-test with $\alpha = 0.05$). These trends are expected with the binder grades for the different mixtures.

The general trends observed from the RA mixtures show that both RAs have a softening effect and relaxation improvement on HRAP mixtures, but not to the level of the virgin mixtures. Also, the comparison in phase angles shows binder B might have potential incompatibility with the HRAP-B, and RA1 seems to have lower incompatibility than RA2. In general, both the dynamic modulus and phase angles show the capacity of compatibility identification, but the phase angle master curves perform better in terms of screening and differentiating the compatibility between the different binders.

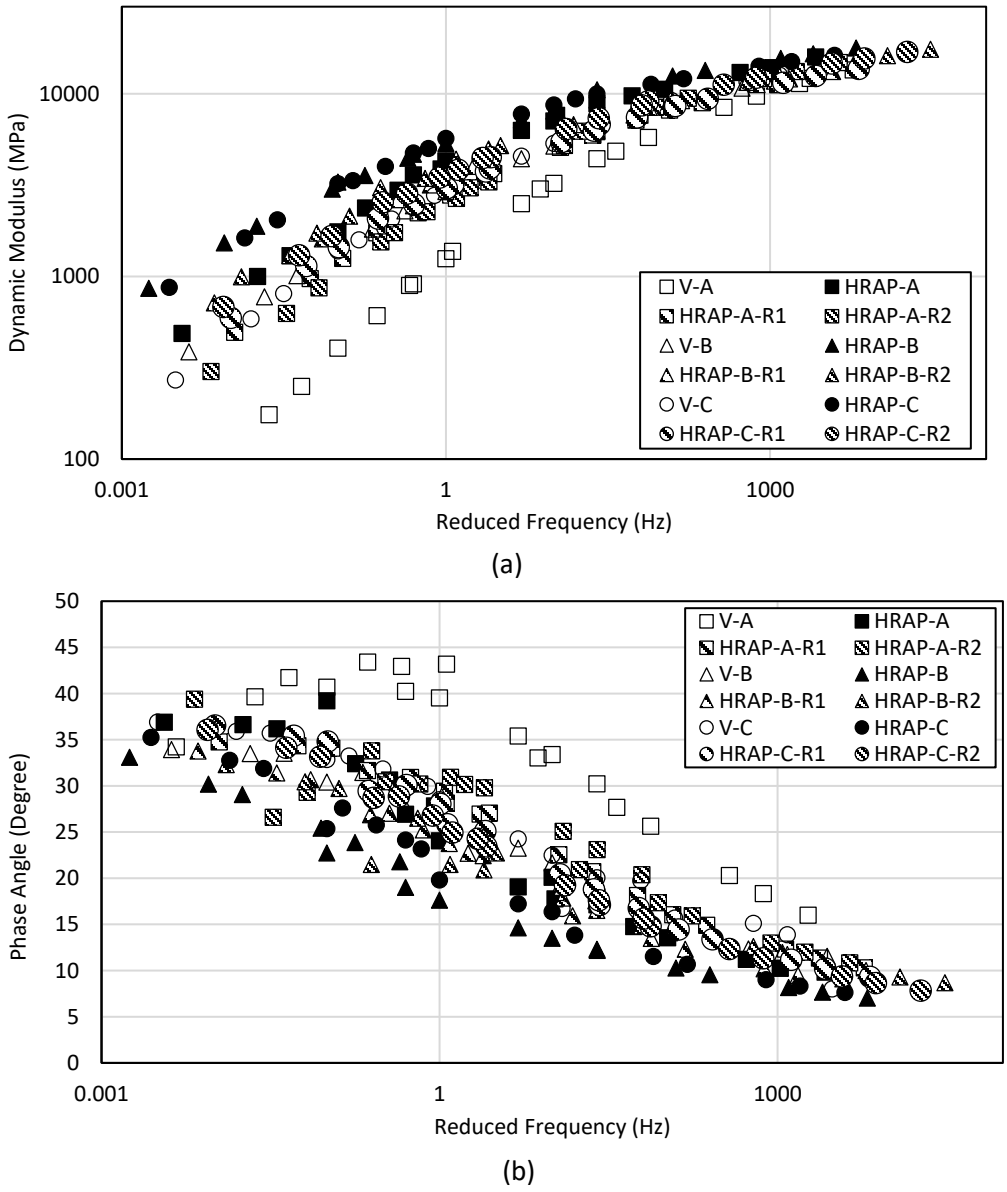

Figure 4-10 Master curves of (a) dynamic modulus on a logarithmic scale and (b) phase angle (δ) for study mixtures (ref = 20 °C)

Several rheological based mixture performance parameters, such as cracking parameter G-R_m and rutting parameter CMRI, can be calculated from the |E*| and phase angle master curves and are presented in **Figure 4-12** and **Figure 4-13**. The general trend shows that all three HRAP mixtures have significantly higher G-R_m and CMRI values than the three virgin mixtures. The results indicate deterioration of the cracking resistance and improvement of the rutting resistance with the inclusion of the RAP material. The impact of the addition of RAP is different for the mixtures with binders B and C, although the two virgin binders have the same PG. All RA treated mixtures show lower G-R_m values than the corresponding HRAP mixtures and higher G-R_m values than virgin mixtures. However, there is no consistent trend observed from the CMRI values of RA treated mixtures. Also notice that the high value

for HRAP-RA2 for binder C is likely a result of an abnormal similarity between the f_A and f_B values in the CMRI calculation.

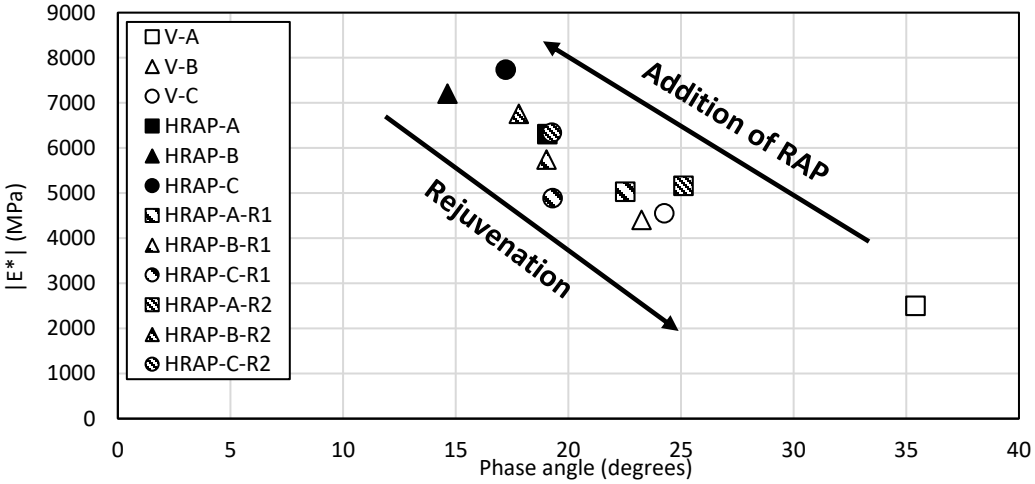

Figure 4-11 Black space diagram for the study mixtures

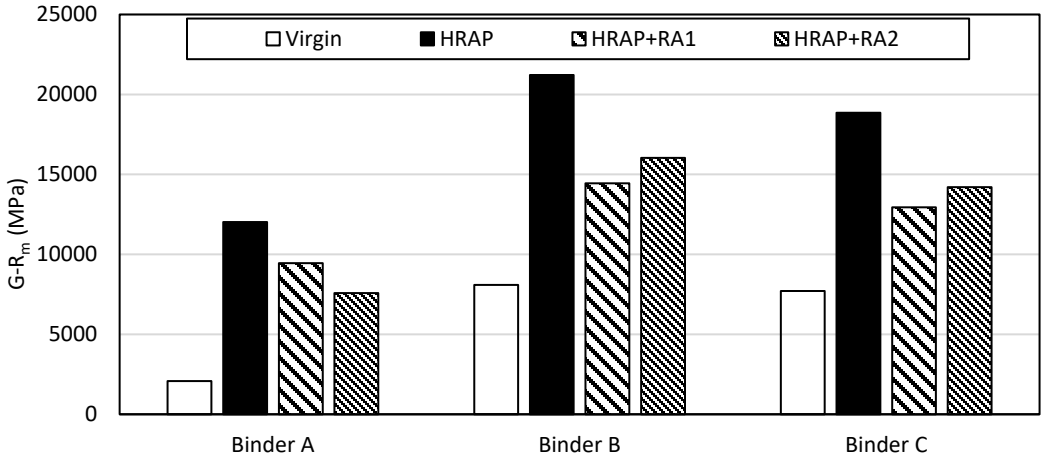

Figure 4-12 G-R_m parameter for the study mixtures

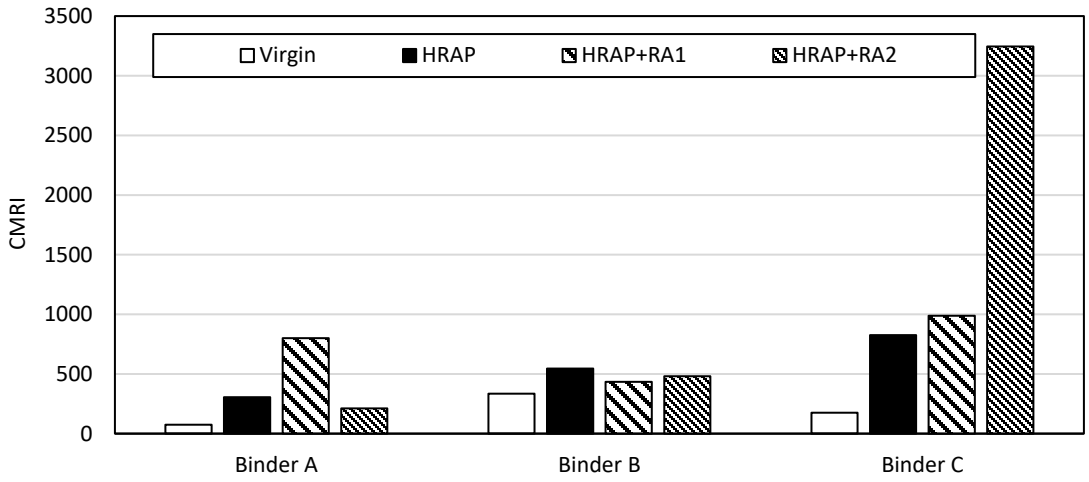

Figure 4-13 CMRI parameter for the study mixtures

4.4.2 Illinois Flexibility Index Semi-Circular Bend (SCB) Test (I-FIT)

Figure 4-14 and **Figure 4-15** show the intermediate-temperature fracture energy (G_f), FI and RDCI parameters determined using the I-FIT testing for the 12 study mixtures. All HRAP mixtures generally show significantly lower fracture energy or indices, as expected. The only exception is materials produced using binder A, where the fracture energy for HRAP-A shows comparable fracture energy with V-A. As expected, binder A mixtures with lower PG (58-28) show the highest values for both indices, indicating better cracking resistance than the other two mixtures with PG 64-22 binders. The lower values for the mixtures with binder B and C indicate inferior cracking properties and potential incompatibility. The inclusion of RA improves the properties as compared to the corresponding HRAP mixtures with RA1 producing higher values of FI and RDCI values than RA2 for all binders; this indicates there may be more incompatibility with the RA2 material, particularly with binder C. However, there is no consistent trend observed from the G_f.

The G_f parameter shown in the **Figure 4-14** is demonstrating that RA1 product may be incompatible with binder A together with control RAP material. This is observed as lower values for G_f for RA treated HRAP-A mixtures as opposed to that without RAs. Comparing results for binder B and C, it can be observed that virgin binder C and control RAP may have greater incompatibility (also discussed in Chapter 3 report), however, RA1 and RA2 material appears to alleviate this incompatibility.

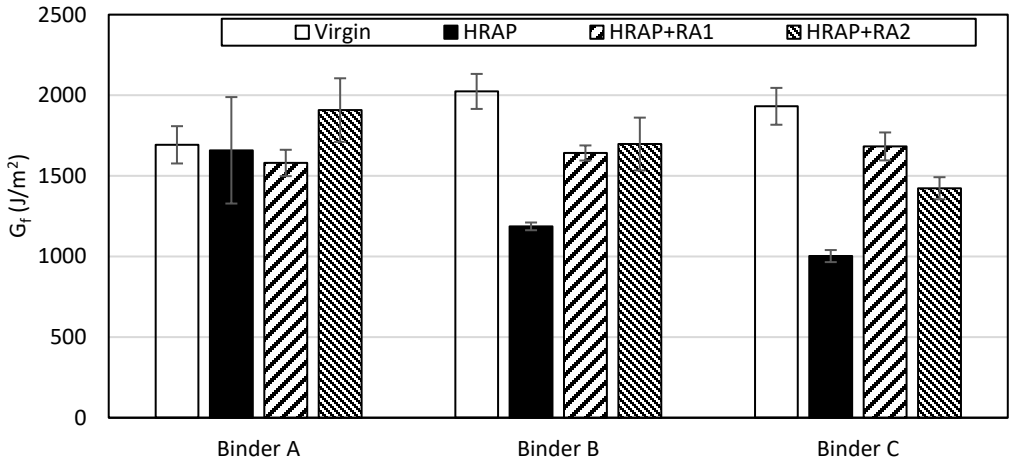

Figure 4-14 G_f parameter measured from I-FIT on RA treated mixtures

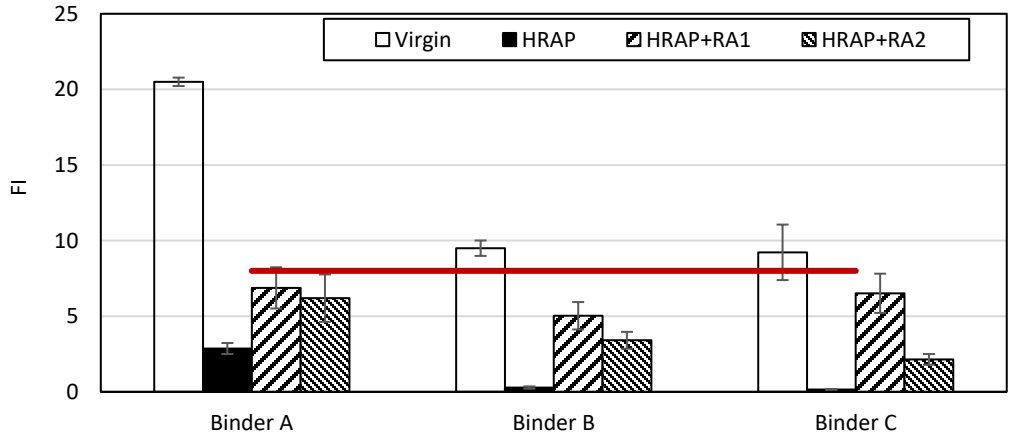

Figure 4-15 FI parameter measured from I-FIT on RA treated mixtures

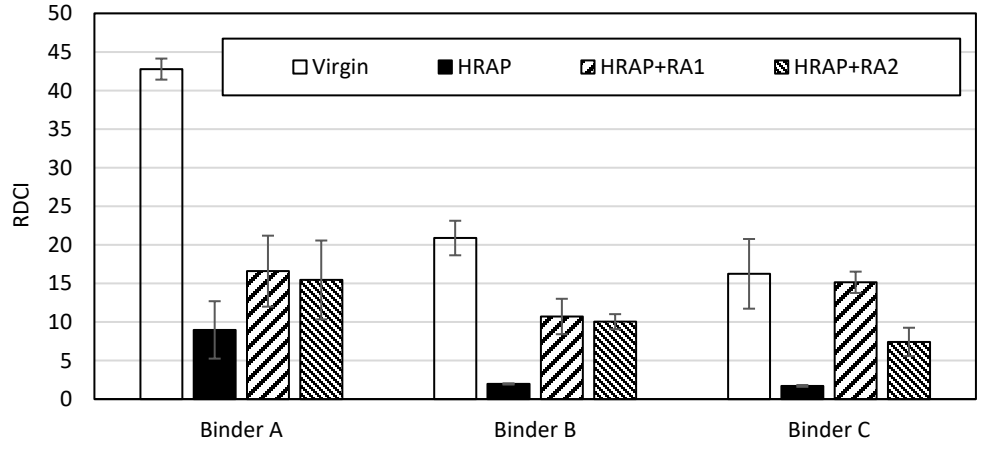

Figure 4-16 RDCI parameter measured from I-FIT on RA treated mixtures

4.4.3 Disk-shaped Compact Test

Figure 4-16 and **Figure 4-17** below show the calculated G_f and FST parameter for the study mixtures. The RAP mixtures have lower G_f and FST values than the virgin mixtures, as expected. Notice that both the virgin and RAP mixture with binder A have the highest G_f and FST values. Mixtures with binder B have slightly higher G_f and FST values than the mixtures with binder C. All virgin mixtures and RAP mixture with binder A meet the current threshold value of 450 J/m^2 for the G_f parameter. With the inclusion of RA, mixtures show higher FST values, indicating an improvement in thermal cracking resistance. However, there is an inconsistent trend with the G_f parameter and additional tests are necessary to confirm the results for the binder A mixtures. From the RA perspective, the mixtures treated RA1 generally show higher G_f and FST values than RA2. It indicates RA1 might have higher compatibility with material in terms of the low temperature properties.

The G_f parameter demonstrates that for binder A and binder B mixtures, both RA1 and RA2 products may be incompatible with binder A and B together with the control RAP material. This is due to lower values for G_f for RA treated HRAP-A mixtures as opposed to that without RAs and only marginal improvements in G_f for HRAP-B mixtures. Comparing results for binder B and C, it can be observed that virgin binder C and control RAP may have greater incompatibility (also discussed in chapter 3), however, RA1 and RA2 material appears to alleviate this incompatibility.

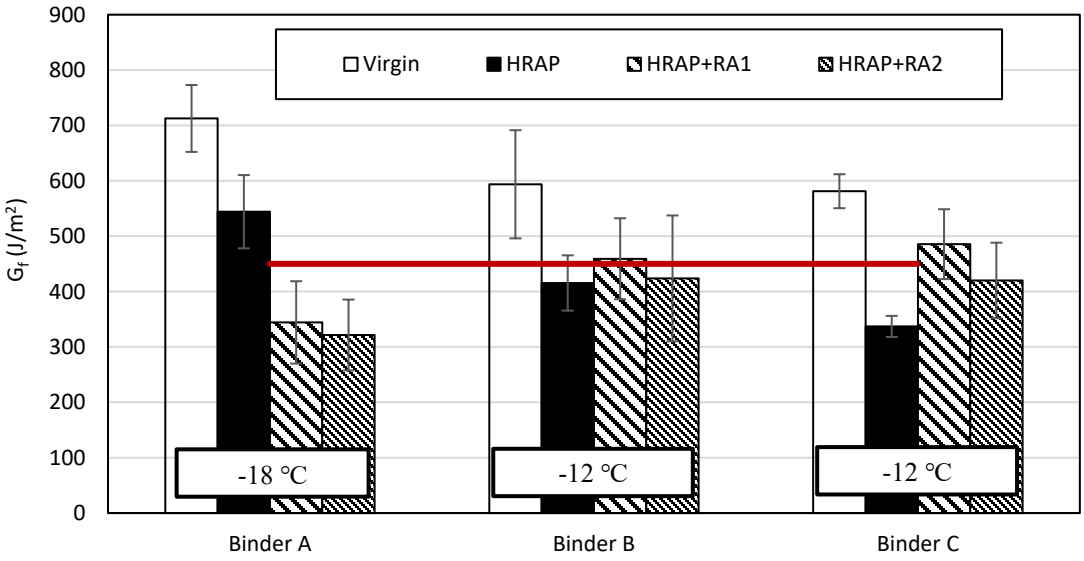

Figure 4-17 G_f parameter measured from DCT

The FST parameter in **Figure 4-18** represents that both RA1 and RA2 may be incompatible with binder A together with the control RAP material. Comparing results between binders A B and C, RA treated HRAP-A mixtures shows lowest improvement of the FST values based on the similar level of HRAP mixtures.

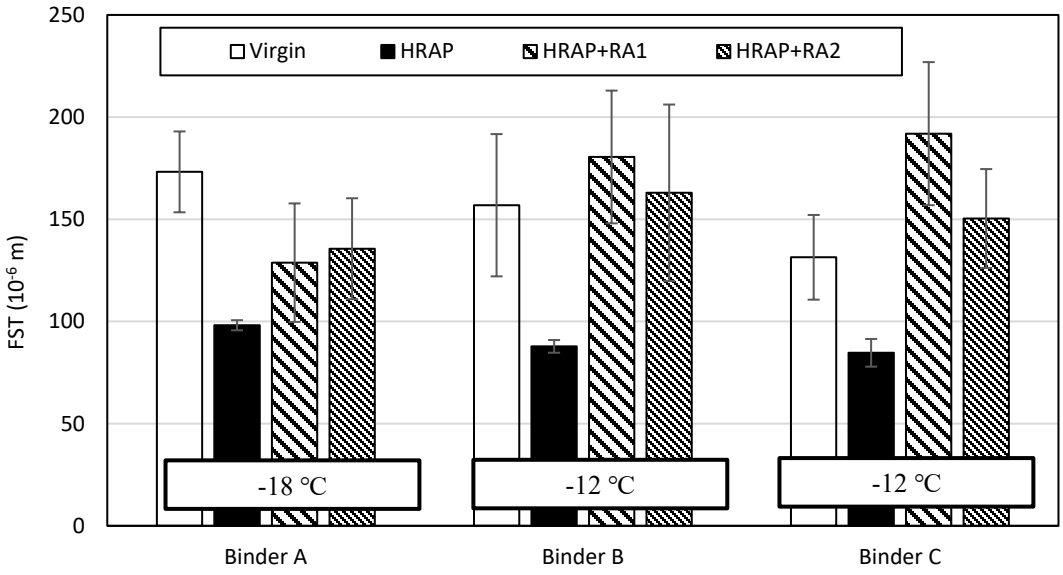

Figure 4-18 FST parameter measured from DCT

4.5 STATISTICAL ANALYSIS OF TESTING RESULTS

In this section, the correlations between mixture testing parameters and corresponding extracted and recovered binder parameters are evaluated using various statistical methods. The evaluated materials include control RAP mixtures with 45% RAP1 blended with three different binders, six RA treated RAP mixtures with 45% RAP and 2 RAs and the corresponding extracted and recovered binders.

4.5.1 Statistical Correlation Methods

Pearson correlation coefficient and Hoeffding's D correlation analysis are selected as the statistical methods in this study. The frequently used Pearson's correlation method is only able to capture linear relationships, so Hoeffding's D correlation method is selected as a supplementary tool to screen the significant relevance between the results.

The Pearson correlation coefficient is a widely accepted measure of the linear relationship between two specified variables. The Pearson correlation coefficient 1 indicates the case of a positive linear relationship, and -1 indicates the case of a negative linear relationship. The closer the coefficient is to either -1 or 1, the stronger the correlation between the variables.

Hoeffding's D correlation is a statistical method which can be used to infer nonlinear and non-monotonic relationships between the variables. The parameter D represents a nonparametric measure of dependence, by testing the independence of two study variables. The intuitive idea of Hoeffding's D correlation is to calculate the distance between the distribution under the null hypothesis and the empirical bivariate distribution. The D coefficient measurements fall between -0.5 and 1, with a larger value of D coefficient indicating a stronger non-linear relevance between parameters. Generally, if the

analysis between two variables shows a low Pearson coefficient but a high Hoeffding's D coefficient, it represents a potential non-linear relationship may exist between the two study parameters.

4.5.2 Binder-Mixture Correlation Analysis

The paired correlation coefficients between 9 mixture testing parameters and 11 binder testing parameters were calculated and summarized in a correlation matrix format. The two different correlation coefficients are presented in this section to preliminarily screen for significant linear/non-linear relationships. The Pearson correlation coefficients between the binder properties and the mixture properties are shown in **Table 4-3**. Values closer to 1 or -1 are shaded by green color indicating the stronger positive/negative relationship between the two parameters. The intensity of the color represents the strength of the correlation. Those correlations with a coefficient below 0.1 are not shaded with color, while those strong correlation (coefficients > 0.7) are also marked bold and italic.

As shown in the **Table 4-3**, most of the fracture (except for G_f@DCT) parameters, D^R fatigue parameter and G-R_m rheological parameter show fair correlation (|correlation coefficient|>0.5) with one or multiple binder parameters. As a contrast, there is lack of significant correlation between G_f@DCT with all the binder parameters. This might be due to the fracture energy showing a high variability at low temperature. All three intermediate temperature fracture parameters from I-FIT testing show moderate to strong negative correlation with most of the binder parameters (except for R value, HTPG, ΔT_c, and ϕ_α). Compared with I-FIT parameters, the low temperature fracture parameters show more significant correlation with thermal parameters from DSC testing than the rheological parameters. The two fatigue parameters D^R and S_{app} generally show similar trends in terms of the correlations, while D^R is observed to have a relatively stronger relationship with binder properties especially for T_c(S). The mixture rheological parameter G-R_m generally shows a positive relationship with all the rheological binder parameters, while the correlation between mixture G-R_m and thermal binder parameters are lower but still significant. As for the rutting parameter CMRI, there's no significant correlation observed with the theoretical parameter, while CMRI shows moderate correlation with the DSC thermal parameter (except for ϕ_α).

From the binder's perspective, rheological parameter R value, HTPG and ΔT_c and thermal parameter ϕ_α do not show a strong relationship with any of the mixture parameters. The most promising binder parameter is T_c(S), which shows significant correlation with almost all mixture parameters including fracture properties. By contrast, T_c(m), LTPG and binder G-R parameter show strong relationships with intermediate cracking and mixture G-R_m, but those parameters show the shortcomings in presenting low temperature cracking and fatigue cracking. As for the thermal binder parameter from DSC testing, Tg_α, Tg_β and Tg show a similar trend for correlation with mixture properties, while Tg shows slightly stronger relevance with fatigue parameters and the rutting parameter.

Table 4-3 Pearson correlation coefficients between the corresponding mixture and binder parameters

			Mixture Properties								
			Fracture Parameters					Fatigue Parameters		Rheological Parameters	
			G_f@I-FIT	FI	RDCI	G_f@DCT	FST	D^R	S_{app}	G-R_m	CMRI
Binder Properties	Rheological Parameters	R	-0.09	0.00	-0.10	0.36	0.49	-0.38	-0.22	0.22	0.09
		HTPG	-0.14	-0.08	-0.24	0.47	0.26	-0.34	-0.18	0.47	-0.27
		T_c(S)	-0.35	-0.46	-0.52	0.14	-0.56	***-0.78***	-0.66	0.60	-0.29
		T_c(m)	-0.44	-0.47	-0.60	0.45	-0.25	-0.41	-0.25	***0.79***	-0.19
		ΔT_c	0.22	0.12	0.25	-0.51	-0.35	0.26	0.10	-0.44	-0.08
		LTPG	-0.32	-0.43	-0.55	0.39	-0.33	-0.23	-0.06	***0.71***	-0.32
		G-R	-0.36	-0.39	-0.50	0.51	-0.08	-0.19	-0.02	***0.74***	-0.21
	DSC Parameters	Tg_α	-0.23	-0.35	-0.35	-0.07	-0.65	-0.03	-0.20	0.40	-0.47
		Tg_β	-0.36	-0.40	-0.39	-0.01	-0.66	0.18	0.01	0.43	-0.37
		Tg	-0.24	-0.41	-0.40	-0.09	-0.63	-0.34	-0.50	0.45	-0.52
		ϕ_α	-0.13	0.11	0.16	-0.19	-0.46	0.48	0.32	-0.18	0.01

Table 4-4 below shows the Hoeffding's D correlation matrix. The values of Hoeffding's D coefficients are generally between -0.02 and 0.21, which indicates relatively weak nonlinear correlations. In other words, a low value of Hoeffding's D coefficients indicates there is not a strong non-monotonic relationship between any pairs of mixture and binder parameters.

Table 4-4 Hoeffding's D correlation between the corresponding mixture and binder parameters

			Mixture Properties						
			Fracture Parameters					Rheological Parameters	
			G_f@I-FIT	FI	RDCI	G_f@DCT	FST	G-R_m	CMRI
Binder Properties	Rheological Parameters	R	-0.01	-0.01	-0.01	0.06	0.04	0.03	0.09
		HTPG	-0.01	-0.02	0	0.03	0.01	0.03	0.01
		T_c(S)	0.05	0.01	0	-0.02	0.18	0.02	0.01
		T_c(m)	0.01	0.01	0.03	0.01	0.03	0.11	0
		ΔT_c	0	-0.02	0.01	0.07	0.01	0.05	0.08
		LTPG	0	0.02	0.03	-0.01	0.1	0.07	-0.01
		G-R	0	0.01	0.04	0.04	-0.01	0.21	0.05
	DSC Thermal Parameters	Tg_α	0.04	0	0.01	-0.02	0.11	0.01	-0.02
		Tg_β	0.01	0.01	0.05	-0.01	0.07	0.01	-0.02
		Tg	0.03	0.04	0	-0.01	0.15	0.03	0.05
		ϕ_α	-0.01	0.03	0.03	-0.01	0.02	0	0.01

In summary, the G-R_m parameter calculated from the mixture complex modulus testing shows the most promising correlation with many binder properties. As a mixture cracking parameter, the G-R_m shows the strong relationship (correlation coefficients >0.7) with those fracture related rheological binder parameters and have a fairly good relationship with the thermal parameter as well. Thus, the G-R_m

parameter is considered as the critical parameter for compatibility characterization in the next step of the analysis. Also notice that the FST parameter from the DCT test shows good relationship with binder thermal properties and the FI parameter from the I-FIT test shows both good relationship with binder rheological and thermal properties. The FST and DCT parameter is also evaluated as a fallback option after G-R_m in the next stage.

4.5.3 Statistical Analysis by Comparing Means

The ability of a test or method to differentiate the effect of different binder types and recycling agents is very important for compatibility characterization. The connecting letter analysis was conducted on replicates for 6 mixture fracture indicators (G_f and FST from DCT test; G-R_m Parameter from E* test; G_f, FI and RDCI from I-FIT test). This report can be used to assess the sensitivity of a test or indicator by means of showing how many groups can be classified statistically and how each group is different from another groups. In the report, group letter A indicates the group has the best value of the property with respect to cracking resistance. Materials with a different group letter (e.g., B) are statistically significantly different. If there's a connecting letter (e.g., AB), it indicates can still be distinguished as a different group, but are statistically part of both groups (e.g., A and B).

Table 4-5 below presents the connecting letter report for the parameters calculated for each of the nine mixtures. The DCT G_f at low temperature fails to differentiate any of the mixtures, since all measurements fall into the same group. The FST parameter not only shows the ability to discriminate between the RA-treated mixtures but also can classify the effect of the binder and RA types. The connecting letter report for FST shows that the combination of RA1 with binder B produces the best FST value, followed by the combination of RA1 and binder C. The significantly different value of FST for these combinations may indicate better compatibility. The connecting letter report indicates that RA2 may have lower compatibility than RA1 with all binders, since all RA2 treated mixtures were classified as "ABC". It also shows that binder A might have lower compatibility with RAs than binder B and C, since HRAP-A starts in a higher category, but only increases to the same or a lower category than materials with binders B or C.

Table 4-5 Summary of connecting letter report for fracture indices (α=0.05)

Tests	DCT		I-FIT			E*
Indicators	**G_f**	**FST**	**G_f**	**FI**	**RDCI**	**G-R_m**
HRAP-A	*A*	*B C*	*A B C*	*B C D*	*A B C*	*A B*
HRAP-B	*A*	*C*	*C D*	*D*	*C*	*D*
HRAP-C	*A*	*C*	*D*	*D*	*C*	*C D*
HRAP-A-RA1	*A*	*A B C*	*A B C*	*A B*	*A*	*A*
HRAP-B-RA1	*A*	*A*	*A B C*	*A B C*	*A B C*	*A B*
HRAP-C-RA1	*A*	*A B*	*A B*	*A*	*A B*	*A B*
HRAP-A-RA2	*A*	*A B C*	*A*	*A B*	*A B*	*A*
HRAP-B-RA2	*A*	*A B C*	*A B*	*B C D*	*A B C*	*B C D*
HRAP-C-RA2	*A*	*A B C*	*B C D*	*C D*	*B C*	*A B C*
Range	A	A~C	A~D	A~D	A~C	A~D
Groups	1	5	6	6	5	6

The intermediate temperature cracking parameters (G_f, FI, RDCI, G-R_m) show the ability to categorize the mixtures into 5 or 6 groups. **Table 4-6** shows the change in number of groups from corresponding HRAP mixtures based on **Table 4-5**. The results indicate that Binder A is more resistant to cracking with the RAP1 material than Binder B and binder C without RA. RA1 appears to be more effective, or potentially more compatible than RA2, particularly with binder C due to the change in groupings. Based on the comparison between 4 parameters in the table, G-R_m and I-FIT G_f shows exorbitant independency from the binder type effect, which shows the mixture "Binder A-NA" has higher ranking than RA-treated mixtures. Notice that FI, RDCI and E* results follow a very consistent trend with respect to differentiating binder types and RAs: Thus, for this case, both FI and RDCI can be considered as good selection for compatibility characterization method in terms of the intermediate temperature cracking property.

Table 4-6 Change in number of groups from HRAP

Tests	DCT		I-FIT		E*	
Indicators	**G_f**	**FST**	**G_f**	**FI**	**RDCI**	**G-R_m**
HRAP-A-RA1	*0*	*1*	*0*	*2*	*2*	*1*
HRAP-B-RA1	*0*	*3*	*2*	*3*	*2*	*4*
HRAP-C-RA1	*0*	*2*	*4*	*5*	*3*	*3*
HRAP-A-RA2	*0*	*1*	*2*	*2*	*1*	*1*
HRAP-B-RA2	*0*	*2*	*3*	*2*	*2*	*2*
HRAP-C-RA2	*0*	*2*	*2*	*1*	*1*	*2*

Table 4-7 below summarizes the connecting letter reports for all fracture Indices for the virgin mixtures and RA treated HRAP mixtures. The groups show that virgin mixtures were successfully classified as the

top groups by FST, FI, RDCI, and G-R_m parameters. However, the fracture energy for both DCT and I-FIT tests fail to distinguish the differences between the virgin mixtures and RA treated HRAP mixtures. From the FST results, the mixture with binder C generally shows better low temperature fracture resistance than the mixture with binder B for both the virgin mixtures and the HRAP mixtures with RAs. The same trend can also be observed from the intermediate temperature cracking indicators (FI, RDCI, and G-R_m). But there's a significant exception HRAP-C-R2, which consistently shows low performance in all indicators. This reveals that the RA2 might have incompatibility with the binder C and RAP mix. Overall, FST, FI, RDCI and G-R_m have the ability to distinguish the incompatible binder. FST has the most promising discrimination ability for low temperature cracking properties. And FI and G-R_m have the most promising discrimination ability for intermediate temperature cracking properties considering their more subdivided groups and wider value ranges. The connecting letter report for each parameter is shown in Appendix A.

Table 4-7 Summary of connecting letter report for fracture indices compared with virgin mixtures (α=0.05)

Tests	DCT		I-FIT			E*
Indicators	G_f	FST	G_f	FI	RDCI	G-R_m
V-A	*A*	*A B C*	*A B C*	*A*	*A*	*A*
V-B	*A*	*A B*	*A*	*B*	*B*	*B*
V-C	*A*	*A*	*A B*	*B*	*B C*	*B*
HRAP-A-RA1	*A*	*B C*	*B C*	*B C*	*B*	*B C*
HRAP-B-RA1	*A*	*B C*	*A B C*	*B C D*	*B C*	*C D E*
HRAP-C-RA1	*A*	*A B C*	*A B C*	*B*	*B C*	*B C*
HRAP-A-RA2	*A*	*C*	*A B*	*B C*	*B C*	*B*
HRAP-B-RA2	*A*	*B C*	*A B C*	*C D*	*B C*	*E*
HRAP-C-RA2	*A*	*B C*	*C*	*D*	*C*	*E*
Range	A~A	A~C	A~C	A~D	A~C	A~E
Groups	1	6	5	6	4	5

4.5.4 Compatibility Ranking

The following performance index was developed to provide a relative comparison of the magnitude of a particular parameter for the various mixtures and binders. The performance index is defined as the percent difference with respect to the best value within the group of materials being compared (equation 10). The higher performance index reveals potential inferior performance.

$$Performance\ Index = \frac{Best\ Value - Value}{Best\ Value} \times 100\% \quad (10)$$

Table 4-8 below shows the performance index calculated from the binder testing results. The color map was shaded based on the performance index ranking within each indicator. The mixture with higher index value and shaded with darker color shows inferior properties. It can be observed that most of the mixture parameters show significant differences between the binders extracted from RA treated mixtures and those extracted from non-RA treated mixtures. This indicates those parameters have the ability to distinguish the RA's effect on the binder, and they are more likely to be affected by the RA. By contrast, the performance index and the color map for phase angle and G-R_m parameter show the significant difference between binder types. That's to say the binder type, instead of RA type, is more likely casting a dominant effect on these parameters. The dominant effect shows that all fracture test results and parts of rheological parameters (E*, CMRI) are more likely controlled by the inclusion of RA. Phase angle and G-R_m parameter are strongly affected by the binder types.

Table 4-8 Performance index identified from the various mixture tests results

Mixture ID	Mixture Evaluation								
	Rheological Analysis				Inter. Temp. Fracture			Low Temp. Fracture	
Test Method	E*	Phase Angle	G-R_m	CMRI	G_f	FI	RDCI	G_f	FST
HRAP-A	25.6	16.3	43.4	45.1	13.1	58.2	41.9	0.0	48.9
HRAP-B	43.3	41.9	0.0	158.8	37.8	95.8	87.2	23.7	54.2
HRAP-C	53.8	31.1	11.1	291.6	47.5	97.7	88.9	38.1	55.9
HRAP-A-R1	0.0	10.3	55.5	279.2	17.2	0.0	7.4	36.7	32.9
HRAP-B-R1	14.2	24.2	31.9	106.1	13.9	26.8	30.7	15.6	6.0
HRAP-C-R1	2.8	23.1	39.0	368.4	11.8	5.1	2.0	10.8	0.0
HRAP-A-R2	2.6	0.0	64.3	0.0	0.0	9.8	0.0	40.9	29.3
HRAP-B-R2	34.4	29.1	24.4	128.0	11.0	50.4	35.0	22.1	15.1
HRAP-C-R2	26.1	23.3	33.1	1438.8	25.4	68.7	52.0	22.8	21.7
Dominant Effect	RA	Binder	Binder	RA	RA	RA	RA	RA	RA

Table 4-9 below shows the performance index calculated from the binder testing results. From the rheological analysis results, it can be observed that T_c(S), T_c(m) and LTPG values are more affected by the RA and show similarity in terms of the binder ranking. As expected, extracted samples with binder A always have a good performance for most of rheological parameters related to cracking. It makes sense since binder A has a lower PG grade. As for the parameters from thermal analysis, both Tg_α, Tg_β and Tg show similar ranking, and both are affected by the inclusion of RA. However, parameter ϕ_α results show that it's more likely affected by the binder types.

Table 4-9 Percent incompatibility identified from the various binder tests results

Binder ID	Binder Evaluation										
	Rheological Analysis (DSR)							Thermal Analysis (DSC)			
Test Method	R	HTPG	T_c(S)	T_c(m)	ΔT_c	LTPG	G-R	Tg_α	Tg_β	Tg	ϕ_α
HRAP-A	23.1	10.7	20.1	14.6	33.3	19.7	116.8	35.3	241.4	32.3	55.2
HRAP-B	10.5	2.7	24.4	33.5	224.5	33.5	2417.3	25.9	172.7	24.6	31.1
HRAP-C	16.6	6.8	24.4	24.9	111.5	24.9	907.3	34.1	218.3	34.4	40.4
HRAP-A-R1	12.5	10.6	0.0	0.0	106.2	0.0	82.8	4.5	35.5	4.0	48.4
HRAP-B-R1	0.0	0.0	7.1	18.2	251.1	18.2	1287.7	3.4	4.5	7.5	2.9
HRAP-C-R1	10.8	5.3	12.0	17.9	182.2	17.9	682.5	9.9	65.9	6.7	39.7
HRAP-A-R2	23.4	12.4	12.9	4.8	0.0	12.4	0.0	18.7	65.2	18.7	31.4
HRAP-B-R2	5.5	4.9	7.6	14.5	196.1	14.5	1114.8	9.6	30.3	12.8	0.0
HRAP-C-R2	12.3	10.9	6.4	8.6	134.9	8.6	254.9	0.0	0.0	0.0	27.8
Dominant Effect	Binder	Binder	RA	RA	Binder	RA	Binder	RA	RA	RA	Binder

4.6 CHAPTER SUMMARY

This chapter evaluated various binder and mixture property indicators for binder blends and mixtures with RAP1 and proposed multiple methods to screen the promising methods for binder compatibility characterization. Binder rheological characterization indicated that binder B is most incompatible with the RAP material as well as with both RAs. DSC parameters such as Tg and ϕ_α have also shown the ability to characterize the compatibility of asphalt materials. Complex modulus testing indicated that both RAs improve the stiffness and relaxation capacity on the study HRAP mixtures. Both dynamic modulus and phase angle showed the capacity of compatibility identification, but the phase angle master curves perform better in terms of screening and differentiating between the different binders. Overall, from mixture testing FI, RDCI, FST and mixture Glover-Rowe showed the potential ability to capture the difference between the study mixtures evaluated in this chapter.

To evaluate the performance of different methods, the following statistical methods are applied: the logistic analysis based on the bar chart of the material property, the correlation analysis between the binder and mixture properties. The correlation analysis showed that the rheological parameters T_c(S) and T_c(m) generally correlate well with most fracture-based mixture parameters. Comparing with other mixture cracking performance, the mixture rheological cracking parameter G-R_m generally showed moderate to strong correlation with most of the DSR and DSC binder testing results. Connecting letter report was utilized to evaluate the discrimination ability of each indicator by comparing the means statistically. It was observed that the RA2 might be significantly incompatible with HRAP1 and binder C. Furthermore, it also indicated that the FST performs well for screening low temperature cracking properties and FI and RDCI perform well for screening intermediate temperature cracking properties. Finally, the ranking of the incompatibility index was utilized to show a possible method to identify the incompatible material and its dominant effect.

Chapter 5: RECOMMENDATION FOR PRACTICAL AND IMPLEMENTABLE CHARACTERIZATION SYSTEM TO DETERMINE COMPATIBILITY

Previous chapter focused on the core material characterization and identified the promising test methods for compatibility evaluation. The main objective of the work conducted within this chapter is to evaluate these test methods and tools to determine those that are sensitive and able to differentiate the compatibility of the binders and mixtures based on the proposed testing plan. The promising methods and tools identified from this chapter are further validated in the next chapter.

5.1 MATERIAL BASE

The material base generated for this chapter is summarized and presented in **Table 5-1** and **Table 5-2** below. Combined with the mixture results from chapter 3 and 4, twenty-one mixtures (3 virgin mixtures, 3 LRAP mixtures, 9 HRAP mixtures and, 6 RA treated HRAP mixtures) were designed or evaluated within this chapter. In addition, a total of twenty-four binder blends (3 virgin binders, 7 HRAP blends and, 14 RA treated HRAP blends) were evaluated within this chapter. It should be noted that this chapter covers testing of RAP2 along with RAP3 and compares the results with control RAP (RAP1) as well as virgin mixtures. Material ID for each variation is also included in the tables. For example, HRAP1-A-R1 indicated RA1 treated RAP1 material (45%) mixed with binder A. It should be noted that all LRAP materials have 25% RAP1 while all HRAP materials have 45% RAP.

Table 5-1 Material base generated for binder evaluation

	Material Base		Binder ID	Testing Methods	Chapter
Binder Evaluation	Virgin Binder	A	V-A	DSC, DSR, APC, SARA	Chapter 3
		B	V-B		
		C	V-C		
	Extracted Binder from HRAP mix	HRAP1 + Binder A (HRBR)	HRAP1-A		
		HRAP1 + Binder B (HRBR)	HRAP1-B		
		HRAP1 + Binder C (HRBR)	HRAP1-C		
		HRAP2 + Binder A (HRBR)	HRAP2-A	DSC, DSR	Chapter 5
		HRAP2 + Binder C (HRBR)	HRAP2-C		
		HRAP3 + Binder A (HRBR)	HRAP3-A		
		HRAP3 + Binder C (HRBR)	HRAP3-C		
	Extracted Binder from RA Treated mix	HRAP1 + Binder A (HRBR)+RA1	HRAP1-A-R1	DSC, DSR	Chapter 4
		HRAP1 + Binder B (HRBR)+RA1	HRAP1-B-R1		
		HRAP1 + Binder C (HRBR)+RA1	HRAP1-C-R1		
		HRAP1 + Binder A (HRBR)+RA2	HRAP1-A-R2		
		HRAP1 + Binder B (HRBR)+RA2	HRAP1-B-R2		
		HRAP1 + Binder C (HRBR)+RA2	HRAP1-C-R2		
		HRAP2 + Binder A (HRBR)+RA1	HRAP2-A-R1	DSC, DSR	Chapter 5
		HRAP2 + Binder C (HRBR)+RA1	HRAP2-C-R1		
		HRAP2 + Binder A (HRBR)+RA2	HRAP2-A-R2		
		HRAP2 + Binder C (HRBR)+RA2	HRAP2-C-R2		
		HRAP3 + Binder A (HRBR)+RA1	HRAP3-A-R1		
		HRAP3 + Binder C (HRBR)+RA1	HRAP3-C-R1		
		HRAP3 + Binder A (HRBR)+RA2	HRAP3-A-R2		
		HRAP3 + Binder C (HRBR)+RA2	HRAP3-C-R2		

Table 5-2 Material base generated for mixture evaluation

	Material Base		Mixture ID	Testing Methods	Chapter
Mixture Evaluation	Virgin Mixtures	Binder A + Aggregate A	V-A	E*, DTCF, IFIT, DCT	Chapter 3
		Binder B + Aggregate A	V-B		
		Binder C + Aggregate A	V-C		
	Mixtures with RAP	HRAP1 (control) + Binder A + Aggregate A (HRBR)	HRAP1-A		
		HRAP1 (control) + Binder B + Aggregate A (HRBR)	HRAP1-B		
		HRAP1 (control) + Binder C + Aggregate A (HRBR)	HRAP1-C		
		HRAP2 + Binder A + Aggregate A (HRBR)	HRAP2-A	E*, IFIT, DCT	Chapter 5
		HRAP2 + Binder B + Aggregate A (HRBR)	HRAP2-B		
		HRAP2 + Binder C + Aggregate A (HRBR)	HRAP2-C		
		HRAP3 + Binder A + Aggregate A (HRBR)	HRAP3-A		
		HRAP3 + Binder B + Aggregate A (HRBR)	HRAP3-B		
		HRAP3 + Binder C + Aggregate A (HRBR)	HRAP3-C		
		LRAP + Binder A + Aggregate A (HRBR)	LRAP-A		
		LRAP + Binder B + Aggregate A (HRBR)	LRAP-B		
		LRAP + Binder C + Aggregate A (HRBR)	LRAP-C		
	Mixtures with RAP and RA	HRAP1 (control) + Binder A + RA1+Aggregate A (HRBR)	HRAP1-A-R1	E*, IFIT, DCT	Chapter 4
		HRAP1 (control) + Binder B + RA1+Aggregate A (HRBR)	HRAP1-B-R1		
		HRAP1 (control) + Binder C + RA1+Aggregate A (HRBR)	HRAP1-C-R1		
		HRAP1 (control) + Binder A + RA2+ Aggregate A (HRBR)	HRAP1-A-R2		
		HRAP1 (control) + Binder B + RA2+Aggregate A (HRBR)	HRAP1-B-R2		
		HRAP1 (control) + Binder C + RA2+Aggregate A (HRBR)	HRAP1-C-R2		

5.2 EXTRACTED BINDER PERFORMANCE TEST RESULTS

This section focuses on the testing results from the binders which are extracted and recovered from the RA treated RAP materials. The compatibility between two recycling agents (5% RA1 and 8% RA2; percentage in terms of RAP binder weight), three base binders (A, B, and C) together with three RAP materials including base RAP material (RAP1) are evaluated in this section. **Table 3.1** summarizes the material combinations that were tested. It is worth mentioning that LRAP and HRAP1 contain the same RAP material but in different amounts, with the former containing 25% RAP and the latter containing 45% RAP by weight of the mixture.

Table 5-3 Extracted and recovered blended binder inforamation and aging level

Binder ID	Binder	RAP Content	Recycling Agent	Aging Level
LRAP-A	A	45% by wt of mixture for HRAP (34% RBR) and 25% by wt of mixture for LRAP mixtures (19% RBR)	None	As-extracted (As-ext)
HRAP1-A				
HRAP2-A				
HRAP3-A				
LRAP-B	B			
HRAP1-B				
HRAP2-B				
HRAP3-B				
LRAP-C	C			
HRAP1-C				
HRAP2-C				
HRAP3-C				
HRAP1-A-RA1	A		RA1	As-ext; 1xPAV; 2xPAV
HRAP1-B-RA1	B			
HRAP1-C-RA1	C			
HRAP1-A-RA2	A		RA2	As-ext; 1xPAV; 2xPAV
HRAP1-B-RA2	B			
HRAP1-C-RA2	C			
HRAP2-A-RA1	A		RA1	As-ext
HRAP3-A-RA1				
HRAP2-C-RA1	C			
HRAP3-C-RA1				
HRAP2-A-RA2	A		RA2	As-ext
HRAP3-A-RA2				
HRAP2-C-RA2	C			
HRAP3-C-RA2				

5.2.1 Rheological Analysis Results (DSR Testing)

Figure 5-1 and **Figure 5-2** summarize the measured continuous PG for the extracted and recovered binder blends for all three RAP materials. The HTPG results for all binder blends in as-extracted condition without PAV aging are presented and discussed in this section. LRAP blends have lower HTPG than the corresponding HRAP1 blends regardless of the binder type, as expected, due to lower RAP content. Blends with binder B have the warmest HTPG, whereas the blends containing binder A have the lowest HTPG values. HRAP1 blends have the highest HTPG, whereas HRAP3 blends have the lowest

HTPG irrespective of the RA and binder type. The effect of RAs is different for each binder and RAP source combination; the magnitude of the variation is generally small, ranging from 0.1 to 3.3 °C, with the exception of HRAP2 blend with binder C and RA2, with a difference of 6 °C.

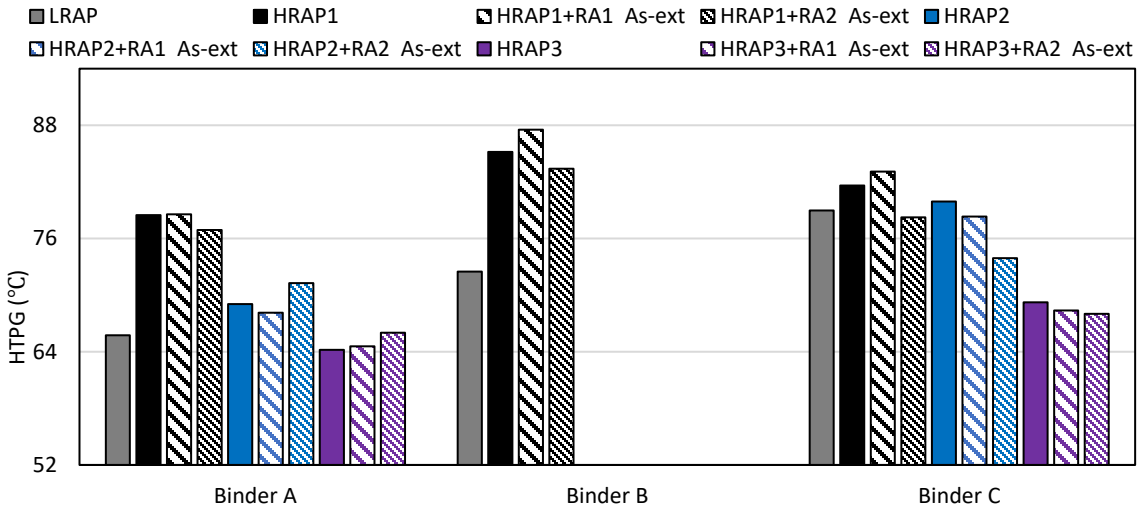

Figure 5-1 HTPG of the extracted and recovered binder blends

Figure 5-2 shows the LTPG and the percent change from the corresponding HRAP blends (i.e., HRAP1, HRAP2 and HRAP3) in the as-extracted condition. It should also be mentioned that aging effect (1xPAV and 2xPAV) was evaluated for binder blends containing HRAP1 only. PAV aging conditions affected LTPG values adversely and the impact of PAV aging is comparable across the board. The addition of both RAs initially improves the LTPG, but the benefits are continuously lost after each PAV aging cycle. The magnitude of the change is different for the various binder blends. Blends with binders B and C demonstrate the largest changes (greater aging susceptibility). This indicates that both RA1 and RA2 improved low temperature performance, but they also may have lower compatibility with binders B and C together with RAP1 blends. Generally, lower LTPG grade when compared to respective HRAP blend shows the better compatibility between the RAP binder and RA, if all other parameters are comparable. Overall, it seems that LTPG and HTPG are not showing significant discrimination between RAP, binder and RAs on the basis of compatibility.

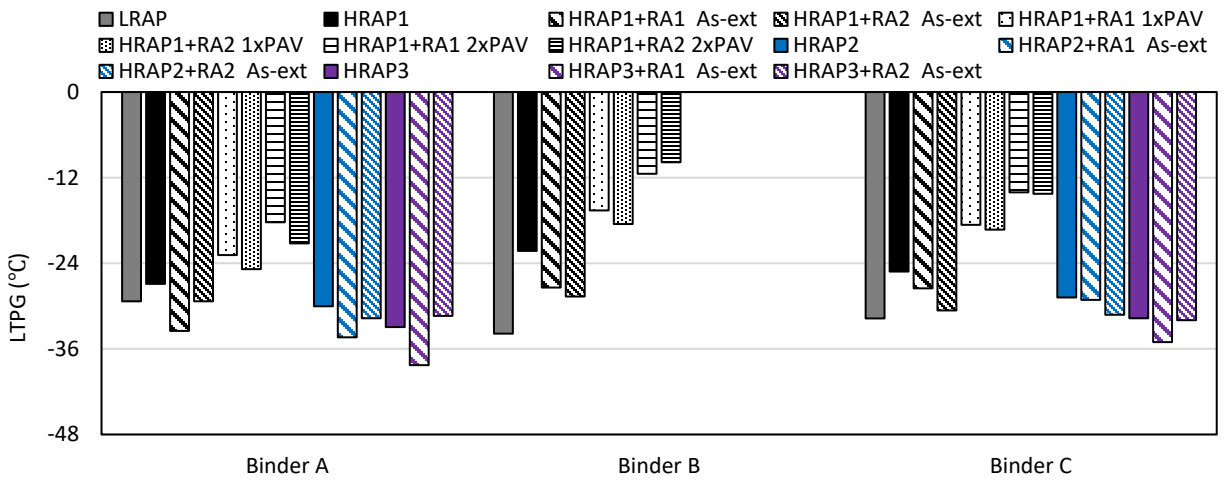

(a)

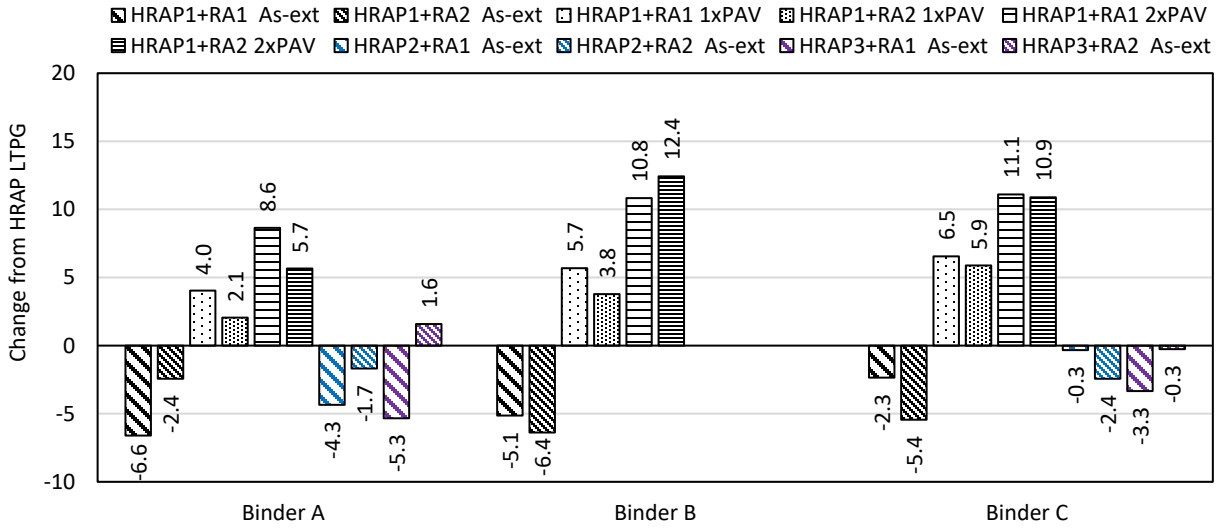

(b)

Figure 5-2 Comparison of (a) LTPG values and (b) change in LTPG as compared to their respective HRAP blends

Figure 5-3 below presents the ΔT_c values for all blends. All as-extracted binders have ΔT_c values above the currently proposed cracking limit threshold of -5 °C and there is a consistent trend that binder B shows the lowest ΔT_c values, indicating inferior cracking resistance. The inclusion of the RA generally decreases the ΔT_c values for the blended binders, except for binder C with RAP2 and RAP3 blends where both RAs show higher ΔT_c values than the corresponding HRAP blend.

After both levels of PAV aging, all blends with RA1 are close to or exceed the cracking threshold of -5 °C, which indicates severe cracking potential. The ΔT_c values for binders with RA2 are generally better than those with RA1. Similar to the trend observed from the as-extracted materials, binder B has the worst ΔT_c values for all long-term aged blends. This is consistent with the assumption that binder B is incompatible as compared to binders A and C. Generally, lower ΔT_c value when compared to respective HRAP indicates the potential incompatibility between RAP binder and RAs and from the results, it seems

that RA1 shows consistent lower ΔT_c values with all HRAP1 binder blends and with binder A for HRAP3. Blends having RA1 with all binders exceed the cracking limit of -5 °C whereas blends with RA2 show overall better performance than RA1.

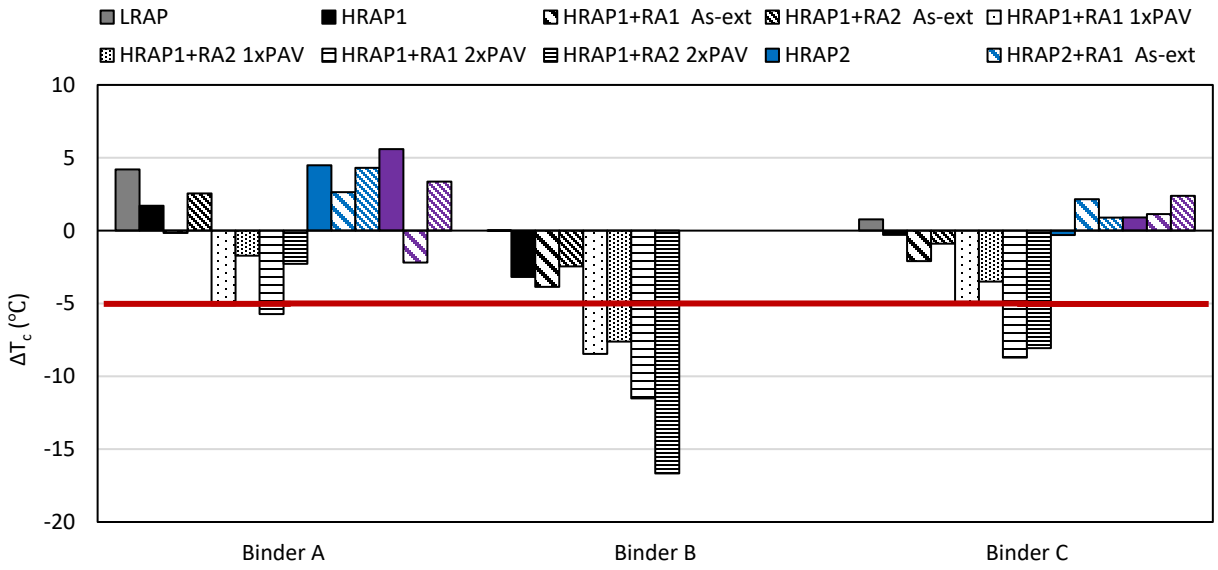

Figure 5-3 ΔT_c parameter of the extracted and recovered binders with aging

Figure 5-4 below presents the Glover-Rowe (G-R) parameter values of extracted and recovered binder blends at different aging levels and the relative changes with respect to corresponding HRAP blends. All blended binders in the as-extracted condition have G-R values that are lower than the warning limit and cracking limit for binders A and C, whereas binder B is near the warning limit. This result indicates that binder B is potentially incompatible as blends with binder B have significantly higher G-R values compared to corresponding blends with binder C even though they have similar PG grades. The inclusion of RA improves (lowers) the G-R values for all three HRAP blends. It can also be observed that RA2 improves the properties of HRAP1 blends more than RA1, which is opposite for RAP2 and RAP3 blends. All G-R values increase with aging, with only Binder A blend within the cracking limit after 1xPAV. Both binder B and C have larger changes with aging, and the relative differences at the 2xPAV as compared to the control materials. Generally, increase in the G-R parameter with inclusion of RA indicates the potential incompatibility of RA with the RAP and virgin binder blend. It can be observed from the results that RA2 shows potential incompatibility with HRAP2 and HRAP3 with binder A as it increased the G-R parameter instead of decreasing.

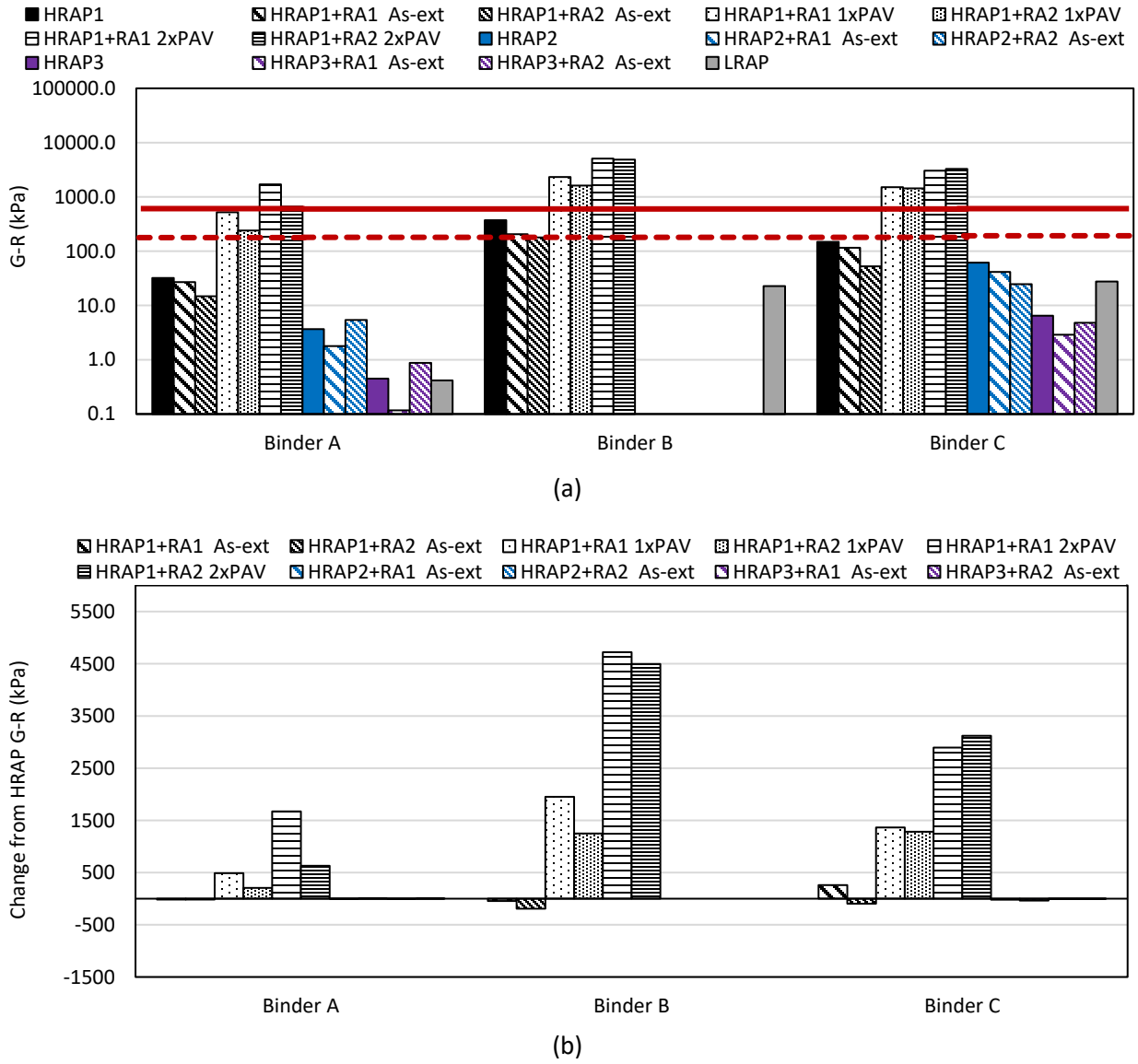

Figure 5-4 Comparison of (a) G-R parameter and (b) change in G-R as compared to their respective HRAP blends

Figure 5-5 below shows the G-R points in Black space. For all blends, both RA1 and RA2 show the softening effect and decreased stiffness and improved phase angle compared to their respective HRAP blends. This can be observed as the results are comparable with corresponding to LRAP blends. It should also be noted that RAs with binder B only soften the blends without restoring relaxation properties as phase angle is similar for all blends which again indicates potential incompatibility. Also, the blends with RA2 show lower stiffness than blends with RA1 for binder type A and B, whereas it is opposite for binder type C. It indicates that RA2 might have more significant softening effect on the blends with HRAP1 and HRAP2 and RA1 have that with HRAP3. **Figure 5-6** below shows the Black space diagram of the RA treated blends with different aging levels. It can be observed that binder B shows a more detrimental impact on stiffness and phase angle of all blends resulting in inferior rheological properties.

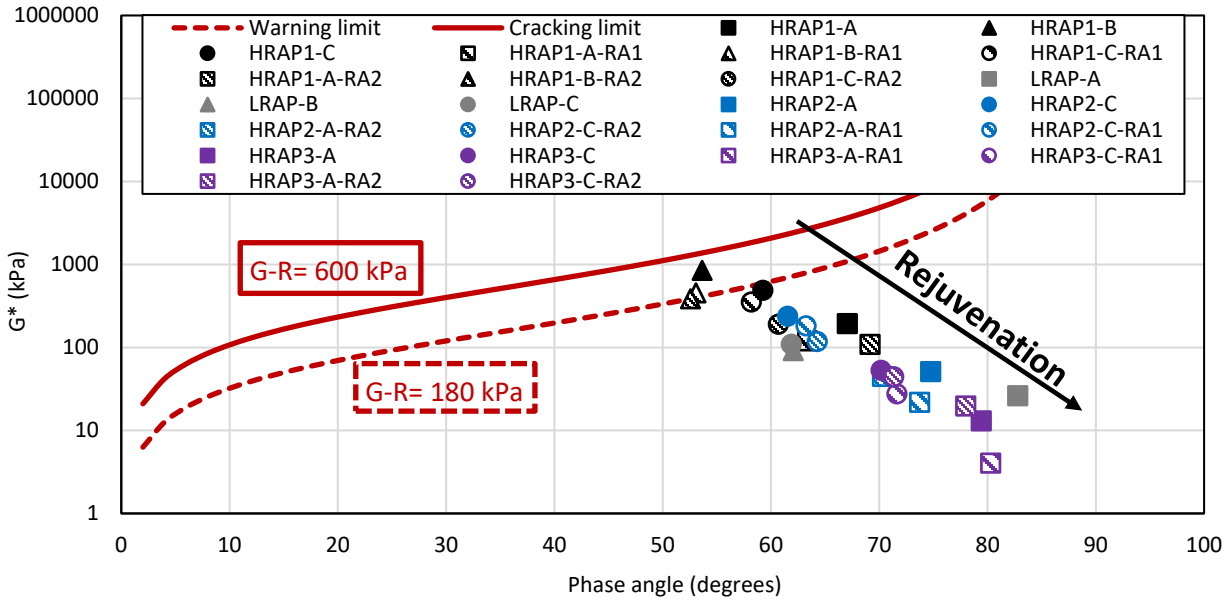

Figure 5-5 G-R points in Black space for as-extracted binder blends

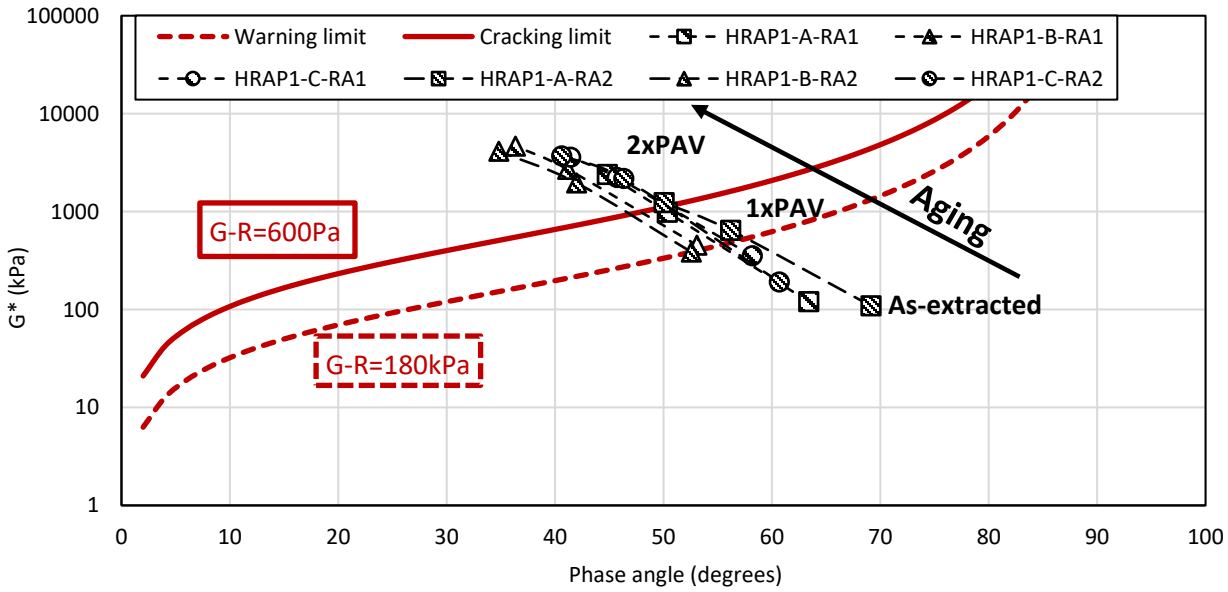

Figure 5-6 G-R points in Black space for rejuvenated binder blends with aging

Figure 5-7 below shows the R-values for all materials and aging conditions. Binder B consistently has the highest R-value for all conditions. The R-values of the as-extracted binder generally increase with the addition of both RAs and aging. There are differences in the R-values of the binder A materials, with the RA1 showing greater changes than RA2, which may indicate RA2 might be more effective with RAP1 material having Binder A. However, the R-value does not show differentiation for blends with RAP2 and RAP3. Overall, it seems that the R-value parameter does not show much discrimination between the study blends.

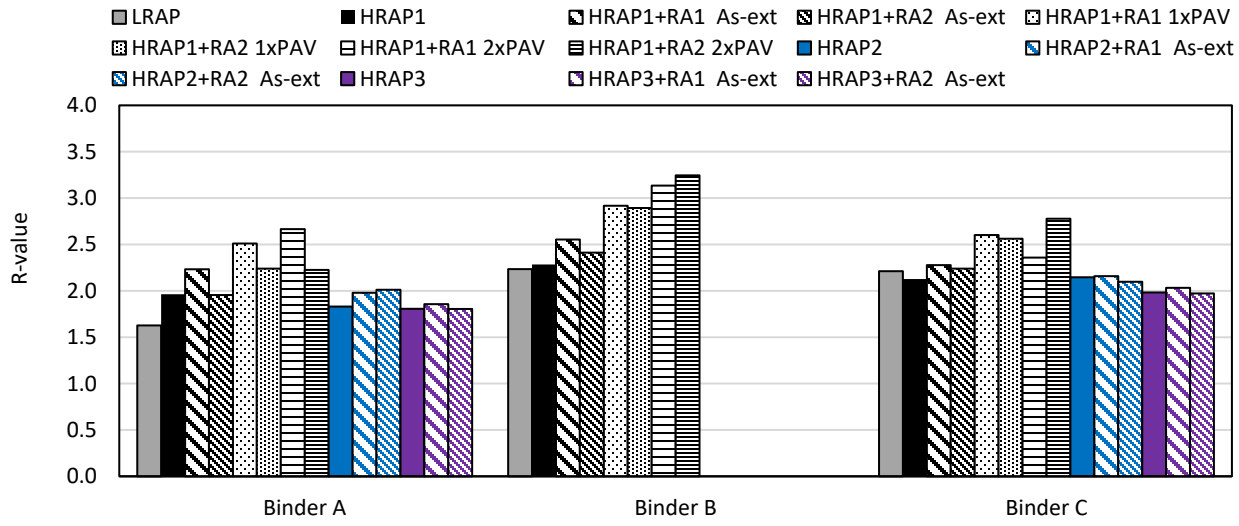

(a)

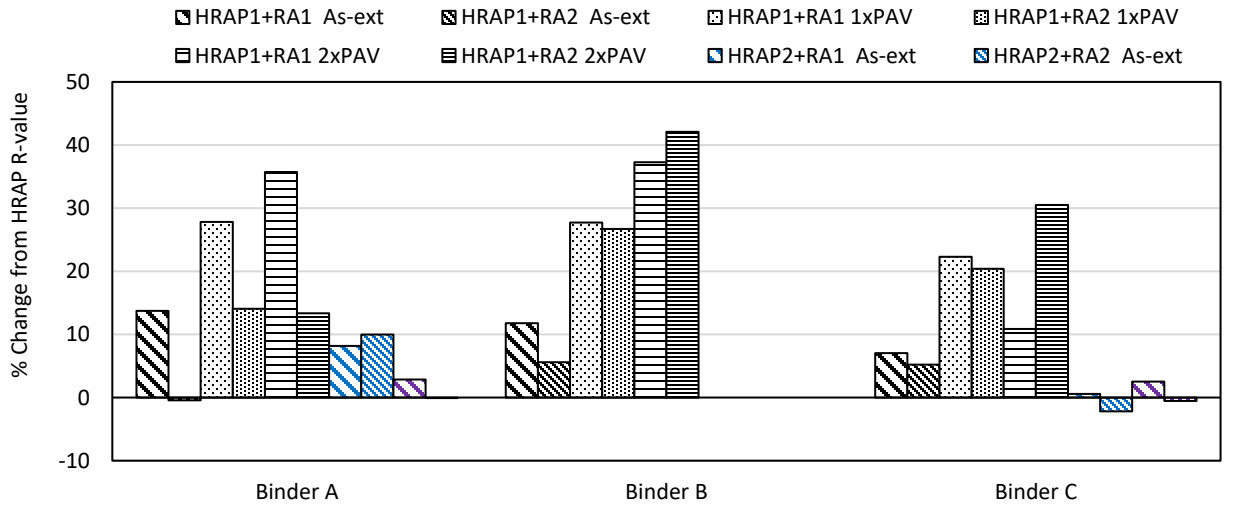

(b)

Figure 5-7 Comparison of (a) G-R parameter and (b) and percent change in R-value as compared to their respective HRAP blends

5.2.2 Thermal Analysis Results (DSC Testing)

Figure 5-8 below shows the Tg_α, Tg_β and Tg values measured from the DSC test results for the extracted and recovered binders from the six RA treated mixtures and corresponding three control mixtures. With the inclusion of the RAs, both Tg_α and Tg_β show decreased values as compared to the corresponding untreated binder. Generally, higher Tg_α, Tg_β and Tg compared to corresponding HRAP material indicate potential incompatibility between RAs and RAP blends.

HRAP1 blends with binder A and C have comparable Tg values which are slightly warmer than the value for Binder B. The inclusion of RA results in slightly decreased Tg values, indicating improved thermal properties. For Tg_α as expected, HRAP had a warmer transition than LRAP for all three binders. Both RA1

and RA2 reversed the impact of the higher RAP on this parameter. Generally, RA1 resulted in lower Tg_{α}, Tg_{β} and Tg values than RA2 indicating that RA1 is more effective than RA2. The impact of RAP content was even more dramatic with the Tg_{β} parameter. This is not unexpected, as the change in this parameter is thought to be more reflective of the impact of aged bitumen on blend compatibility. It is observed that for all three binders, the increase in RAP content shifted Tg_{β} to positive temperatures. Inclusion of both RAs reversed this trend, with RA1 generally resulting in a larger reversal, except for binder C with HRAP1 in which RA2 showed a higher impact for Tg_{α}, Tg_{β} and Tg.

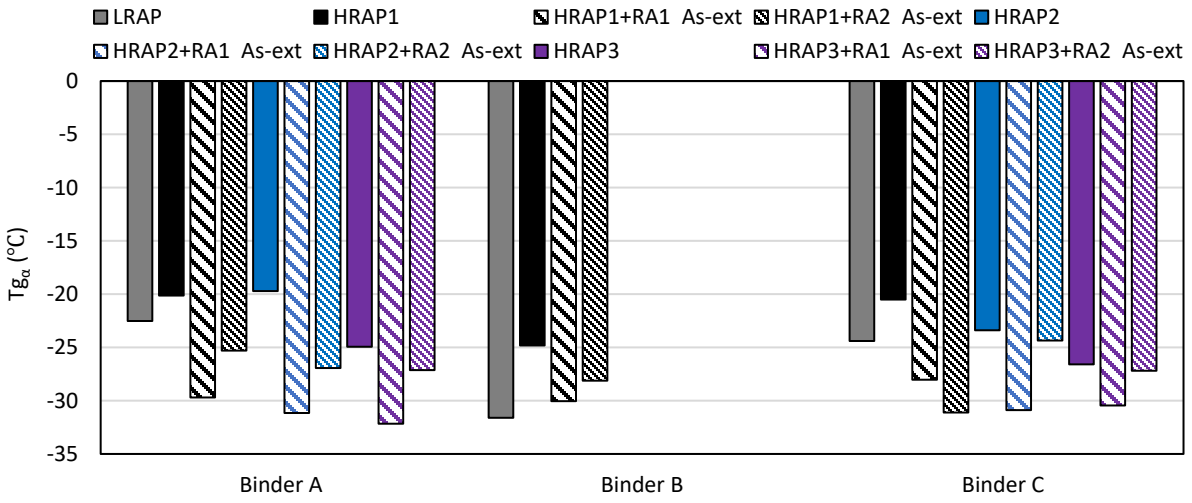

(a)

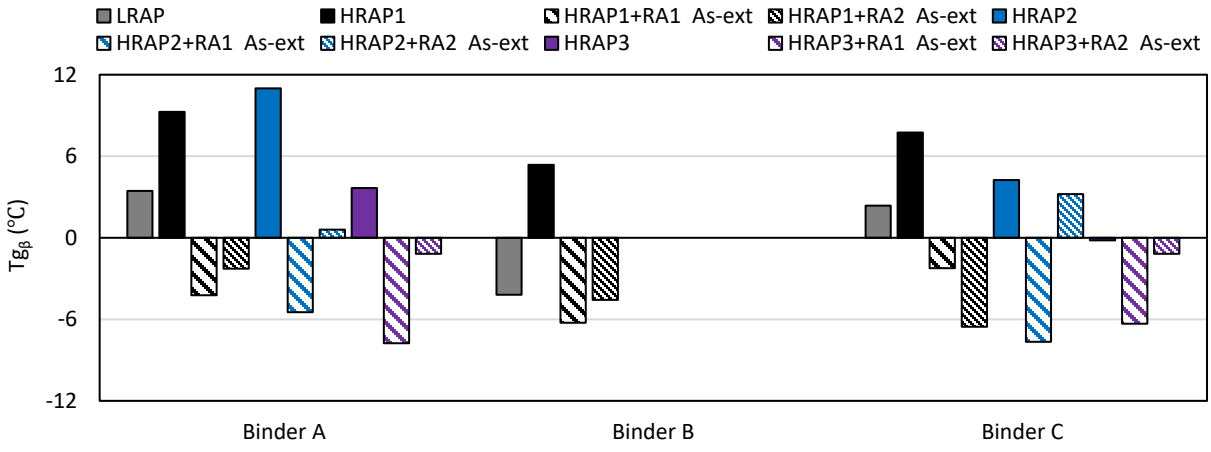

(b)

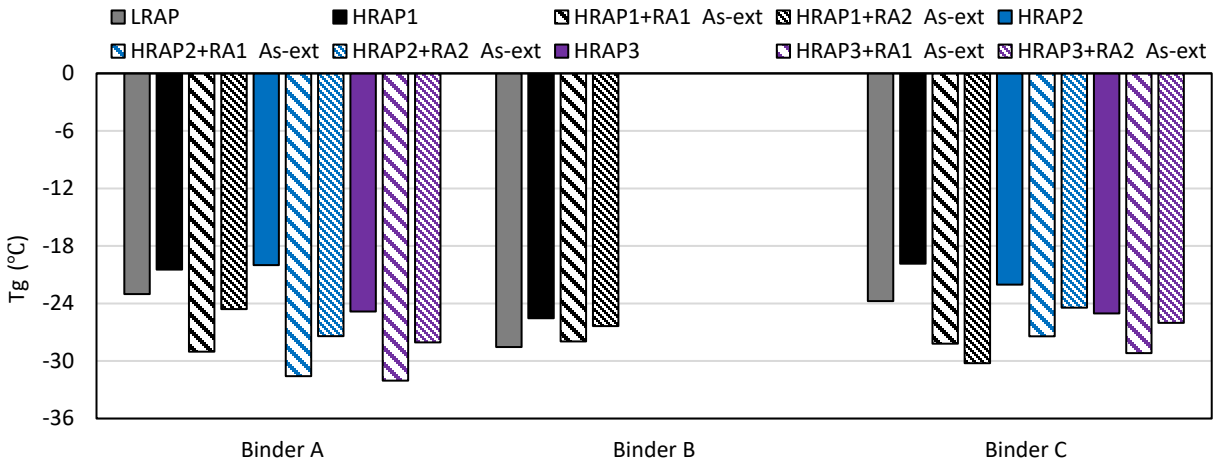

(c)

Figure 5-8 DSC analysis results of extracted and recovered binders: (a) Tg_{α}, (b) Tg_{β}, and (c) Tg

Figure 5-9 shows the ϕ_{α} parameter for the study binders. As expected, all RA treated binders have higher ϕ_{α} parameter than the corresponding extracted and recovered HRAP binders. Generally, lower ϕ_{α} value when compared to respective HRAP indicates the potential incompatibility between the binder components (i.e., RAP binder, virgin binder, and RAs). From the results, it seems that both RA1 and RA2 show lower relative ϕ_{α} impact with RAP1 material and binder B. Based on the more significant impact of the RAs on the basis of the temperature shift of Tg_{α} and Tg_{β} as a result of both RAP content and use of recycling agents, shift-based composite parameters should be evaluated for relation to other observed measures of potential compatibility in this study, in addition to ϕ_{α}.

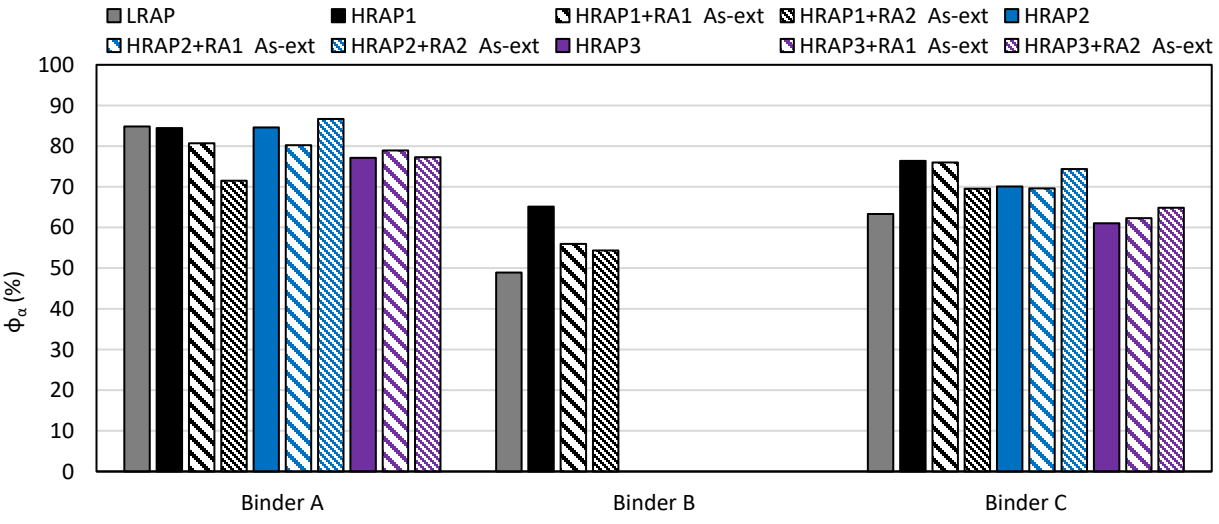

Figure 5-9 ϕ_{α} parameter for extracted and recovered binder blends

Figure 5-10 further extends the thermal analysis to the Tg_{Aave} parameter, which as previously discussed is the weighted average of the deconvoluted Tg peaks. The results show a trend similar to that of the total Tg, in which higher content of aged RAP binder causes a shift towards warmer temperatures, which

the rejuvenation in each case results in a reversal of this process, with the RA1 impact typically being higher in all cases except for HRAP1 with Binder C. Generally, lower Tg_{Aave} parameter for a blend compared to respective HRAP blend shows the better compatibility between the binder and RA, if all other parameters are comparable.

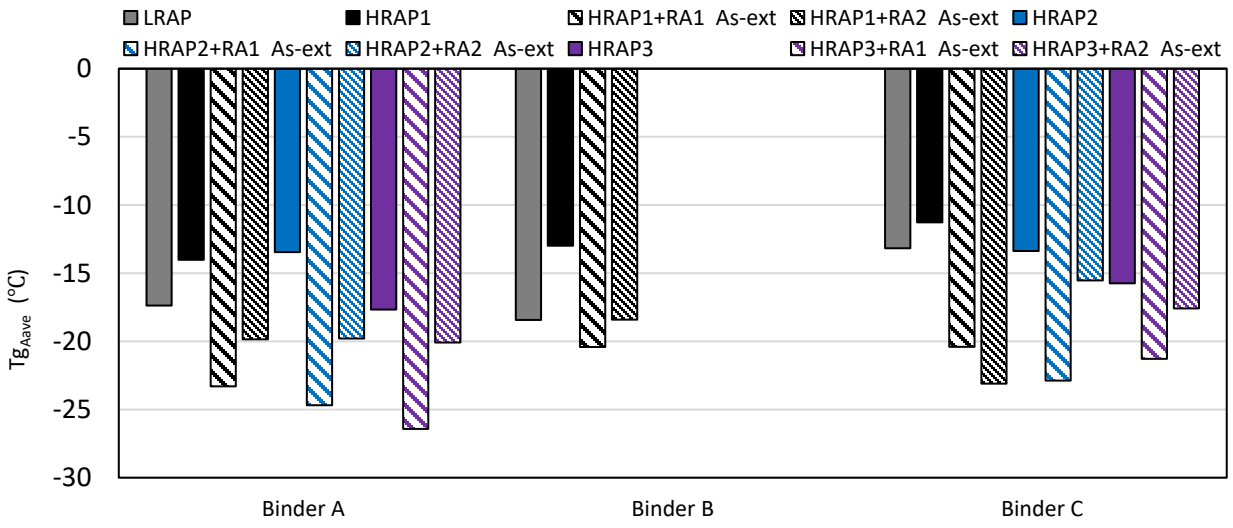

Figure 5-10 Tg_{Aave} parameter for extracted and recovered binder blends

5.3 MIXTURE PERFORMANCE TEST RESULTS

In this section, results of various mixture tests on the lab-produced samples with 45% RAP and recycling agents are compared with their control groups (45% RAP without RA), 30% RAP mixtures and virgin mixtures (without RAP or RA).

5.3.1 Rheological Properties

Dynamic modulus and phase angle master curves constructed from the complex modulus testing are presented in **Figure 5-11** below. Each series represents an average of three replicates. Compared to virgin mixtures, all HRAP mixtures show higher |E*| values and lower phase angle over all frequencies. The mixtures with binder A have significantly lower dynamic modulus and higher phase angles for both virgin mixtures and all HRAP mixtures than corresponding mixtures blended with binder B and binder C. The |E*| values for HRAP mixtures with binder B and binder C are statistically similar over all frequencies (based on t-test with $\alpha = 0.05$). These trends are expected with the binder grades for the different mixtures. It seems that HRAP1 shows the worst rheological properties as mixtures with HRAP1 show higher dynamic modulus and lower phase angle values with all binders when compared to corresponding HRAP2 and HRAP3 mixtures.

The general trends observed from the RA mixtures shows that both RAs have a softening effect and relaxation improvement on HRAP mixtures, but not to the level of the virgin mixtures. Also, the comparison in phase angles shows that binder B has lower relaxation property with the HRAP1, and RA1

seems to allow for higher relaxation than RA2. In general, both the dynamic modulus and phase angles show the capacity to be able to identify potential incompatibility within binder constituents, but the phase angle master curves show more differentiation between the different binders.

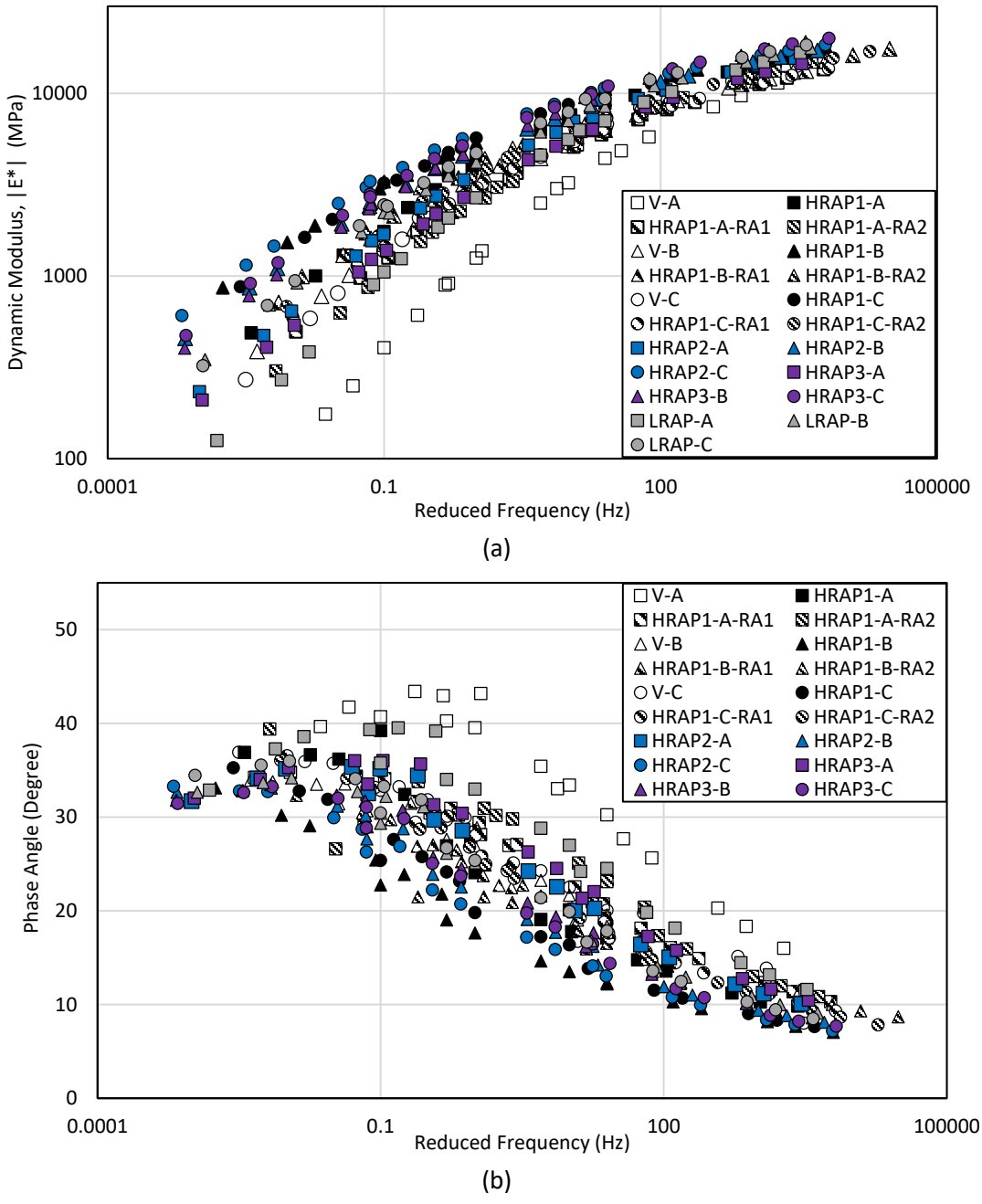

Figure 5-11 Master curves of (a) dynamic modulus on a logarithmic scale and (b) phase angle (δ) for study mixtures at 20 °C

Rheological based mixture performance cracking parameter G-R_m can be calculated from the |E*| and phase angle master curves which are presented in **Figure 5-12**. Generally, higher G-R_m value indicates the higher potential for incompatibility among the RAP material and the binder. It can be observed that

binder B is potentially less compatible with HRAP2 as it has higher G-R_m than that with binder C having similar binder PG. Similarly, binder C also shows poor rheological properties with HRAP2. The general trend shows that all three HRAP mixtures have significantly higher G-R_m than the corresponding virgin mixtures. The results indicate deterioration of the cracking resistance with the inclusion of the RAP material. The impact of the addition of RAP is different for the mixtures with binders B and C, although the two virgin binders have the same PG. All RA treated mixtures show lower G-R_m values than the corresponding HRAP mixtures but higher than that of virgin mixtures.

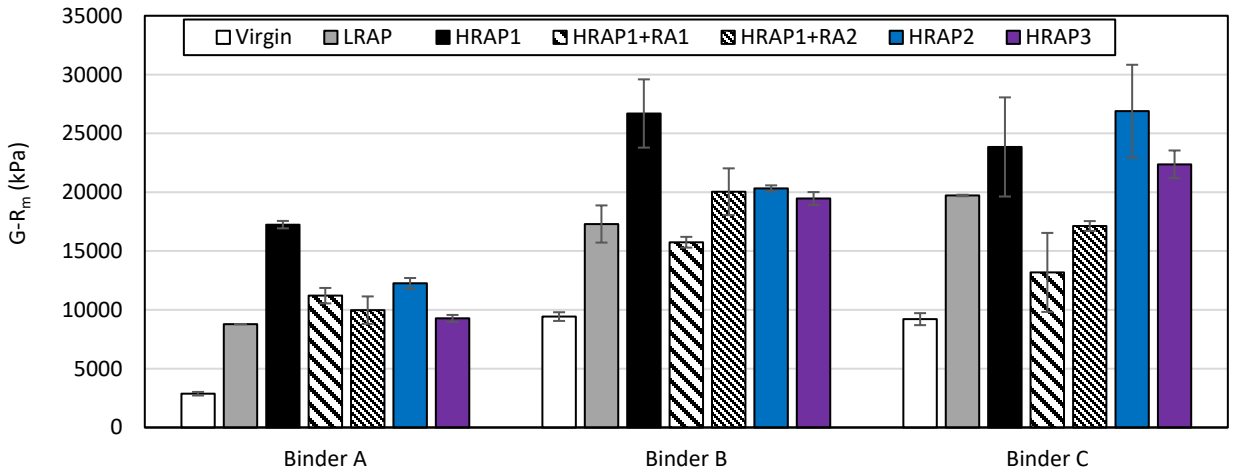

Figure 5-12 Glower-Rowe mix parameter (G-R_m) parameter for the study mixtures

Figure 5-13 shows the G-R_m values in Black space to evaluate the effect of addition of RAP and rejuvenators on the rheological properties. It is observed that addition of rejuvenators restores the properties of HRAP1 to that of corresponding LRAP mixtures for all binders. The results show that overall RAP1 shows poor rheological properties in comparison with corresponding RAP2 and RAP3 mixtures. From the results, it seems that RA1 shows higher improvement with binders B and C than RA2.

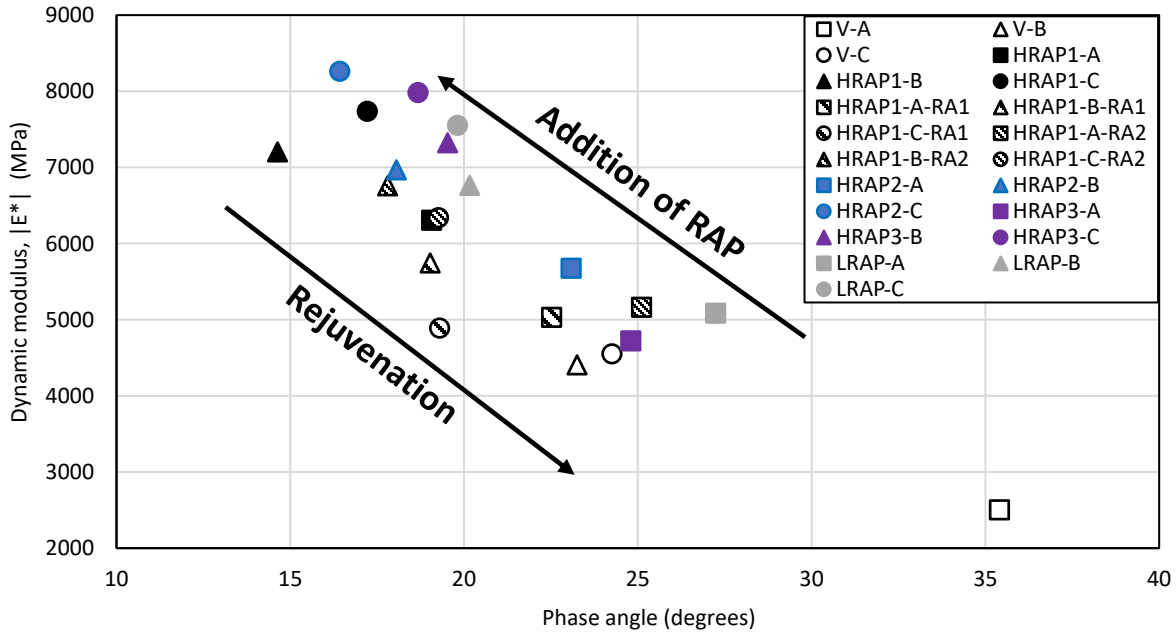

Figure 5-13 G-R_m points in Black space for the study mixtures

5.3.2 Illinois Flexibility Index Semi-Circular Bend (SCB) Test (I-FIT)

Figures 5-14 and **5-15** show FI and RDCI parameters, determined using the I-FIT, and their normalized values with respect to the corresponding virgin mix for all study mixtures. Generally, lower FI value indicates the potential incompatibility among the RAP material, binder and RAs. It can be observed from the results that HRAP1 has low FI values for the mixtures having binder B and C indicating poor cracking performance. Mixtures with binder A show the highest values for both the indices, indicating better cracking resistance than corresponding mixtures with binder B and C which are PG 64-22 binders. Mixtures with binder B and C have lower values for the indices indicating inferior cracking properties. The inclusion of RA improves the fracture properties when compared to corresponding HRAP mixtures. It seems that RAs are more effective for mixtures with binder B and C than mixtures with binder A as improvement compared to corresponding HRAP mixture is more however, it is important to note that the FI values of the corresponding HRAP material were extremely low. It can also be noted that RA1 shows more effectiveness than RA2 in restoring the fracture resistance for mixtures with all three binders. RAP3 mixtures show better fracture properties compared to RAP1 and RAP2 mixtures due to lower HTPG of RAP binder. Furthermore, it is worth noting that RAP2 might be potentially more compatible than RAP1 as it shows better fracture properties for mixtures but they both have comparable aged binder PGs.

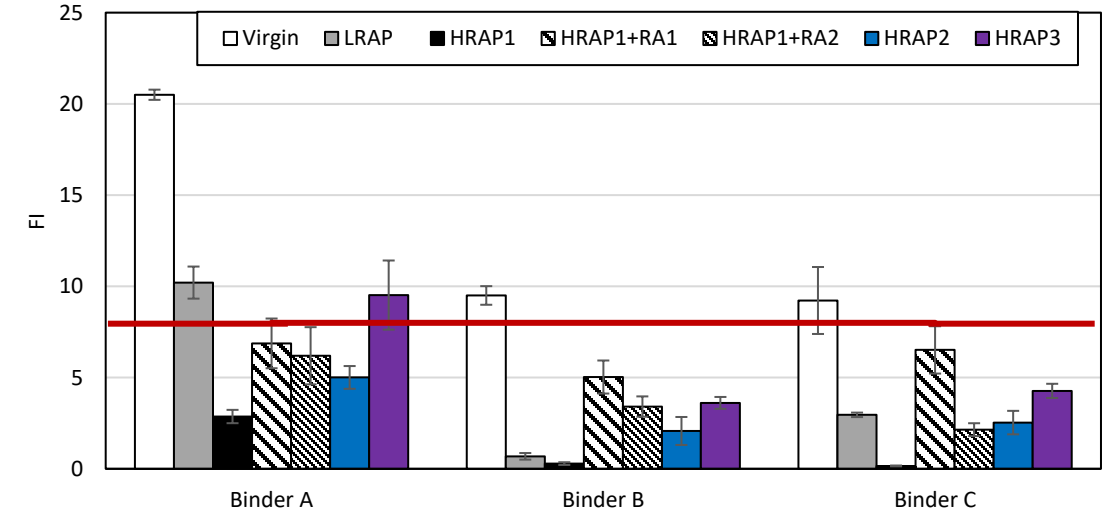

(a)

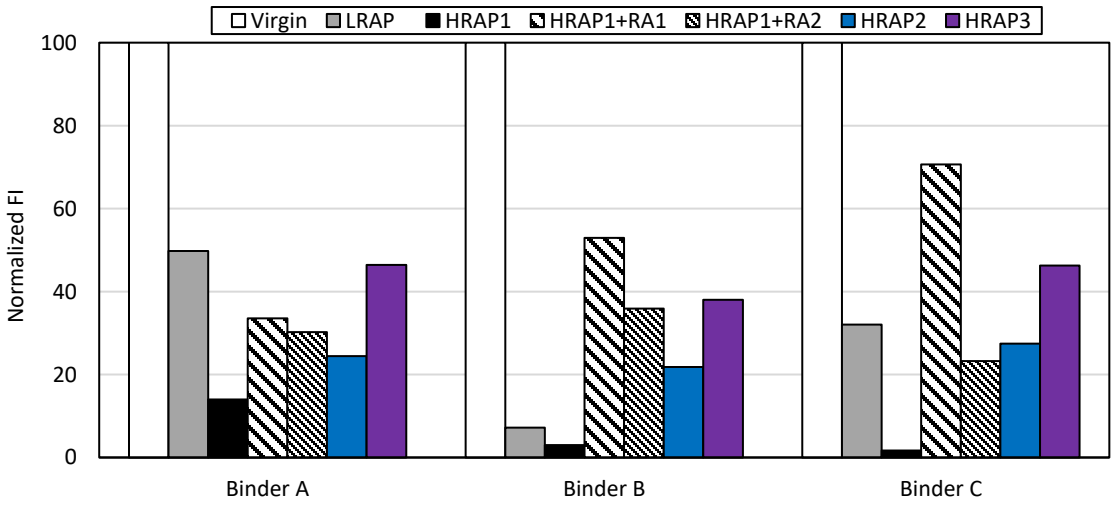

(b)

Figure 5-14 (a) FI parameter measured from I-FIT on study mixtures and (b) normalized FI values with respect to corresponding virgin mix

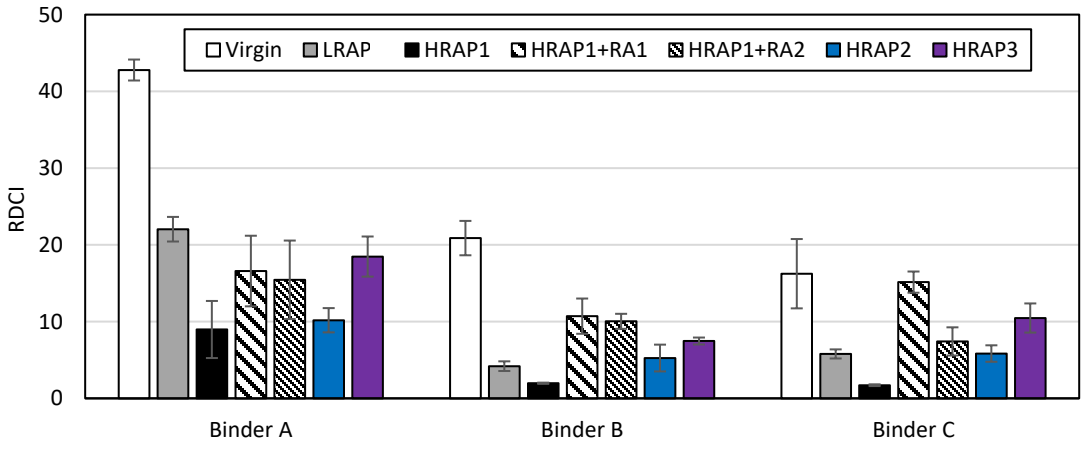

(a)

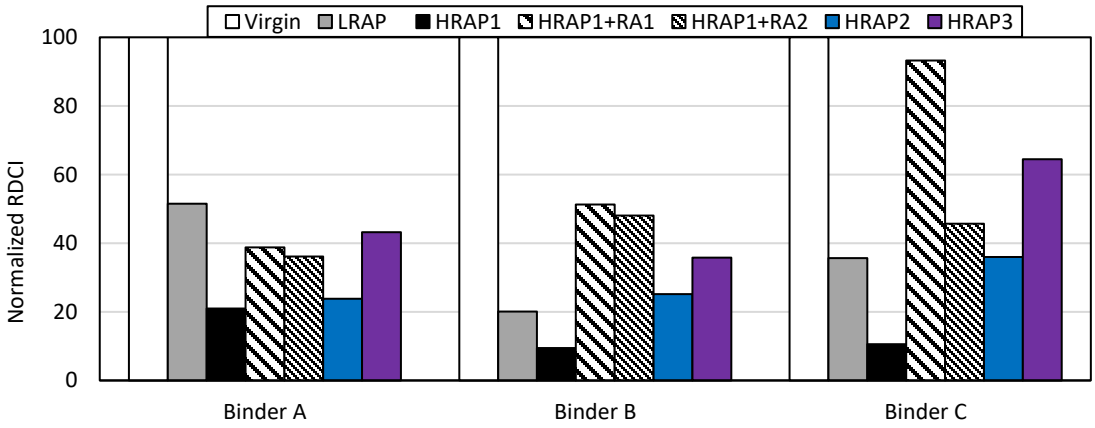

(b)

Figure 5-15 (a) RDCI parameter measured from I-FIT on study mixtures and (b) normalized RDCI values with respect to corresponding virgin mix

5.3.3 Disk-shaped Compact Tension Test

Figures 5-16 and **5-17** below show the calculated fracture energy and FST parameter and their normalized values with respect to corresponding virgin mix for all study mixtures. The RAP mixtures have lower G_f and FST values than the virgin mixtures, as expected. It can be noted that both the virgin and RAP1 mixture with binder A have the highest G_f and FST values whereas RAP2 and RAP3 have similar properties with all three binders. Mixtures with binder B have slightly higher G_f and FST values than the mixtures with binder C. All virgin mixtures and RAP mixture with binder A meet the current threshold value of 450 J/m^2 for the G_f parameter except HRAP2 mixture which is slightly less than the threshold. With the inclusion of RA, mixtures show higher FST values, indicating an improvement in thermal cracking resistance. However, there is an inconsistent trend with the G_f parameter. The mixtures treated with RA1 generally show higher G_f and FST values than RA2 which indicates that RA1 is more effective in improving the low temperature properties of control RAP which is in-line with fracture properties at intermediate temperature.

The case of HRAP1 with Binder A offers a puzzling response. When looking at the FI results this mix performs significantly more poorly than the LRAP1 + Binder A mix. However, the DCT results show a surprising opposite trend, with the HRAP1 mix showing better performance than the LRAP1 version. The results become more surprising when compared to the HRAP1 + RA1 or RA2, in which a relatively lower performance is observed. Based on these results one of two possible explanations come to mind: There is a potential lack of impact for either RA1 or RA2 products with binder A the control RAP material in terms of low temperature DCT. However, another explanation could be that the observed HRAP1 + Binder A DCT result is an outlier. This explanation can be further supported by the inconsistency with other mix performance tests (FI) and binder low temperature results (DCT and rheology).

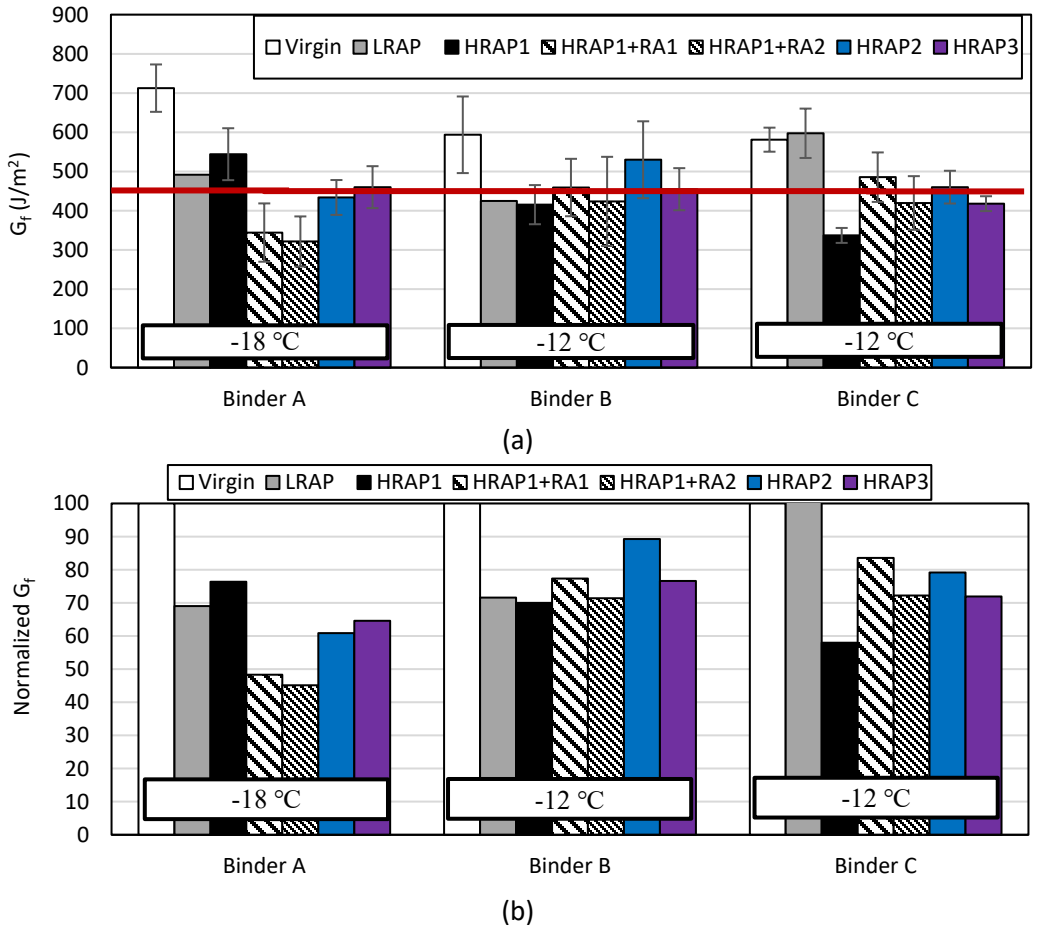

Figure 5-16 (a) G_f parameter from DCT and (b) normalized G_f values with respect to corresponding virgin mix

Generally, lower FST value compared to corresponding HRAP mixtures indicates the potential incompatibility between RAs and RAP material. As observed from **Figure 5-17,** the inclusion of both RA1 and RA2 decreases the FST value, instead of increasing, with binder A compared with the control RAP material indicating potential incompatibility of RAs with binder A.

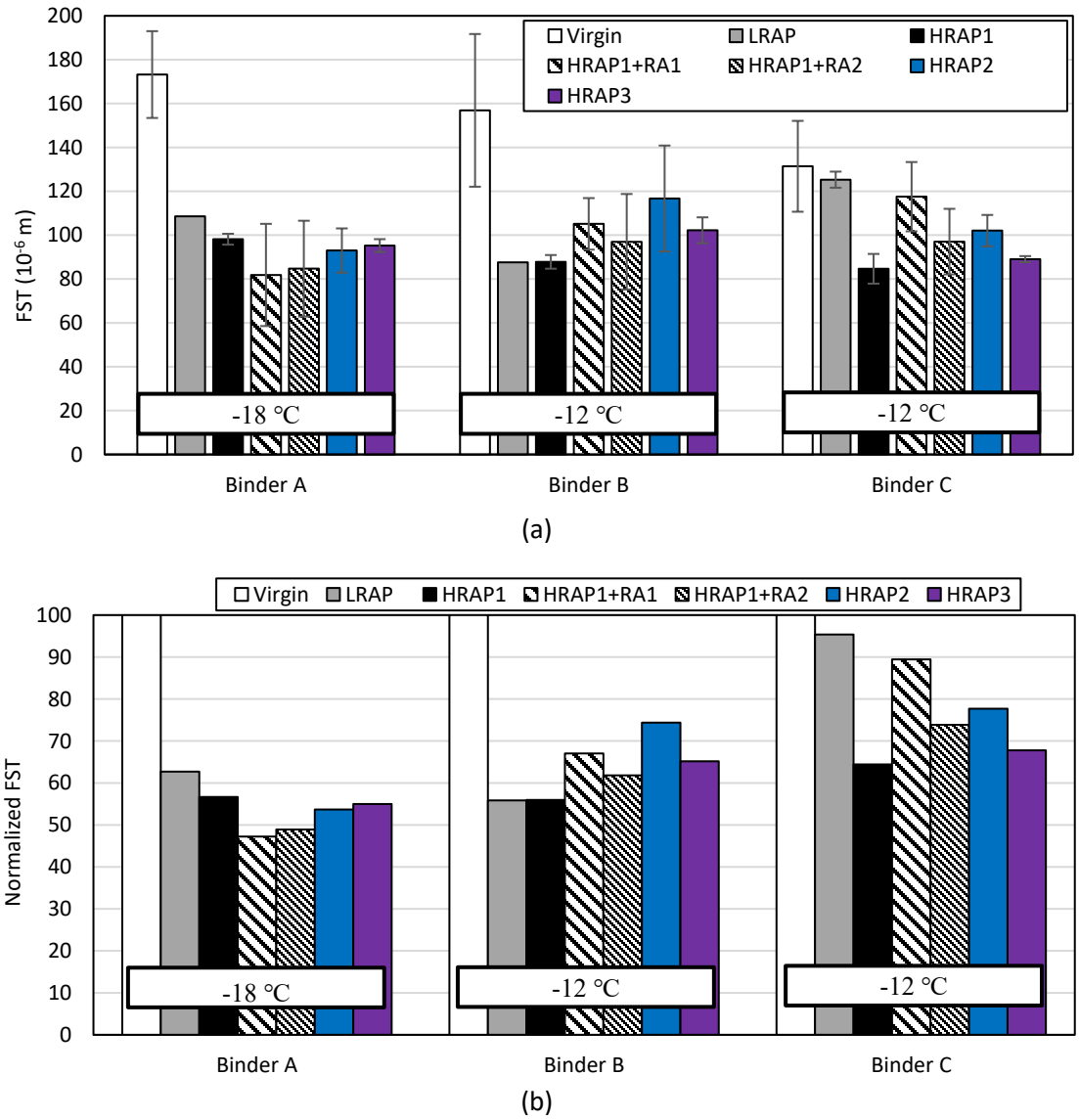

Figure 5-17 (a) FST parameter measured from DCT test on study mixtures and (b) normalized FST values with respect to corresponding virgin mix

5.4 STATISTICAL ANALYSIS OF TESTING RESULTS

In this section, the correlations between mixture testing parameters and corresponding extracted and recovered binder parameters are evaluated using various statistical methods. The evaluated materials include four RAP mixtures, six RA treated RAP mixtures with 45% RAP and 2 RAs and the corresponding extracted and recovered binders.

5.4.1 Statistical Correlation Methods

Pearson correlation coefficient and Hoeffding's D correlation analysis are selected as the statistical methods in this study. The frequently used Pearson's correlation method is only able to capture linear relationships, so Hoeffding's D correlation method is selected as a supplementary tool to screen the significant relevance between the results.

The Pearson correlation coefficient is a widely accepted measure of the linear relationship between two specified variables. Hoeffding's D correlation is a statistical method which can be used to infer nonlinear and also non-monotonic relationships between the variables. Generally, if the analysis between two variables shows a low Pearson coefficient but a high Hoeffding's D coefficient, it represents a potential non-linear relationship may exist between the two study parameters.

5.4.2 Binder-Mixture Correlation Analysis

The paired correlation coefficients between 5 mixture testing parameters and 12 binder testing parameters were calculated and summarized in a correlation matrix format. The two different correlation coefficients are presented in this section to screen significant linear/non-linear relationships. The Pearson correlation coefficients between the binder properties and the mixture properties are presented in **Table 5-4**. Values closer to 1 are shaded by green color indicating the stronger positive/negative relationship between the two parameters. The intensity of the color represents the strength of the correlation. Those correlations with a coefficient below 0.1 are not shaded with color, while those strong correlation (coefficients > 0.7) are also marked bold and italic.

As shown in the **Table 5-4**, most of the fracture parameters (except for G_f@DCT), and rheological parameter G-R_m show fair correlation (0.7 > correlation coefficient ≥ 0.5) to strong correlation (correlation coefficient ≥ 0.7) with multiple binder parameters. As a contrast, there is lack of significant correlation between G_f@DCT with most of the binder parameters. This might be due to the fracture energy showing a high variability at low temperature. All intermediate temperature fracture parameters from I-FIT testing show moderate to strong correlation with most of the binder parameters (except for ΔT_c, Tg, Tg_α and ϕ_α). Compared with I-FIT parameters, the low temperature fracture parameter FST shows more significant correlation with thermal parameters from DSC testing than the rheological parameters. The mixture rheological parameter G-R_m generally shows a fair to strong relationship with all the rheological and thermal binder parameters.

From the binder perspective, rheological parameter ΔT_c and thermal parameters Tg_α and Tg do not show significant relationship with any of the mixture parameters. The most promising binder parameter is

Tg_{Aave}, which shows significant correlation with almost all mixture parameters including fracture properties. By contrast, rheological parameters R, HTPG, T_c(m) and binder G-R parameter show strong relationships with intermediate cracking and mixture G-R_m, but those parameters show the shortcomings in representing low temperature cracking. As for the thermal binder parameter from DSC testing, Tg_β and Tg_{Aave} show a similar trend for correlation with mixture properties. Overall, thermal parameters have slightly stronger relevance with low temperature performance parameters.

Table 5-4 Pearson correlation coefficients between the corresponding mixture and binder parameters

			Mixture Properties				
			Fracture Parameters				Rheological Parameters
			FI	RDCI	G_f@DCT	FST	G-R_m
Binder Properties	Rheological Parameters	R	0.65	0.62	0.39	0.37	0.51
		T_c(S)	0.46	0.48	0.25	0.30	0.52
		T_c(m)	0.59	0.58	0.29	0.27	0.66
		ΔT_c	0.45	0.41	0.20	0.13	0.48
		HTPG	**0.91**	**0.90**	0.11	0.16	**0.84**
		LTPG	0.48	0.49	0.27	0.30	0.54
		G-R	0.46	0.45	0.30	0.28	0.54
	DSC Parameters	Tg_α	0.36	0.37	0.27	0.42	0.40
		Tg_β	0.50	0.52	0.35	0.55	0.52
		Tg_{Aave}	**0.73**	**0.76**	0.41	0.61	**0.78**
		ϕ_α	0.48	0.52	0.21	0.27	0.38
		Tg	0.44	0.44	0.35	0.49	0.48

Table 5-5 below shows the Hoeffding's D correlation matrix. The values of Hoeffding's D coefficients are generally between -0.04 and 0.22, which indicates relatively weak nonlinear correlations. In other words, a low value of Hoeffding's D coefficients indicates there is not a strong non-linear relationship between any pairs of mixture and binder parameters.

Table 5-5 Hoeffding's D correlation between the corresponding mixture and binder parameters

			Mixture Properties				
			Fracture Parameters				Rheological Parameters
			FI	RDCI	G_f@DCT	FST	G-R_m
Binder Properties	Rheological Parameters	R	0.10	0.08	0.00	-0.01	0.10
		T_c(S)	0.17	0.14	0.04	0.03	0.15
		T_c(m)	-0.02	-0.03	-0.04	-0.03	-0.02
		ΔT_c	0.08	0.07	0.01	-0.02	0.07
		HTPG	0.10	0.06	0.00	-0.01	0.12
		LTPG	0.01	0.03	-0.03	-0.02	0.02

		G-R	0.22	0.15	0.03	0.01	0.12
	DSC Parameters	Tg_{α}	-0.01	-0.02	-0.02	-0.01	0.01
		Tg_{β}	0.02	0.04	-0.03	0.06	0.09
		Tg_{Aave}	0.13	0.19	-0.04	0.00	0.16
		ϕ_{α}	0.07	0.07	0.01	-0.03	0.06
		Tg	0.04	0.01	-0.03	0.02	0.06

In summary, the G-R_m parameter calculated from the mixture complex modulus testing shows the most promising correlation with many binder properties. As a mixture cracking parameter, the G-R_m shows a strong relationship (correlation coefficients >0.7) with the thermal parameters and has a fairly good relationship with fracture related rheological binder parameters as well. Thus, the G-R_m parameter is considered as the critical parameter for compatibility characterization in the next step of the analysis. Also notice FI parameter from the I-FIT test shows good relationship with both rheological and thermal properties of binder.

5.4.3 Statistical Analysis by Comparing Means

The ability of a test or method to differentiate the effect of different binder types and recycling agents is very important for compatibility characterization. The connecting letter analysis was conducted on replicates for 5 mixture fracture indicators (FI and RDCI from I-FIT test; G_f and FST from DCT test; and G-R_m parameter from E* test). These results can be used to assess the sensitivity of a test or indicator by means of showing how many groups can be classified statistically and how each group is different from another groups. In the report, group letter A indicates the group has the best value of the property with respect to cracking resistance. Materials with a different group letter (e.g., B) are statistically significantly different. If there's a connecting letter (e.g., AB), it indicates that it can still be distinguished as a different group, but is statistically part of both groups (e.g., A and B).

Table 5-6 below presents the connecting letter report for the parameters calculated for each of the nine mixtures. Intermediate temperature cracking parameters (FI, RDCI, G-R_m), especially FI, categorize the mixtures into 12 groups without significant overlap between the groups as represented. They can classify the effect of the binder and RA types in addition to the ability to discriminate between the RA-treated mixtures and untreated mixtures. The connecting letter report for FI shows that virgin mixtures have better fracture resistance compared to all other mixtures having RAP. The results indicate that Binder A is more resistant to cracking with the RAP1 material than Binder B and binder C without RA indicating potential compatibility of binder A. It is also worth to note that results show better compatibility of RA1 with all RAP material than RA2 which did not show significant improvement in fracture performance compared to corresponding RAP mixtures without any RA. It can be concluded that RA2 is potentially incompatible with binders B and C because it did not improve the fracture performance of mixtures containing these binders, whereas it did improve the fracture performance of mixtures containing binders A and made it comparable to that of RA1. Overall, RA1 appears to be more effective, or potentially more compatible than RA2, particularly with binder C due to the change in groupings. From binder's perspective, it seems that binder A is compatible with all RAP materials

whereas binder B is potentially incompatible with all RAP materials. It can be observed that FI, RDCI and E* results follow a very consistent trend with respect to differentiating binder types and RAs. Consequently, both FI and RDCI are a suitable choice for compatibility characterization methods in terms of their cracking at intermediate temperatures.

It seems that G_f at low temperature fails to effectively differentiate the mixtures, since most mixtures are classified under several groups due to higher variability in G_f at low temperatures. However, the FST parameter not only shows the ability to discriminate between the RA-treated mixtures but also can classify the effect of the binder and RA types. It is interesting to note that the connecting letter report indicates that RAs are unable to improve the low temperature performance as they did not increase the cracking resistance of any of the mixtures. It also shows that binder A might have lower compatibility with both RAs than binder B and C, since HRAP-A starts in a higher category, but only increases to the same or a lower category than materials with binders B or C. The connecting letter report for each parameter is shown in Appendix B.

Table 5-6 Summary of connecting letter report for fracture indices (α=0.05)

Tests	I-FIT		E*	DCT	
Indicators	**FI**	**RDCI**	**G-R_m**	**G_f**	**FST**
V-A	A	A	A	A B C D	B C D
V-B	B C	B C	B C	A B C	A B
V-C	B C	C D	B	A	A
LRAP-A	B	B	B C	B C D E F G H	B C D E F
LRAP-B	I	F G H	E F	C D E F G H	C D E F
LRAP-C	G H	E F G	F G H	A B C D	B C D E
HRAP1-A	G H	E F	E F	E F G H	E F
HRAP1-B	I	G H	I	B C D E	E F
HRAP1-C	I	H	I	G H	D E F
HRAP2-A	E F	E	B C D	E F G H	E F
HRAP2-B	H I	F G H	F G H	A B	A B C
HRAP2-C	H	F G H	I	C D E F G	D E F
HRAP3-A	B	B C D	B	C D E F G	E F
HRAP3-B	F G H	E F	F G	C D E F G H	D E F
HRAP3-C	F G	E	G H	E F G H	D E F
HRAP1-A-RA1	D E	C D	C D	F G H	F
HRAP1-B-RA1	E F	E	E F	D E F G	D E F
HRAP1-C-RA1	C D	D	D E	B C D E F	C D E F
HRAP1-A-RA2	D E	D	B C D	H	E F
HRAP1-B-RA2	F G H	E	H	E F G H	D E F
HRAP1-C-RA2	H I	E F	F G H	E F G H	D E F
Ranges	A~I	A~H	A~I	A~H	A~F
Groups	12	12	12	14	10

5.4.4 Compatibility Ranking

The following performance index was developed to provide a relative comparison of the magnitude of a particular parameter for the various mixtures and binders. The performance index is defined as the percent difference with respect to the best value within the group of materials being compared (equation 13). The higher performance index reveals potentially inferior performance. Variable (such as binder type, RAP and RA type) which cover broader range of performance index variation, i.e., difference between maximum and minimum index values of a group analyzed, is considered to have a dominant effect.

$$Performance\ Index = \frac{Best\ Value - Value}{Best\ Value} \times 100\% \quad (13)$$

Table 5-7 below shows the performance index calculated from the mixture testing results evaluating compatibility of both rejuvenators. The color map was shaded based on the performance index ranking within each indicator. The mixture with a higher index value and shaded with a darker color shows inferior properties. It can be observed that most of the mixture parameters show significant differences between the RA treated mixtures and non-RA treated mixtures. This indicates that selected parameters can distinguish the RA's effect on the binder, and they are more likely to be affected by the RA. From the table, all mixture properties were improved when RAs are used, covering the broader range of performance index. When considering the binder type, it can be concluded that it also affects the mixture properties but not as significantly as the RA type, as it covers a smaller range than that covered by the RA type. For example, for the FI parameter, the ranges covered by RA for binder A, B, and C are from 0% to 58.32%, 26.82% to 95.85%, 5.19% to 97.74%, respectively, whereas the ranges covered by binder type for without any RA, with RA1 and with RA2 are from 58.32% to 97.74%, 0% to 26.82% and 9.87% to 68.79% respectively. As RA variation covers a broader range than that by binder type variation, it can be concluded that RA shows a dominant effect, as shown in the last row of the table. Both rejuvenators improve the intermediate fracture properties; however, they could not improve their low-temperature performance, especially for RAP1 mixtures with binder A. This inability to discriminate between mixtures at low temperatures may be caused by different testing temperatures, which are adjusted based on the LTPG of the binder, i.e., -18 ℃ for mixes with binder A and -12 ℃ for mixes with binder B and C. Overall, using RA1 improved the mixture's properties, while using RA2 improved them as well, though not as much as using RA1. This suggests that RA1 is more compatible with all RAP materials than RA2.

Table 5-7 Performance index identified from mixture test results to evaluate compatibility of RA and binder

Mixture Performance Index (%)					
Mixture ID	**Rheological Analysis**	**Inter. Temp. Fracture**		**Low Temp. Fracture**	
	G-R_m	**FI**	**RDCI**	**G_f**	**FST**
HRAP1-A	72.84	58.32	45.92	0.00	16.50
HRAP1-B	167.55	95.85	88.11	23.65	25.29
HRAP1-C	139.04	97.74	89.66	38.06	27.98
HRAP1-A-RA1	12.32	0.00	0.00	36.73	30.36
HRAP1-B-RA1	57.84	26.82	35.43	15.62	10.54

HRAP1-C-RA1	32.13	5.19	8.70	10.77	0.00
HRAP1-A-RA2	0.00	9.87	6.88	40.91	27.92
HRAP1-B-RA2	100.88	50.39	39.49	22.12	17.49
HRAP1-C-RA2	71.67	68.79	55.27	22.80	17.43
Dominant Effect	**RA**	**RA**	**RA**	**-**	**-**

Table 5-8 below shows the performance index calculated from the mixture testing results of mixtures containing different RAP materials and binders. From the results, RAP1 (control RAP) and RAP3 have the worst and best intermediate fracture properties respectively for all binder, indicating potential incompatibility and compatibility respectively. It seems that binder type shows more dominant effect (highest range coverage) for G-R_m, whereas RAP type dominates the intermediate temperature cracking property such as FI. Furthermore, at low temperatures, it is observed that neither binder nor RAP can show dominant effect which again may be due to adjusted testing temperatures based on the LTPG of the binder. Overall, it seems that RAP3 is potentially more compatible with binder A than any other binders.

Table 5-8 Performance index identified from mixture test results to evaluate compatibility of RAP and binder

Mixture Performance Index (%)					
Mixture ID	**Rheological Analysis**	**Inter. Temp. Fracture**		**Low Temp. Fracture**	
	G-R_m	**FI**	**RDCI**	**G_f**	**FST**
HRAP1-A	85.89	69.91	51.44	0.00	15.91
HRAP1-B	187.75	97.01	89.33	23.65	24.75
HRAP1-C	157.09	98.37	90.71	38.06	27.46
HRAP2-A	32.13	47.40	44.90	20.27	20.32
HRAP2-B	119.12	78.23	71.54	2.61	0.00
HRAP2-C	189.85	73.40	68.38	15.44	12.54
HRAP3-A	0.00	0.00	0.00	15.45	18.39
HRAP3-B	109.80	62.05	59.55	16.41	12.40
HRAP3-C	141.17	55.15	43.33	23.18	23.69
Dominant Effect	**Binder**	**RAP**	**-**	**-**	**-**

Tables 5-9 and 5-10 below show the performance index calculated from the binder testing results. From the rheological analysis results, it can be observed that T_c(S), T_c(m), ΔT_c, LTPG and log(G-R) values can differentiate among RAP materials, RA and binder type. Extracted samples with binder A always have a good performance for most of rheological parameters related to cracking, which is reasonable considering the lower PG of binder A. G-R parameter indicates that RAP3 blends among all RAP materials showed better results and RAP1 (control RAP) blends showed worst results. These results agree with the mixture results. HRAP1 blends showed inferior performance with binder B indicating potential incompatibility of binder B. From thermal analysis results, it is evident that Tg_α, Tg_β and Tg_{Aave} are the most relevant parameters to mixture cracking results as they showed the potential ability to differentiate between the effects of RAs and RAP materials. Furthermore, results also indicate that RA1 may be generally more compatible with mixtures with all binders than RA2. The performance index for the remaining parameters evaluated in the report is also reported in Appendix B.

Table 5-9 Performance index identified from binder test results to evaluate compatibility of RAP and binder

Binder ID	Binder Evaluation							
	Rheological Analysis					Thermal Analysis		
	$T_c(S)$	$T_c(m)$	ΔT_c	LTPG	Log(G-R)	Tg_α	Tg_β	Tg_{Aave}
V-A	0.00	7.66	67.96	0.20	0.00	2.41	0.00	0.00
V-B	6.17	13.55	71.24	6.36	122.53	9.13	25.55	16.27
V-C	13.40	19.76	70.32	13.58	123.89	0.00	12.25	22.43
HRAP1-A	20.44	25.81	69.56	20.60	155.05	38.58	179.07	52.65
HRAP1-B	24.67	42.20	156.82	34.22	193.98	24.30	145.88	56.14
HRAP1-C	24.68	34.71	105.22	25.69	179.44	37.45	166.16	61.92
HRAP2-A	11.14	10.44	19.81	11.32	120.67	39.86	193.89	54.55
HRAP2-C	13.90	25.30	105.49	14.98	165.43	28.64	136.32	54.85
HRAP3-A	2.51	0.00	0.00	2.71	87.29	23.91	131.23	40.33
HRAP3-C	6.15	15.36	83.79	6.34	129.71	18.90	98.39	46.83
LRAP-A	13.20	12.99	24.90	13.37	86.07	31.28	129.46	41.31
LRAP-B	0.88	13.06	99.85	0.00	149.62	3.60	64.16	37.77
LRAP-C	6.09	15.64	86.14	6.28	152.67	25.58	120.23	55.52

Table 5-10 Performance index identified from binder test results to evaluate compatibility of RAP, binder, and RA

Binder ID	Binder Evaluation							
	Rheological Analysis					Thermal Analysis		
	$T_c(S)$	$T_c(m)$	ΔT_c	LTPG	Log(G-R)	Tg_α	Tg_β	Tg_{Aave}
HRAP1-A	33.10	25.81	69.56	29.75	261.53	37.39	219.30	46.93
HRAP1-B	36.66	42.20	156.82	41.80	375.78	22.83	169.22	50.85
HRAP1-C	36.66	34.71	105.22	34.26	333.10	36.24	199.82	57.32
HRAP1-A-RA1	16.27	13.10	102.82	12.50	253.57	7.63	45.59	11.82
HRAP1-B-RA1	22.21	28.89	168.92	28.40	348.03	6.57	19.44	22.75
HRAP1-C-RA1	26.33	28.62	137.48	28.13	321.33	12.83	71.23	22.78
HRAP1-A-RA2	27.03	17.28	54.38	23.38	225.47	21.32	70.67	24.88
HRAP1-B-RA2	22.60	25.66	143.82	25.14	341.83	12.55	41.16	30.34
HRAP1-C-RA2	21.62	20.58	115.94	20.04	284.49	3.26	15.61	12.56
HRAP2-A	25.28	10.44	19.81	21.55	160.65	38.69	241.66	49.06
HRAP2-C	27.60	25.30	105.49	24.79	291.98	27.26	154.80	49.40
HRAP2-A-RA1	14.47	3.97	52.89	10.20	126.98	3.11	29.53	6.55
HRAP2-C-RA1	27.53	18.84	61.49	23.91	273.54	3.97	1.38	13.42
HRAP2-A-RA2	21.10	6.54	22.92	17.16	178.57	16.24	107.70	25.11
HRAP2-C-RA2	22.32	16.66	83.93	18.44	249.31	24.28	141.41	41.20
HRAP3-A	18.03	0.00	0.00	13.93	62.71	22.44	147.12	33.13
HRAP3-C	21.09	15.36	83.79	17.14	187.17	17.33	97.56	40.41
HRAP3-A-RA1	0.00	1.41	139.14	0.00	0.00	0.00	0.00	0.00
HRAP3-C-RA1	12.78	6.10	79.65	8.42	149.40	5.32	18.47	19.45
HRAP3-A-RA2	20.85	8.73	39.82	18.05	93.78	15.64	84.86	23.98
HRAP3-C-RA2	20.44	10.84	57.28	16.47	173.07	15.44	84.81	33.42

5.5 CHAPTER SUMMARY

This chapter evaluated core materials of the study and proposed promising methods for characterization of binder and mixture compatibility based on the extracted binder and mixture test results of the core materials. Binders were evaluated for rheological and thermal properties using DSR and DSC, respectively. Rheological characterization indicates that binder B among all binders shows more incompatibility with RAP1 material as well as with both RAs. Black space diagram is clearly able to capture the effect of RAs and different RAP materials and also indicates the potential incompatibility of binder B with all RAP1 material and potential compatibility of RAP3 material with all binders. Furthermore, DSC thermal analysis shows that the ϕ_α and Tg related parameters have the greatest ability to characterize the compatibility of materials. From mixture results, FI, RDCI, FST and mixture Glover-Rowe parameters were identified as the potential indicators for mixture compatibility characterization as they can differentiate between various binders and RAP materials. The correlation analysis shows that the rheological parameter Tc(m), R and G-R generally correlate well with most fracture-based mixture parameters. FI from I-FIT generally shows moderate to strong correlation with most of the rheological and thermal parameters of binder. The connecting letter report shows that the RA2 shows a significant incompatibility with all RAP materials and binders. It also indicates that the FST performs well for screening low temperature cracking properties and RDCI and FI perform well for screening intermediate temperature cracking properties. Finally, compatibility ranking analysis also supports that binder B is the most incompatible binder and RAP1 is the most incompatible RAP material among all the core materials evaluated in the study.

Chapter 6: VALIDATION MATERIALS AND FIELD PERFORMANCE

The previous chapter focused on the evaluation and determination of the test methods and tools that are sensitive and able to differentiate the compatibility of the asphalt materials. Various binder and mixture test methods that are able to characterize the compatibility were also recommended. The main objective of this chapter is to validate the parameters recommended in the previous chapter and to correlate with the field performance by testing validation materials. Moreover, the effects of various mixture components such as binder, RAP, and RAs are evaluated. Finally, the correlation analysis of binder and mixture properties has been conducted for both core and validation materials.

6.1 VALIDATION MATERIALS

The material base that was generated for this chapter is summarized and presented in **Table 6-1** below. Eight mixtures were selected and evaluated as validation materials in this chapter in order to cover geographical variation as much as possible.

Table 6-1 Material base generated for validation materials

Binder/ Mixture ID	Material Source	Virgin Binder PG	Testing Methods for Evaluation of Extracted Binder	Testing Methods for Mixture
MO-VL	Missouri (30% RAP & 3% RAS)*	46-34	DSC, DSR	IFIT, DCT
MN-VL	Minnesota (45% RAP+RA)	58-28		
TX10-VL	Texas (10% RAP)	70-22		
TX30-VL	Texas (30% RAP)	64-22		
VA-VL	Virginia (35% RAP+RA)	58-28		
IL-VL	Illinois (22% RAP+2.5% RAS)	58-28		
NCAT30-VL	NCAT (30% RAP)	64-22		
NCAT45-VL	NCAT (45% RAP+RA)	64-22		

* % RAP and RAS shows % of recycled binder ratio (RBR) in the mix.

6.2 FIELD PERFORMANCE

Performance history of the test sections laid with some of the validation materials are also collected to correlate with the laboratory evaluation. For both NCAT mixtures, 5-year field performance data on cracking, rutting, IRI (international roughness index), and texture were collected and presented below. Although both sections were subjected to more than 13 million equivalent standard axle loads (MESALs) by November 2022, they did not show any signs of inferior performance. The measured performances of NCAT mixtures are represented in **Table 6-2**. Cracking, rutting, IRI and texture have been tracked to evaluate the field performance. The performance graphs of these mixtures are attached in Appendix C. Overall, it can be concluded that NCAT mixtures are showing very good performance in the field.

Table 6-2 Summary of field performance of the validation materials

Field Section (Traffic) / Performance Parameters	NCAT30-VL (>13 MESALs)	NCAT45-VL (>13 MESALs)
Cracking (% of lane)	<3%	<2%
Rutting (mm)	<2	<5
Mean IRI (in/mile)	<100	<100
Texture (mm)	<1	<1

6.3 TESTING OF MATERIALS

This section covers the testing methods and information about the evaluated materials. Eight mixtures were selected as validation materials, and their binder and mixture properties were assessed.

6.3.1 Testing Methods Overview

Recommended binder and mixture testing methods from chapter 5 are presented in **Table 6-3**. The binder tests include rheological characterization using the DSR and thermal analysis using the DSC. Assessment of mixture fracture properties is also conducted because of the presence of RAP and use of RAs as these materials are fully blended during the extraction and recovery process but not in the field.

Table 6-3 Selected binder and mixture testing methods

Binder Test Methods	**Thermal Analysis**	Modulated Differential Scanning Calorimeter (DSC)
	Rheological Tests	Dynamic shear rheometer testing (DSR; with 4-mm, 8-mm and 25-mm plate)
Mixture Test Methods	**Intermediate Temperature Cracking Test**	Illinois-Flexibility Index Semi-Circular Bend Test (I-FIT)
	Low Temperature Cracking Test	Disc-shaped Compact Tension Test (DCT)

6.4 EXTRACTED BINDER AND MIXTURE PERFORMANCE TEST RESULTS

This section focuses on the testing results of the recovered binders and mixtures for the validation materials. The section first discusses the binder results and corresponding observations, followed by the mixture results and discussion. Binder results include rheological and thermal properties, while mixture testing covers cracking characterization at intermediate and low temperatures.

6.4.1 Extracted Binder Performance Results

6.4.1.1 Rheological Analysis Results (DSR Testing)

Figure 6-1 and **Figure 6-2** summarize the measured continuous PGs of the extracted and recovered binder blends for all eight validation materials. MO-VL shows the lowest HTPG, as expected, as it has the softer virgin binder (PG 46-34) (**Figure 6-1**). Although the TX30-VL has a higher RBR, it shows lower HTPG than that of TX10-VL. This can be explained by the softer binder used in TX30-VL to compensate for the higher RBR. RA imparts a softening effect in NCAT45-VL and compensates for a higher RBR. This results in lower HTPG of the blend.

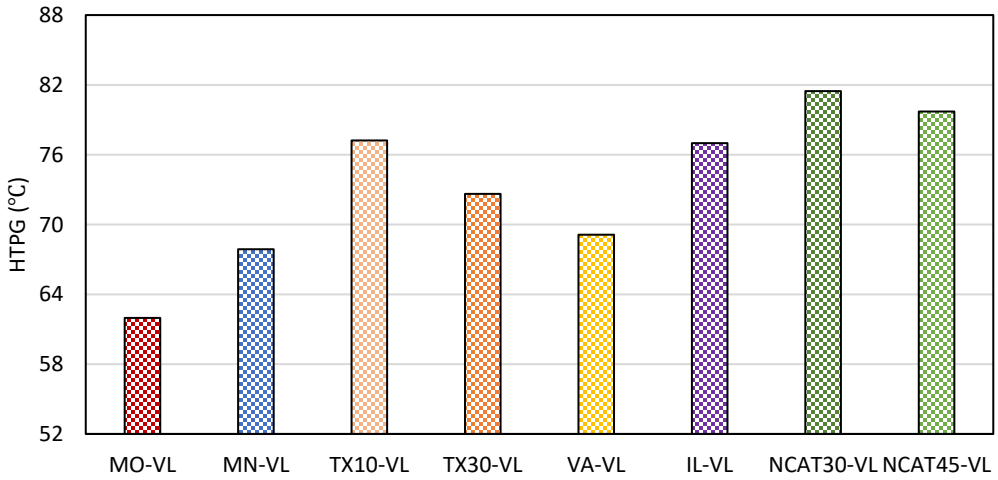

Figure 6-1 HTPG of the extracted and recovered binder blends

Figure 6-2 shows the LTPG of the blends for all validation mixtures in an as-extracted condition. MO-VL shows the lowest LTPG due to softer virgin binder (PG 46-34). Even though the MN-VL does not have RA and has higher RAP content, it managed to show comparatively lower LTPG indicating good low temperature characteristic. Furthermore, both NCAT mixtures show similar LTPG values indicating the capability of RA to compensate for the adverse impact of additional RAP for NCAT45-VL mixture.

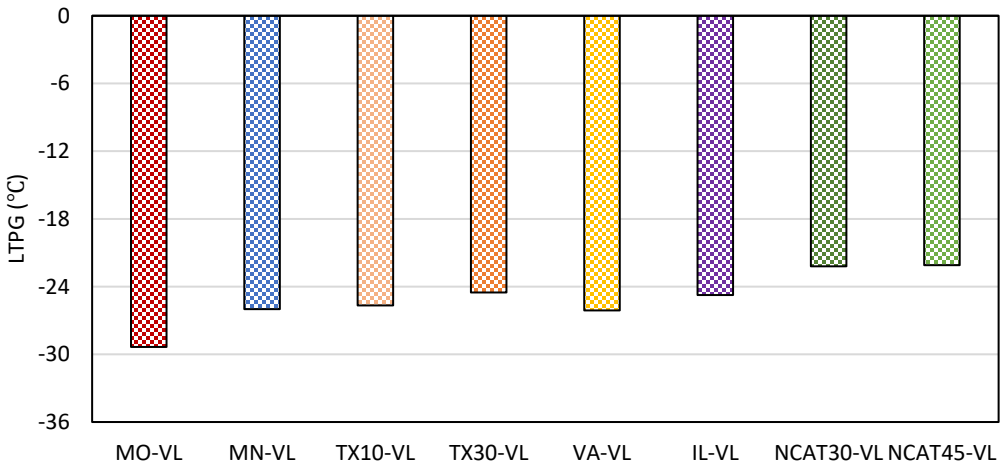

Figure 6-2 Comparison of LTPG values

Figure 6-3 below presents the ΔT_c values for all 1xPAV aged blends. All 1xPAV binders have ΔT_c values above the currently proposed cracking limit threshold of -5 °C. The inclusion of the RA generally decreases the ΔT_c values for the blended binders as both NCAT30-VL (no RA) and NCAT45-VL (with RA) show comparable ΔT_c values. MN-VL shows exceptionally high ΔT_c value, indicating higher low temperature cracking resistance.

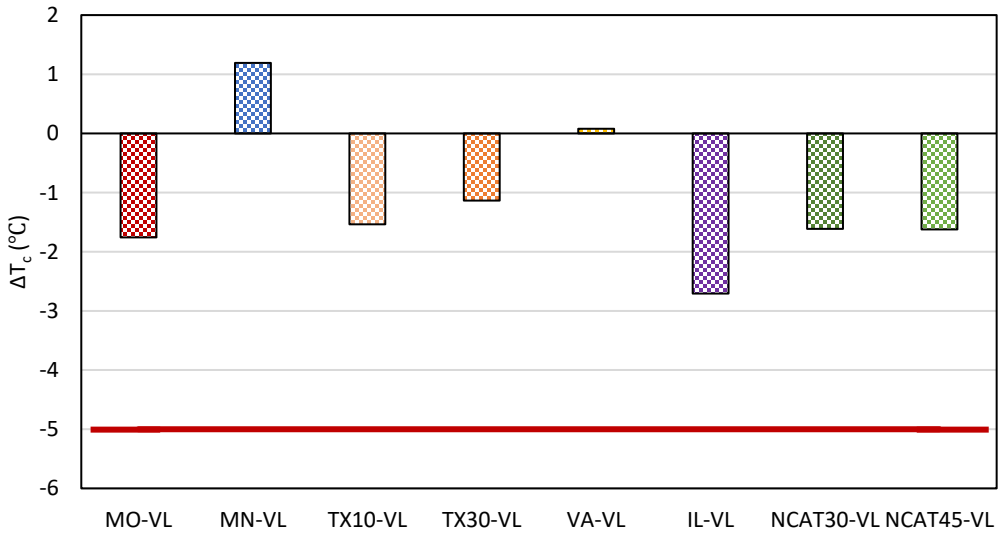

Figure 6-3 ΔT_c parameter of the extracted and recovered binders with aging

Figure 4-4 and **Figure 6-5** below show the G* vs phase angle of blends in the Black space and the Glover-Rowe (G-R) parameters binder blends in 1xPAV aged condition. It can be observed that only MO-VL, VA-VL and MN-VL blends are below the warning and cracking limits of 180 kPa and 600 kPa respectively. Given it has 45% RAP, the MN-VL RAP may be more compatible because G-R is below the warning limit and has the highest phase angle. Furthermore, both NCAT30-VL and NCAT45-VL are above the cracking limit indicating potential for cracking. It is interesting to observe that NCAT45-VL has better properties than NCAT30-VL although it has higher RAP content. This could imply that the incorporated RA has

alleviated the effect of higher RAP amount. MO-VL shows lowest stiffness and highest phase angle value indicating better rheological properties from cracking perspective whereas the NCAT30-VL shows the highest stiffness indicating potential for inferior rheological properties.

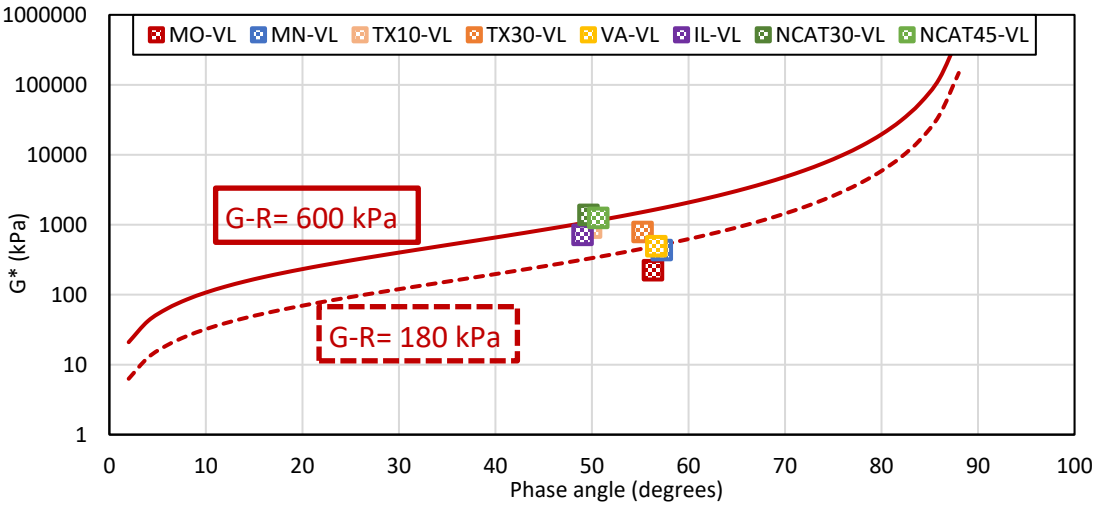

Figure 6-4 G-R Black space diagram for as-extracted binder blends

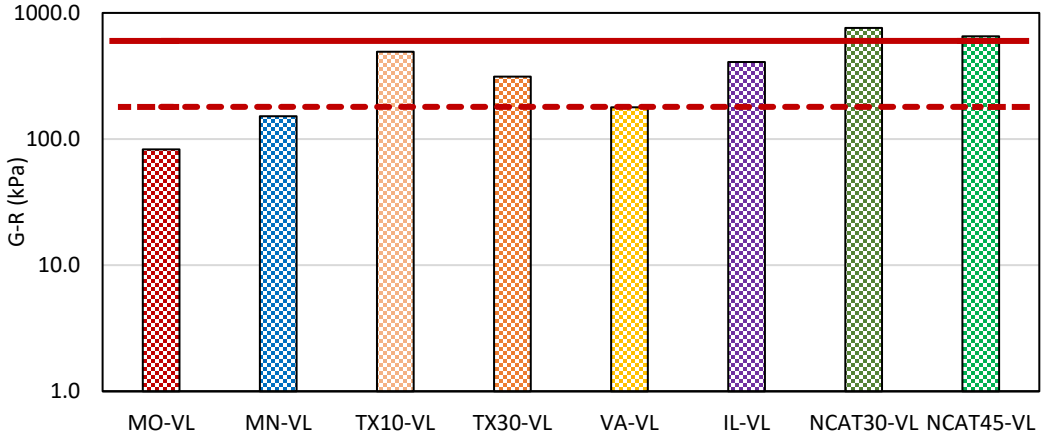

Figure 6-5 G-R parameter for all validation binder blends

Figure 6-6 below shows the R-values for all blends in as-extracted condition. Generally, the R-values of the binder generally increase with the addition of both RAs and aging levels. TX10-VL has the highest R-value among all blends. Both NCAT30-VL and NCAT45-VL show similar R-values, aligning with the previous observations, emphasizing the effectiveness of RA.

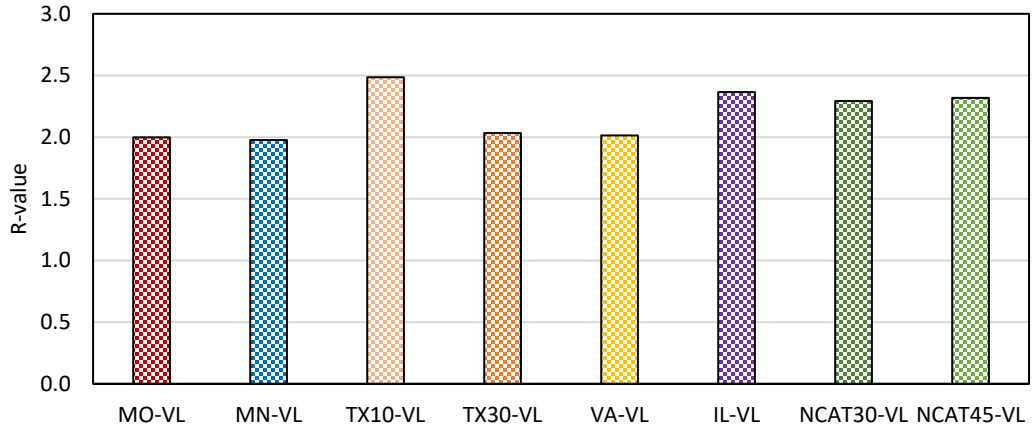

Figure 6-6 R-value parameter for all validation binder blends

6.4.1.2 Thermal Analysis Results (DSC Testing)

Figure 6-7Figure 6-8, andFigure 6-9 below show the Tg_{α}, Tg_{β} and Tg values measured from the DSC test results for the extracted and recovered binders from the eight-validation mixtures. Comparing the results to the mixture compositions (previously shown in **Table 6-1**) a few trends can be observed: the Tg_{α} seems to roughly correspond to the overall virgin binder low temperature grade, or in the case of the NCAT45 mix, the virgin binder including the RA. Whereas the Tg_{β} did not generally follow the grade trends, but it demonstrate a couple of interesting datapoints: in the TX mixes, the higher RAP version resulted in a warmer $Tg_{\beta,}$ which is to be expected, on the other hand, despite the increase in RAP content between the NCAT30 to NCAT45 (30 to 45% RAP), the inclusion of the RA in the NCAT45 section seems to have resulted in an overall lower Tg temperature. The overall experimentally derived Tg shows a somewhat similar trend.

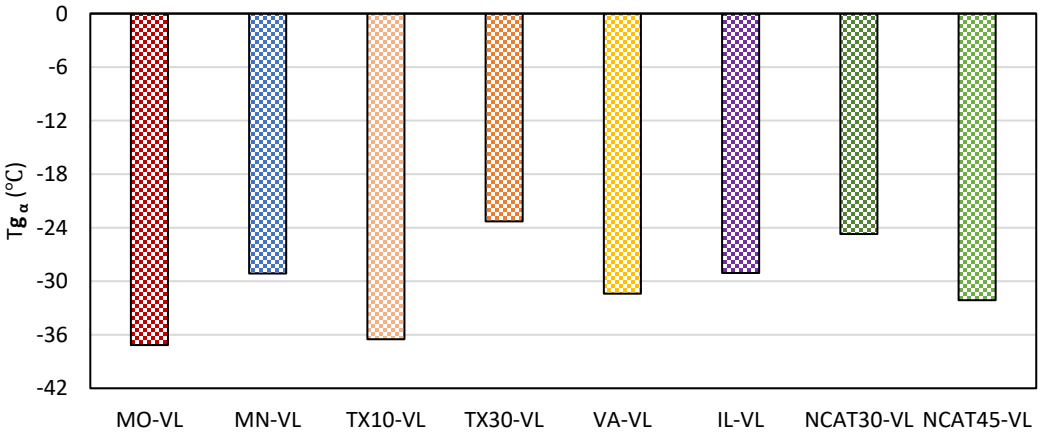

Figure 6-7 Tg_{α} parameter for extracted and recovered validation binder blends

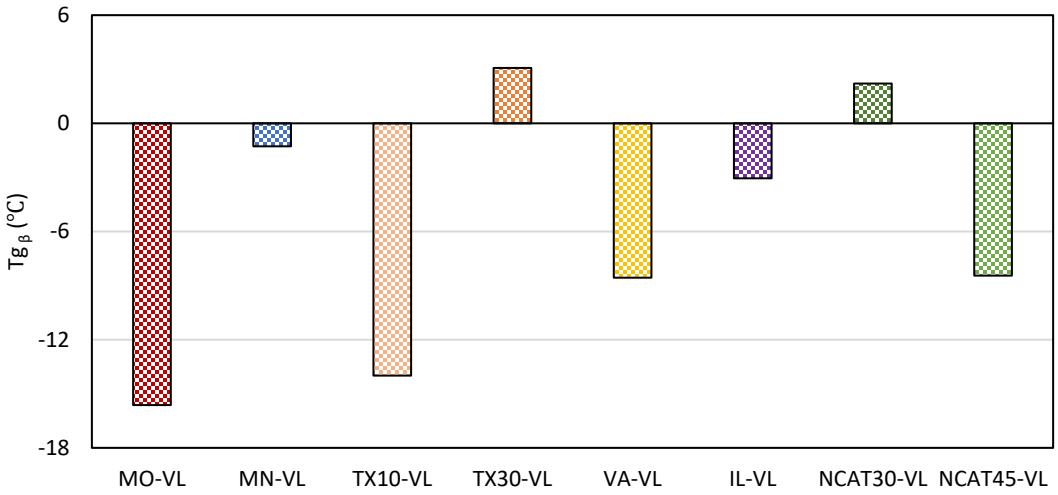

Figure 6-8 Tg_β parameter for extracted and recovered validation binder blends

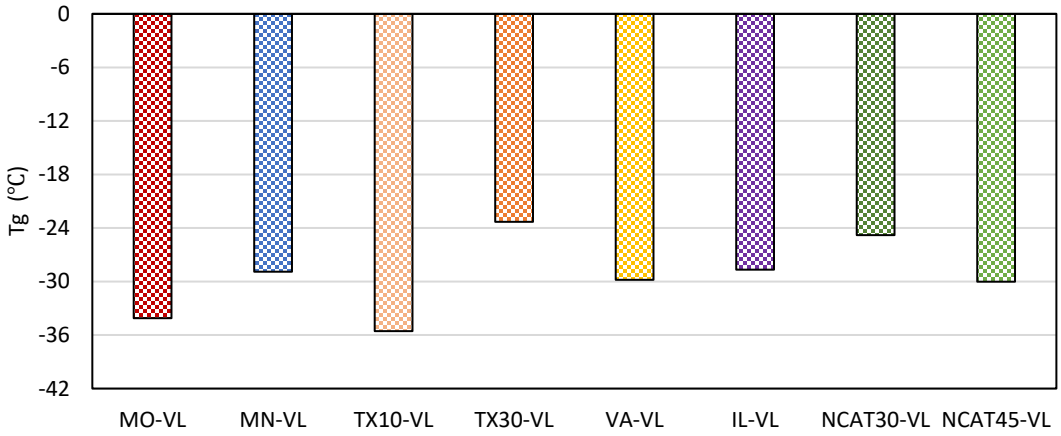

Figure 6-9 Tg parameter for extracted and recovered validation binder blends

The ϕ_α parameter, shown in **Figure 6-10**, shows a more discriminating trend. The MO-VL mix which contains the highest RAS content, had the lowest ϕ_α, which may be an indication of the impact of the RAS binder on compatibility, despite this mix using a very soft virgin binder (PG46-34). The shift from 30% to 45% RAP in the NCAT mixes also resulted in a decrease in the ϕ_α value. With the TX mixes, the increased RAP did not correspond to a decrease in ϕ_α, which may be a reflection of the different virgin binder used in the two mixes.

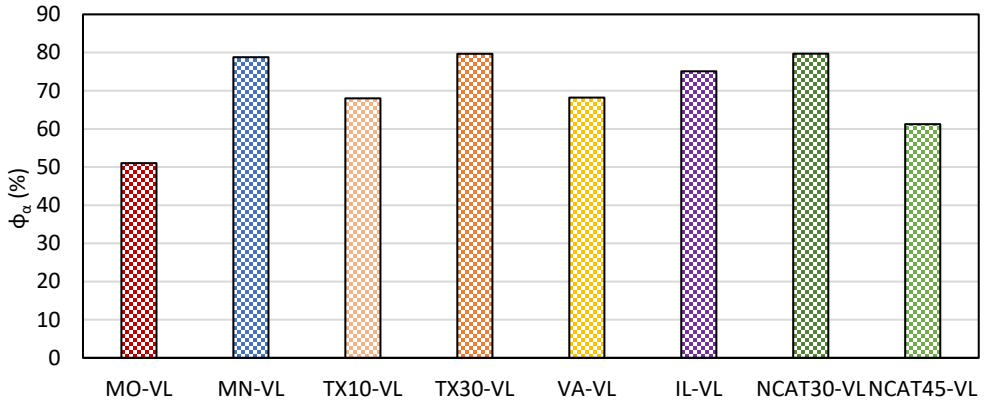

Figure 6-10 ϕ_α parameter for extracted and recovered validation binder blends

Figure 6-11 further extends the thermal analysis to the Tg_{Aave} parameter, which as previously discussed is the weighted average of the deconvoluted Tg peaks. The results show a trend similar to that of the total Tg, in which higher content of aged RAP binder generally causes a shift towards warmer temperatures. Generally, a relatively lower Tg_{Aave} parameter for a blend may be an indicator of improved compatibility between the binder components, however it may not be possible to accurately interpret results from directly compare values from completely different mixes and materials.

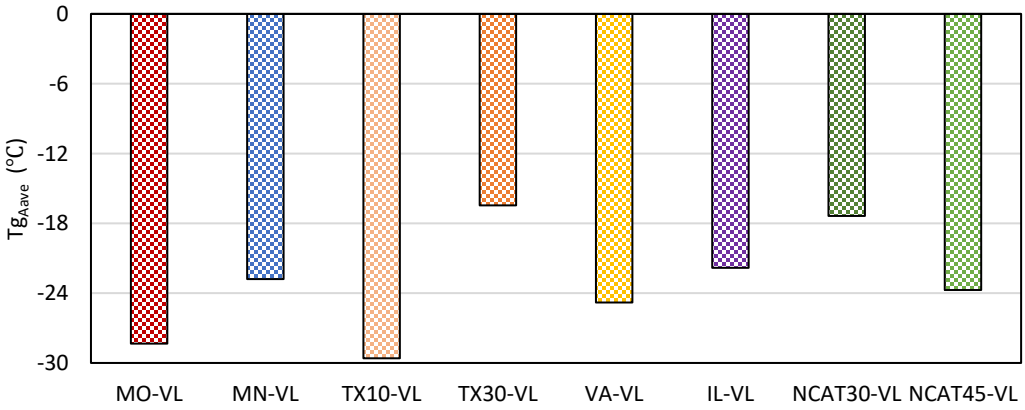

Figure 6-11 Tg_{Aave} parameter for extracted and recovered validation binder blends

6.4.2 Mixture Performance Test Results

In this section, mixture test results for the validation materials are presented. Recommended tests from task 6 have been performed on these materials to evaluate their cracking performance. I-FIT and DCT tests have been performed on validation mixtures to evaluate their intermediate and low temperatures cracking performances respectively.

6.4.2.1 Illinois Flexibility Index Semi-Circular Bend (SCB) Test (I-FIT)

Figure 6-12**6-12** and **Figure** 4-16 **6-13** show the FI and RDCI parameters for all validation material determined by performing I-FIT. It seems that only Missouri mix passes the current threshold value of 8 for FI among all validation materials. This may be because it has a softer virgin binder. It is interesting

that NCAT mixtures have brittle failure which resulted in the minimum FI values. However, the field sections having these mixtures did not show any inferior performance indications. This might be explained by the fact that the intermediate PGs for NCAT30-VL and NCAT45-VL are 33.6 and 32.8 °C respectively, significantly higher than 25 °C (I-FIT test temperature). Furthermore, loose material (implying higher air voids) in closed buckets were not stored in climate control conditions for 5 years which might have caused significant aging of the mix in the buckets. These reasons might have resulted in higher stiffness and brittle mixture behavior at 25 °C for NCAT mixtures. So, storing the loose mixtures in climate-controlled conditions and performing the test at site specific intermediate temperature might resolve this problem. The RDCI parameter also showed a similar trend to FI as expected. Hence, the research team also tested the field cores to explore the performance behavior of NCAT mixtures in detail. The results comparison is presented in the following subsection.

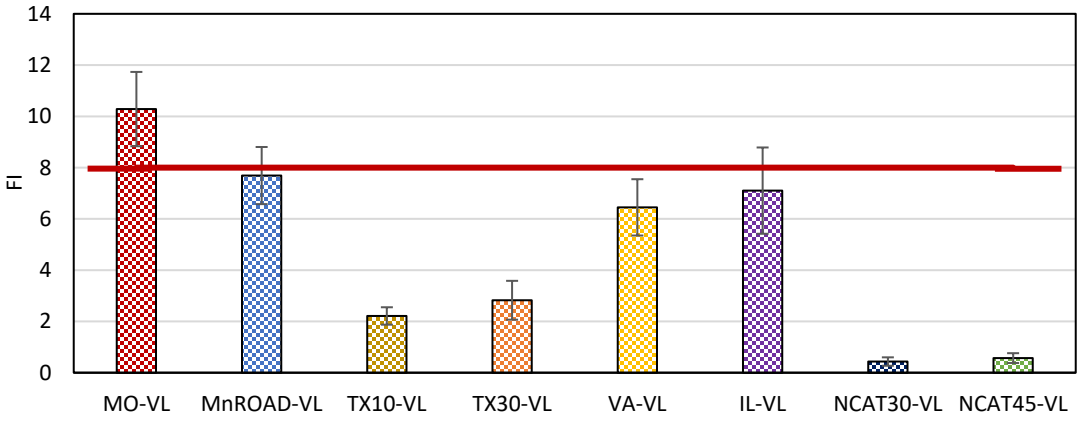

Figure 6-12 FI parameter measured from I-FIT on validation mixtures

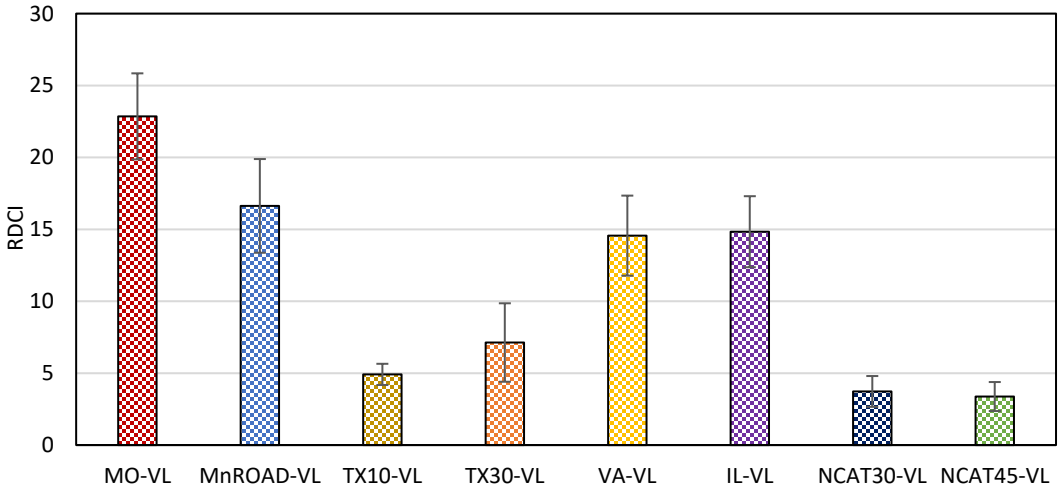

Figure 6-13 RDCI parameter measured from I-FIT on validation mixtures

I-FIT RESULTS OF NCAT MIXTURES

This section compares the I-FIT results of NCAT mixtures to explore the strange performance behavior of NCAT mixtures in detail. **Figure 6-14** shows the comparison of FI at four conditions. 'CR' refers to the results as per construction report (short-term aged) whereas, 'CR-Critically Aged' refers to the results as

per construction report after 8 hours of aging at 135 °C. 'UNH' refers to the results reported by UNH with 5-years bucket stored (Uncontrolled climate storage) aging condition and 'Field Cores' refers to the results of field cores from pavements subjected to four years of field aging. It is very interesting to notice that, in general, both NCAT mixtures have higher susceptibility to aging. It is surprising that 5-years bucket stored (Uncontrolled climate storage) aging is similar to the aging level of CR-Critically Aged condition, given that the field aging has still not reached to the aging level of CR-Critically Aged condition. These results support the hypothesis that ambient storage of loose mixtures may significantly affect the performance of asphalt mixtures. However, it should be noted that the observation is based on a very limited amount of data and should be explored more to verify the adverse impact of ambient aging on asphalt mixtures stored without temperature control.

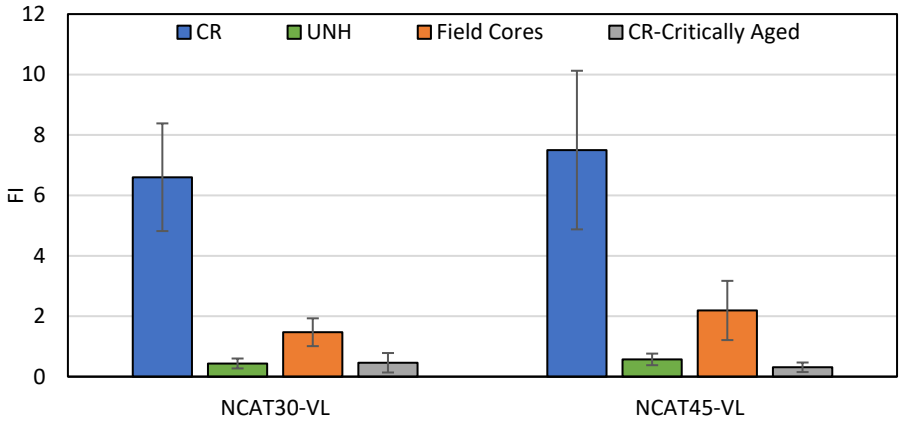

Figure 6-14 Comparison of FI for NCAT mixtures at various conditions

6.4.2.2 Disk-shaped Compact Tension Test

Figure 4-17 and **Figure** 4-18 **6-16** below show the calculated fracture energy and FST parameter for all validation material determined by performing DCT test. The corresponding testing temperatures are shown on the respective data bars. It can be observed that only VA-VL, NCAT30-VL and NCAT45-VL mixtures have passed the current threshold limit of 450 J/m^2 (**Figure** 4-17 **6-15)**. The importance of testing temperature adjustment based on geographic location can be observed in the results as both NCAT mixtures show improved thermal cracking properties. These results align with the field performance and contradict with the FI results. Both NCAT mixtures have shown similar thermal cracking properties emphasizing the effectiveness of RA (used in NCA45-VL mixture) with the RAP. The FST parameter in Figure 4-18 FST parameter measured from DCT**Figure** 4-18 **6-16** shows the similar trend as that of G_f parameter.

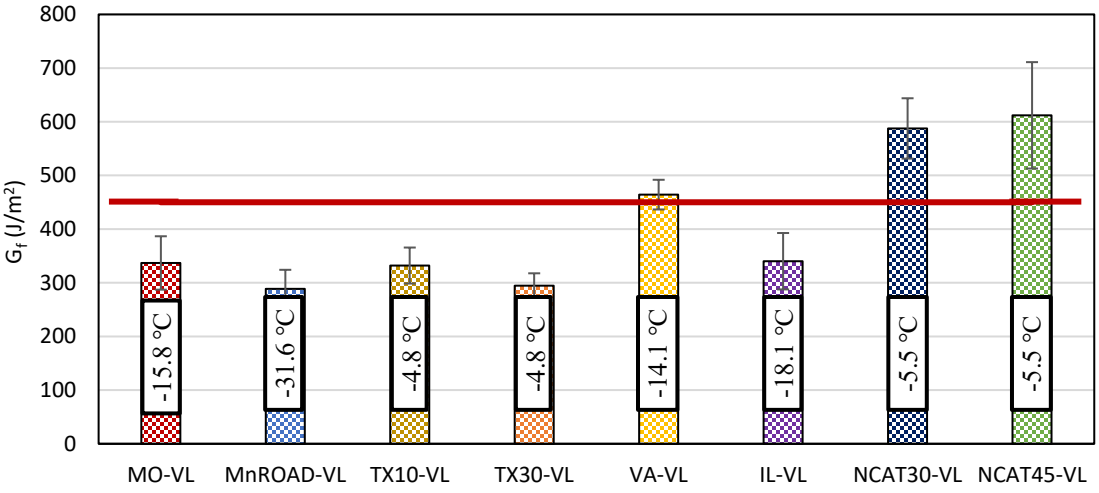

Figure 6-15 G_f parameter measured from DCT test

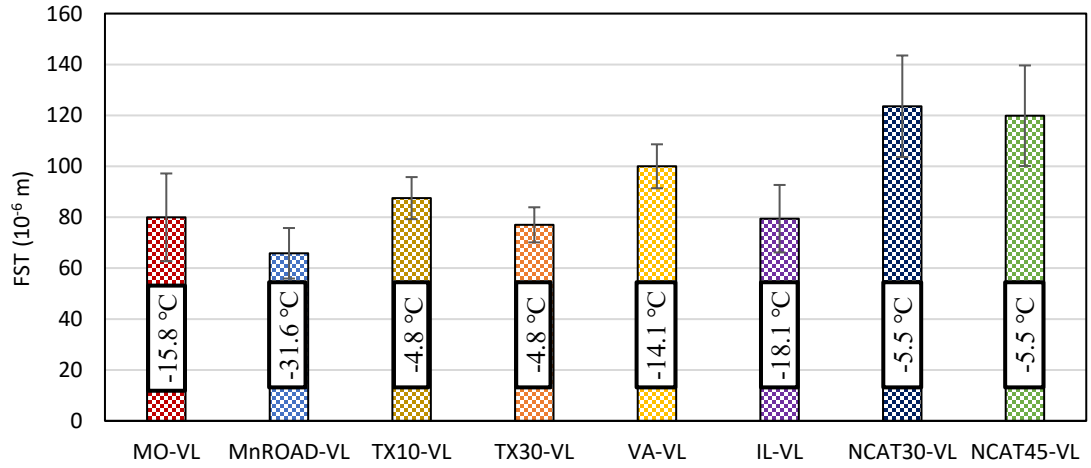

Figure 6-16 FST parameter calculated from DCT test results

6.4.3 Effect of ambient aging on asphalt material properties

To evaluate the effect of ambient aging, the virgin binders were retested for DSC parameters after two years of ambient aging in a closed container and the results are presented in **Figure 6-176-17**. Ambient storage for two years has had a negative impact on all binders. It is interesting to note that Binder A was the most impacted, which was the softest binder (PG 58-28) among all. These findings highlight the sensitivity of the DSC parameters to aging and emphasize that ambient storage can have a negative impact on asphalt materials. However, these findings need to be validated further by testing additional binders in the future. These findings may support the research team's hypothesis (presented earlier) regarding the inferior cracking properties of NCAT mixtures tested after 5 years of ambient storage in buckets.

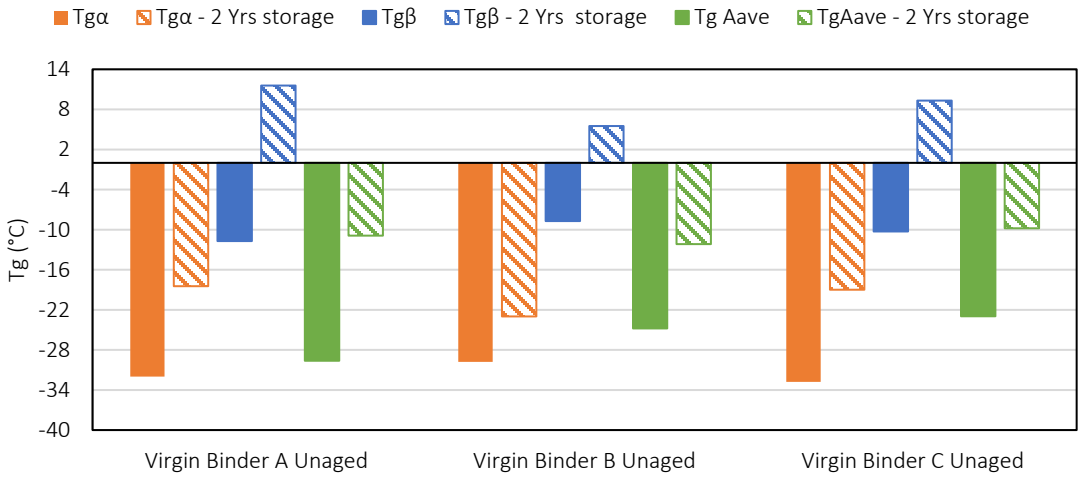

Figure 6-17 Effect of ambient aging on thermal properties of asphalt

6.5 STATISTICAL ANALYSIS OF TEST RESULTS

In this chapter, the correlations between mixture testing parameters and corresponding extracted and recovered binder parameters are evaluated using various statistical methods. The evaluated materials include four RAP mixtures, six RA treated RAP mixtures with 45% RAP and 2 RAs and the corresponding extracted and recovered binders.

6.5.1 Statistical correlation methods

Pearson correlation coefficient and Hoeffding's D correlation analysis are selected as the statistical methods in this study. The frequently used Pearson's correlation method is only able to capture linear relationships, so Hoeffding's D correlation method is selected as a supplementary tool to screen the significant relevance between the results. The Pearson correlation coefficient is a widely accepted measure of the linear relationship between two specified variables. The Pearson correlation coefficient 1 indicates the case of a positive linear relationship, and -1 indicates the case of a negative linear relationship. The closer the coefficient is to either -1 or 1, the stronger the correlation between the variables.

Hoeffding's D correlation is a statistical method which can be used to infer nonlinear and also non-monotonic relationships between the variables. The parameter D represents a nonparametric measure of dependence, by testing the independence of two study variables. The intuitive idea of Hoeffding's D correlation is to calculate the distance between the distribution under the null hypothesis and the empirical bivariate distribution. The D coefficient measurements fall between -0.5 and 1, with a larger value of D coefficient indicating a stronger non-linear relevance between parameters. Generally, if the analysis between two variables shows a low Pearson coefficient but a high Hoeffding's D coefficient, it represents a potential non-linear relationship may exist between the two study parameters.

6.5.2 Binder-Mixture correlation Analysis

The paired correlation coefficients between 5 mixture testing parameters and 12 binder testing parameters were calculated and summarized in a correlation matrix format. The two different correlation coefficients are presented in this section to screen significant linear/non-linear relationships. The Pearson correlation coefficients between the binder properties and the mixture properties are shown in **Table 6-4**. Values closer to 1 are shaded by green color indicating the stronger positive/negative relationship between the two parameters. The intensity of the color represents the strength of the correlation. Those correlations with a coefficient below 0.1 are not shaded with color, while those strong correlation (coefficients > 0.7) are also marked bold and italic.

As shown in the **Table 6-4**, most of the fracture parameters (except for G_f@DCT) show fair correlation (0.7 > correlation coefficient ≥ 0.5) to strong correlation (correlation coefficient ≥ 0.7) with multiple binder parameters. As a contrast, there is lack of significant correlation between G_f@DCT with most of the binder parameters. This might be due to the fracture energy showing a high variability at low temperature. All intermediate temperature fracture parameters from I-FIT testing show moderate to strong correlation with most of the binder parameters (except for T_c(S), LTPG, G-R, ΔT_c, Tg and ϕ_α). The low temperature fracture parameter FST shows comparatively fair correlation with thermal parameters from DSC testing as well as with the rheological parameters. The mixture cracking parameters FI and RDCI generally show fair to strong relationship with all the rheological and thermal binder parameters. Similar observations were made from core material results.

From the binder's perspective, rheological parameters T_c(S), and LTPG and thermal parameters Tg_α, Tg_β, and ϕ_α do not show a strong relationship with low temperature cracking parameters. The most promising binder parameters are Tg and Tg_{Aave}, which show significant correlation with almost all mixture parameters including fracture properties. As for the thermal binder parameter from DSC testing, Tg and Tg_{Aave} show a similar trend for correlation with mixture properties.

Table 6-4 Pearson correlation coefficients between the corresponding mixture and binder parameters

			Mixture Properties			
			Fracture Parameters			
			FI	RDCI	G_f@DCT	FST
Binder Properties	Rheological Parameters	R	0.66	0.68	0.52	0.60
		T_c(S)	0.74	0.74	0.25	0.30
		T_c(m)	0.90	0.92	0.42	0.51
		ΔT_c	0.91	0.93	0.45	0.54
		HTPG	0.86	0.88	0.58	0.64
		LTPG	0.80	0.79	0.40	0.42
		G-R	0.76	0.77	0.55	0.64
	DSC Parameters	Tg_α	0.66	0.67	0.42	0.42
		Tg_β	0.71	0.72	0.37	0.40
		Tg_{Aave}	0.64	0.65	0.47	0.47
		ϕ_α	0.76	0.79	0.06	0.19
		Tg	0.72	0.72	0.55	0.54

Table 6-5 below shows the Hoeffding's D correlation matrix. The values of Hoeffding's D coefficients are generally between -0.11 and 0.71, which indicates relatively weak nonlinear correlations except for ΔT_c. In other words, a low value of Hoeffding's D coefficients indicates there is not a strong non-linear relationship between any pairs of mixture and binder parameters. However, it should be noted that ΔT_c is a composite parameter which depends on the $T_c(S)$ and $T_c(m)$ meaning that trends with ΔT_c should be evaluated with caution.

Table 6-5 Hoeffding's D correlation between the corresponding mixture and binder parameters

			Mixture Properties			
			Fracture Parameters			
			FI	RDCI	G_f@DCT	FST
Binder Properties	Rheological Parameters	R	0.36	0.39	-0.04	0.11
		$T_c(S)$	0.08	0.11	-0.05	-0.11
		$T_c(m)$	0.30	0.32	-0.09	-0.04
		ΔT_c	0.68	0.71	-0.02	0.07
		HTPG	0.08	0.11	-0.05	-0.11
		LTPG	0.30	0.32	0.02	0.07
	DSC Parameters	G-R	0.00	0.02	0.02	-0.05
		Tg_α	0.03	0.05	-0.05	-0.05
		Tg_β	0.00	0.04	0.13	-0.04
		Tg_{Aave}	0.04	0.05	-0.05	-0.05
		ϕ_α	0.00	0.04	0.13	-0.04

In summary, the intermediate temperature cracking parameters calculated from the I-FIT test show the most promising correlation with many rheological and thermal properties of binder. The G-R, $T_c(m)$, Tg and Tg_{Aave} show a fair to strong relationship with all cracking parameters. Thus, these parameters are considered as the critical parameter for compatibility characterization.

6.6 EFFECT OF MIXTURE COMPONENTS ON SELECTED BINDER AND MIXTURE PARAMETERS

6.6.1 Effect of Binder Type on Binder Properties

6.6.1.1 Glover-Rowe Parameter (G-R)

It can be clearly observed that mixtures with binder A shows better G-R than mixtures with binder B and C that may be a result of softer binder grade of A (**Figure 6-18**). However, it is interesting to note that mixtures with binder C show better G-R parameter than binder B even though they both have similar PG grade. This indicates the potential incompatibility of binder B with HRAP1 as virgin mixture blends without HRAP1 have similar G-R. **Figure 6-19** shows the effect of binder on G-R for all HRAP materials evaluated in the study. It can be observed that blends with binder A have better G-R than blends with binder C due to softer binder grade. It can also be observed that inclusion of RA2 in Binder A with HRAP2 and HRAP3 adversely affected, indicating its potential incompatibility.

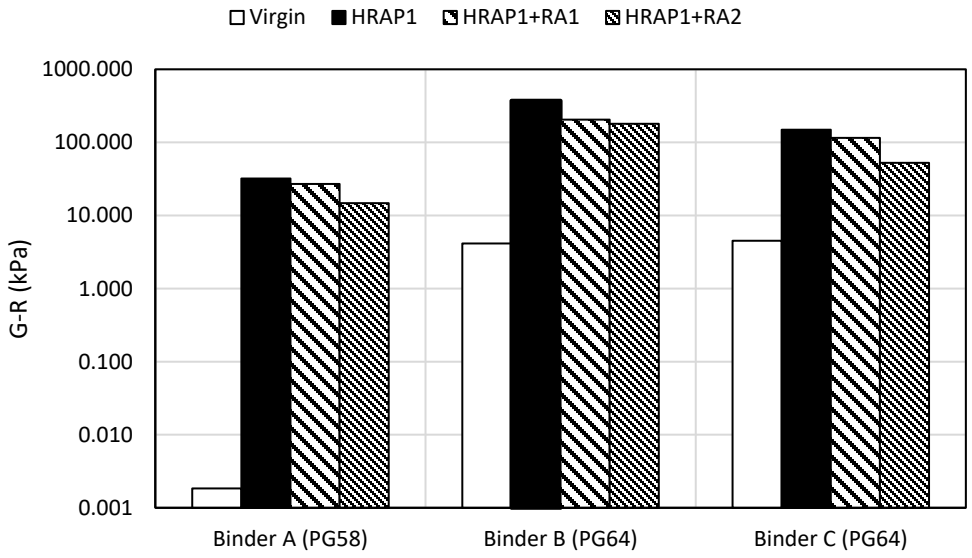

Figure 6-18 Effect of binder type on G-R for HRAP1 blends

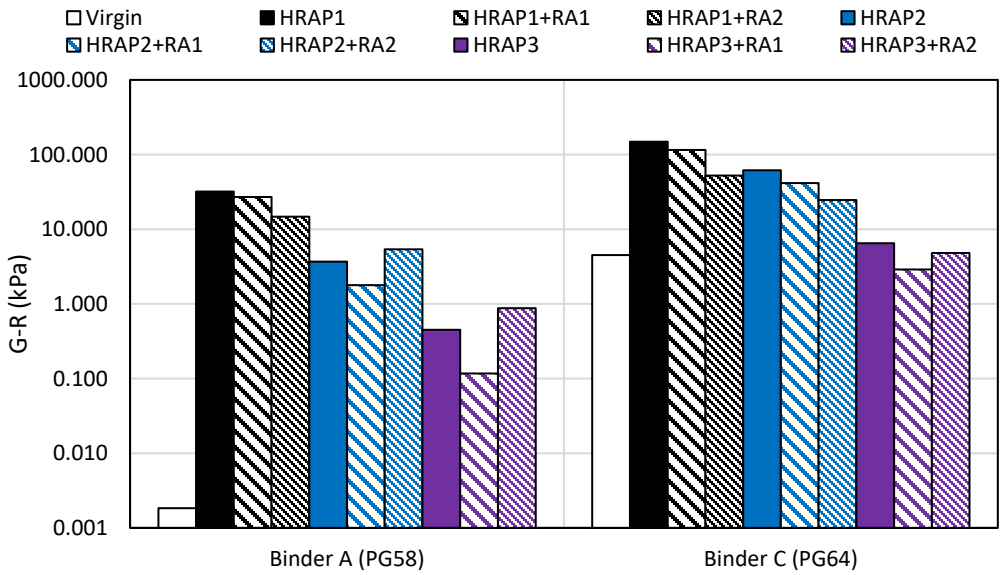

Figure 6-19 Effect of binder type on G-R for all HRAP blends

6.6.1.2 Critical Low Temperature Based on Relaxation Rate (T_c(m))

It can be clearly observed that mixtures with binder A shows better T_c(m) than mixtures with binder B and C that may be a result of softer binder grade of A (**Figure 6-20**). However, it is interesting to note that mixtures with binder C show better or comparable T_c(m) parameter than with binder B even though the latter had better value to start with (Virgin results). This indicates the potential incompatibility of binder B with HRAP1 as virgin mixtures without HRAP1 have similar T_c(m). **Figure 6-21** shows the effect of binder on T_c(m) for all HRAP materials evaluated in the study. It can be observed that blends with binder A have better T_c(m) than blends with binder C due to softer binder grade.

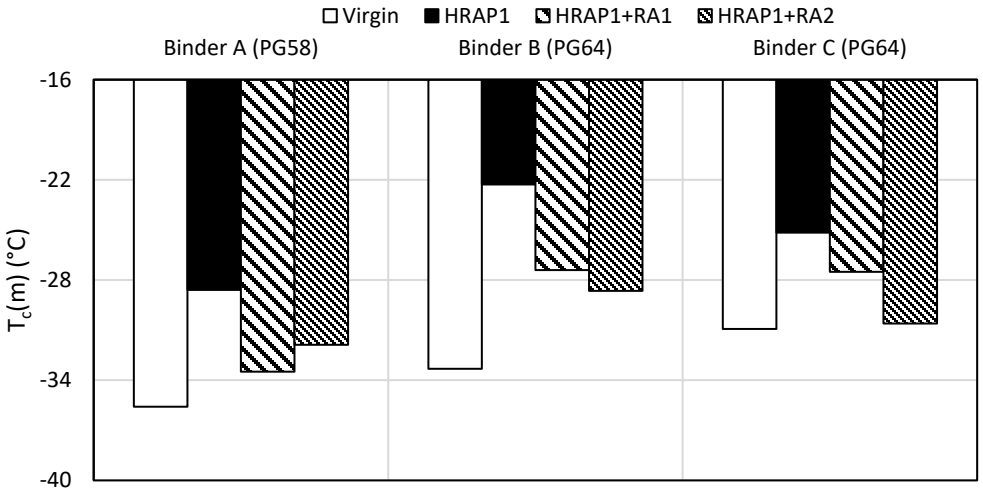

Figure 6-20 Effect of binder type on T_c(m) for HRAP1 blends

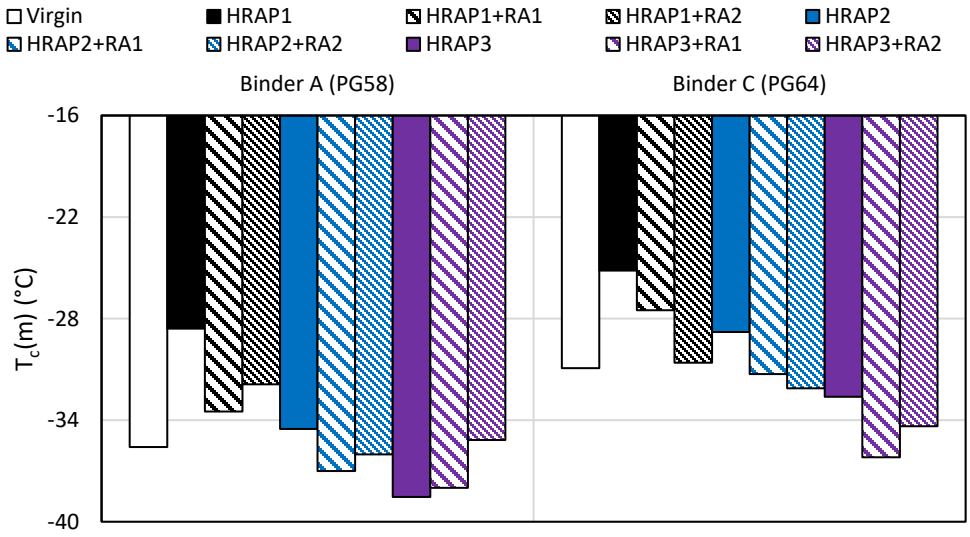

Figure 6-21 Effect of binder type on T_c(m) for all HRAP blends

6.6.1.3 Change in Critical Low Temperature (ΔT_c)

It can be clearly observed that mixtures with binder A shows better ΔT_c than mixtures with binder B and C that may be a result of softer binder grade of A (**Figure 6-22**). However, it is interesting to note that mixtures with binder C show better ΔT_c parameter than with binder B even though they both have similar PG grade. This indicates the potential incompatibility of binder B with HRAP1 as virgin mixture blends without HRAP1 have similar ΔT_c, which also supports the findings from G-R parameter. **Figure 6-23** shows the effect of binder on ΔT_c for all HRAP materials evaluated in the study. It can be observed that blends with binder A have better ΔT_c than blends with binder C due to softer binder grade. However, it is interesting to note that RA1 with HRAP3 and binder A has surprisingly very inferior ΔT_c than expected indicating potential incompatibility which need to be confirmed by other parameters as well.

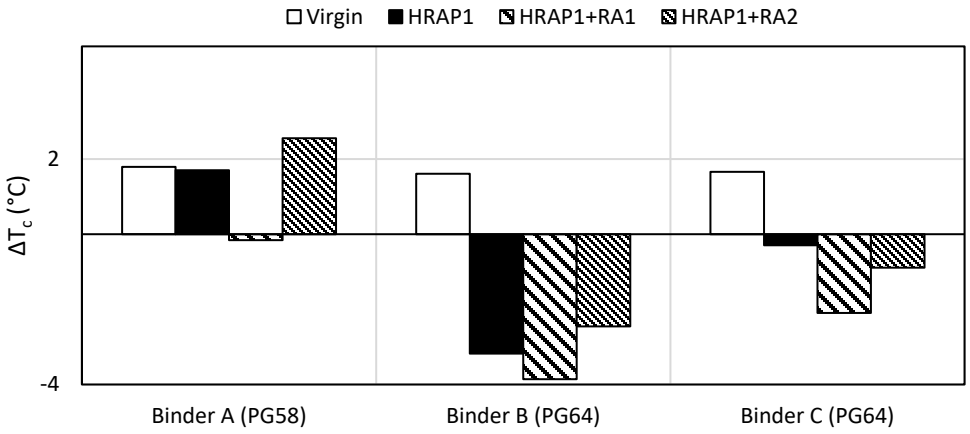

Figure 6-22 Effect of binder type on ΔT_c for HRAP1 blends

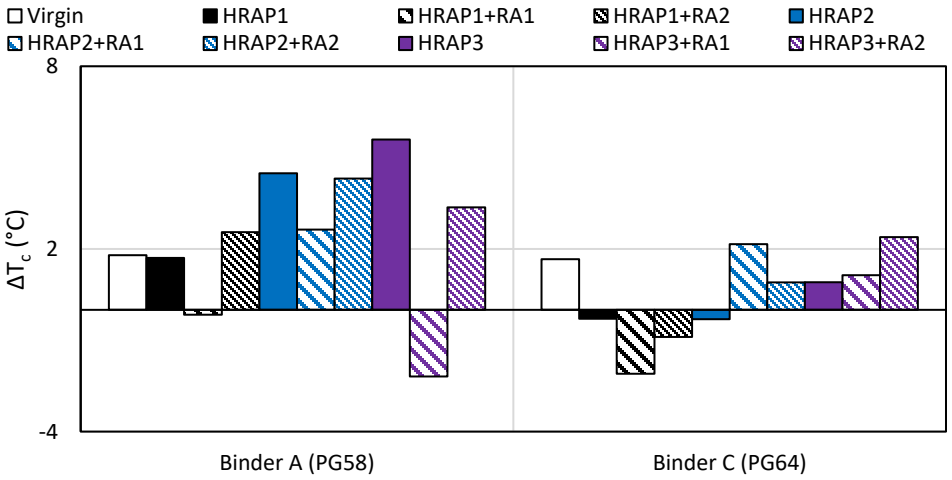

Figure 6-23 Effect of binder type on ΔT_c for all RAP blends

6.6.1.4 ϕ_α Index

Figure 6-24 shows the effect of binder type on ϕ_α index. More compatible binders generally have a higher ϕ_α index. It can be observed that with the inclusion of RAP2 adversely affects the ϕ_α index. However, the binder B blends show a significantly larger decrease than other binders indicating the potential incompatibility of binder B. **Figure 6-25** shows the effect of binder on ϕ_α index for all HRAP materials evaluated in the study. It is observed from the plot that blends with binder A have better ϕ_α index than blends with binder C. It is interesting to note that inclusion of RA did not have significant impact on the ϕ_α index.

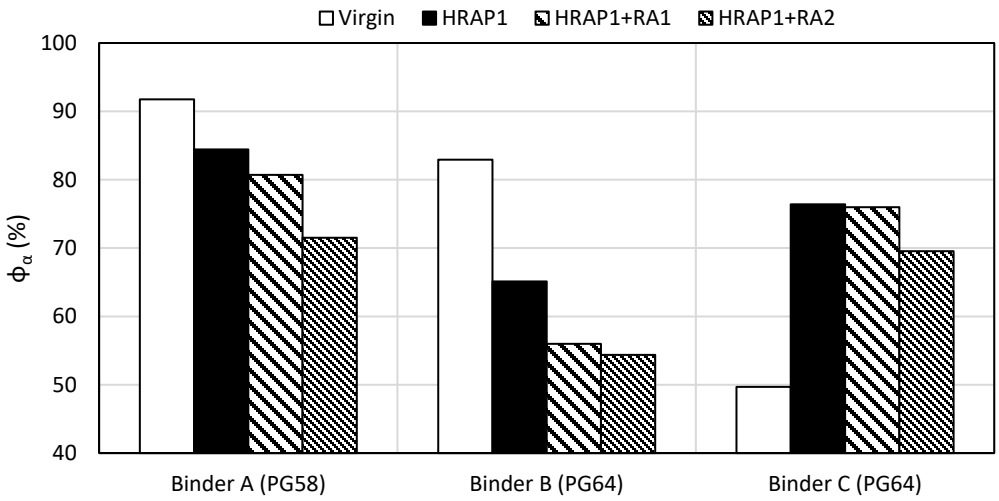

Figure 6-24 Effect of binder type on ϕ_α for HRAP1 blends

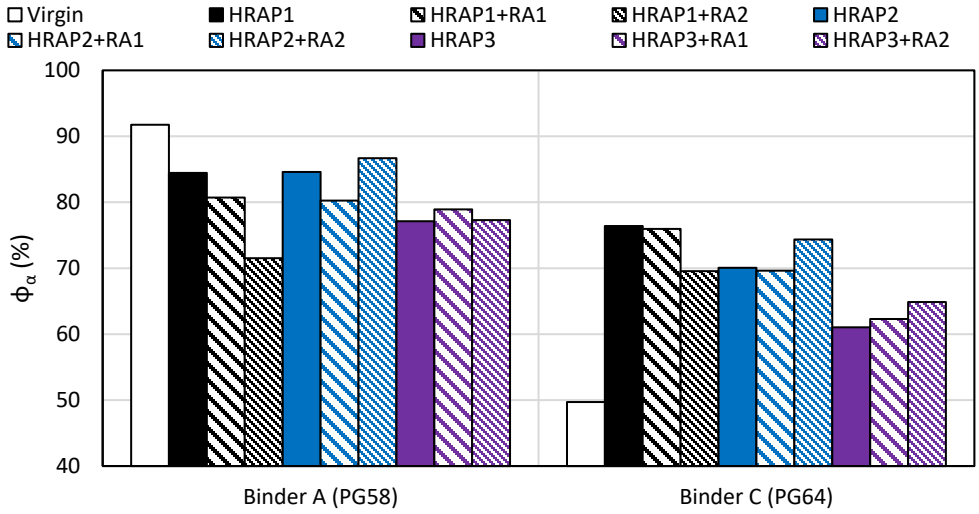

Figure 6-25 Effect of binder type on ϕ_α for all RAP blends

6.6.1.5 Glass Transition Temperature (Tg)

It can be clearly observed that virgin blends with all binder show better Tg than blends with RAP binders (**Figure 6-26**). It is worth noting that inclusion of HRAP1 with binder A and C had high impacted and affected more adversely than with binder B. However, RA improved the Tg for both of them and made it comparable for all three binders. **Figure 6-27** shows the effect of binder on Tg for all HRAP materials evaluated in the study. It is observed that binder C shows better Tg with HRAP2 than HRAP1, even though they both have similar PG grades, indicating potential compatibility of HRAP3 with binder C. It can be noted that the effect of RA is similar across the board and improves the Tg with all binders.

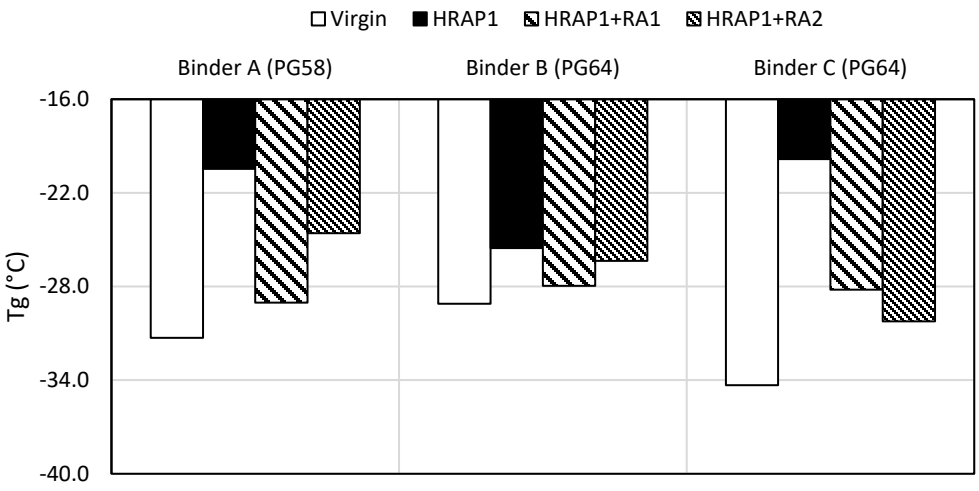

Figure 6-26 Effect of binder type on Tg for HRAP1 blends

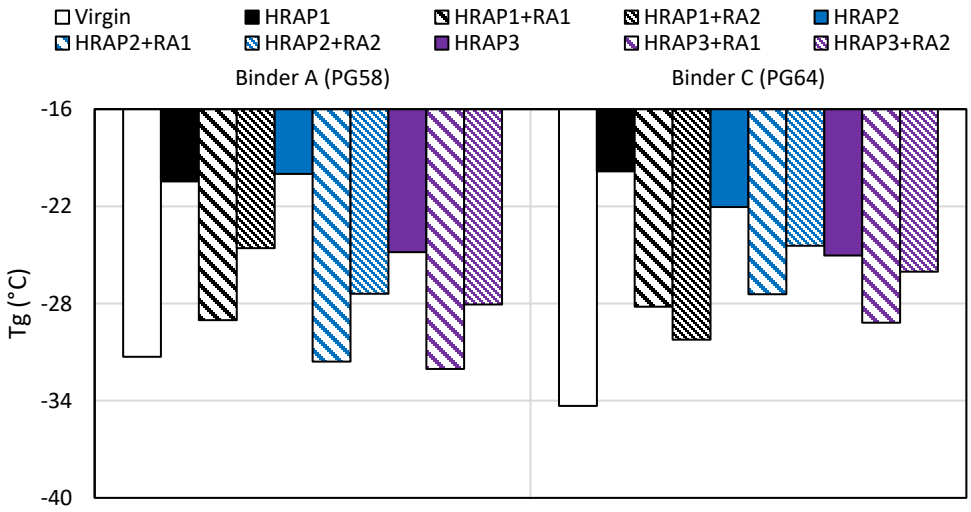

Figure 6-27 Effect of binder type on Tg for all RAP blends

6.6.1.6 Tg_{Aave} Parameter

It can be clearly observed that virgin blends with all binder show better Tg_{Aave} than blends with RAP binders (**Figure 6-28**). Inclusion of rejuvenators is able to partly compensate for the adverse impact of RAP. **Figure 6-29** shows the effect of binder on Tg_{Aave} for all HRAP materials evaluated in the study. It can be observed that blends with binder A have slightly better Tg_{Aave} than blends with binder C due to softer binder grade.

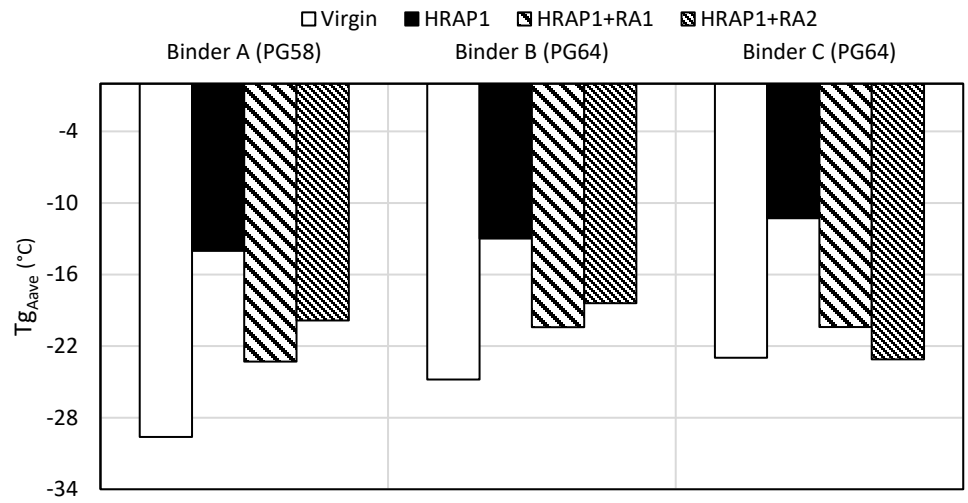

Figure 6-28 Effect of binder type on Tg_{Aave} for HRAP1 blends

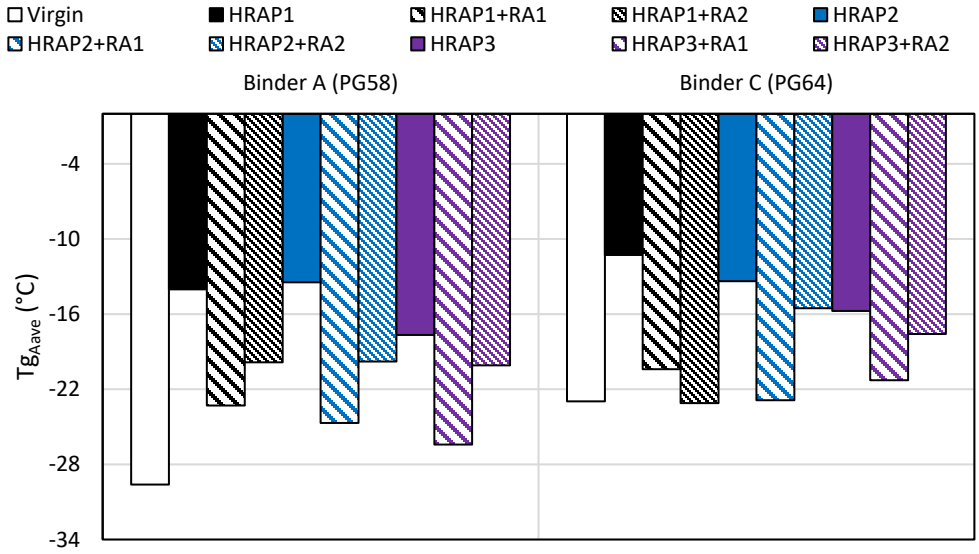

Figure 6-29 Effect of binder type on Tg_{Aave} for all RAP blends

6.6.1.7 Span of Glass Transition Temperature (Tg_{Range})

It has been observed that virgin binders with binder C have the highest span of DSC curve and hence corresponding higher Tg_{Range} value. (**Figure 6-30**) Generally, higher compatible binders have narrower span of DSC curve. **Figure 6-31** shows the effect of binder on Tg_{Range} for all HRAP materials evaluated in the study. It can be observed that rejuvenated blends with binder A have slightly better Tg_{Range} than rejuvenated blends with binder C due to softer binder grade, especially with RA2.

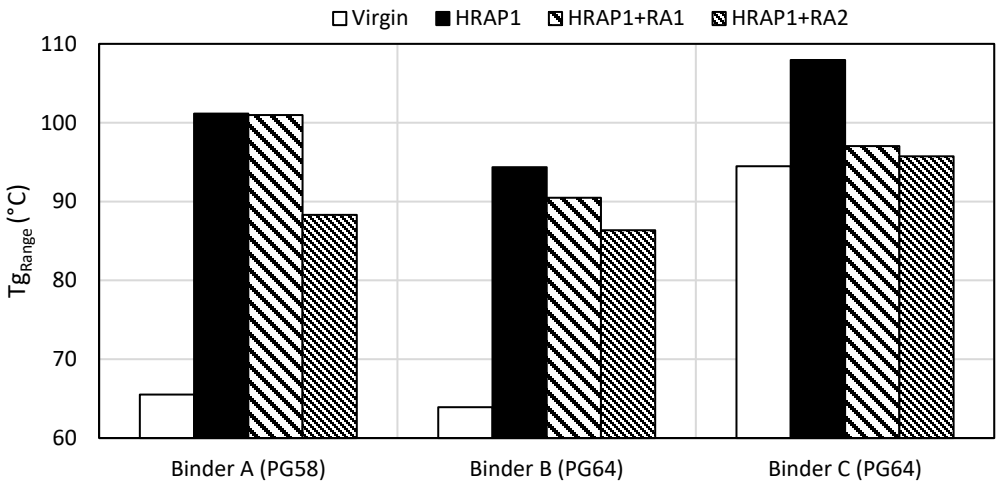

Figure 6-30 Effect of binder type on Tg_{Range} for HRAP1 blends

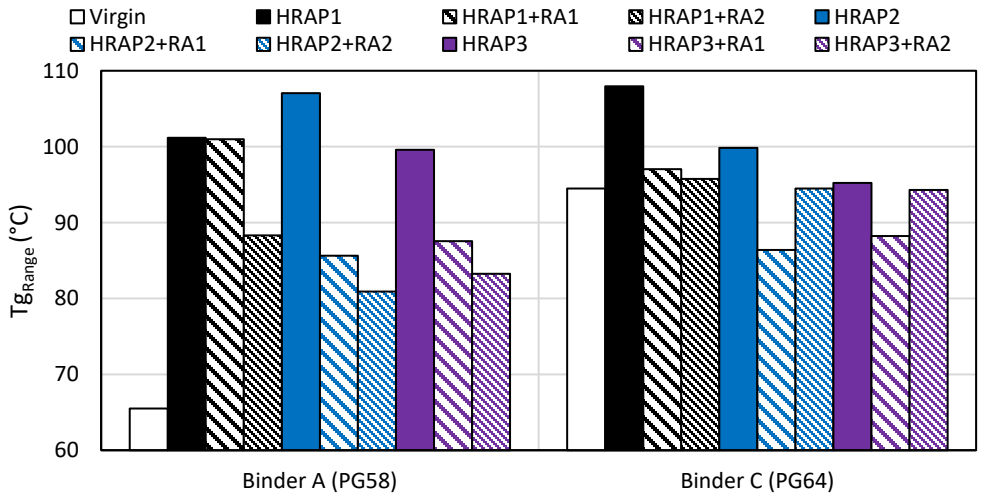

Figure 6-31 Effect of binder type on Tg_{Range} for all RAP blends

6.6.2 Effect of RA Type on Binder Properties

This section discusses the effect of RA type on selected binder parameters. In subsequent bar plots, bars of blends having binder A, B, and C are represented by hatch with □, △, and ○ patterns respectively, whereas the bars of blends having HRAP1, HRAP2 and HRAP3 are shown with black-, blue- and magenta-colored patterns.

6.6.2.1 Glover-Rowe Parameter (G-R)

Figure 6-32 shows the effect of RA on G-R for all HRAP materials evaluated in the study. It can be observed that inclusion of RA generally improves the G-R. However, it is interesting to note that inclusion of RA2 adversely affected the G-R with RAP2 and RAP3 with binder A, when compared to blends without any RA, which might indicate the potential incompatibility of RA2 with HRAP2 and HRAP3.

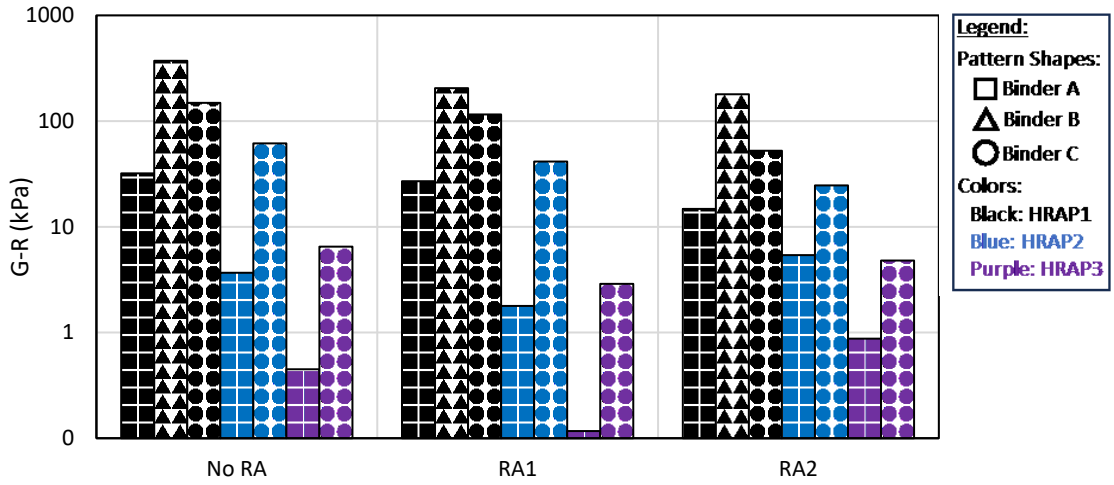

Figure 6-32 Effect of RA type on G-R for all RAP blends

6.6.2.2 Critical Low Temperature Based on Relaxation Rate (T_c(m))

Figure 6-33 shows the effect of RA on T_c(m) for all HRAP materials evaluated in the study. It can be observed that inclusion of RA generally improves the T_c(m). However, it is interesting to note that RA1 is more effective with HRAP2 and HRAP3 than with HRAP1.

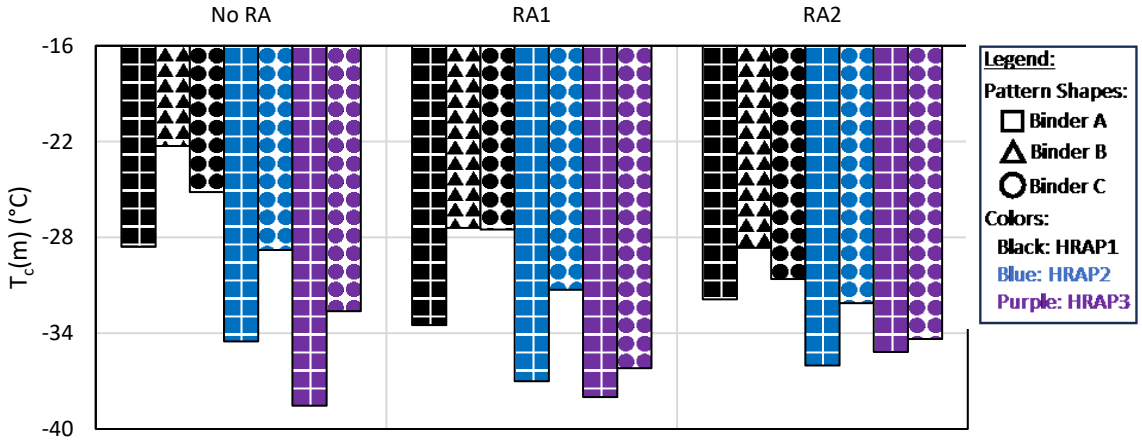

Figure 6-33 Effect of RA type on T_c(m) for all RAP blends

6.6.2.3 Change in Critical Low Temperature (ΔT_c)

Figure 6-34 shows the effect of RA on ΔT_C for all HRAP materials evaluated in the study. It can be observed that inclusion of RA generally improves the ΔT_C. However, this trend is not consistent across the board, which might be due to dependence of ΔT_c on both T_c(S) and T_c(m). Inclusion of RA generally improves both T_c(S) and T_c(m) and relative improvement determines the ΔT_C.

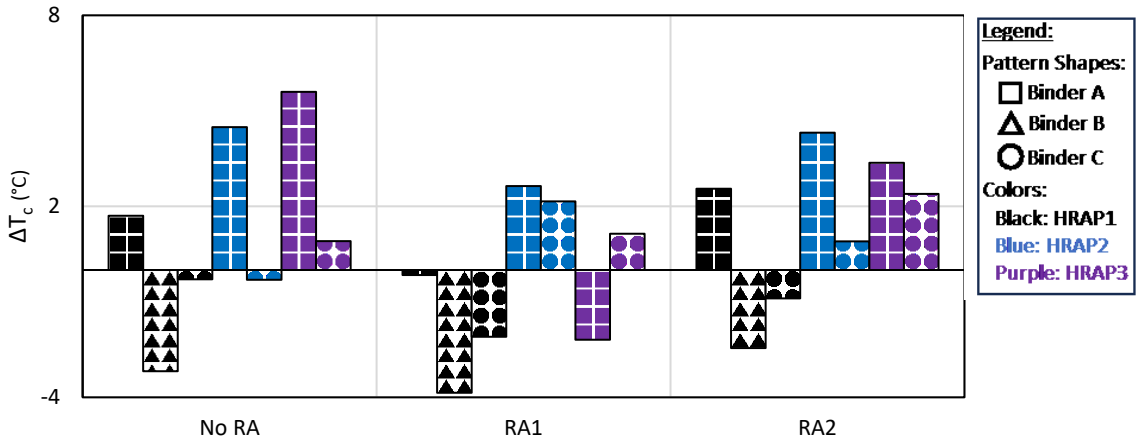

Figure 6-34 Effect of RA type on ΔT_c for all RAP blends

6.6.2.4 ϕ_α Index

Figure 6-35 shows the effect of RA on ϕ_α Index for all HRAP materials evaluated in the study. It can be observed that inclusion of RA overall did not affect the ϕ_α Index for HRAP2 and HRAP3. However, it is interesting to note that inclusion of RA2 adversely affected the ϕ_α Index with all binders for HRAP1 blends, indicating the potential incompatibility of RA2 with HRAP1.

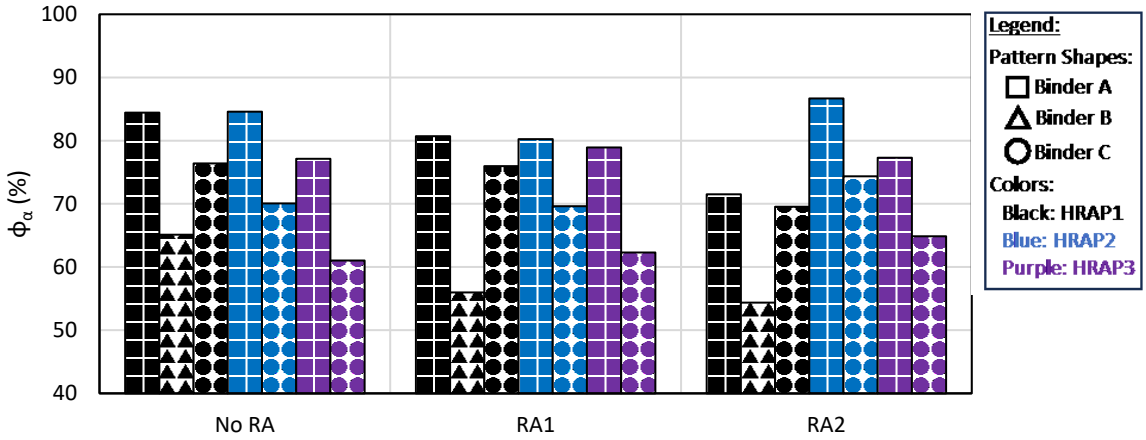

Figure 6-35 Effect of RA type on ϕ_α for all RAP blends

6.6.2.5 Glass Transition Temperature (Tg)

Figure 6-36 shows the effect of RA on Tg for all HRAP materials evaluated in the study. It can be observed that inclusion of RA generally improves the Tg. It is interesting to note that inclusion of RA1 improves Tg more than RA2. This again aligns with the findings from rheological parameters.

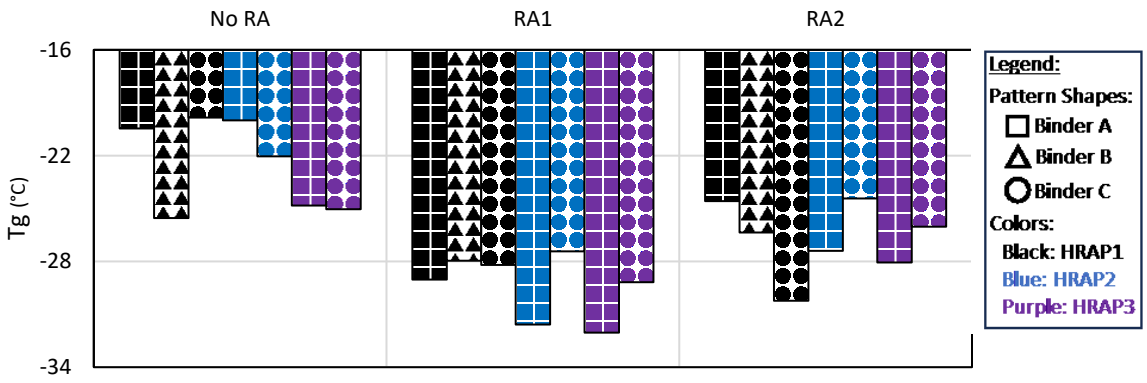

Figure 6-36 Effect of RA type on Tg for all RAP blends

6.6.2.6 Tg_{Aave} Parameter

Figure 6-37 shows the effect of RA on Tg_{Aave} for all HRAP materials evaluated in the study. It can be observed that inclusion of RA generally improves the Tg_{Aave}. It is interesting to note that inclusion of RA1 improves Tg_{Aave} more than RA2 except for HRAP1 blend with binder C. This also supports the findings from Tg parameter.

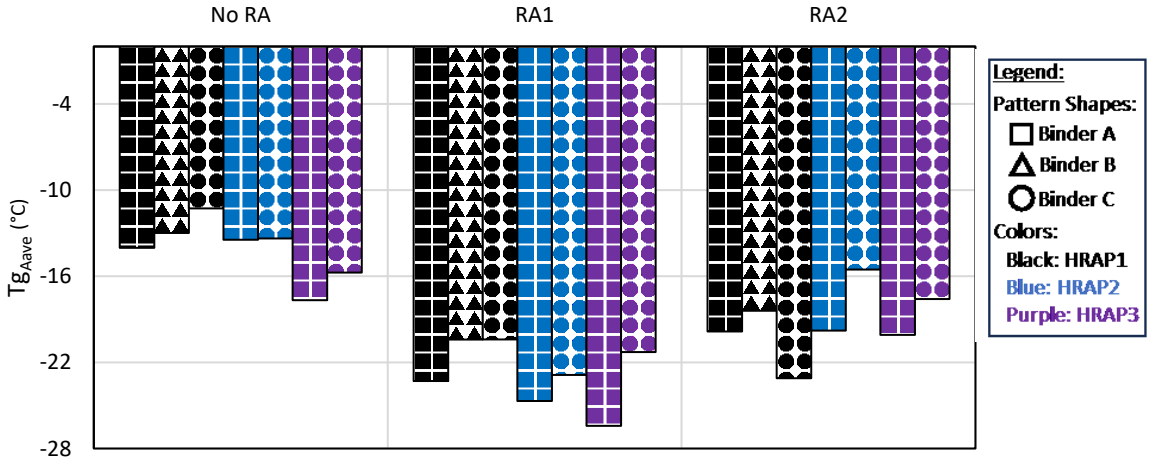

Figure 6-37 Effect of RA type on Tg_{Aave} for all RAP blends

6.6.2.7 Span of Glass Transition Temperature (Tg_{Range})

Figure 6-38 shows the effect of RA on Tg_{Range} for all HRAP materials evaluated in the study. It can be observed that inclusion of RA generally decreases the Tg_{Range}. It is interesting to note that inclusion of RA1 did not show any improvement with HRAP1 blends, however, it improved the parameter with HRAP2 and HRAP3 blends. Tg_{Range} more than RA2 except for HRAP1 blend with binder C. This also supports the findings from other DSC parameters.

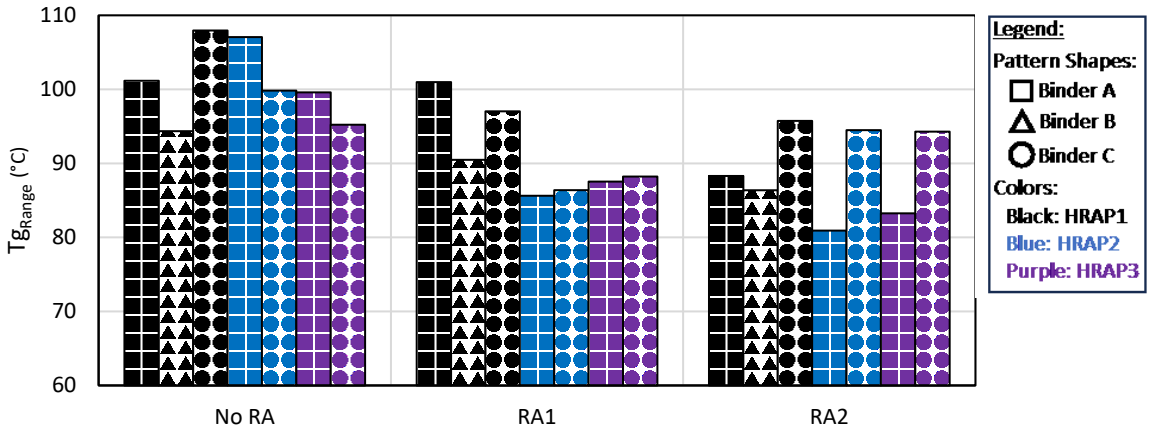

Figure 6-38 Effect of RA type on Tg_{Range} for all RAP blends

6.6.3 Effect of RAP Type on Binder Properties

6.6.3.1 Glover-Rowe Parameter (G-R)

From **Figure 6-39**, it can be clearly observed that HRAP2 shows better G-R than HRAP1 with all binders even though HRAP1 and HRAP2 have similar PG grades. Furthermore, it can also be observed that all HRAP with Binder A and B show best and worst G-R respectively even though binder B and C have same binder PG grade.

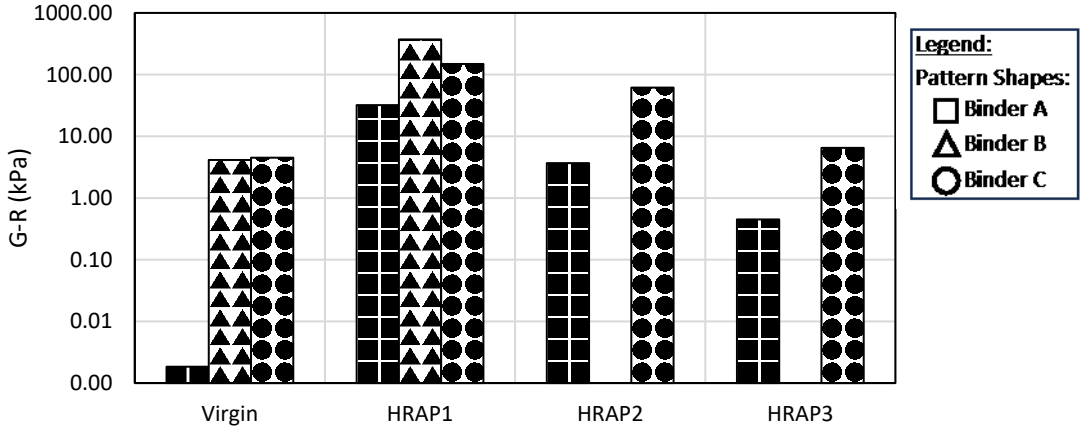

Figure 6-39 Effect of RAP type on G-R

6.6.3.2 Critical Low Temperature Based on Relaxation Rate (T_c(m))

Figure 6-40 shows the effect of HRAP on T_c(m) for all binders evaluated in the study. It can be clearly observed that HRAP2 shows better T_c(m) than HRAP1 with all binders even though HRAP1 and HRAP2 have similar PG grades. All HRAP with Binder A shows best T_c(m) than all other binders due to its softer binder grade. However, it is interesting to note that HRAP blends with binder C have better T_c(m) than binder B even though both have same PG grade and binder B had better value to start with. This

indicates potential incompatibility of binder B with HRAP1. The finding also aligns with the findings from G-R.

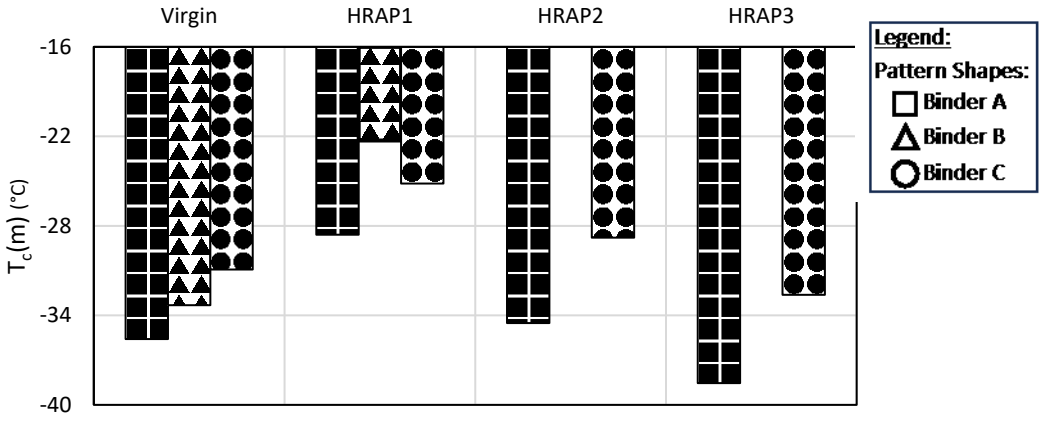

Figure 6-40 Effect of RAP type on T_c(m)

6.6.3.3 Change in Critical Low Temperature (ΔT_c)

From **Figure 6-41**, it can be clearly observed that HRAP2 shows better ΔT_c than HRAP1 with all binders even though HRAP1 and HRAP2 have similar PG grades. All HRAP with Binder A shows best ΔT_c than all other binders due to its softer binder grade. However, it is interesting to note that HRAP blends with binder C have better ΔT_c than binder B even though both have same PG grade had similar value to start with. This indicates potential incompatibility of binder B with HRAP1. However, the overall trend is not consistent across the board, which might be due to dependence of ΔT_c on both T_c(S) and T_c(m) and inclusion of RAP does not have same effect on both critical temperatures.

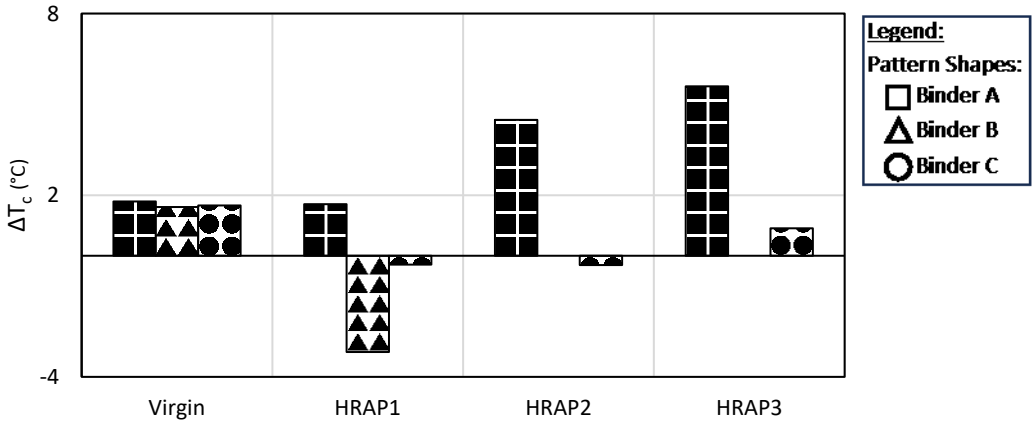

Figure 6-41 Effect of RAP type on ΔT_c

6.6.3.4 ϕ_α Index

It can be clearly observed that HRAP1 shows better ϕ_α Index than HRAP2 with binder C even though HRAP1 and HRAP2 have similar PG grades (**Figure 6-42**). All HRAP with Binder A shows best T_c(m) than all other binders due to its softer binder grade.

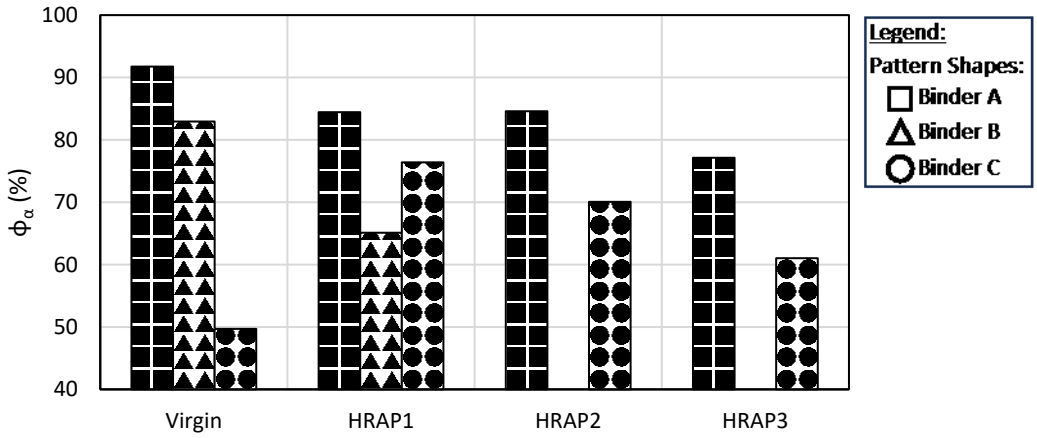

Figure 6-42 Effect of RAP type on ϕ_α

6.6.3.5 Glass Transition Temperature (Tg)

Figure 6-43 shows the effect of RAP on Tg. It can be clearly observed that inclusion of RAP results in inferior Tg which is true across the board. HRAP1 and HRAP2 show similar Tg values for both binder A and C as they have similar PG grades. HRAP3 blends show the better Tg values for all binder as it has the softer PG grade RAP binder.

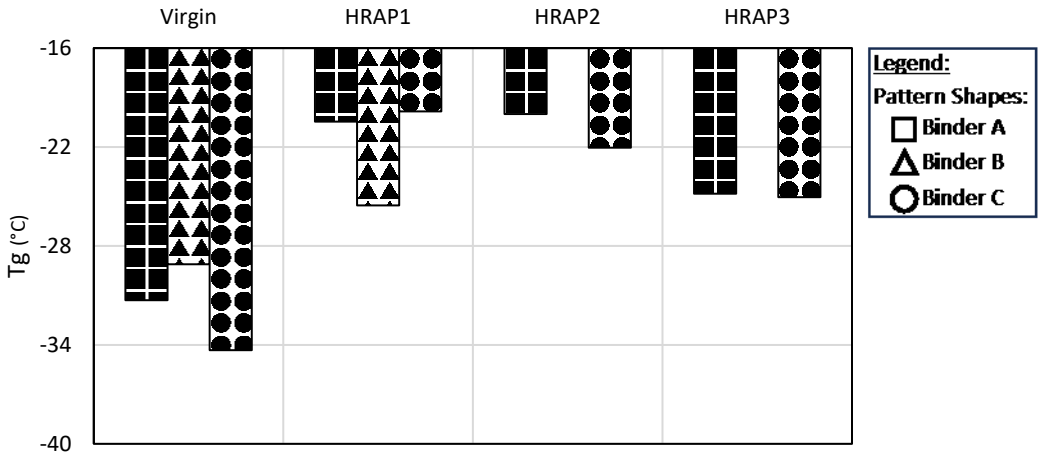

Figure 6-43 Effect of RAP type on ϕ_α

6.6.3.6 Tg_{Aave} Parameter

Figure 6-44 shows the effect of RAP on Tg_{Aave}. It can be clearly observed that inclusion of RAP results in inferior Tg_{Aave} which is true across the board. HRAP1 and HRAP2 show similar Tg_{Aave} values for both

binder A and C as they have similar PG grades. HRAP3 blends show the better Tg values for all binder as it has the softer PG grade RAP binder.

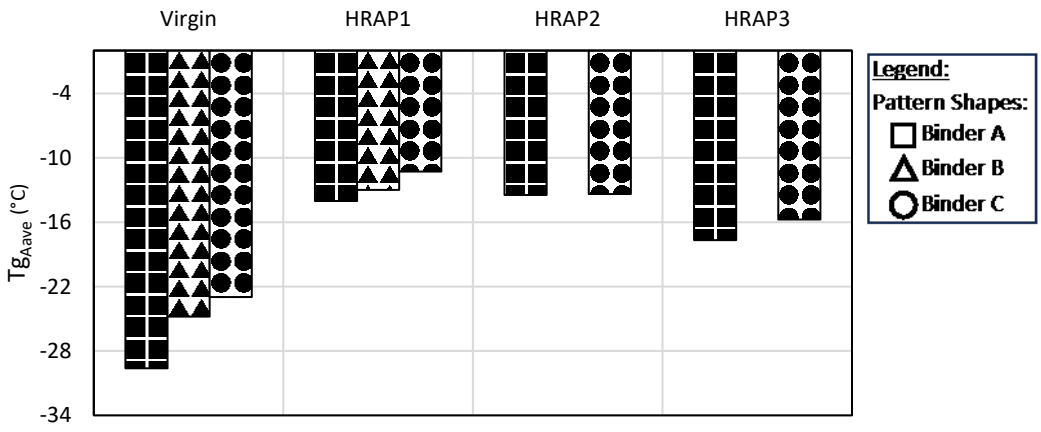

Figure 6-44 Effect of RAP type on Tg_{Aave}

6.6.3.7 Span of Glass Transition Temperature (Tg_{Range})

Figure 6-45 shows the effect of RAP on Tg_{Range}. It can be clearly observed that inclusion of RAP results in increased Tg_{Range} which holds true across the board. HRAP1 and HRAP2 show similar Tg_{Range} values for both binder A and C as they have similar PG grades. HRAP3 blends show the better Tg_{Range} values for all binder because of softer PG grade RAP binder.

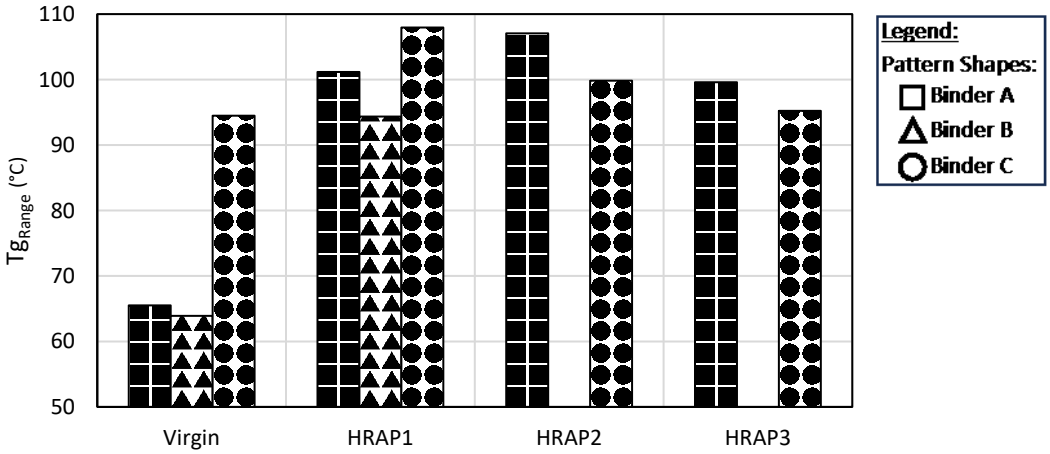

Figure 6-45 Effect of RAP type on Tg_{Range}

6.6.4 Comparison of Binder Properties with Mixture Properties

This section shows the scatter plot of selected binder parameters and mixture parameters to correlate them with each other. The selected mixture parameters include FI and FST whereas selected binder parameters include rheological parameters (G-R, T_c(m), and ΔT_c) and DSC parameters (ϕ_α Index, Tg, Tg_{Aave}, and Tg_{Range}). In the subsequent figures, binder A, B, and C data points are represented with □, △, and ○ respectively. Furthermore, results of virgin mixture and mixtures having RAP are shown with

hollow and solid bullets. Coarser and finer patterns indicate the data points of mixtures with RA1 and RA2 respectively.

6.6.4.1 Scatter Plots for FI (Core Materials)

This subsection discusses the correlations between FI and binder parameters for core materials.

GLOVER-ROWE PARAMETER (G-R)

It can be observed that as the G-R decreases the FI increases with virgin mixtures having the best properties (**Figure 6-46**). Although the G-R is inferior with RA1, it is interesting to note that mixtures with RA1 show better FI than their corresponding mixtures with RA2. This may imply that the mixture test results, and binder test results may not always align with each other, showcasing the potential for variation in results. The results indicate that RA1 is more compatible with RAP1 than RA2. Furthermore, it can be inferred from the results that mixtures with RAP2 outperform the corresponding mixtures with RAP1 even though the continuous PG grades of both RAP are similar. This suggests that RAP2 is more compatible with all binders than RAP1.

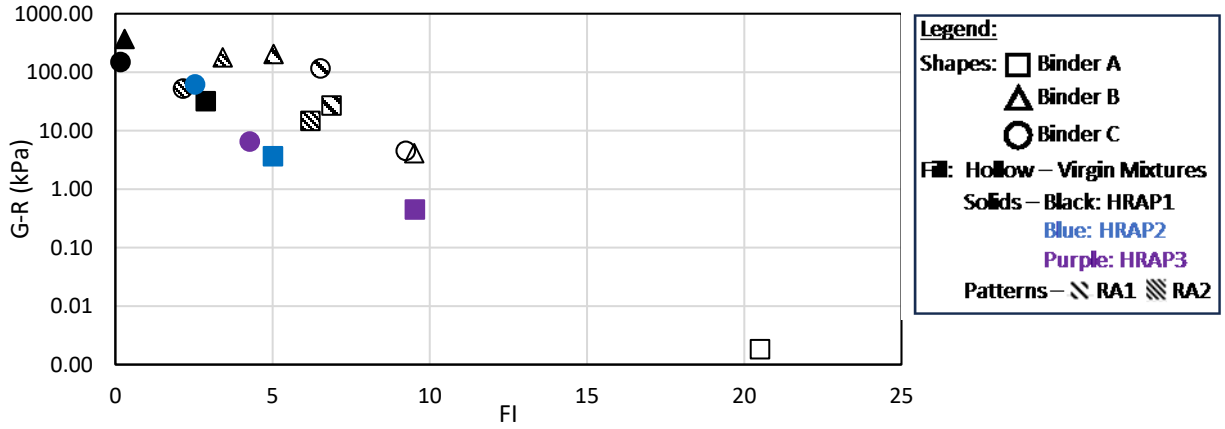

Figure 6-46 Scatter plot of G-R and FI for core materials

CRITICAL LOW TEMPERATURE BASED ON RELAXATION RATE (T_c(M))

It can be observed that as the T_c(m) decreases the FI increases with virgin mixtures having the best properties (**Figure 6-47**). It is interesting to note that mixtures with RA1 show better FI than their corresponding mixtures with RA2. The results indicate that RA1 is more compatible with RAP1 than RA2. Furthermore, it can be inferred from the results that mixtures with RAP2 outperform the corresponding mixtures with RAP1 even though the continuous PG grades of both RAP are similar. This suggests that RAP2 is more compatible with all binders than RAP1.

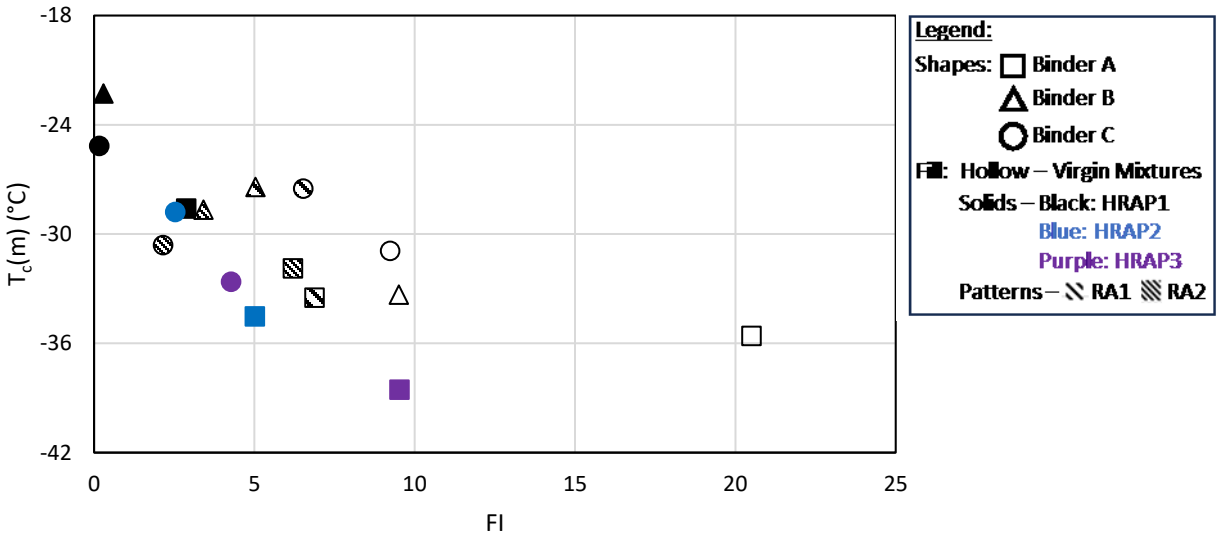

Figure 6-47 Scatter plot of T_c(m) and FI for core materials

CHANGE IN CRITICAL LOW TEMPERATURE (ΔT_C)

It can be observed that ΔT_c increases with the increase in the FI and virgin mixtures showing the best properties (**Figure 6-48**). Although the ΔT_c is inferior with RA1, it is interesting to note that mixtures with RA1 show better FI than their corresponding mixtures with RA2. However, it should be noted that the overall trend from the plot is not as promising as that of T_c(m), which might be due to dependence of ΔT_c on both T_c(S) and T_c(m). The threshold for ΔT_c is not proposed due to its composite nature. The mixture results indicate that RA1 is more compatible with RAP1 than RA2. It can also be inferred from the results that mixtures with RAP2 outperform the corresponding mixtures with RAP1 even though the continuous PG grades of both RAP are similar. This suggests that RAP2 is more compatible with all binders than RAP1.

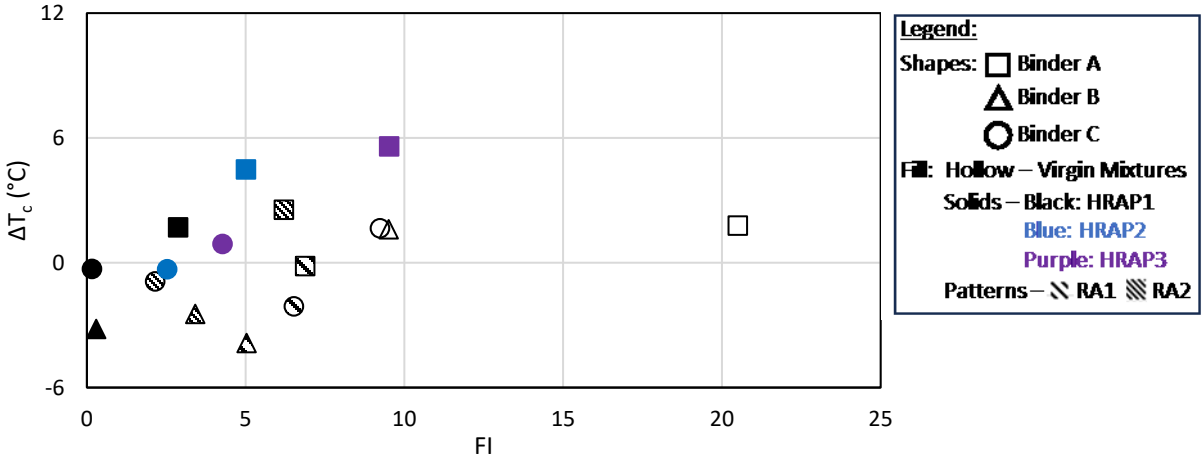

Figure 6-48 Scatter plot of ΔT_c and FI for core materials

Φ_A INDEX

It can be observed that ϕ_α increases with the increase in the FI and virgin mixtures showing the best properties except with binder C (**Figure 6-49**). It is interesting to note that mixtures with RA1 show better FI and ϕ_α than their corresponding mixtures with RA2 indicating that RA1 is more compatible with RAP1 than RA2. However, it should be noted that the threshold for ϕ_α is not proposed as the overall trend from the plot is not as promising as that of other rheological parameters.

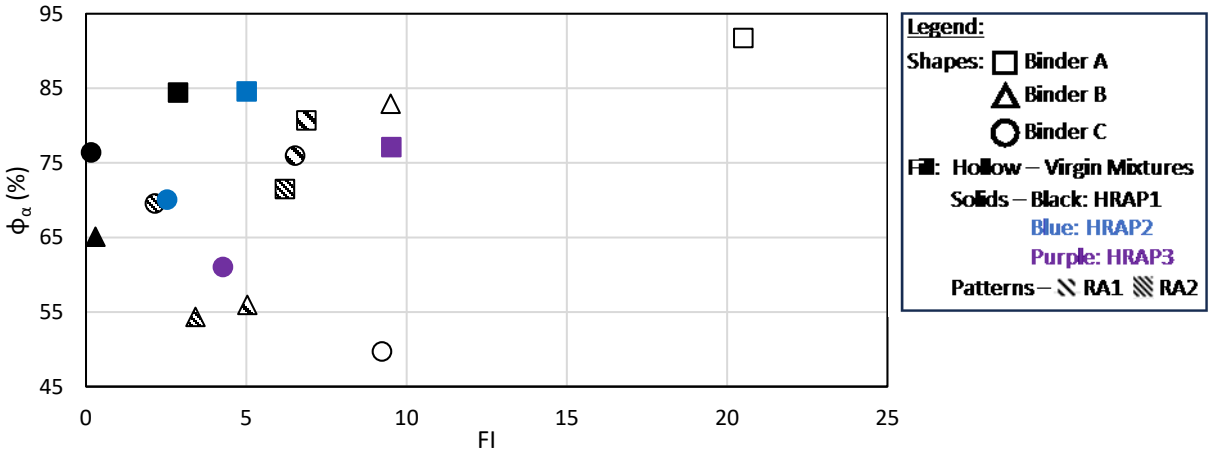

Figure 6-49 Scatter plot of ϕ_α and FI for core materials

GLASS TRANSITION TEMPERATURE (TG)

It can be observed that Tg decreases with the increase in FI and virgin mixtures show the best properties (**Figure 6-50**). It is interesting to note that mixtures with RA1 show better FI and Tg than their corresponding mixtures with RA2 indicating that RA1 is more compatible with RAP1 than RA2. Furthermore, it can be inferred from the results that mixtures with RAP2 outperform the corresponding mixtures with RAP1 even though the continuous PG grades of both RAP are similar. This suggests that RAP2 is more compatible with all binders than RAP1.

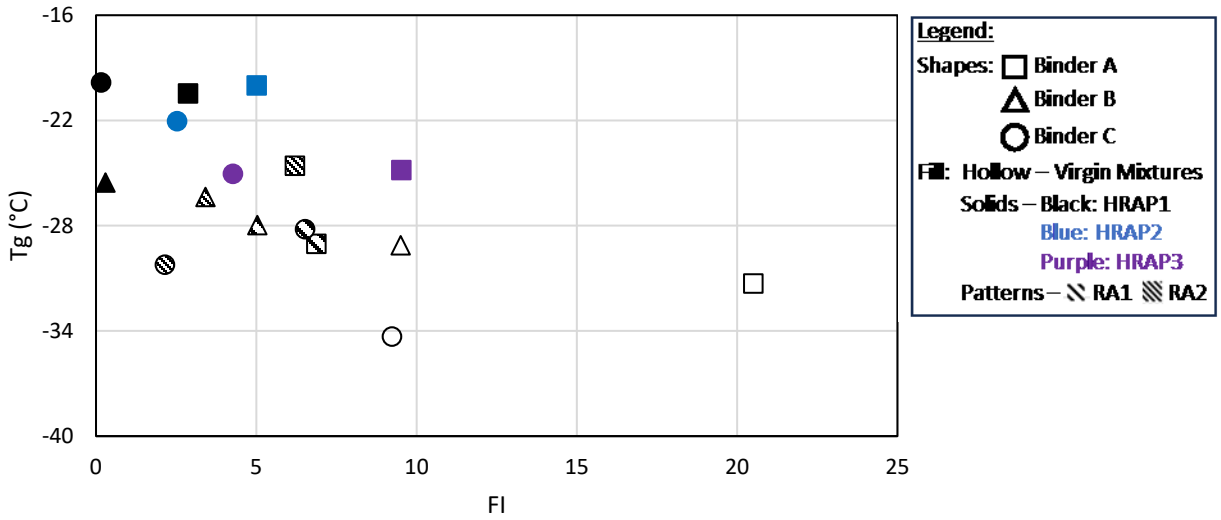

Figure 6-50 Scatter plot of Tg and FI for core materials

TG_{AAVE} PARAMETER

It can be observed that Tg_{Aave} decreases as the FI increases with virgin mixtures show the best properties (**Figure 6-51**). It is interesting to note that mixtures with RA1 show better FI and Tg_{Aave} than their corresponding mixtures with RA2 indicating that RA1 is more compatible with RAP1 than RA2.

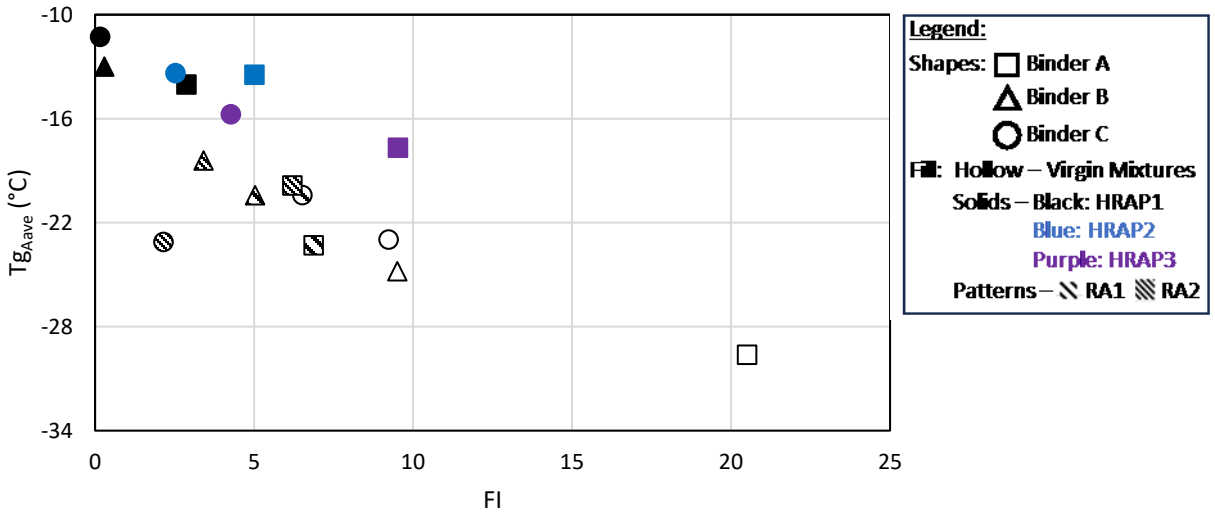

Figure 6-51 Scatter plot of Tg_{Aave} and FI for core materials

6.6.4.2 Scatter Plots for FI (Validation Materials)

This subsection discusses the correlations between FI and binder parameters for validation materials.

GLOVER-ROWE PARAMETER (G-R)

It can be observed that as the G-R decreases, the FI increases with MO-VL having the best properties (**Figure 6-52**). This trend aligns with the core materials' findings. There is a consistent trend between G-R and FI.

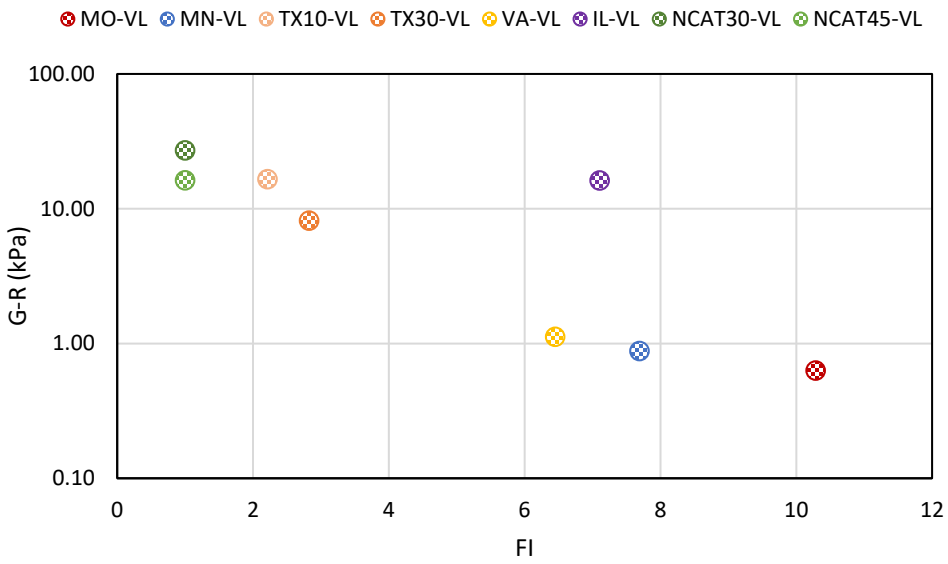

Figure 6-52 Scatter plot of G-R and FI for validation materials

CRITICAL LOW TEMPERATURE BASED ON RELAXATION RATE (T_C(M))

It can be observed that as the T_c(m) decreases, the FI increases with virgin mixtures having the best properties (**Figure 6-53**). This trend is consistent and in line with the results of core materials.

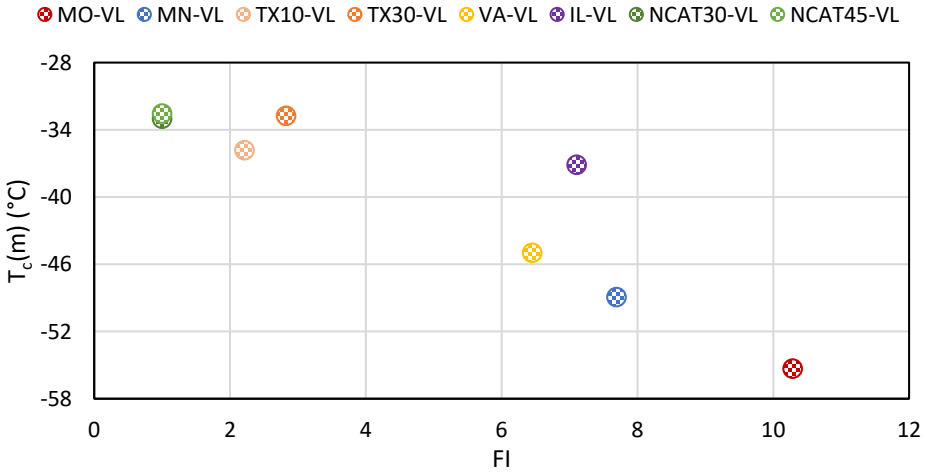

Figure 6-53 Scatter plot of T_c(m) and FI for validation materials

CHANGE IN CRITICAL LOW TEMPERATURE (ΔT_C)

It can be observed from **Figure 6-54** that ΔT_c increases with the increase in the FI value with MO-VL having the best ΔT_c value. This trend confirms the findings of core materials; however, it should be noted that the overall trend from the plot is not as promising as that of T_c(m) due to dependence of ΔT_c on both T_c(S) and T_c(m).

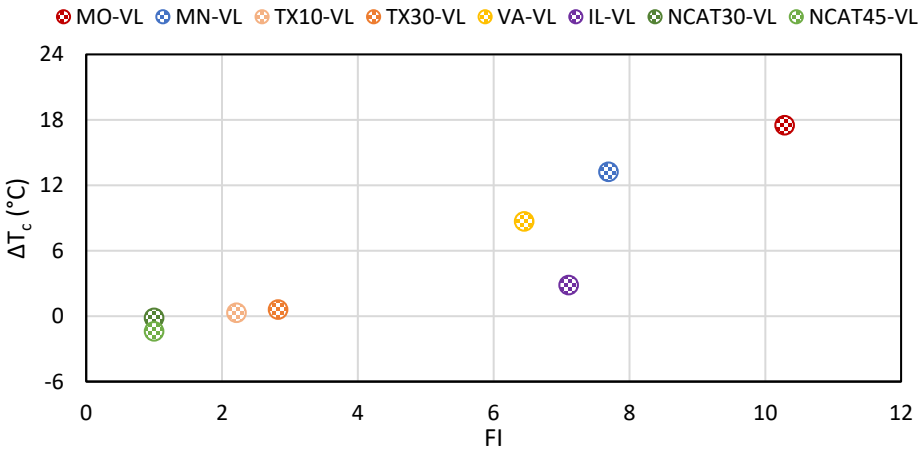

Figure 6-54 Scatter plot of ΔT_c and FI for validation materials

Φ_A INDEX

It can be observed from **Figure 6-55** that the trend between ϕ_α and FI is not consistent and does not align with the core materials. Larger dataset and more mixture results are necessary in order to achieve more meaningful data given that core materials have shown meaningful results.

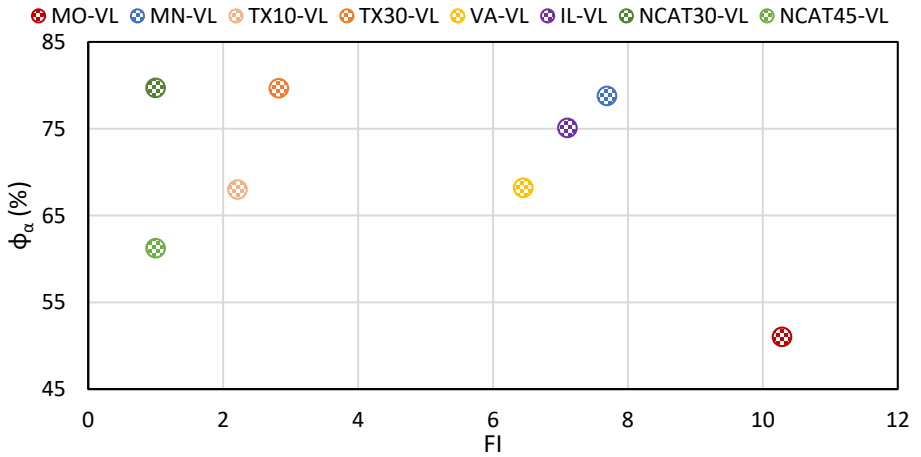

Figure 6-55 Scatter plot of ϕ_α and FI for validation materials

GLASS TRANSITION TEMPERATURE (TG)

It can be observed that Tg decreases with the increase in FI indicating that if Tg is lower than there are high chances of better intermediate temperature performance (**Figure 6-56**). It is interesting to note TX30-VL shows more than 10 °C drop in Tg compared to TX10-VL which might indicate incompatibility of RAP material given that TX30-VL and TX10-VL had PG 64-22 and PG 70-22 virgin binder respectively. Overall, this trend is consistent and in line with the results of core materials.

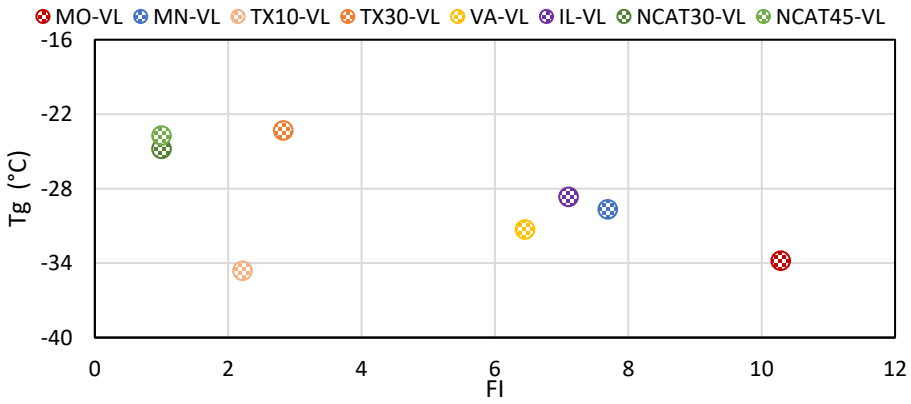

Figure 6-56 Scatter plot of Tg and FI for validation materials

TG_{AAVE} PARAMETER

It can be observed that Tg_{Aave} decreases as the FI increases with virgin mixtures show the best properties (**Figure 6-57**). It is interesting to note that TX30-VL shows more than 12 °C drop compared to its counterpart TX10-VL, as observed with Tg as well. Overall, this trend looks promising and is in line with the results of core materials. This highlights the potential of Tg_{Aave} as a parameter to evaluate the compatibility of the asphalt materials.

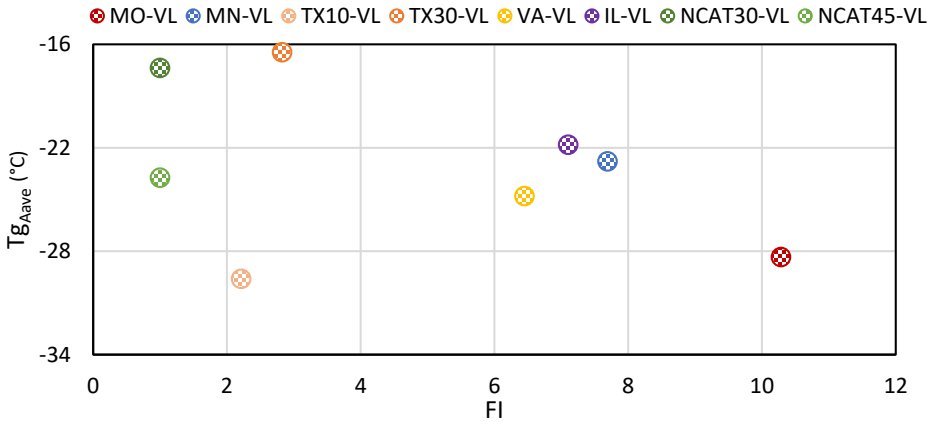

Figure 6-57 Scatter plot of Tg_{Aave} and FI for validation materials

6.6.4.3 Scatter Plots for FST (Core Materials)

This subsection discusses the correlations between FST and Tg_{Aave} for core materials. Scatter plots for other binder parameters are shown in Appendix C.

TG_{AAVE} PARAMETER

The FST increases with the decrese in G-R, however the trend is not as clear as that with FI (**Figure 6-58**). It is interesting to note that mixtures with RAs show comparable FST to that of mixtures without RAs. However, Tg_{Aave} shows improvement with RAs. Overall, FST for all mixtures has a narrow range than FI which might be due to adjusted testing temperature based on binder LTPG as all HRAP mixtures have a similar FST value resulting in no clear trend.

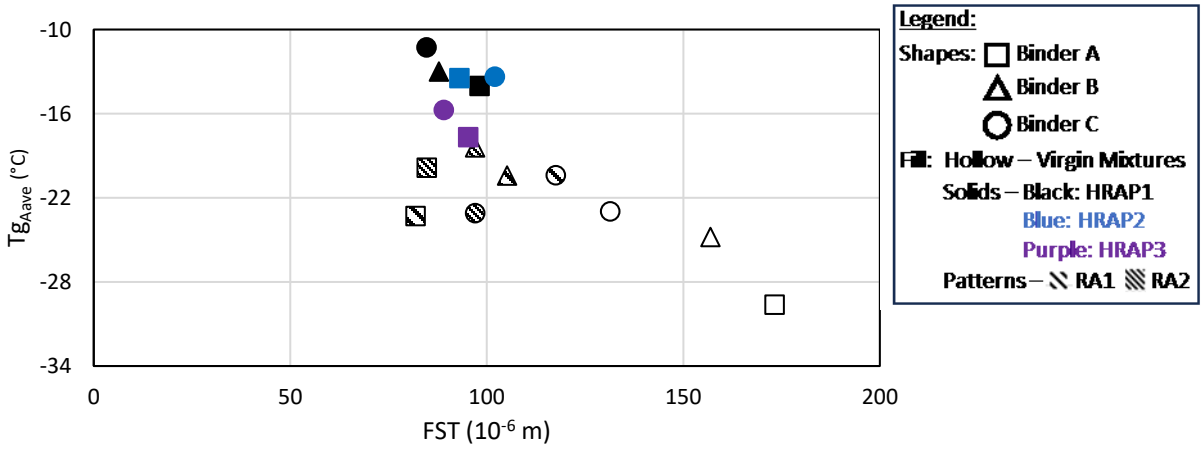

Figure 6-58 Scatter plot of Tg_{Aave} and FST for core materials

6.6.4.4 Scatter Plots for FST (Validation Materials)

This subsection discusses the correlations between FST and Tg_{Aave} for validation materials. Scatter plots for other binder parameters are shown in Appendix C.

TG_{AAVE} PARAMETER

It can be observed that Tg_{Aave} decreases as the FI increases with virgin mixtures show the best properties (**Figure 6-59**). It is interesting to note that TX30-VL shows more than 12 °C drop compared to its counterpart TX10-VL. This potentially indicates the incompatibility of TX30 RAP. Overall, this trend looks promising and is in line with the results of core materials. This highlights the potential of Tg_{Aave} as a parameter to evaluate the compatibility of the asphalt materials. Overall, FST for all mixtures has a narrow range than FI which might be due to adjusted testing temperature based on binder LTPG as all RAP mixtures have a similar FST value resulting in no clear trend.

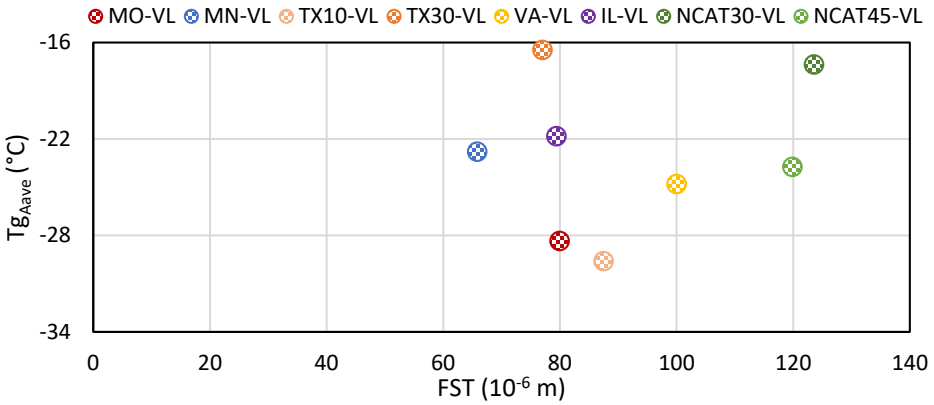

Figure 6-59 Scatter plot of Tg_{Aave} and FST for validation materials

6.7 CHAPTER SUMMARY

This task report assessed the selected binder and mixture property indicators to validate the findings of the core materials, based on the testing results of asphalt mixtures and asphalt binders recovered from eight validation mixtures. Similar to core materials, extracted binders from validation mixtures were evaluated for rheological and thermal properties using DSR and DSC, respectively. The Black space diagram and G-R parameter capture the effect of RAs and different RAP materials and also indicate the potential compatibility of the rejuvenator used in NCAT45-VL, thus validating the effectiveness of these parameters in compatibility characterization. Furthermore, DSC thermal analysis also shows that ϕ_α and Tg-related parameters have the greatest ability to characterize the compatibility of materials. From validation mixture test results, FI, FST, and mixture Glover-Rowe parameters are recommended as potential indicators for mixture compatibility characterization as they can differentiate between different binders, RAPs, and RAs. Furthermore, correlation analysis shows that the rheological parameters $T_c(m)$, ΔT_c, and G-R generally correlate well with most fracture-based mixture parameters. Intermediate cracking parameters for validation mixtures correlate better with the rheological and thermal parameters of the binder than low-temperature cracking parameters. Moreover, it is worthwhile noting that preliminary results show that ambient aging may significantly have an adverse impact on the performance properties and consequently the performance of the asphalt materials. Hence, ambient aging should be considered in the mixture and binder tests. In addition, intermediate cracking parameters such as FI might be misleading sometimes, as they do not account for the binder grade. For example, the mixture with a stiffer binder (necessary for hot climate conditions) may have lower indices, but in the field, because of the warmer average temperature, they can perform well. This can be addressed by testing the mixtures at their ITPG or having location-based thresholds.

Chapter 7: PROJECT SUMMARY, CONCLUSIONS AND RECOMMENDATIONS FOR FUTURE RESEARCH

7.1 SUMMARY

Modern asphalt mixtures are usually a combination of various materials from different sources, including RAP and RAs, and are used to attain sustainable growth. However, the lack of a well-established method for determining compatibility between various sources and types of virgin binder, aged binder extracted from RAP, and RAs is a major impediment in current asphalt material selection and specification restricting the allowable recycled material content in the mixture. Therefore, this research aims to provide a framework for agencies to select the most compatible component materials from various sources for their projects.

The main objective of this project was to develop a practical and implementable characterization system to determine compatibility between virgin asphalt binder and recycled asphalt pavement (RAP) as well as that between virgin asphalt binder, RAP and rejuvenating agents. The core material matrix consisted of three RAP sources, three asphalt binders (one with PG 58–28, two with PG 64–22), and two RAs (petroleum-based and bio-oil-based) to develop a methodology for compatibility characterization of these materials. Finally, eight validation mixtures and limited field performances were assessed to verify the findings from the primary materials.

The following subsections provide a list of key conclusions based on the research completed as part of this project, as well as recommendations for future extension of this research topic.

7.2 CONCLUSIONS

The following is a list of conclusions made based on research completed during this project from (1) primary binder test results, (2) primary mixture test results, and (3) validation materials.

Binder Test Results of Core Materials:

- Rheological and thermal characterization methods have been identified suitable for compatibility characterization.
- Rheological characterizations such as G-R, ΔT_c have consensually indicated that RAP1 is potentially incompatible whereas RAP2 is potentially compatible with virgin binders and rejuvenators evaluated in the study given that both RAPs have comparable PGs.
- DSC thermal analysis also supported the findings of the rheological characterization as RAP1 showed the warmest Tg of all.
- Binder B showed potential for inferior performance than binder C given that both binders had similar PGs based on results of G-R and ΔT_c parameters. The findings were also supported by the results of ϕ_α parameter from thermal analysis. The blends having RAs also suggested potential for inferior performance of binder B.

- G-R plotted in Black space diagram was clearly able to capture the effect of RAs and different RAP materials and also indicated the potential incompatibility of binder B with all RAP1 material and potential compatibility of RAP3 material with all binders.
- DSC thermal analysis showed that the ϕ_α and Tg related parameters have the greatest ability to characterize the compatibility of materials.
- Overall, ΔT_c, Glover-Rowe, ϕ_α and other Tg related parameters such as Tg_{Aave} and Tg were recommended as the potential indicators for binder compatibility characterization.

Mixture Test Results of Core Materials:

Core mixtures include 21 mixtures produced using various combinations of core materials. All core mixtures were designed with similar aggregate gradation to facilitate direct comparison.

- Rheological and cracking characterization tests have been identified suitable for compatibility characterization for mixtures.
- Complex modulus test along with Black space diagram clearly differentiated between the mixtures with RAs and different RAP materials. The results also indicated that binder B was potentially more incompatible than binder C and mixtures with RAP1 showed the most inferior performance among all RAP materials.
- I-FIT (intermediate temperature cracking characterization) indicated that mixtures with RAP1 had the most inferior properties followed by RAP2 and RAP3, respectively, irrespective of the presence of RA. The effect of the rejuvenation was also captured by the test. These results also supported the observations from binder tests.
- DCT (low temperature cracking characterization) results indicated that low-temperature performance was less discriminating between various RAPs and binders than intermediate-temperature performance properties. Furthermore, FST parameter from DCT showed better discrimination potential than the fracture energy.
- Overall, FI and FST parameters were recommended as the potential indicators for compatibility characterization of mixtures.

Results of Validation Materials:

Validation materials include 8 mixtures to cover geographical variation as much as possible.

- Rheological parameters such as G-R and Black space analysis validate the effectiveness of the RA used in NCAT45-VL, which had 45% RAP, and improved the properties to that of NCAT30-VL, which had 30% RAP.
- ϕ_α and Tg-related parameters from DSC thermal analysis also show promising results in differentiating between different validation materials and effect of RA.
- Ambient aging may significantly have an adverse impact on the properties and consequently the performance of the asphalt materials. Hence, ambient aging should be considered in the test. Furthermore, binder grade should be accounted in intermediate temperature test.
- The correlation analysis shows that the rheological parameters $T_c(m)$, ΔT_c, and G-R generally correlate well with most fracture-based mixture parameters especially with intermediate cracking parameters.

7.3 RECOMMENDATIONS FOR FUTURE RESEARCH

- The selection of test temperatures for intermediate cracking tests should be based on the geographical location of the project or the performance grade (PG) of the binder (The approach is documented and a paper in *Construction and Building Materials* is currently in review process).
- The impact of ambient aging on the intermediate cracking properties of the mixture and the thermal properties of the binder should be thoroughly evaluated. Preliminary results indicate that these properties undergo significant changes depending on ambient aging conditions.
- Field validation with ongoing and upcoming test sections is recommended. This will be instrumental in corroborating the findings of the study.
- Thresholds for proposed binder parameters should be developed. The preliminary methodology for threshold development based on existing thresholds (for example, FI threshold of 8) of mixtures is explained in the following steps (**Figure 7-1**):
    1. Determine the extreme points on either side of the existing threshold for mixture property.
    2. Determine the corresponding target binder properties (3 and 5 in this case). The threshold for the proposed property lies within this range. The threshold for the proposed binder property can be finetuned and determined from larger data set results.

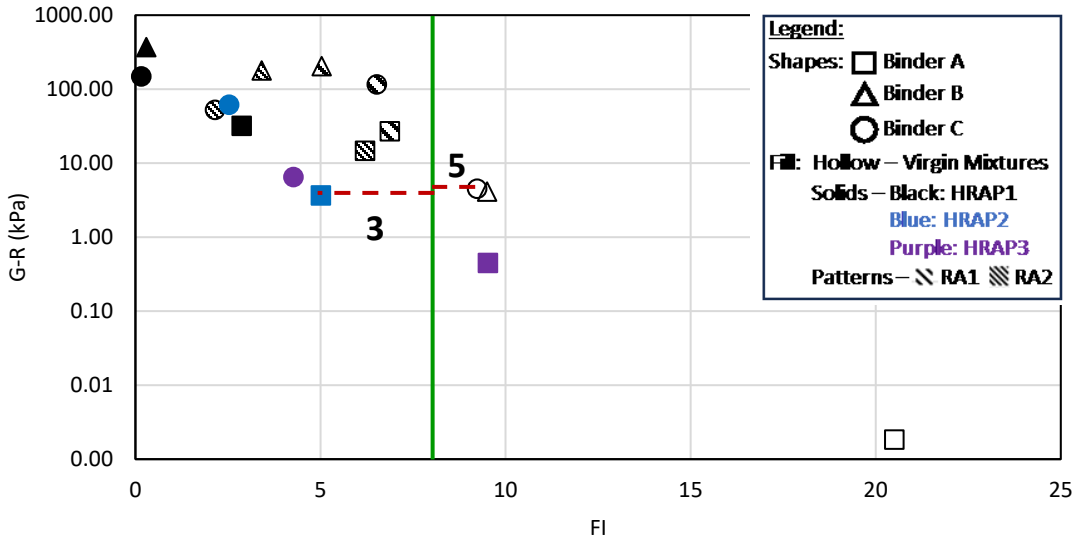

Figure 7-1 Approach for threshold development for the proposed binder parameters

REFERENCES

Adams, J. J., Elwardany, M. D., Planche, J. P., Boysen, R. B., & Rovani, J. F. (2019). Diagnostic techniques for various asphalt refining and modification methods. *Energy Fuels*, *33*(4), 2680-2698.

Al-Qadi, I. L., Wu, S., Lippert, D. L., Ozer, H., Barry, M. K., & Safi, F. R. (2017). Impact of high recycled mixed on HMA overlay crack development rate. *Road Materials and Pavement Design*, *18*(sup4), 311–327.

Anderson, M. (2010). Using the multiple-stress creep-recovery (MSCR) test. Paper presented at the Association of Modified Asphalt Producers Annual Meeting, Savannah, GA, February 2–3, 2010.

Anderson, R., King, G., Hanson, D., & Blankenship, P. (2011). Evaluation of the relationship between asphalt binder properties and non-load related cracking. *J. Assoc. Asphalt Paving Technol.*, *80*, 615-664.

Andriescu, A., & Hesp, S. A. M. (2009). Time–temperature superposition in rheology and ductile failure of asphalt binders. *Int. J. Pavement Eng.*, *10*(4), 229–240.

Andriescu, A., Iliuta, S., Hesp, S. A. M., & Youtcheff, J. S. (2004). Essential and plastic works of ductile fracture in asphalt binders and mixtures. *Proc. Can. Tech. Asphalt Assoc., 49*, 93–121.

Angius, E., Ding, H., & Hesp, S. A. M. (2018). Durability assessment of asphalt binder. *Constr. Build. Mater.*, *165*, 264–271.

Apostolidis, P., Liu, X., Erkens, S., & Scarpas, A. (2019). Evaluation of epoxy modification in bitumen. *Constr. Build. Mater.*, *208*, 361–368. https://doi.org/10.1016/j.conbuildmat.2019.03.013

Arnold, T. (2017). What's in your asphalt? Public Roads, *81*(2), 14–19.

Bahia, H. U., Hanson, D. I., Zeng, M., Zhai, H., Khatri, M. A., & Anderson, R. (2001). Characterization of modified asphalt binders in Superpave mix design (NCHRP Project 9-10), NCHRP Report 459, The National Academic Press, Washington DC.

Barborak, R. C., Coward, J., Clifton, E., & Lee, R. (2016). Detection and estimation of re-refined engine oil bottoms in asphalt binders. *Transp. Res. Rec.*, *2574*, 48–56.

Barth, E. J. (1962). *Asphalt science and technology.* New York: Gordon and Breach Science Publishers.

Boduszynski, M. M. (1981). Asphaltene in petroleum asphalts: Composition and formation. In *Advances in chemistry series: Chemistry of asphalts* (pp. 119–135), J. W. Bunger and N. C. Li (Eds.). Washington, DC: Am. Chem. Soc.

Bowers, B. F., Huang, B., Shu, X., & Miller, B. C. (2014). Investigation of reclaimed asphalt pavement blending efficiency through GPC and FTIR. *Constr. Build. Mater.*, *50*, 517–523.

Bullard, J. W., Pauli, A. T., Garboczi, E. J., & Martys, N. S. (2009). A comparison of viscosity concentration relationships for emulsions. *J. Colloid Interface Sci.*, *330*, 186–193.

Buszewski, B., & Noga, S. (2012). Hydrophilic interaction liquid chromatography (HILIC)—A powerful separation technique. *Anal. Bioanal. Chem.*, *402*, 231–247.

Canto, L. B., Mantovani, G. L., Deazevedo, E. R., Bonagamba, T. J., Hage, E., & Pessan, L. A. (2006). Molecular characterization of styrene-butadiene-styrene block copolymers (SBS) by GPC, NMR, and FTIR. *Polym. Bull.*, *57*(4), 513–524.

Claudy, P., Letoffe, J. M., King, G. N., & Planche, J. P. (1992). Characterization of asphalt cements by thermomicroscopy and differential scanning calorimetry: Correlation to classic physical properties. *Fuel Sci. Technol. Int.*, *10*(4–6), 735–765.

Claudy, P., Letoffe, J. M., King, G. N., Planche, J. P., & Brule, B. (1991). Characterization of paving asphalts by differential scanning calorimetry. *Fuel Sci. Technol. Int.*, *9*(1), 71–92.

Clopotel, C., Velasquez, R., Bahia, H., Pérez-Jiménez, F., Miró, R., & Botella, R. (2012). Relationship between binder and mixture damage resistance at intermediate and low temperatures. *Transp. Res. Rec.*, *2293*(1), 39–47.

Corbett, L. W. (1969). Composition of asphalt based on generic fractionation using solvent deasphalting, elution adsorption chromatography, and densitometric characterization. *Anal. Chem.*, *41*(4), 576–579.

Corbett, L. W. (1970). Relationship between composition and physical properties of asphalt and discussion. *Assoc. Asphalt Paving Technol. Proc.*, *39*, 481−491.

Cortizo, M. S., Larsen, D. O., Bianchetto, H., & Alessandrini, J. L. (2004). Effect of the thermal degradation of SBS copolymers during the ageing of modified asphalts. *Polym. Degrad. Stab.*, *86*(2), 275–282.

Cotterell, B., & Reddel, J. K. (1977). Essential work of plane stress fracture. *Int. J. Fract.*, *13*(3), 267–277.

Daly, W. H., Negulescu, L., & Balamurugan, S. S. (2013). Implementation of GPC characterization of asphalt binders at Louisiana Materials Laboratory (HWA/LA.13/505). Baton Rouge, LA: Louisiana Department of Transportation.

Das, O., Kim, N. K., Hedenqvist, M. S., & Bhattacharyya, D. (2015). The flammability of biocomposites. *Durability and Life Prediction in Biocomposites, Fibre-Reinforced Composites and Hybrid Composites, Volume*, 335-365.

Desbief, S., Hergué, N., Douhéret, O., Surin, M., Dubois, P., Geerts, Y., Lazzaroni, R., & Leclère, P. (2012). Nanoscale investigation of the electrical properties in semiconductor polymer–carbon nanotube hybrid materials. Nanoscale, 4, 2705.

DiBenedetto, A. T. (1987). Prediction of the glass transition temperature of polymers: A model based on the principle of corresponding states. *J. Polym. Sci.: Part B: Polym. Phys.*, *25*, 1949–1969.

Ding, H., Gotame, Y., Nie, Y., & Hesp, S. A. M. (2018). Acceptance testing of extracted and recovered asphalt cements for provincial and municipal paving contracts in Ontario. *Proc. Can. Tech. Asphalt Assoc.*, *63*, 43–60.

Ding, H., Tetteh, N., & Hesp, S. A. M. (2017). Preliminary experience with improved asphalt cement specifications in the City of Kingston, Ontario, Canada. *Constr. Build. Mater.*, *157*, 467–475.

Dong, S., & Striegel, A. M. (2013). Size-exclusion chromatography of asphaltenes: An experimental comparison of commonly used approaches. Chromatographia, 76(13–14), 725–733.

Einstein, A. (1966). Eine neve bestimmung der Moleküldimensionen. *Annalen der Physik*, *19*, 289–307.

Elkashef, M., Jones, D., Jiao, L., Williams, R. C., & Harvey, J. (2019). Using thermal analytical techniques to study rejuvenators and rejuvenated reclaimed asphalt pavement binders. *Energy Fuels*, *33*(4), 2651-2658.

Elwardany, M. D., Planche, J. P., & Adams, J. J. (2019). Determination of binder glass transition and crossover temperatures using 4-mm plates on a dynamic shear rheometer. *Transp. Res. Rec.*, *2673*. https://doi.org/10.1177/0361198119849571

Erskine, J. E., Hesp, S. A. M., & Kaveh, F. (2012). Another look at accelerated aging of asphalt cements in the pressure aging vessel. Paper presented at 5th Eurasphalt and Eurobitume Congress, Istanbul, Turkey.

Eyerer, S., Eyerer, P., Eicheldinger, M., Tübke, B., Wieland, C., & Spliethoff, H. (2018). Theoretical analysis and experimental investigation of material compatibility between refrigerants and polymers. Energy, 163, 782–799. https://doi.org/10.1016/j.energy.2018.08.142

Ge, D., Yan, K., You, Z., & Xu, H. (2016). Modification mechanism of asphalt binder with waste tire rubber and recycled polyethylene. *Constr. Build. Mater.*, *126*, 66–76.

Gilar, M., Olivova, P., & Daly, A. E. (2005). Orthogonality of separation in two-dimensional liquid chromatography. *J. C. Gebler Anal. Chem.*, *77*, 6426–6434.

Glaser, R., Turner, T. F., Loveridge, J. L., Salmans, S. L., & Planche, J. P. (2013). Fundamental properties of asphalts and modified asphalts, Volume III (Quarterly Technical Report). Washington, DC: Federal Highway Administration (FHWA).

Glover, C. J., Davison, R. R., Domke, C. H., Ruan, Y., Juristyarini, P., Knorr, D. B., & Jung, S. H. (2005). Development of a new method for assessing asphalt binder durability with field validation (Final report). City, State: Publisher.

Grieshaber, S. E., Farran, A. J., Lin-Gibson, S., Kiick, K. L., & Jia, X. (2009). Synthesis and characterization of elastin−mimetic hybrid polymers with multiblock, alternating molecular architecture and elastomeric properties. *Macromolecules, 42*(7), 2532–2541.

Gulmine, J. V., Janissek, P. R., Heise, H. M., & Akcelrud, L. (2002). Polyethylene characterization by FTIR. *Polym. Test.*, *21*(5), 557–563.

Gutierrez, J., Mondragon, I., & Tercjak, A. (2014). Quantitative nanoelectrical and nanomechanical properties of nanostructured hybrid composites by peak force tunneling atomic force microscopy. *J. Phys. Chem. C.*, *118*, 1206–1212.

Harrison, I. R., Wang, G., & Hsu, T. C. (1992). A differential scanning calorimetry study of asphalt binders (*SHRP-A/UFR-92-612*). Washington, DC: Strategic Highway Research Program (SHRP), National Academy of Science.

Heithaus, J. J. (1960). Measurement and significance of asphaltene peptization. *Am. Chem. Soc. D, Petrol. Chem. Prepr.*, *5*, A23–A37.

Hesp, S. A. M., & Shurvell, H. F. (2010). X-ray fluorescence detection of waste engine oil residues in asphalt and its effect on cracking in service. Int. J. Pavement Eng., 11(6), 541–553.

Hesp, S. A. M., Genin, S. N., Scafe, D., Shurvell, H. F., & Subramani, S. (2009). Five-year performance review of a northern Ontario pavement trial. Proc. Can. Tech. Asphalt Assoc., 54, 99–126.

Hesp, S. A. M., Iliuta, S., & Shirokoff, J. W. (2007). Reversible aging in asphalt binders. Energy Fuels, 21(2), 1112–1121.

Hesp, S. A. M., Johnson, K. N., McEwan, R. G., Samy, S., Ritchie, S., & Thomas, M. (2014). Effect of ten commercial warm mix additives on the quality and durability of Cold Lake asphalt cement. Int. J. Pavements, 13(1), 1–11.

Hesp, S. A. M., Soleimani, A., Subramani, S., Phillips, T., Smith, D., Marks, P., & Tam, K. (2009). Asphalt pavement cracking: Analysis of extraordinary life cycle variability in eastern and northeastern Ontario. Int. J. Pavement Eng., 10(3), 209–277.

Hintz, C., Velasquez, R., Johnson, C., & Bahia, H. (2011). Modification and validation of linear amplitude sweep test for binder fatigue specification. *Transp. Res. Rec.*, *2207*, 99–106.

Horan, B. (2011). Multiple stress creep recovery (MSCR) task force. Paper presented at the Southeastern Asphalt User/Producer Group (SEAUPG) Meeting, Savannah, GA, November 11–17, 2011.

Huang, S. C., & Pauli, A. T. (2008). Particle size effect of crumb rubber on rheology and morphology of asphalt binders with long-term aging. Road Mater. Pavement Des., 9(9), 73–95.

Jafarzadeh, S., Claesson, P. M., Sundell, P. E., Pan, J., & Thormann, E. (2014). Nanoscale electrical and mechanical characteristics of conductive polyaniline network in polymer composite films. ACS Appl. Mater. Interfaces, 6, 19168–19175.

Jimenez-Mateos, J. M., Quintero, L. C., & Rial, C. (1966). Characterization of petroleum bitumens and their fractions by thermogravimetric analysis and differential scanning calorimetry. *Fuel*, *75*(15), 1691–1700.

Johnson, K.-A. N., & Hesp, S. A. M. (2014). Effect of waste engine oil residue on quality and durability of SHRP materials reference library binders. *Transp. Res. Rec.*, *2444*(1), 102–109. https://doi.org/10.3141/2444-12

Kakroodi, A. R., Kazemi, Y., Rodrigue, D., & Park, C. B. (2018). Facile production of biodegradable PCL/PLA in situ nanofibrillar composites with unprecedented compatibility between the blend components. *Chemical Engineering Journal*, *351*, 976–984.

Kamal, M. R., & Sourour, S. (1973). Kinetics and thermal characterization of thermoset cure. *Polym. Eng. Sci.*, *13*(1), 59–64.

Karlsson, R., & Isacsson, U. (2003). Application of FTIR-ATR to characterization of bitumen rejuvenator diffusion. *J. Mater. Civil Eng.*, *15*(2), 157–165.

Karlsson, R., Isacsson, U., & Ekblad, J. (2007). Rheological characterization of bitumen diffusion. *J. Mater. Sci.*, *42*(1), 101–108.

Kartsova, L. A., Bessonova, E. A., & Somova, V. D. (2019). Hydrophilic interaction chromatography. *J. Anal. Chem.*, *74*, 415–424.

Kaskow, J., van Poppelen, S., & Hesp, S. A. M. (2018). Methods for the quantification of recycled engine oil bottoms in performance-graded asphalt cement. *J. Mater. Civ. Eng.*, *30*(2), p.04017269.

Kim, Y. R., Castorena, C., Elwardany, M., Rad, F. Y., Underwood, B. S., Gundla, A., Gudipudi, P. P., Farrar, M. J., & Glaser, R. R. (2018). Long-term aging of asphalt mixtures for performance testing and prediction (NCHRP research report 871). Washington DC: Transportation Research Board.

Koots, J. A., & Speight, J. G. (1975). Relationship of petroleum resins to asphaltenes. *Fuel*, *54*(2), 179–184.

Kriz, P., Stastna, J., & Zanzotto, L. (2008). Glass transition and phase stability in asphalt binders. *Road Mater. Pavement Des.*, *9*(sup1), 37–65. https://doi.org/10.1080/14680629.2008.9690158

Kuang, D., Yu, J., Feng, Z., Li, R., Chen, H., Guan, Y., & Zhang, Z. (2014). Performance evaluation and preventive measures for aging of different bitumens. *Constr. Build. Mater.*, *66*, 209–213.

Kudva, R. A., Keskkula, H., & Paul, D. R. (1998). Compatibilization of nylon 6/ABS blends using glycidyl methacrylate/methyl methacrylate copolymers. *Polymer*, *39*(12), 2447–2460.

Lamontagne, J., Durrieu, F., Planche, J. P., Mouillet, V., & Kister, J. (2021). Direct and continuous methodological approach to study the aging of fossil organic material by infrared micro spectrometry imaging: Application to polymer-modified bitumen. *Anal. Chim. Acta*, *444*(2), 241–250.

Laval, C., & Quivoron, C. (1973). Mise en evidence d'une corrélation entre le rapport hydrophile/lipophile des résines epoxydes et leur compatibilité avec le bitumen routier. *C. R. Acad. Sci. IIc.*, *256*, 743.749.

Le Guern, M., Chailleux, E., Farcas, F., Dreessen, S., & Mabille, I. (2010). Physico-chemical analysis of five hard bitumens: Identification of chemical species and molecular organization before and after artificial aging. *Fuel*, *89*(11), 3330–3339.

Lei, Z., Bahia, H., & Yi-qiu, T. (2015). Effect of bio-based and refined waste oil modifiers on low-temperature performance of asphalt binders. *Constr. Build. Mater.*, *86*, 95–100.

Li, R., Xiao, F., Amirkhanian, S., You, Z., & Huang, J. (2017). Developments of nanomaterials and technologies on asphalt materials: A review. *Constr. Build. Mater.*, *143*, 633–648.

Liang, M., Sun, C., Yao, Z., Jiang, H., Zhang, J., & Re, S. (2020). Utilization of wax residue as compatibilizer for asphalt with ground tire rubber/recycled polyethylene blends. *Constr. Build. Mater.*, *230*, 116966. https://doi.org/10.1016/j.conbuildmat.2019.116966

Liang, M., Xin, X., Fan, W., Ren, S., Shi, J., & Luo, H. (2018). Thermo-stability and aging performance of modified asphalt with crumb rubber activated by microwave and TOR. *Mater. Des.*, *127*, 84–96.

Lima, F. S. G., & Leite, L. F. M. (2004). Determination of asphalt cement properties by near infrared spectroscopy and chemometrics. *Pet. Sci. Technol.*, *22*(5), 589–600.

Liu, H. Y., Zhang, H. L., Hao, P. W., & Zhu, C. Z. (2015). The effect of surface modifiers on ultraviolet aging properties of nano-zinc oxide modified bitumen. *Pet. Sci. Technol.*, *33*(1), 72–78.

Liu, H., Al-Qadi, I. L., Lambros, J., El-Khatib, A., Singhvi, P., & Doll, B. (2016). Development of the fracture-based flexibility index for asphalt concrete cracking potential using modified semi-circle bending test parameters. *Constr. Build. Mater.*, *115*, 390–401.

Lu, X., & Isacsson, U. (1998). Chemical and rheological evaluation of ageing properties of SBS polymer modified bitumens. *Fuel*, *77*(9), 961–972.

Lu, X., & Isacsson, U. (2002). Effect of aging on bitumen chemistry and rheology. *Constr. Build. Mater.*, *16*, 15–22.

Ma, T., Huang, X., Zhao, Y., & Yuan, H. (2012). Aging behavior and mechanism of SBS modified asphalt. J. Test. Eval., 40(7), 663–681.

Mansourkhaki, A., Ameri, M., Habibpour, M., & Underwood, B. S. (2020). Relations between colloidal indices and low-temperature properties of reclaimed binder modified with softer binder, oil-rejuvenator and polybutadiene rubber. *Construction and Building Materials*, *239*, 117800.

Martin, A. E., Kaseer, F., Arambula, E., Bajaj, A., Daniel, J. S., Hajj, E., Morian, N., & Ogbo, C. (2018). Component materials selection guidelines and evaluation tools for binder blends and mixtures with high recycled materials content and recycling agents. Submitted to the AAPT Conference.

Martin, A. E., Zhou, F., Arambula, E., Park, E. S., Chowdhury, A., Kaseer, F., Carvajal, J., Hajj, E., Daniel, J. S., & Glover, C. (2015). The effects of recycling agents on asphalt mixtures with high RAS and RAP binder ratios (Interim report NCHRP 09-58 Project). Washington DC: Transportation Research Board.

Menapace, I., Cucalon, L. G., Kaseer, F., Masad, E., & Martin, A. E. (2018). Application of low field nuclear magnetic resonance to evaluate asphalt binder viscosity in recycled mixes. *Constr. Build. Mater.*, *170*, 725–736.

Menapace, I., Masad, E., Papavassiliou, G., & Kassem, E. (2015). Evaluation of aging in asphalt cores at room temperature using low field nuclear magnetic resonance. *Bituminous Mixtures Pavements*, *VI*, 395.

Mensching, D. J., Rowe, G. M., & Daniel, J. S. (2017). A mixture-based black space parameter for low-temperature performance of hot mixture asphalt. *Road Materials and Pavement Design*, *18*(1), 404–425.

Miknis, F., & Michon, L. C. (1998). Some applications of nuclear magnetic resonance imaging to crumb rubber modified asphalts. *Fuel*, *77*(5), 393–397.

Mogawer, W., Li, H., Andriescu, A., & Copeland, A. (2012). Evaluation of fatigue tests for characterizing asphalt binders. *J. Mater. Civ. Eng.*, *25*, 610–617.

Morea, F., Marcozzi, R., & Castaño, G. (2012). Rheological properties of asphalt binders with chemical tensoactive additives used in warm mix asphalts (WMAs). *Constr. Build. Mater.*, *29*, 135–141.

Mouillet, V., Lamontagne, J., Durrieu, F., Planche, J. P., & Lapalu, L. (2018). Infrared microscopy investigation of oxidation and phase evolution in bitumen modified with polymers. *Fuel*, *87*(7), 1270–1280.

Nahar, S. N. (2016). Phase-separation characteristics of bitumen and their relation to damage healing (Doctoral dissertation). Delft University of Technology, Delft, Netherlands.

Nemati, R., Dave, E. V., & Sias, J. E. (2020). Development of complex modulus-based rutting index parameter for asphalt mixtures. *J. Transp. Eng., Part B: Pavements*, *146*(2), 04020026.1-04020026.11.

Nemati, R., Haslett, K., Dave, E. V., & Sias, J. E. (2019). Development of a rate-dependent cumulative work and instantaneous power-based asphalt cracking performance index. *Road Mater. Pavement Des.*, *20*(sup1), S315–S331. https://doi.org/10.1080/14680629.2019.1586753

Ning-Li, L., Zhao, X. P., Sun, J. S., & Xiao, Q. Y. (2015). Study on aging mechanism of rubber modified asphalt. *J. Highway Transport. Res. Dev.*, *32*, 18-27.

Notional Center for Asphalt Technology (NCAT). (n.d.). Retrieved from http://www.eng.auburn.edu/research/centers/ncat/newsroom/2018-spring/aging.html

Oliver, J. W. H. (1974). Diffusion of oils in asphalts. *Ind. Eng. Chem. Prod. Res. Dev.*, *13*(1), 76–82.

Oliver, J. W. H. (2009). Changes in the chemical composition of Australian bitumens. *Road Mater. Pavement Des.*, *10*(3), 569–586.

Omari, I., Aggarwal, V., & Hesp, S. A. M. (2016). Investigation of two warm mix asphalt additives. *Int. J. Pavement Res. Technol.*, *9*(2), 83–88.

Oyekunle, L. O. (2006). Certain relationships between chemical composition and properties of petroleum asphalts from different origins. *Oil Gas Sci. Technol. IFP*, *61*(3), 433–441.

Paliukaite, M., Assuras, M., & Hesp, S. A. M. (2016). Effect of recycled engine oil bottoms on the ductile failure properties of straight and polymer-modified asphalt cements. *Constr. Build. Mater.*, *126*, 190–196. https://doi.org/10.1016/j.conbuildmat.2016.08.156.

Paliukaitė, M., Assuras, M., & Silva, S. C. (2017). Implementation of the double-edge-notched tension test for asphalt cement acceptance. *Transp. Dev. Econ.*, *3*(6), 1-10. https://doi.org/10.1007/s40890-017-0034-0

Paliukaite, M., Vaitkus, A., & Zofka, A. (2014). Evaluation of bitumen fractional composition depending on the crude oil type and production technology in environmental engineering. *Proc. Int. Conf. Environ. Eng.*, *9*, 1.

Pasandín, A. R., Pérez, I., Gómezmeijide, B., & Pérezbarge, N. (2015). The effect of hydrated lime on the bond between asphalt and recycled concrete aggregates. *Pet. Sci. Technol.*, *33*(10), 1141-1148.

Pauli, A. T., & Branthaver, J. F. (1998). Relationship between asphaltenes, Heithaus compatibility parameters, and asphalt viscosity. *Petroleum Science and Technology*, *16*(9&10), 1125–1147.

Pauli, A. T., & Branthaver, J. F. (1999). Rheological and compositional definitions of compatibility as they relate to the colloidal model of asphalt and residua. *American Chemical Society Division of Petroleum Chemistry, Preprints*, *44*, 190–193.

Petersen, J. C. (2009). A review of the fundamentals of asphalt oxidation (*Transportation Research Circular E-C140*). Washington, DC: Transportation Research Board.

Pieri, N., Jacquot, F., Mille, G., Planche, J. P., & Kister, J. (1996). GC-MS identification of biomarkers in road asphalts and in their parent crude oils: Relationships between crude oil maturity and asphalt reactivity towards weathering. *Org. Geochem.*, *2*(1–2), 51–68.

Planche, J. P., Claudy, P. M., Leé Toffé, J. M., & Martin, D. (1998). Using thermal analysis methods to better understand asphalt rheology. *Thermochim. Acta*, *324*, 223–227.

Polacco, G., Filippi, S., Paci, M., Giuliani, F., & Merusi, F. (2012). Structural and rheological characterization of wax-modified bitumens. *Fuel*, *95*(1), 407–416.

Polacco, G., Stastna, J., Biondi, D., Antonelli, F., Vlachovicova, Z., & Zanzotto, L. (2004). Rheology of asphalts modified with glycidylmethacrylate functionalized polymers. *J. Colloid Interface Sci.*, *280*(2), 366–373.

Qin, Q., Farrar, M. J., Pauli, A. T., & Adams, J. J. (2014). Morphology, thermal analysis, and rheology of Sasobit modified warm mix asphalt binders. *Fuel*, *115*, 416–425.

Qin, Q., Schabron, J. F., Boysen, R. B., & Farrar, M. J. (2014). Field aging effect on chemistry and rheology of asphalt binders and rheological predictions for field aging. *Fuel*, *121*(2), 86–94.

Rebelo, L. M., De Sousa, J., Abreu, A., Baroni, M., Alencar, A., & Soares, S. (2014). Aging of asphaltic binders investigated with atomic force microscopy. *Fuel*, *117*, 15–25.

Redelius, P., & Soenen, H. (2015). Relation between bitumen chemistry and performance. *Fuel*, *140*, 34–43.

Rigg, A., Duff, A. R., Nie, Y., Somuah, M., Tetteh, N., & Hesp, S. A. M. (2017). Non-isothermal kinetic analysis of reversible ageing in asphalt cements. *Road Materials and Pavement Design*, *18*(4), 185–210.

Roberts, F. L., Kandhal, P. S., Brown, E. R., & Dunning, R. L. (1989). Investigation and evaluation of ground tire rubber in hot mix asphalt (*NCAT Report, 89-3*). Auburn, AL, National Center for Asphalt Technology.

Romberg, J. W., Nesmith, S. D., & Traxler, R. N. (1959). Some chemical aspects of the components of asphalt. *J. Chem. Eng. Data*, *4*(2), 159–161.

Rowe, G. M. (2011). Prepared discussion for the AAPT paper by Anderson et al.: Evaluation of the relationship between asphalt binder properties and non-load-related cracking. *Journal of the Association of Asphalt Paving Technologists*, *80*, 649–662.

Schmets, A., Kringos, N., Pauli, T., Redelius, P., & Scarpas, T. (2010). On the existence of wax induced phase separation in bitumen. *Int. J. Pavement Eng.*, *11*(6), 555–563.

Shastry, A., & Arnold, T. (2015). The analysis of asphalt binders for recycled engine oil bottoms by X-ray fluorescence spectroscopy. Paper presented at the 94th Annual Meeting of the Transportation Research Board, Washington, DC.

Sheu, E. Y. (2002). Petroleum asphaltenes: Properties, characterization, and issues. *Energy & Fuel*, *16*, 74–82.

Sheu, E., DeTar, M., & Storm, D. (1991). Rheological properties of vacuum residue fractions. *Organic Solvents, Fuel*, *70*, 1151–1156.

Sias, J. E., Dave, E. V., Zhang, R., & Rahbar-Rastegar, M. R. (2019). Incorporating impact of aging on cracking performance of mixtures during design (*Technical Report, No. FHWA-NH-RD-26962O*). New Hampshire Department of Transportation, Concord, NH.

Soenen, H., Lu, X., & Laukkanen, O. V. (2016). Oxidation of bitumen: Molecular characterization and influence on rheological properties. *Rheol. Acta*, *55*(4), 315–326.

Spadafora, A., Gilna, C., Krupp, D., Fisher, J., & Siegel, J. A. (1985). Fluorescence of petroleum products I. Three-dimensional fluorescence plots of motor oils and lubricants. *J. Forensic Sci.*, *30*(3), 741–759.

Tabatabaee, H. A., & Sylvester, T. (2011). Relating thermal and rheological analysis to phase compatibility of bitumen modified with rejuvenating and softening recycling agents. *Proceedings of the Eurobitumen and Euroasphalt Congress*, Madrid, 2021.

Tabatabaee, H. A., Sylvester, T., & Calcanas, C. (2011). Phase-compatibility of bitumen defined through deconvolution of modulated differential scanning calorimetry response. *Proceedings of the European Association of Asphalt Technologists (EATA) Conference*, Vienna, 2021.

Thomas, W. H., & Tester, H. E. (1993). The effect of paraffin wax in asphaltic bitumen and its estimation. *1st World Petroleum Congress*, *1933*, 547–550.

Traxler, R. N., & Romberg, J. W. (1952). Asphalt, a colloidal material. *Ind. Eng. Chem.*, *44*(1), 155–158.

Trujillo, P. (2011). Long-term aging study of WMA binder (Masters thesis). University of Texas at Austin, Austin, TX.

Turner, T. F., & Branthaver, J. F. (1997). DSC studies of asphalts and asphalt components. In A. Usmani (Ed.), Asphalt Science and Technology (pp. 59–102). Boca Raton, FL: CRC Press.

Wang, S., Wang, Q., Wu, X., & Zhang, Y. (2015). Asphalt modified by thermoplastic elastomer based on recycled rubber. Constr. Build. Mater., 93, 678–684.

Wang, S., Yuan, C., & Jiaxi, D. (2014). Crumb tire rubber and polyethylene mutually stabilized in asphalt by screw extrusion. J. Appl. Polym. Sci., 131, 41189.

Wang, Y., & Kim, Y. R. (2017). Development of a pseudo strain energy-based fatigue failure criterion for asphalt mixtures. *Int. J. Pavement Eng.*, *20*(10), 1182–1192.

Xiao, F., Punith, S., Amirkhanian, N., & Putman, B. (2013). Rheological and chemical characteristics of warm mix asphalt binders at intermediate and low performance temperatures. *Can. J. Civ. Eng.*, *40*, 861–868.

Yang, X., You, Z., & Mills-Beale, J. (2015). Asphalt binders blended with a high percentage of biobinders: Aging mechanism using FTIR and rheology. *J. Mater. Civ. Eng.*, *27*(4), 04014157.1- 04014157-11.

Yani, Q. I. (2013). Analysis of aging characteristics of rubber asphalt with FTIR method. *New Build. Mater.*, *3*, 47-48,58.

Yousefi, A., Lafleur, P. G., & Gauvin, R. (1997). Kinetic studies of thermoset cure reactions: A review. *Polym. Compos.*, *18*(2), 157–168.

Yu, M. A., Zhao-Yi, H. E., Liang, H. E., Ling, T. Q., S. O., & Sciences, C. J. (2015). University analysis on aging characteristics and infrared spectroscopy of warm mix asphalt rubber. *J. Highway Transport. Res. Dev.*, 32*(1)*, 13-18.

Zelelew, H., Paugh, C., & Corrigan, M. (2011). Warm-mix asphalt laboratory permanent deformation performance in the state of Pennsylvania: A case study. Paper presented at the 90th Transportation Research Board Annual Meeting, Washington, D.C., January 23–27, 2011.

Zhang, H., Zhu, C., Yu, J., Tan, B., & Shi, C. (2015). Effect of nano-zinc oxide on ultraviolet aging properties of bitumen with 60/80 penetration grade. *Mater. Struct.*, *48*(10), 1–9.

Zhang, R. (2020). Evaluation and identification of cracking susceptibility of asphalt binders and mixtures by incorporation of effects of aging on performance (Doctoral dissertation). University of New Hampshire, Durham, NH.

Zhou, H., Wang, Z., Zhu, Y., Li, Q., & Zou, H. J. (2013, December). Quantitative determination of trace metals in high-purity silicon carbide powder by laser ablation inductively coupled plasma mass spectrometry without binders. *Spectrochimica Acta Part B, Atomic Spectroscopy*, *90*, 55–60.

Zhu, Y., Dave, E. V., Rahbar-Rastegar, R., Daniel, J. S., & Zofka, A. (2017). Comprehensive evaluation of low-temperature cracking fracture indices for asphalt mixtures. *Road Mater. Pavement Des.*, *18*(sup4), 467-490.

Appendix A:

CONNECTING LETTER REPORTS FOR CONTROL RAP MIXTURES

Table A-1 Connecting letter report for fracture energy from DCT (α=0.05)

Mixture ID	Connecting Letter	Means	Group
Binder B-NA	A	544.16	A
Binder B-RA1	A	495.44	
Binder C-RA1	A	485.57	
Binder B-RA2	A	454.66	
Binder C-RA2	A	420.10	
Binder A-NA	A	415.48	
Binder A-RA1	A	344.29	
Binder C-NA	A	337.04	
Binder A-RA2	A	321.56	

Table A-2 Connecting letter report for FST form DCT (α=0.05)

Mixture ID	Connecting Letter			Means	Group
Binder B-RA1	A			193.60	A
Binder C-RA1	A	B		191.91	AB
Binder B-RA2	A	B	C	172.16	ABC
Binder C-RA2	A	B	C	150.36	
Binder A-RA2	A	B	C	135.61	
Binder A-RA1	A	B	C	128.77	
Binder A-NA		B	C	98.14	BC
Binder B-NA			C	87.81	C
Binder C-NA			C	84.65	

Table A-3 Connecting letter report for fracture energy from I-FIT (α=0.05)

Mixture ID	Connecting Letter				Means	Group
Binder A-RA2	A				1908.03	A
Binder C-RA1	A	B			1750.24	AB
Binder B-RA2	A	B			1697.39	
Binder A-NA	A	B	C		1658.55	ABC
Binder B-RA1	A	B	C		1641.99	
Binder A-RA1	A	B	C		1580.19	
Binder C-RA2		B	C	D	1423.28	BCD
Binder B-NA			C	D	1186.79	CD
Binder C-NA				D	1002.67	D

Table A-4 Connecting letter report for FI from I-FIT (α=0.05)

Mixture ID	Connecting Letter				Means	Group
Binder C-RA1	A				7.45	A
Binder A-RA1	A	B			6.27	AB
Binder A-RA2	A	B			6.20	
Binder B-RA1	A	B	C		5.03	ABC
Binder B-RA2		B	C	D	3.41	BCD
Binder A-NA		B	C	D	2.87	
Binder C-RA2			C	D	2.15	CD
Binder B-NA				D	0.29	D
Binder C-NA				D	0.16	

Table A-5 Connecting letter report for RDCI from I-FIT (α=0.05)

Mixture ID	Connecting Letter			Means	Group
Binder A-RA1	A			16.59	A
Binder C-RA1	A	B		15.49	AB
Binder A-RA2	A	B		15.45	
Binder B-RA1	A	B	C	10.71	ABC
Binder B-RA2	A	B	C	10.04	
Binder A-NA	A	B	C	8.97	
Binder C-RA2		B	C	7.42	BC
Binder B-NA			C	1.97	C
Binder C-NA			C	1.72	

Table A-6 Connecting letter report for mixture Glover Rowe parameter from E* Test(α=0.05)

Mixture ID	Connecting Letter				Means	Group
HRAP-A-R2	A				10022.28	A
HRAP-A-R1	A				11216.78	
HRAP-C-R1	A	B			13164.34	AB
HRAP-A	A	B			15362.85	
HRAP-B-R1	A	B			15740.78	
HRAP-C-R2	A	B	C		17128.99	ABC
HRAP-B-R2		B	C	D	20008.53	BCD
HRAP-C			C	D	24118.75	CD
HRAP-B				D	27015.48	D

Appendix B:

CONNECTING LETTER REPORTS AND PERFORMANCE INDEX FOR CORE MIXTURES

Table B-7 Connecting letter report for fracture energy from DCT (α=0.05)

Level	Connecting Letter								Mean	Group
V-C	A								712.59	A
HRAP2-B	A	B							603.10	AB
LRAP-C	A	B	C	D					597.44	ABCD
V-B	A	B	C						593.68	ABC
V-A	A	B	C	D					581.19	ABCD
HRAP1-B		B	C	D	E				544.16	BCDE
LRAP-A		B	C	D	E	F	G	H	491.76	BCDEFGH
HRAP1-C-R1		B	C	D	E	F			485.57	BCDEF
HRAP2-C			C	D	E	F	G		460.16	CDEFG
HRAP3-A			C	D	E	F	G		460.10	CDEFG
HRAP1-B-R1				D	E	F	G		459.15	DEFG
HRAP3-B			C	D	E	F	G	H	454.89	CDEFGH
LRAP-B			C	D	E	F	G	H	445.39	CDEFGH
HRAP2-A					E	F	G	H	433.85	EFGH
HRAP1-B-R2					E	F	G	H	423.80	EFGH
HRAP1-C-R2					E	F	G	H	420.10	EFGH
HRAP3-C					E	F	G	H	418.02	EFGH
HRAP1-A					E	F	G	H	415.48	EFGH
HRAP1-A-R1						F	G	H	344.29	FGH
HRAP1-C							G	H	337.04	GH
HRAP1-A-R2								H	321.64	H

Table B-8 Connecting letter report for FST form DCT (α=0.05)

Level	Connecting Letter						Mean	Group
V-C	A						173.21	A
V-B	A	B					156.89	AB
HRAP2-B	A	B	C				138.94	ABC
V-A		B	C	D			131.39	BCD
LRAP-C		B	C	D	E		125.29	BCDE
HRAP1-C-R1			C	D	E	F	117.54	CDEF
LRAP-A		B	C	D	E	F	108.60	BCDEF
HRAP1-B-R1				D	E	F	105.14	DEF
HRAP3-B				D	E	F	102.23	DEF
HRAP2-C				D	E	F	102.06	DEF
HRAP1-C				D	E	F	98.14	DEF
HRAP1-C-R2				D	E	F	97.05	DEF
HRAP1-B-R2				D	E	F	96.98	DEF
HRAP3-A					E	F	95.24	EF
HRAP2-A					E	F	92.99	EF
HRAP3-C				D	E	F	89.06	DEF
HRAP1-B					E	F	87.81	EF
LRAP-B			C	D	E	F	87.63	CDEF
HRAP1-A-R2					E	F	84.72	EF
HRAP1-A					E	F	84.65	EF
HRAP1-A-R1						F	81.85	F

Table B-9 Connecting letter report for FI from I-FIT (α=0.05)

Level	Connecting Letter									Mean	Group
V-A	A									20.50	A
LHRAP-A		B								10.21	B
HRAP3-A		B								9.52	B
V-B		B	C							9.50	BC
V-C		B	C							9.23	BC
HRAP1-C-R1			C	D						7.45	CD
HRAP1-A-R1				D	E					6.27	DE
HRAP1-A-R2				D	E					6.20	DE
HRAP1-B-R1					E	F				5.03	EF
HRAP2-A					E	F				5.01	EF
HRAP3-C						F	G			4.27	FG
HRAP3-B						F	G	H		3.61	FGH
HRAP1-B-R2						F	G	H		3.41	FGH
LRAP-C							G	H		3.25	GH
HRAP1-A							G	H		2.87	GH
HRAP2-C								H		2.53	H
HRAP1-C-R2								H	I	2.15	HI
HRAP2-B								H	I	2.07	HI
LRAP-B									I	0.69	I
HRAP1-B									I	0.29	I
HRAP1-C									I	0.16	I

Table B-10 Connecting letter report for RDCI from I-FIT (α=0.05)

Level	Connecting Letter								Mean	Group
V-A	A								42.78	A
LRAP-A		B							22.04	B
V-B		B	C						20.88	BC
HRAP3-A		B	C	D					18.48	BCD
HRAP1-A-R1			C	D					16.59	CD
V-C			C	D					16.24	CD
HRAP1-C-R1				D					15.49	D
HRAP1-A-R2				D					15.45	D
HRAP1-B-R1					E				10.71	E
HRAP3-C					E				10.47	E
HRAP2-A					E				10.18	E
HRAP1-B-R2					E				10.04	E
HRAP1-A					E	F			8.97	EF
HRAP3-B					E	F			7.47	EF
HRAP1-C-R2					E	F			7.42	EF
LRAP-C					E	F	G		6.88	EFG
HRAP2-C						F	G	H	5.84	FGH
HRAP2-B						F	G	H	5.26	FGH
LRAP-B						F	G	H	5.16	FGH
HRAP1-B							G	H	1.97	GH
HRAP1-C								H	1.72	H

Table B-11 Connecting letter report for mixture Glover Rowe parameter from E* test (α=0.05)

Level	Connecting Letter									Mean	Group
V-A	A									2080.45	A
V-C		B								7705.94	B
HRAP3-A		B								7887.87	B
V-B		B	C							8086.4	BC
LRAP-A		B	C							8784.45	BC
HRAP1-A-R2		B	C	D						10022.28	BCD
HRAP2-A		B	C	D						10594.37	BCD
HRAP1-A-R1			C	D						11216.78	CD
HRAP1-C-R1				D	E					13164.34	DE
HRAP1-A					E	F				15362.85	EF
LRAP-B					E	F				15410.68	EF
HRAP1-B-R1					E	F				15740.78	EF
HRAP3-B						F	G			16466.86	FG
HRAP1-C-R2						F	G	H		17128.99	FGH
LRAP-C						F	G	H		17477.33	FGH
HRAP2-B						F	G	H		17548.98	FGH
HRAP3-C							G	H		19381.17	GH
HRAP1-B-R2								H		20008.53	H
HRAP2-C									I	23996.85	I
HRAP1-C									I	24118.75	I
HRAP1-B									I	27015.48	I

Table B-12 Compatibility evaluation of RAP, binder and RA based on performance index identified from binder test results

Binder ID	Binder Evaluation											
	Rheological Analysis							Thermal Analysis				
	R	T_c(S)	T_c(m)	ΔT_c	HTPG	LTPG	Log(G-R)	$T_{g\,\alpha}$	$T_{g\,\beta}$	$T_{g\,Aave}$	ϕ_α	T_g
HRAP1-A	8.85	33.10	25.81	69.56	10.34	29.75	261.53	37.39	219.30	46.93	2.59	36.14
HRAP1-B	26.58	36.66	42.20	156.82	2.68	41.80	375.78	22.83	169.22	50.85	24.88	20.29
HRAP1-C	17.95	36.66	34.71	105.22	6.75	34.26	333.10	36.24	199.82	57.32	11.86	38.08
HRAP1-A-RA1	23.79	16.27	13.10	102.82	10.25	12.50	253.57	7.63	45.59	11.82	6.90	9.39
HRAP1-B-RA1	41.49	22.21	28.89	168.92	0.00	28.40	348.03	6.57	19.44	22.75	35.42	12.73
HRAP1-C-RA1	26.24	26.33	28.62	137.48	5.06	28.13	321.33	12.83	71.23	22.78	12.36	11.99
HRAP1-A-RA2	8.37	27.03	17.28	54.38	12.14	23.38	225.47	21.32	70.67	24.88	17.50	23.28
HRAP1-B-RA2	33.68	22.60	25.66	143.82	4.72	25.14	341.83	12.55	41.16	30.34	37.28	17.73
HRAP1-C-RA2	24.11	21.62	20.58	115.94	10.60	20.04	284.49	3.26	15.61	12.56	19.77	5.65
HRAP2-A	1.44	25.28	10.44	19.81	21.12	21.55	160.65	38.69	241.66	49.06	2.42	37.58
HRAP2-C	18.93	27.60	25.30	105.49	8.69	24.79	291.98	27.26	154.80	49.40	19.17	31.21
HRAP2-A-RA1	9.73	14.47	3.97	52.89	22.16	10.20	126.98	3.11	29.53	6.55	7.43	1.44
HRAP2-C-RA1	19.60	27.53	18.84	61.49	10.52	23.91	273.54	3.97	1.38	13.42	19.68	14.39
HRAP2-A-RA2	11.56	21.10	6.54	22.92	18.58	17.16	178.57	16.24	107.70	25.11	0.00	14.48
HRAP2-C-RA2	16.33	22.32	16.66	83.93	15.56	18.44	249.31	24.28	141.41	41.20	14.22	23.75
HRAP3-A	0.08	18.03	0.00	0.00	26.66	13.93	62.71	22.44	147.12	33.13	11.02	22.50
HRAP3-C	9.92	21.09	15.36	83.79	20.90	17.14	187.17	17.33	97.56	40.41	29.59	21.85
HRAP3-A-RA1	2.94	0.00	1.41	139.14	26.23	0.00	0.00	0.00	0.00	0.00	8.95	0.00
HRAP3-C-RA1	12.70	12.78	6.10	79.65	21.88	8.42	149.40	5.32	18.47	19.45	28.13	8.93
HRAP3-A-RA2	0.00	20.85	8.73	39.82	24.59	18.05	93.78	15.64	84.86	23.98	10.82	12.42
HRAP3-C-RA2	9.34	20.44	10.84	57.28	22.30	16.47	173.07	15.44	84.81	33.42	25.17	18.76

Appendix C:

FIELD PERFORMANCE GRAPHS OF NCAT MIXTURES AND FST SCATTER PLOTS FOR STUDY MIXTURES

Preliminary Field Performance Data of NCAT30-VL

0 to 10 MESALs:

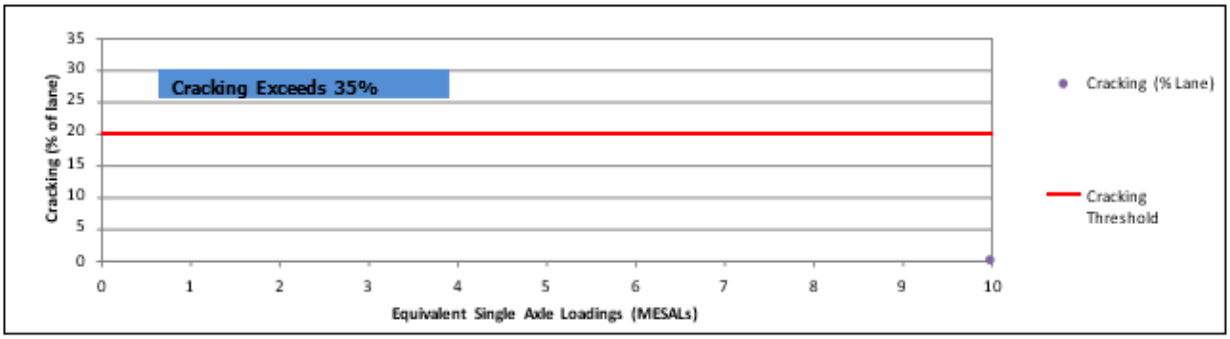

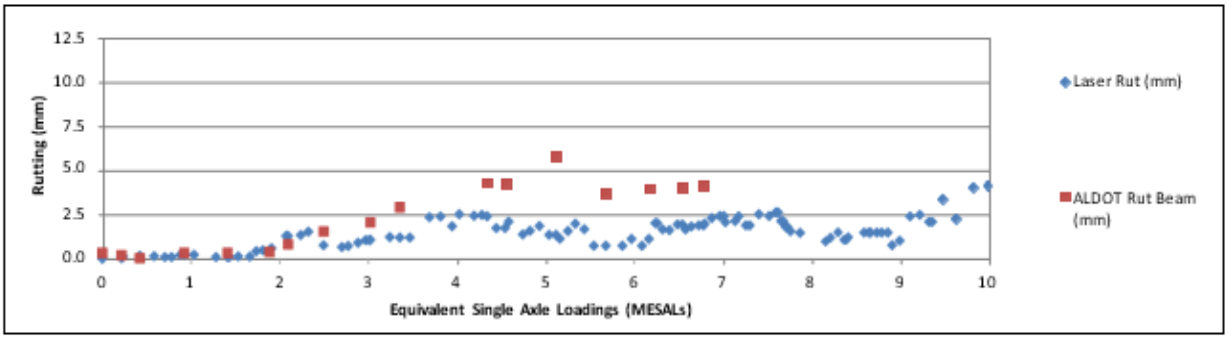

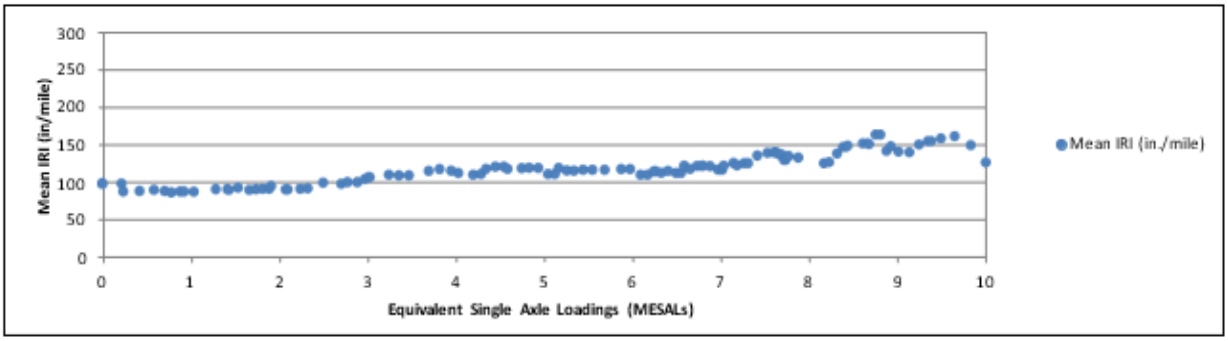

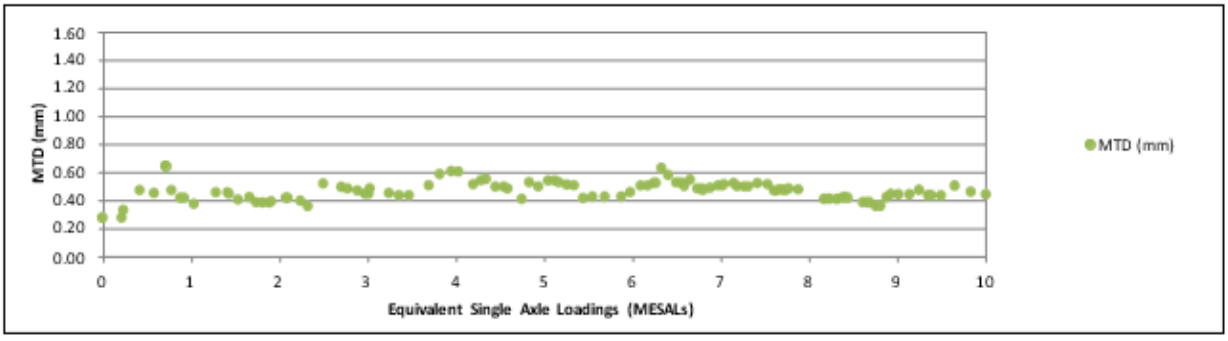

10 to 13 MESALs:

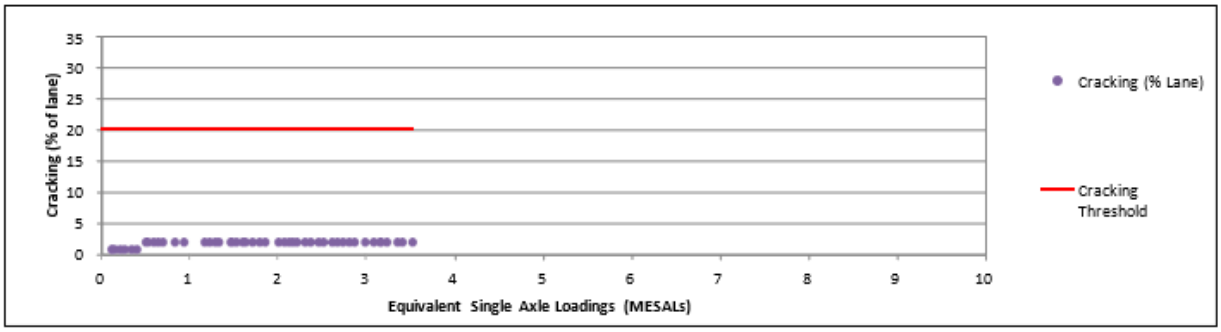

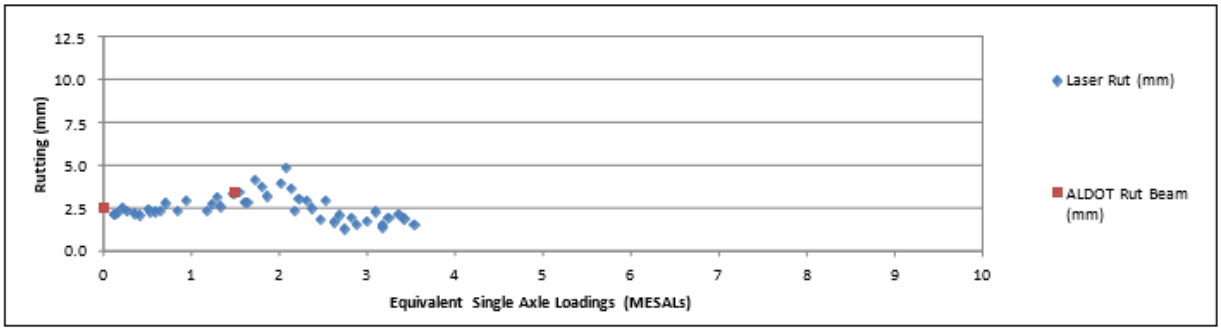

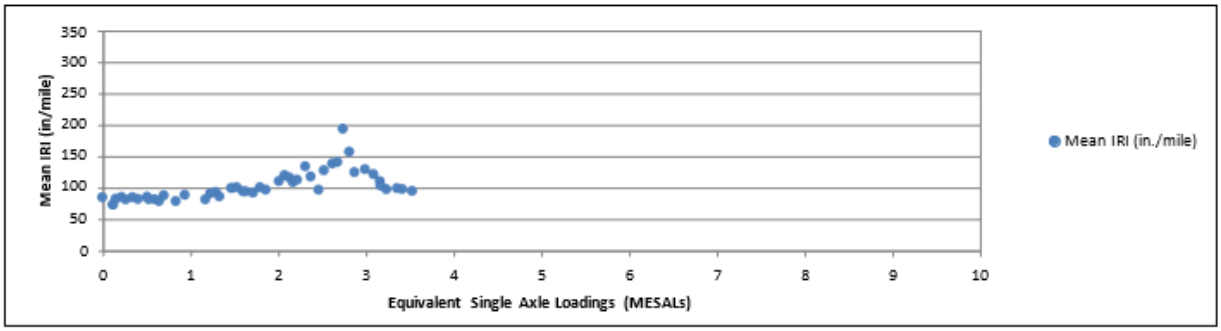

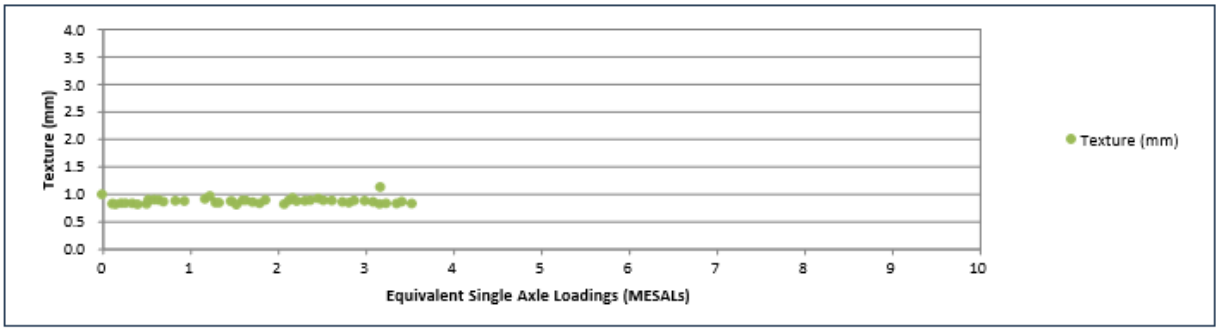

Preliminary Field Performance Data of NCAT45-VL

0-10 MESALs:

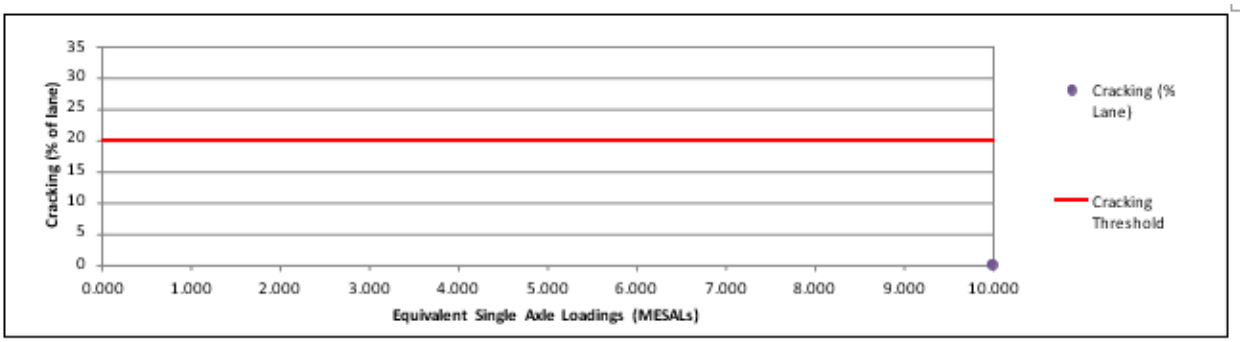

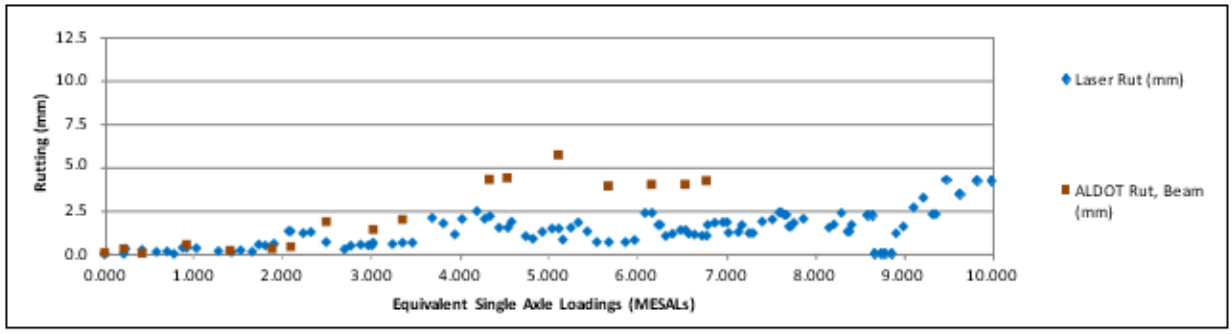

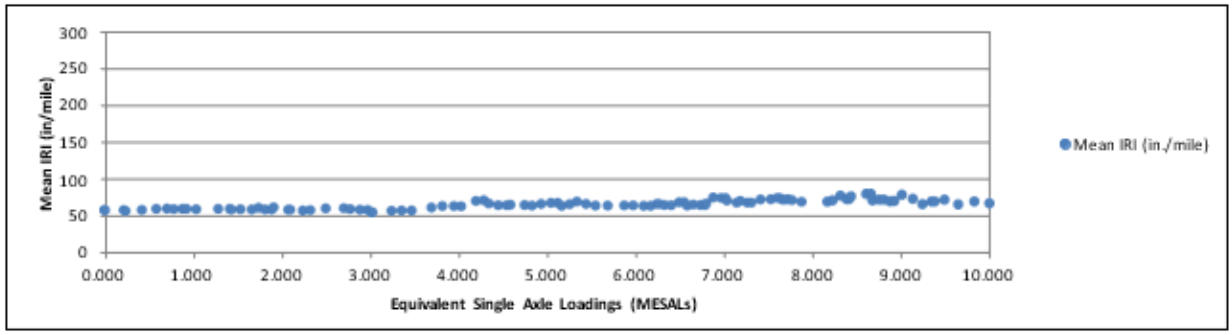

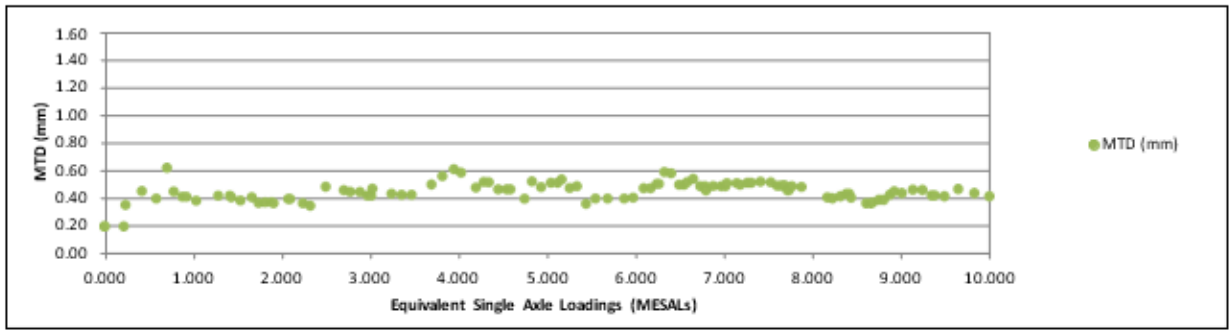

10 to 13 MESALs:

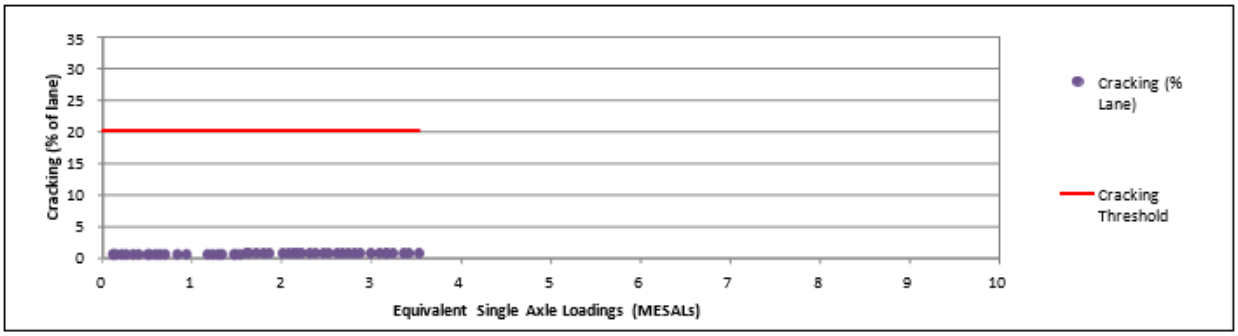

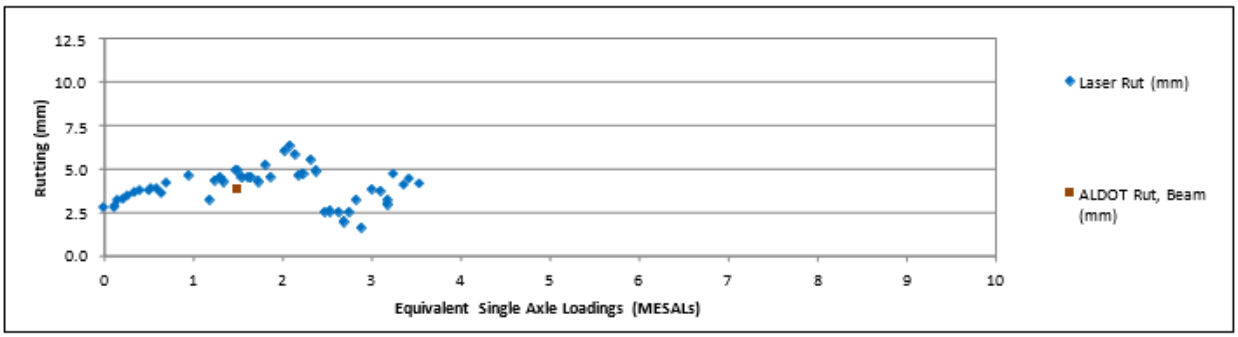

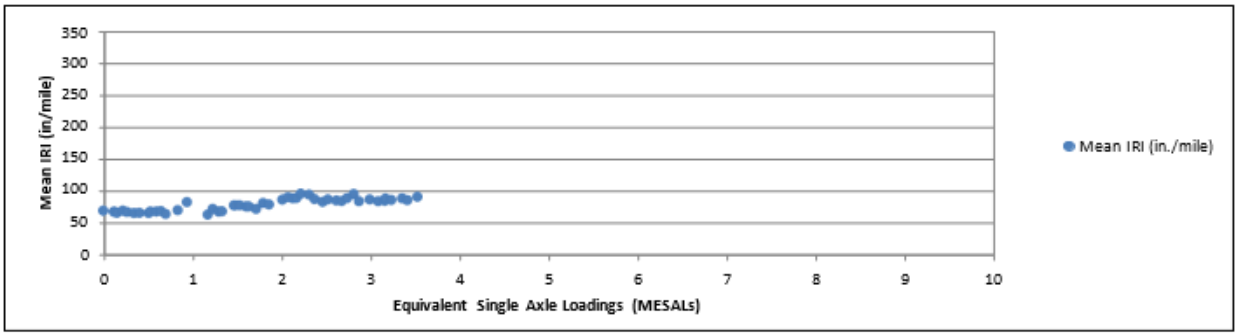

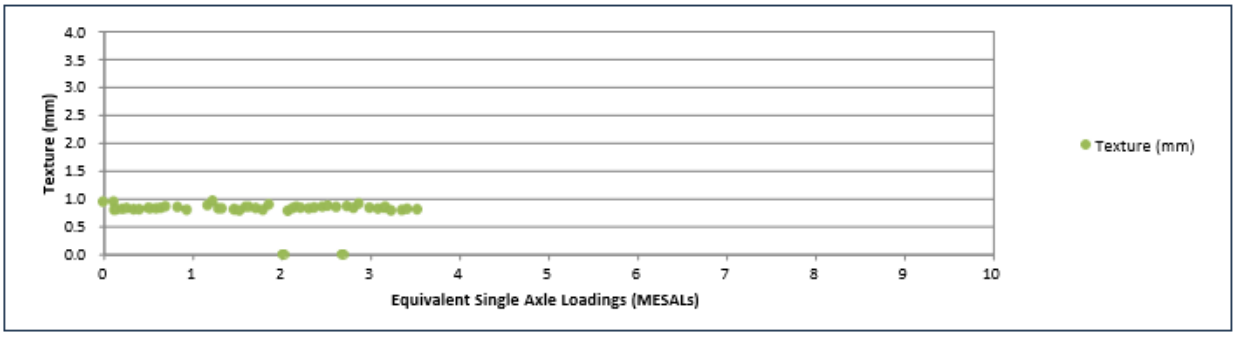

FST Scatter Plots (Core Materials)

Glover-Rowe Parameter (G-R)

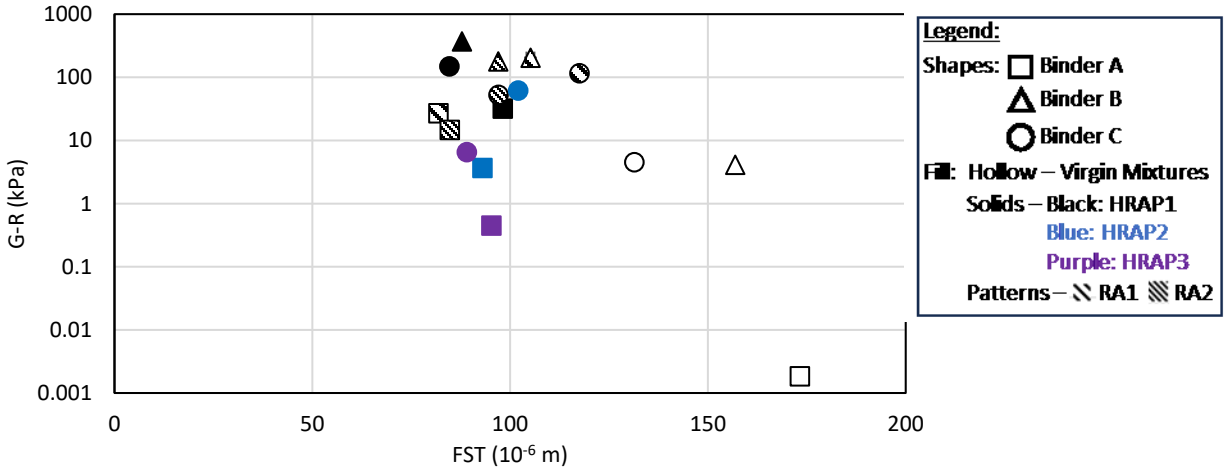

Figure C-1 Scatter plot of G-R and FST for core materials

Critical Low Temperature Based on Relaxation Rate (T_c(m))

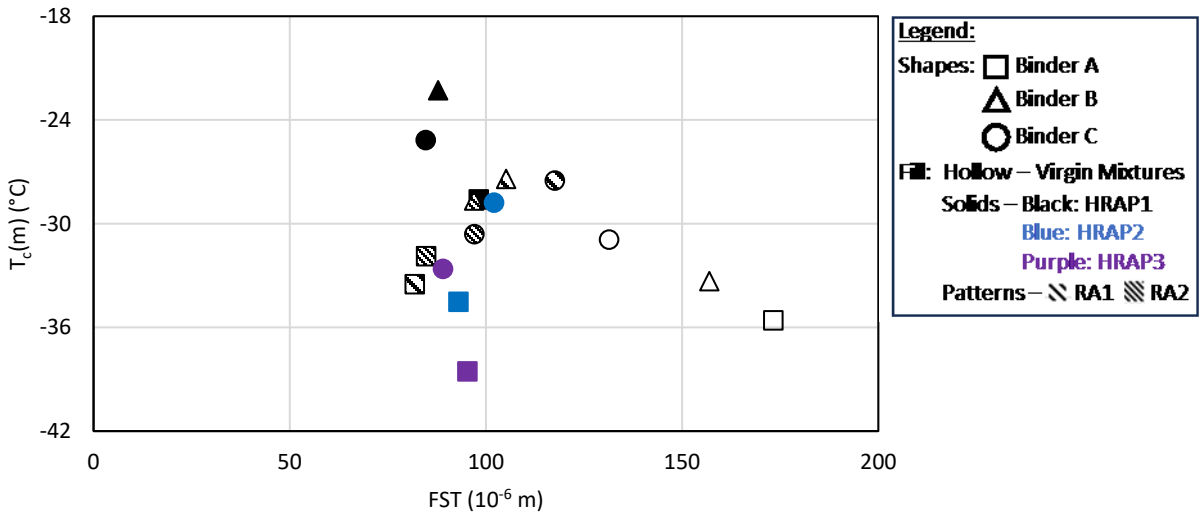

Figure C-2 Scatter plot of T_c(m) and FST for core materials

Change in Critical Low Temperature (ΔT_c)

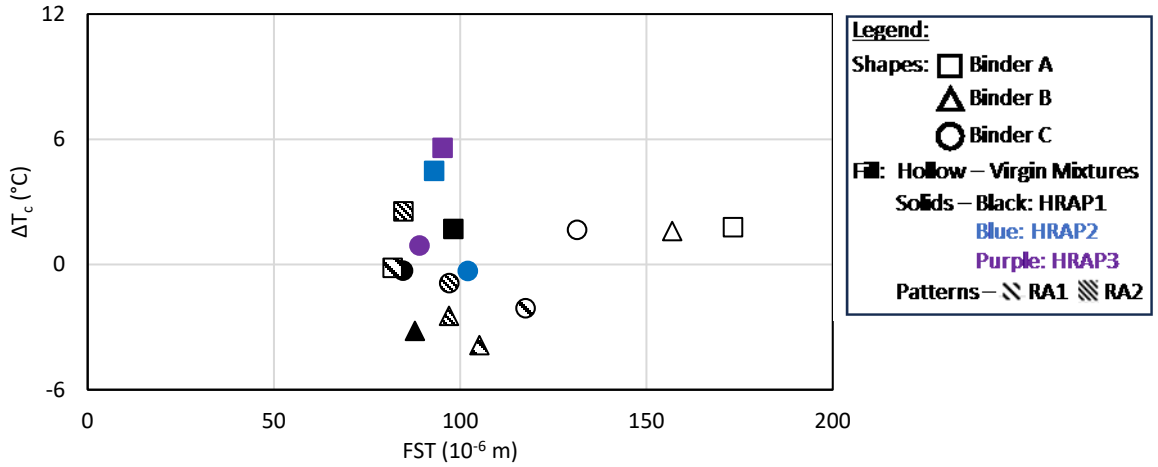

Figure C-3 Scatter plot of ΔT_c and FST for core materials

ϕ_α Index

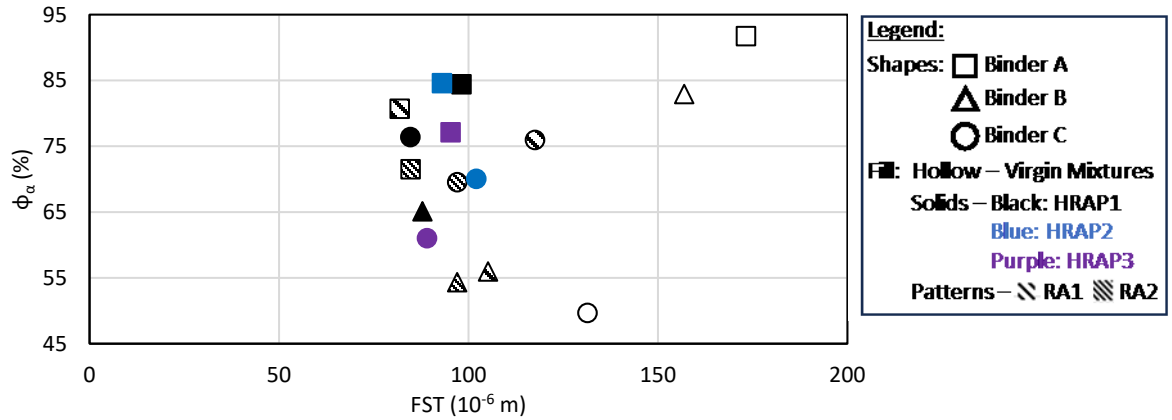

Figure C-4 Scatter plot of ϕ_α and FST for core materials

Glass Transition Temperature (Tg)

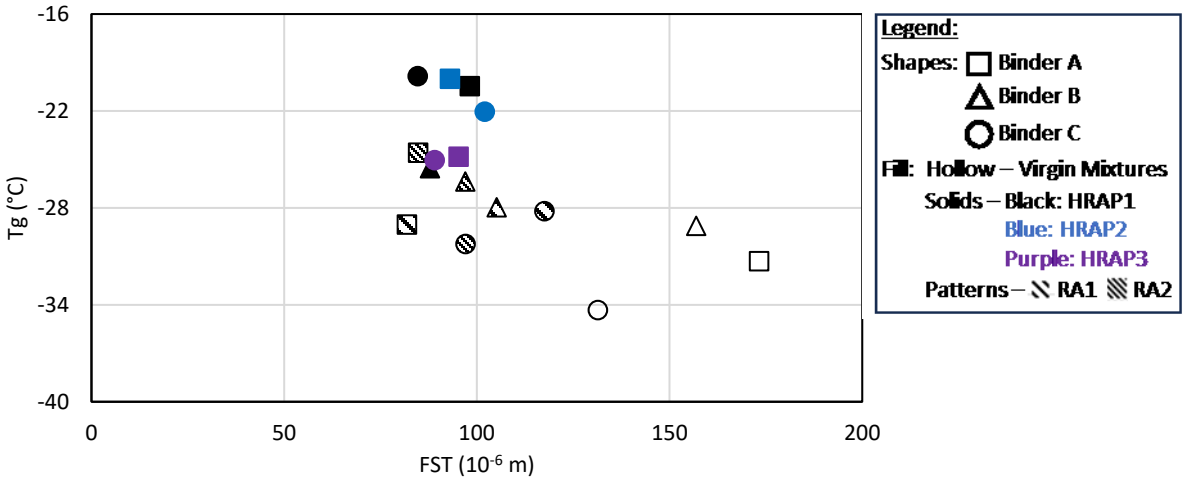

Figure C-5 Scatter plot of Tg and FST for core materials

FST Scatter Plots (Validation Materials)

Glover-Rowe Parameter (G-R)

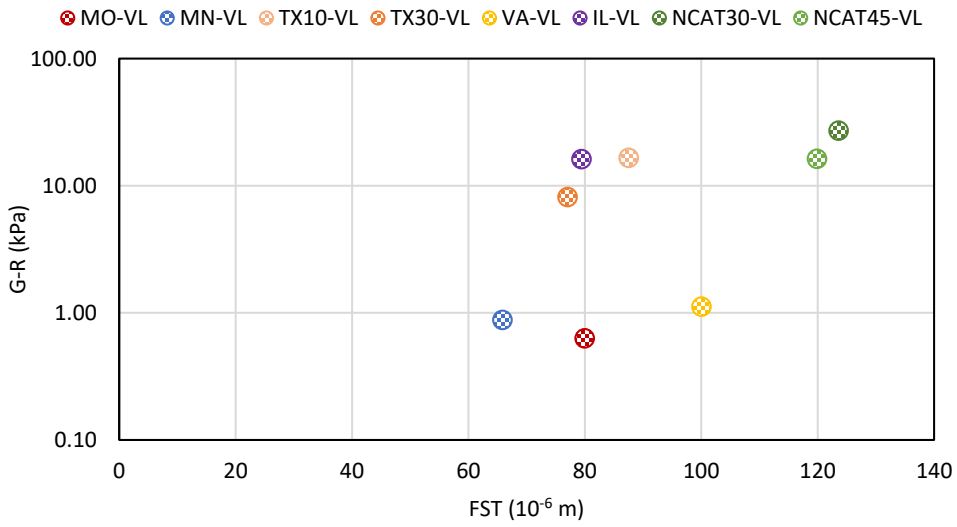

Figure C-6 Scatter plot of G-R and FST for validation materials

Critical Low Temperature Based on Relaxation Rate (T_c(m))

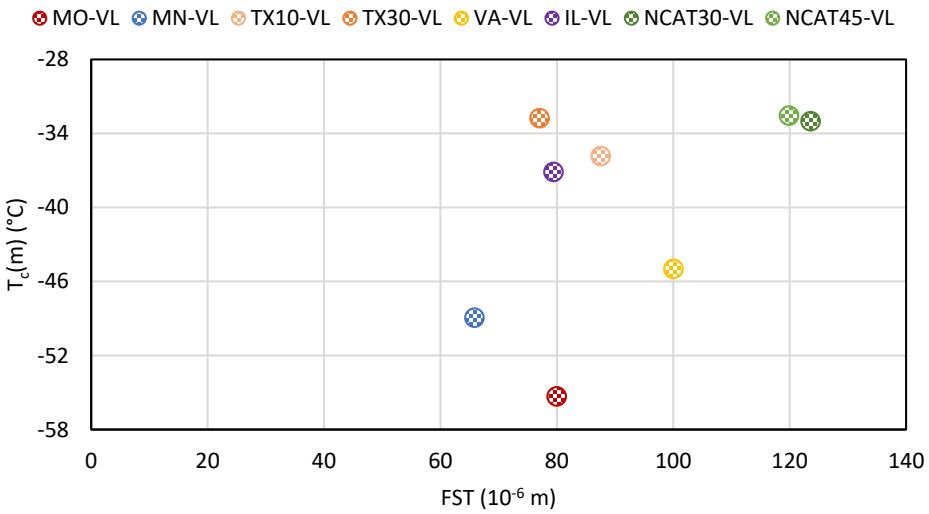

Figure C-7 Scatter plot of T_c(m) and FST for validation materials

Change in Critical Low Temperature (ΔT_c)

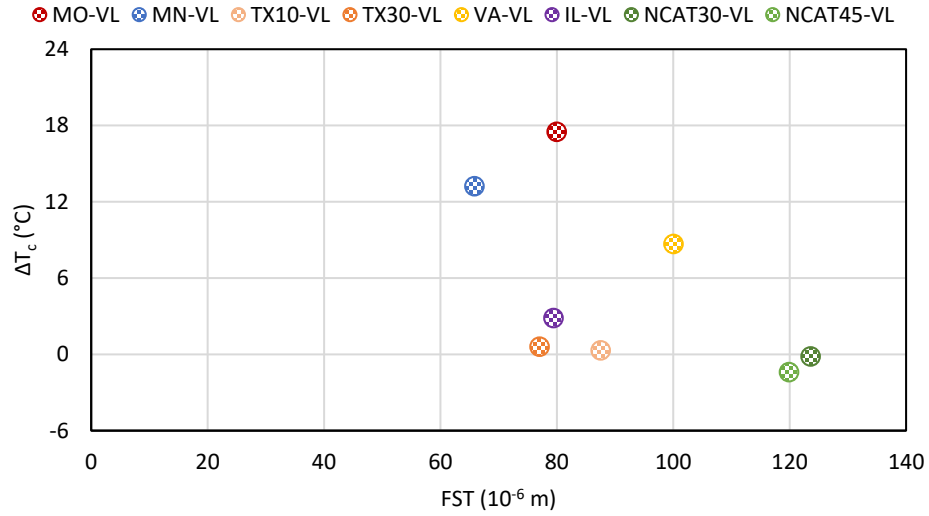

Figure C-8 Scatter plot of ΔT_c and FST for validation materials

ϕ_α Index

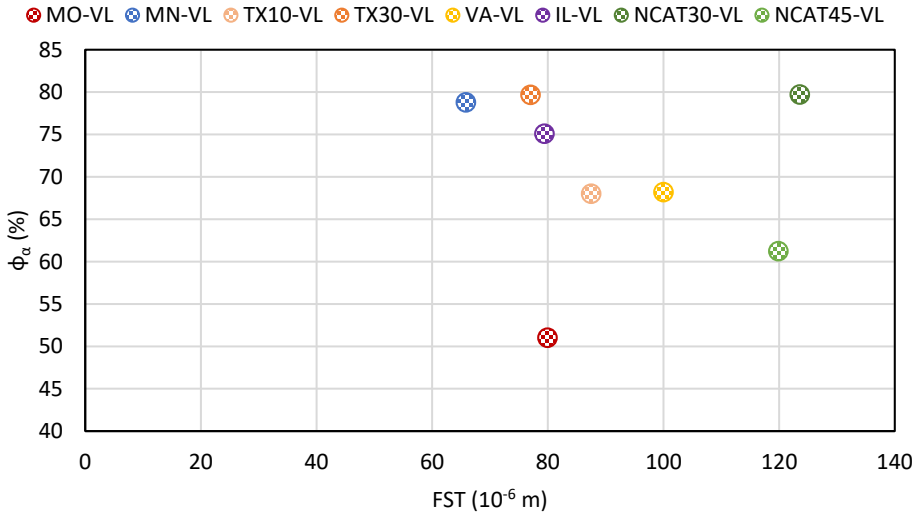

Figure C-9 Scatter plot of ϕ_α and FST for validation materials

Glass Transition Temperature (Tg)

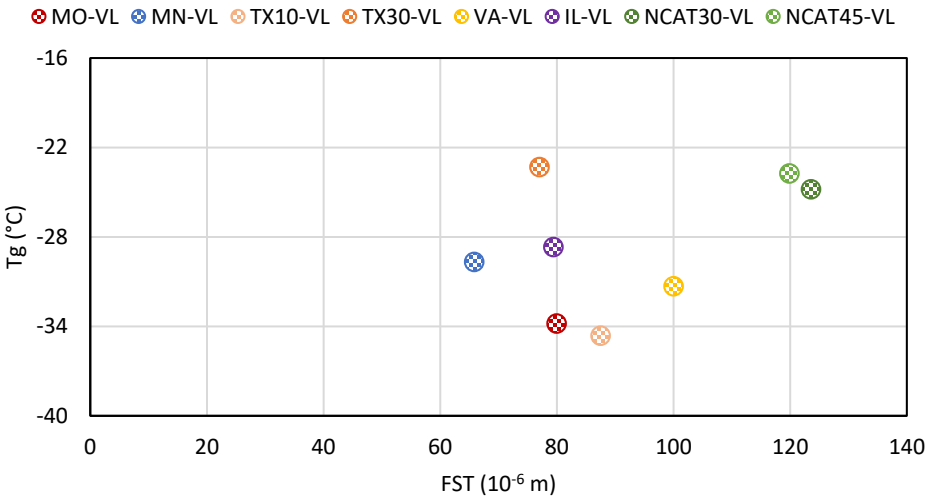

Figure C-10 Scatter plot of Tg and FST for validation materials